# The role of stromal Wnt/Beta-catenin and epidermal Ras-Raf-MEK-ERK MAPK signaling in human squamous cell carcinoma

**Dissertation**

Faculty of Biosciences
Ruperto-Carola University of Heidelberg

Marius Tham
2015

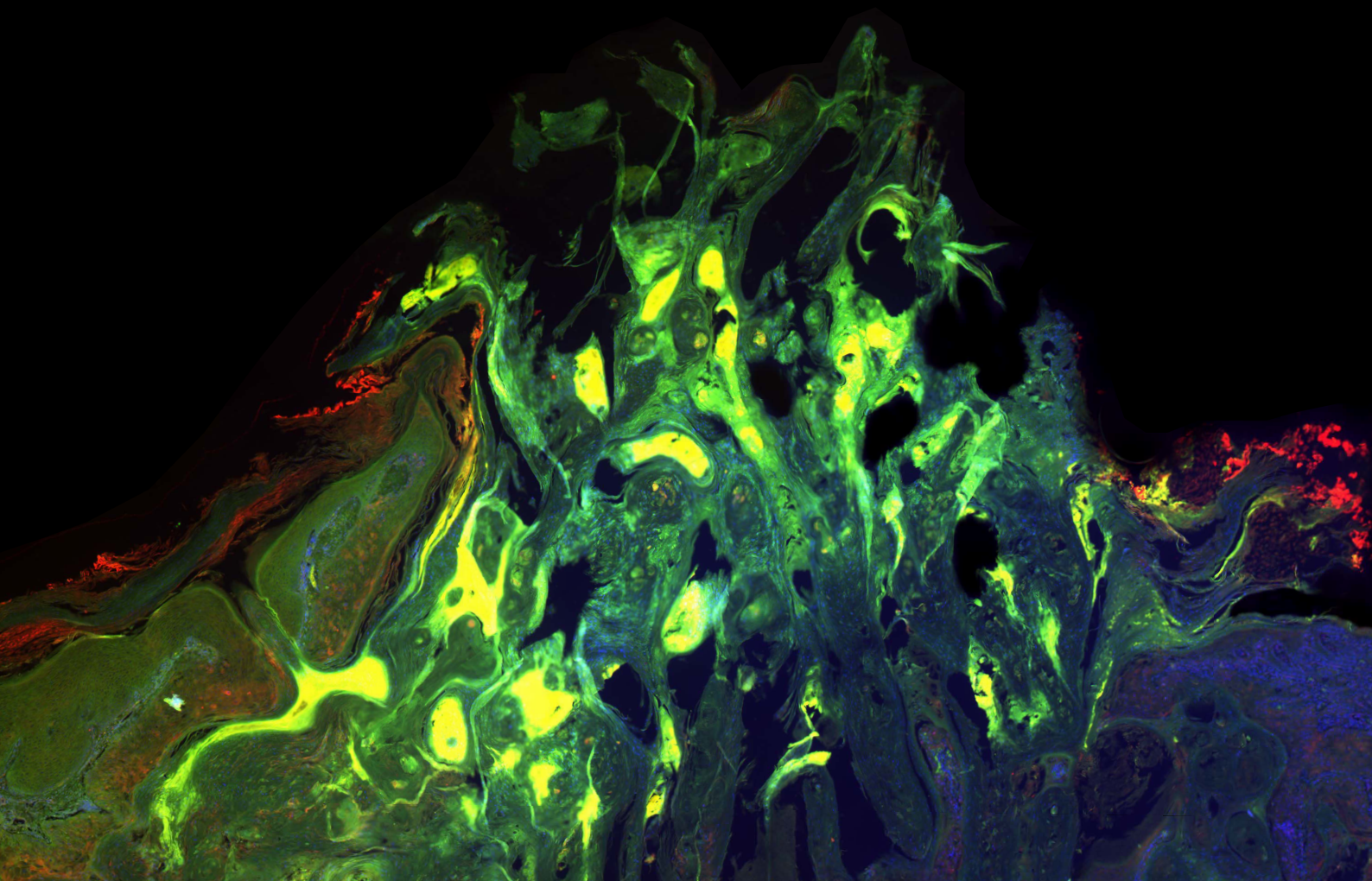

**Cover Illustration:**

Immunofluorescence staining of human cSCC for the proliferation marker Ki67 (red), the regulator of cell-cell adhesion and gene transcription Beta-catenin (green) as well as nuclei (blue).

**Dissertation**

submitted to the

Combined Faculties for the Natural Sciences and for Mathematics
of the Ruperto-Carola University of Heidelberg, Germany

for the degree of
Doctor of Natural Sciences

presented by

Marius Tham, M.Sc.
born in Wiesbaden, Germany

Oral examination:
21.09.2015

# The role of stromal Wnt/Beta-catenin and epidermal Ras-Raf-MEK-ERK MAPK signaling in human squamous cell carcinoma

Referees:

Prof. Dr. Peter Angel
Prof. Dr. Petra Boukamp

This work was conducted in the Division Genetics of Skin Carcinogenesis at the German Cancer Research Center (DKFZ) Heidelberg, Germany from April 2011 to June 2015.

# Acknowledgements

First, I would like to thank Prof. Dr. Petra Boukamp for giving me the opportunity to complete my Master Thesis and subsequently my PhD Thesis in her lab. Petra, thank you for your trust, continuous support and valuable discussions over the years that steadily improved this work. I also appreciate the numerous opportunities to visit scientific conferences. Your scientific spirit and motivation is exceptional!

I am grateful to Prof. Dr. Peter Angel for valuable support during the Thesis Advisory Committee-meetings and supervising this thesis. I would also like to thank Prof. Dr. Dr. Cornelia Mauch not only for being part of my Thesis Advisory Committee, but also for her medical contributions to the discussions.

My special thanks go to Dr. Katrin Sobel for her great support from the first months in the lab to the final submission of our publication. Katrin, I appreciated our steady and well-coordinated discussions and manuscript preparations through numerous phone calls and E-Mails. It was always a pleasure working with you! Hans-Jürgen Stark, I am grateful for our discussions, the manuscript revision, all antibody donations and your jokes! Lisa Schardt and Manuel Berning, our “group meetings” and discussions were always fun and very helpful. I would also like to thank our trainee Larissa Brunner for her very efficient helping hands. Furthermore, I would like to acknowledge Herman Stammer and Iris Martin for their expert help with molecular and cellular work. Herman, without you, I would still be pipetting qPCRs and Iris, you have always been the pillar of the lab! My thanks also go to Prof. Dr. Anna Jauch for the fruitful M-FISH collaboration.

My very special thanks go to all members of A110 throughout the years! The atmosphere in the lab was unmatched mainly when the space was still overcrowded. With you my colleagues and friends work was always entertaining: Angelika Krischke, Angelika Lampe, Anja Bort, Benedikt Müller, Berit Falkowska-Hansen, Christin Elßner, Christine Leufke, Damir Krunic, Elisa Specker, Elizabeth Pavez Loriè, Elke Laport, Ezgi Hacer Karakas, Gaby Blaser, Hans-Jürgen Stark, Heinrich Steinbauer, Herman Stammer, Iris Martin, Jannike Scharm, Jasmin Kollar, Jutta Leykauf, Karin Greulich-Bode, Karsten Böhnke, Katharina Nöske, Katrin Schmidt, Katrin Sobel, Larissa Brunner, Leonard Nevaril, Lisa Schardt, Lutz Langbein, Manuel Berning, Marco Nici, Marion Eryilmaz, Milena Barf, Nina Linde, Philipp Scholz, Philipp Worst, Sabrina Bauer, Silke Prätzel-Wunder, Stefanie Frick, Svenja Ewert, Yetunde Odunsi. (I hope, I have not forgotten anyone!).

Personal thanks go to my parents and grandparents for their great support in every life situation. Especially, I would like to mention my grandfather Adolf Tham for the special training on the 1st floor. Without all of you, I would have never made it that far. Anja, thanks a lot for all your support, reading and understanding during the last months. I am looking forward to our time afterwards.

# Table of Contents

# List of Abbreviations

| | |
|---|---|
| AGE | Agarose gel electrophoresis |
| AK | Actinic keratoses |
| BCC | Basal cell carcinoma |
| BM | Basement membrane |
| bp | Base pair |
| BrdU | 5'Brom-2'-desoxyuridin / 5'-Brom2'-Desoxycytidin |
| BSA | Bovine serum albumin |
| CAF | Carcinoma-associated fibroblasts |
| CAM | Cell adhesion molecule |
| cDNA | Complementary DNA |
| CIS | Carcinoma *in situ* |
| CLL | Chronic lymphocytic leukemia |
| CMML | Chronic myelomonocytic leukemia |
| $CO_2$ | Carbon dioxide |
| COBI (GDC-0973) | Cobimetinib (MEK inhibitor) |
| CP | Crossing point |
| cSCC | Cutaneous squamous cell carcinoma |
| Cy3 | Indocarbocyanine (fluorochrome) |
| DAPI | 4',6-Diamidino-2-phenylindole |
| $ddH_2O$ | Double distilled water |
| DIG | Digoxigenin |
| DMBA | 7,12-dimethylbenz-(a)anthracene |
| DMEM | Dulbecco's modified eagle's medium |
| DMSO | Dimethyl sulfoxide |
| DNA | Deoxyribonucleic acid |
| dNTP | Deoxyribonucleotide triphosphate |
| ECM | Extracellular matrix |
| EDTA | Ethylenediaminetetraacetic acid |
| ELISA | Enzyme-linked immunosorbent assay |
| EMT | Epithelial-mesenchymal transition |
| FBS | Fetal bovine serum |
| fdm | Fibroblast-derived matrix |
| FFPE | Formalin-fixed paraffin-embedded |
| FITC | Fluorescein isothiocyanate |
| H/ E | Haematoxylin/ eosin |
| HPV | Human papillomavirus |
| HPyV | Human polyomavirus |
| HRP | Horseradish peroxidase |
| HSPG | Heparin-sulphate proteoglycan |
| IgG | Immunoglobulin G |
| IHC | Immunohistochemistry |
| IIF | Indirect immunofluorescence |
| ISH | *In situ* hybridization |
| KA | Keratoacanthoma |
| M-FISH | Multiplex-fluorescence *in situ* hybridization |
| MAPK | Mitogen-activated protein kinase |
| MCPyV | Merkel cell polyomavirus |
| MM | Malignant melanoma |
| mRNA | Messenger RNA |
| nCCL-2 | Neutralizing antibodies targeting CCL-2 |
| NHDF | Normal human dermal fibroblasts |
| NHEK | Normal human epidermal keratinocytes |
| nIL-8 | Neutralizing antibodies targeting IL-8 |
| OS | Overall survival |
| OTC (col/ sca/ fdm) | Organotypic culture (collagen/ scaffold/ fibroblast-derived matrix) |
| PBS | Phosphate buffered saline |
| PCR | Polymerase chain reaction |

| | |
|---|---|
| PFS | Progression-free survival |
| PI | Propidium iodide |
| qPCR | Quantitative PCR |
| qRT-PCR | Quantitative RT-PCR |
| RIPA buffer | Radioimmunoprecipitation assay buffer |
| RNA | Ribonucleic acid |
| rpm | Rounds per minute |
| RT | Room temperature |
| RT-PCR | Reverse transcription PCR |
| RTK | Receptor tyrosine kinase |
| SDS-PAGE | Sodium dodecyl sulfate-polyacrylamide gel electrophoresis |
| TAM | Tumor-associated macrophages |
| TBE | Tris, Boric acid and EDTA |
| TEMED | Tetramethylethylenediamine |
| TPA | 12-O-tetradecanoyl-phorbol-13-acetate |
| UPL | Universal Probe Library |
| UV | Ultraviolet |
| VEM (PLX4032) | Vemurafenib (B-Raf inhibitor) |

Additionally, the well-established SI units as well as chemical symbols were used.

Table 1 | **Human gene and protein abbreviations according to HUGO Gene Nomenclature.**

| Gene symbol | Protein symbol | Protein name |
|---|---|---|
| alphaSMA | alpha-SMA | Alpha smooth muscle actin |
| APC | APC | Adenomatous polyposis coli protein |
| APCDD1 | Protein APCDD1 | Adenomatosis polyposis coli down-regulated 1 protein |
| ARAF | A-Raf | Serine/threonine-protein kinase A-Raf |
| AXIN2 | Axin-2 | Axis inhibition protein 2 |
| BCL9 | Bcl-9 | B-cell CLL/lymphoma 9 protein |
| BRAF | B-Raf | Serine/threonine-protein kinase B-Raf |
| CCL2 | CCL-2/ MCP-1 | C-C motif chemokine 2 |
| CDKN1A | p21 | Cyclin-dependent kinase inhibitor 1 |
| CDKN2A | p16-INK4a | Cyclin-dependent kinase inhibitor 2A |
| CREBP | CBP | CREB-binding protein |
| CSF2 | GM-CSF | Granulocyte-macrophage colony-stimulating factor |
| CSNK1A1 | CKI-alpha | Casein kinase I isoform alpha |
| CTNNB1 | Beta-catenin | Catenin beta-1 |
| CXCL10 | CXCL-10 | C-X-C motif chemokine 10 |
| CXCL12 | CXCL-12 | C-X-C motif chemokine 12 |
| CXCR4 | CXCR-4 | C-X-C chemokine receptor type 4 |
| DVL | DSH homolog | Dishevelled |
| EGF | EGF | Epidermal growth factor |
| EGFR | EGFR | Epidermal growth factor receptor |
| FBXW1 | beta-TrCP | Beta-transducin repeat-containing protein |
| FGF7/ KGF | FGF-7 | Fibroblast growth factor 7 |
| FGF10 | FGF-10 | Fibroblast growth factor 10 |
| FLG | Filaggrin | Filaggrin |

| | | |
|---|---|---|
| FZD | Fz | Frizzled |
| GAPDH | GAPDH | Glyceraldehyde-3-phosphate dehydrogenase |
| GSK3B | GSK-3 beta | Glycogen synthase kinase-3 beta |
| HGF | HGF | Hepatocyte growth factor |
| HRAS | H-Ras | GTPase HRas |
| IL1A | IL-1 alpha | Interleukin-1 alpha |
| IL1B | IL-1 beta | Interleukin-1 beta |
| IL6 | IL-6 | Interleukin-6 |
| IL8 | IL-8/ CXCL-8 | Interleukin-8 |
| IVL | Involucrin | Involucrin |
| KIT | c-Kit | Mast/stem cell growth factor receptor Kit |
| KRAS | K-Ras | GTPase KRas |
| KRT1 | Keratin-1 | Keratin, type II cytoskeletal 1 |
| KRT5 | Keratin-5 | Keratin, type II cytoskeletal 5 |
| KRT10 | Keratin-10 | Keratin, type I cytoskeletal 10 |
| KRT14 | Keratin-14 | Keratin, type I cytoskeletal 14 |
| LEF | LEF | Lymphoid enhancer-binding factor |
| LRP5/ 6 | LRP-5/ -6 | Low-density lipoprotein receptor-related protein 5/ 6 |
| MAP2K1 | MEK 1 | Mitogen-activated protein kinase/ ERK kinase 1 |
| MAP2K2 | MEK 2 | Mitogen-activated protein kinase/ ERK kinase 2 |
| MAPK1 | ERK 2 | Extracellular signal-regulated kinase 2 |
| MAPK3 | ERK 1 | Extracellular signal-regulated kinase 1 |
| MMP1 | MMP-1 | Matrix metalloproteinase-1 |
| MMP3 | MMP-3 | Matrix metalloproteinase-3 |
| MMP9 | MMP-9 | Matrix metalloproteinase-9 |
| MMP14 | MMP-14 | Matrix metalloproteinase-14 |
| NRAS | N-Ras | Neuroblastoma RAS viral oncogene |
| PIK3C | PI3K | Phosphatidylinositol 4,5-bisphosphate 3-kinase |
| PTEN | PTEN | Phosphatidylinositol 3,4,5-trisphosphate 3-phosphatase and dual-specificity protein phosphatase |
| PYGO | Pygopus | Pygopus homolog |
| RAF1 | Raf-1/ C-Raf | Serine/threonine-protein kinase Raf-1/ C-Raf |
| SNAI2 | Snail homolog 2 | Zinc finger protein SNAI2 |
| SOS | SOS | Son of sevenless homolog |
| TCF | TCF | T-cell factor |
| TGFA | TGF-alpha | Transforming growth factor alpha |
| TGFB1 | TGF-beta-1 | Transforming growth factor beta-1 |
| TGFB3 | TGF-beta-3 | Transforming growth factor beta-3 |
| TNFAIP6 | TNF alpha-induced protein 6 | Tumor necrosis factor alpha-induced protein 6 |
| TP53 | p53 | Cellular tumor antigen p53 |
| VEGF | VEGF | Vascular endothelial growth factor |
| WNT2 | Wnt-2 | Protein Wnt-2 |
| WNT3 | Wnt-3 | Protein Wnt-3 |

# 1. Zusammenfassung

Weltweit steigt die Prävalenz kutaner Plattenepithelkarzinome (cSCCs), während die an der Tumorentstehung beteiligten Mechanismen noch nicht vollständig verstanden sind. Das Ziel dieser Studie war es, den Einfluss der Wnt/Beta-catenin und Ras-Raf-MEK-ERK MAPK-Signalwege an cSCC Entstehung und Wachstum mit Hilfe von 2D kultivierten Keratinozyten, 3D organotypischen Kulturen der Haut (OTCs) sowie primären humanen cSCC-Biopsien zu untersuchen.

Eine Deregulierung des Wnt Signalwegs, welche durch eine nukleäre Translokation von Beta-catenin detektiert werden kann, wurde bereits für cSCC Tumorzellen beschrieben. Wir konnten nicht nur eine abnormale Wnt/Beta-catenin-Aktivierung im Tumor, sondern auch oder ausschließlich in Fibroblasten des Stromas nachweisen, was eine zusätzliche Rolle eines deregulierten Wnt-Signalwegs impliziert. In Fibroblasten identifizierte eine Genexpressionsanalyse Interleukin-8 (IL-8), C-C motif chemokine 2 (CCL-2) und Matrix metalloproteinase-1 (MMP-1) als Wnt/Beta-catenin induzierte Gene. Darüber hinaus wurden IL-8 und CCL-2 durch Wnt-3a-stimulierte Fibroblasten in OTCs sezerniert und konnten ebenso in humanen cSCCs nachgewiesen werden. Funktionell führte IL-8 und CCL-2 Stimulation von nicht-tumorigenen HaCaT-Zellen zu Hyperproliferation und ersten Invasionsmerkmalen. Die zusätzliche Behandlung von OTCs mit neutralisierenden Antikörpern gegen IL-8 und CCL-2 verhinderte diese Wnt-abhängigen Effekte. MMP-1 wurde ebenfalls in Wnt-3a-stimulierten OTCs sowie in humanen cSCCs exprimiert und aktiviert. Ein Basalmembran-Abbau begünstigte invasives Wachstum von gutartig-tumorigenen H-Ras$^{G12V}$ transfizierten HaCaT-RAS A-5-Zellen, was zusätzlich die Bedeutung einer Wnt-abhängige Interaktion zwischen Fibroblasten und Keratinozyten in der Karzinogenese aufzeigte.

Der Ras-Raf-MEK-ERK MAPK Signalweg ist in den meisten Melanomen aufgrund einer B-Raf$^{V600E}$-Mutation konstitutiv aktiv und führt zu erhöhtem Wachstum und Überleben der Tumorzellen. Klinische Studien von Melanom-Patienten, die mit B-Raf$^{V600E}$-Inhibitoren, wie Vemurafenib, behandelt wurden, zeigen eine deutliche Wachstumsreduktion dieser Tumore. Andererseits führte diese Therapie zu einer stark beschleunigten Entwicklung von cSCCs und legte daher eine direkte Beteiligung von Vemurafenib in der Progression bestehender Läsionen nahe. Vemurafenib-Stimulation von B-Raf$^{V600E}$ A375 Melanomzellen bestätigte einen Block des MEK-ERK-Signalwegs, führte allerdings in Fibroblasten und verschiedenen Keratinozyten zu einer MEK-ERK Hyperaktivierung. Trotz der stark erhöhten MAPK-Aktivität, waren weder Proliferation noch das Überleben der Keratinozyten verändert. Bei kontinuierlicher Vemurafenib-Behandlung von HaCaT-Zellen kam es zu einem selektiven Wachstumsvorteil von Sub-Populationen. Um die Rolle einer abnormalen B-Raf-Aktivierung im Gewebe zu untersuchen, wurden OTCs kontinuierlich mit Vemurafenib behandelt. Zum einen erhöhte Vemurafenib direkt die Differenzierung von normalen und transformierten Keratinozyten, was auch als hyperkeratotische Haut in vielen Melanom-Patienten beobachtet wurde. Zum anderen verursachte Vemurafenib in HaCaT-RAS A-5-Zellen eine hohe MMP-1 und MMP-3-Expression, die mit Collagen-Umbau und Invasion verbunden war. Da sowohl Differenzierung, als auch Invasion durch eine zusätzliche Behandlung mit dem MEK-Inhibitor Cobimetinib verhindert wurden und dies auch bei Melanom-Patienten zu einer verminderten cSCC-Anzahl führte, zeigte, dass die Phänotypen *in vitro* sowie die sich rasch entwickelnden und gut differenzierten cSCCs *in vivo* eine Folge der Vemurafenib-induzierten ERK-Aktivierung darstellen.

Diese Arbeit beschreibt Wnt/Beta-catenin Deregulierung im Stroma sowie eine abnomale Raf-MEK-ERK MAPK Aktivität in Keratinozyten als unabhängige Aspekte die zur cSCC-Progression beitragen.

# 2. Summary

The prevalence of cutaneous squamous cell carcinoma (cSCC) is constantly increasing worldwide, however, the mechanisms driving tumorigenesis are not yet understood. The aim of this study was to understand the contribution of the Wnt/Beta-catenin and the Ras-Raf-MEK-ERK mitogen-activated protein kinase (MAPK) signaling pathways in cSCC development and progression using 2D keratinocyte monolayer cultures, 3D organotypic cultures of the skin (OTCs) as well as primary human cSCC samples.

Deregulated canonical Wnt signaling in tumor cells, as detected by nuclear translocation of Beta-catenin, is well described for a number of human cSCCs. Here, we found that aberrant Wnt/Beta-catenin activation is not restricted to tumor cells, but was additionally or exclusively detected in stromal fibroblasts. This suggested a second role of aberrant Wnt signaling in the stroma of developing cSCCs. Gene expression analysis of fibroblasts identified Interleukin-8 (IL-8), C-C motif chemokine 2 (CCL-2) and Matrix metalloproteinase-1 (MMP-1) as targets of Wnt/Beta-catenin. In agreement, IL-8 and CCL-2 were secreted by Wnt-3a-stimulated fibroblasts in OTCs and could also be detected in human cSCCs *in situ*. As consequence, IL-8 and CCL-2 caused hyper-proliferation and early invasion of non-tumorigenic HaCaT keratinocytes. Importantly, neutralizing antibodies against IL-8 and CCL-2 abolished these Wnt-dependent effects in OTCs. MMP-1 was also highly expressed in Wnt-3a-stimulated OTCs as well as in human cSCCs and was shown to be active. Furthermore, degradation of the basement membrane correlated with invasive growth of benign-tumorigenic H-Ras$^{G12V}$-transfected HaCaT-RAS A-5 cells, demonstrating the importance of the Wnt-dependent fibroblast-keratinocyte cross-talk for skin cancer progression.

Ras-Raf-MEK-ERK MAPK signaling is constitutively active in most melanomas due to a B-Raf$^{V600E}$-mutation leading to increased proliferation and survival. Clinical trials targeting oncogenic B-Raf in melanoma by mutation-specific inhibitors like Vemurafenib displayed high response rates, but caused at the same time development of cSCCs. This suggested a direct involvement of Vemurafenib in the progression of pre-existing lesions. Vemurafenib stimulation of B-Raf$^{V600E}$-mutant A375 melanoma cells confirmed a block in MEK-ERK signaling, while all B-Raf$^{wild\text{-}type}$ cells, such as dermal fibroblasts and different keratinocytes, revealed MEK-ERK hyper-activation. Despite MAPK-activation, neither proliferation nor survival was altered in the keratinocytes. Analyses of continuously Vemurafenib treated HaCaT cells did not show genomic instability, but rather led to a selective growth advantage of genetic subpopulations. To study the role of aberrant B-Raf signaling in the tissue context, OTCs were treated with Vemurafenib. As result, Vemurafenib directly increased differentiation of the normal and transformed keratinocytes, resembling the hyperkeratotic skin phenotype of many melanoma patients. Remarkably, Vemurafenib stimulation of HaCaT-RAS A-5 cells caused high MMP-1 and MMP-3 expression, which correlated with Collagen remodeling and invasion into the stroma. Since both, differentiation and invasion were abolished by co-treatment with the MEK-inhibitor Cobimetinib and as patients receiving the same therapy showed highly decreased cSCC numbers, this strongly suggests that the phenotypes in *in vitro* as well as the rapidly developing well-differentiated cSCCs *in vivo* are direct results of Vemurafenib-induced ERK-activation.

Taken together, this work unraveled two novel aspects, namely Wnt/Beta-catenin deregulation in the tumor-stroma and aberrant Raf-MEK-ERK MAPK signaling in keratinocytes as oncogenic events driving cSCC progression.

# 3. Introduction

## 3.1 Human skin

The Human skin covers a body surface of about 1.5-1.8 $m^2$ and provides approximately 16% of the body mass. It fulfills a dual role since the skin protects the body from physical, chemical and biological hazards and in addition, it forms a barrier to retain fluids, thus preventing dehydration of the body. Furthermore, the skin also regulates temperature, electrolyte as well as water balance and has crucial functions in sensation and immune defense (Elias, 2005; Haake et al., 2001).

### 3.1.1 Compartments of the human skin

The human skin consists of three compartments: The subcutaneous fat represents the innermost layer, followed by the mesenchymally derived dermis and the epidermis, forming the protective body surface (Haake et al., 2001). The dermis is a connective tissue, mainly composed of extracellular matrix (ECM). This matrix mostly consists of Collagen type I + III fibrils and elastic fibers that are embedded in a gel of different glycosaminoglycans and proteoglycans. These proteins and polysaccharides are mainly secreted by fibroblasts, the major cell type of the dermis and provide the skin with tensile strength and elasticity. Besides fibroblasts, macrophages, mast cells, blood vessels and nerve endings are additionally found in the dermis (Fuchs, 2007; Haake et al., 2001). The epidermis on the other hand is a stratified squamous epithelium that forms the outer covering of the skin. The predominant cell type of this compartment are the keratinocytes but also other specialized cells like melanocytes, Langerhans cells and Merkel cells are present in a smaller number (Watt, 1989). Dermis and epidermis are divided by the basement membrane (BM), an amorphous and electron-dense structure (Kalluri, 2003), which serves as structural support, but has also regulatory functions (Aumailley and Timpl, 1986; Paulsson, 1992). The main component of the BM is Collagen type IV but also other ECM proteins like laminins and heparin-sulphate proteoglycans (HSPGs) are present (Kalluri, 2003).

### 3.1.2 Epithelial proliferation and differentiation

Keratinocytes give rise to four distinct epidermal layers representing the different stages of cell differentiation: *Stratum basale*, *Stratum spinosum*, *Stratum granulosum* and *Stratum corneum* (Fuchs, 1993; Green, 1977) (Fig. 1). The *stratum basale* harbors a single layer of highly proliferative keratinocytes with a cuboidal morphology. These cells are connected to the BM by hemidesmosomes, consisting of Integrin alpha-6 beta-4 heterodimers. In addition, keratinocytes interact laterally and suprabasally through desmosomes and other cell-cell junctions (Jones and Green, 1991). Both, hemidesmosomes and desmosomes are associated with the intracellular cytoskeleton, particularly with keratin intermediate filaments. Basal epidermal cells characteristically form keratin networks composed of Keratin-5 (K5) and Keratin-14 (K14). The suprabasal *stratum spinosum* is composed of several layers of keratinocytes that change their morphology to flattened polygonal cells. Once basal cells differentiate, the expression of K5/ K14 is downregulated and Keratin-1 (K1) and Keratin-10 (K10) are predominantly expressed within the suprabasal layers (Fuchs, 1993). Moving outwards through the 1-5 cell layers that compose

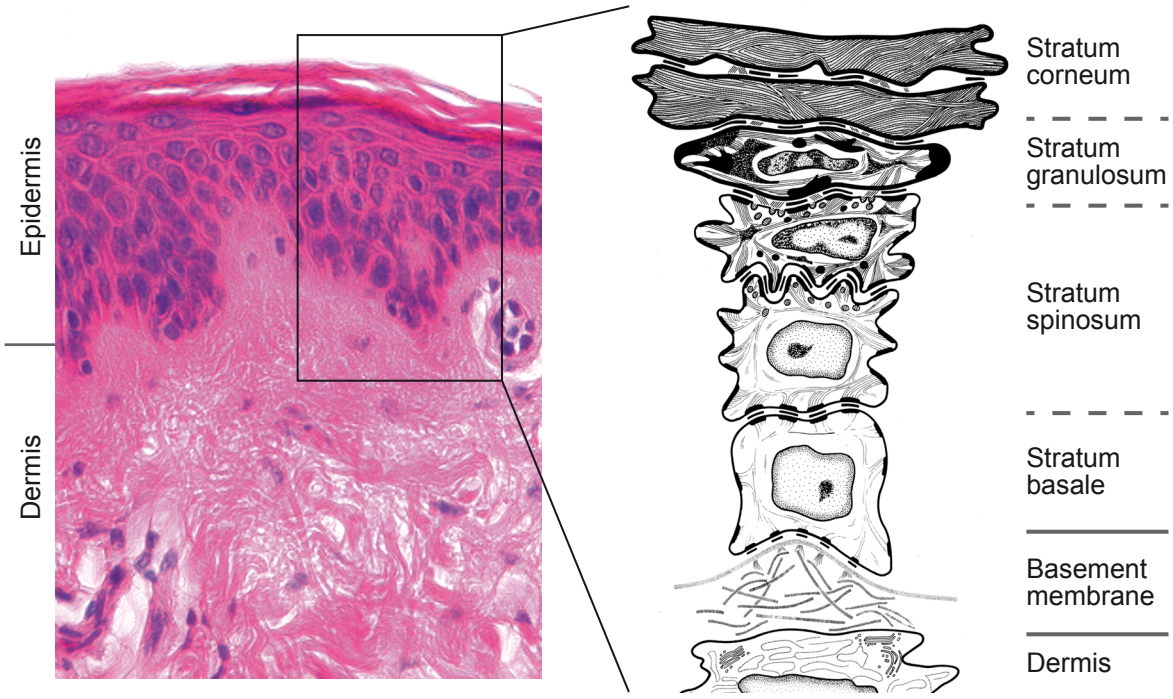


Figure 1 | **Organization of the human skin.**
According to organization and function, the human skin is divided into compartments. The basement membrane seperates dermis from epidermis. The epidermis represents a multi-layered squamous epithelium, which can be further subdivided into *Stratum basale*, *Stratum spinosum*, *Stratum granulosum* and *Stratum corneum* (adopted from Fusenig *et al.* 1986 and kindly provided by Karsten Böhnke).

the *stratum granulosum*, keratinocytes dehydrate and thereby become further flattened. Moreover, cells are characterized by keratohyalin granules, which are mainly composed of pro-Filaggrin and synthesize the precursors of the cornified envelope such as Involucrin and Loricrin (Haake et al., 2001). As closer keratinocytes approach the outside, they prepare to degrade their cell organelles. By reaching the outermost layer, the *stratum corneum*, cells terminally differentiate into dead horn squamous (corneocytes). In particular, these cells contain a Filaggrin-stabilized keratin filament network, which is covalently linked to the proteinous cornified envelope that replaces the plasma membrane. Embedded in a lipid matrix and interconnected by modified desmosomes, the corneocytes form the permeability barrier of the skin (Fuchs, 1990; Nemes and Steinert, 1999).

The epidermis is a continuously renewing tissue. However, cell proliferation is limited to cells within the *stratum basale* that gives rise to the entire epidermis (Watt and Hogan, 2000). In this layer most cells are rapidly dividing progenies of stem cells, referred to as transiently amplifying cells. These keratinocytes undergo a limited number of cell divisions (Fuchs and Raghavan, 2002; Watt et al., 2006), before detaching from the basal layer, stop dividing and induce a program of terminal differentiation. Ultimately, they form the barrier of the skin and thereby replace cells which are constantly shed off (Fuchs, 1990).

## 3.2 Skin cancer

Skin cancer is the most common cancer worldwide and the incidence steadily increases, while the age of the patients decreases (Molho-Pessach and Lotem, 2007). It includes a number of tumor entities that arise from transformation of different cells: The malignant melanoma (MM) represents the most

aggressive skin tumor, which is derived from the pigment-producing melanocytes within the epidermis, dermis or mucosa. Basal cell carcinoma (BCC) as well as squamous cell carcinoma (SCC) derive from keratinocytes and are the most frequent skin carcinomas. Merkel cell carcinoma (MCC) originates from neuroendocrine cells of epidermis, hair follicle and mucosa. MCCs are rare but highly aggressive (Boukamp, 2005; Manola et al., 2000).

### 3.2.1 Malignant melanoma

Melanomas are the most aggressive skin tumor entity with high invasion, metastasis and mortality rates. It is believed that melanomas arise from intermitted UV exposure and in particular from severe sunburns during childhood. The risk for developing melanoma was also associated with specific mutations in the melanocortin-1 receptor, which is important in determining the type of melanin that is produced by melanocytes. Cells harboring these mutations may not be able to synthesize the photoreactive eumelanin, but instead express the photosensitizing pheomelanin, which causes mutations and drives the transformation of melanocytes (Boukamp, 2005). The most prevalent genetic change in MMs represents the deregulation of the Ras-Raf-MEK-ERK mitogen-activated protein kinase (MAPK) pathway. In normal cells, this highly conserved signaling pathway regulates cell proliferation, differentiation, senescence and apoptosis (Heidorn et al., 2010), depending on environmental cues (Marshall, 1995). In malignant melanoma, mutations in this pathway lead to a constitutive activation accompanied by cell cycle progression (Heidorn et al., 2010; Libra et al., 2005). The majority of mutations are found at amino acid position 600 of the B-Raf kinase. In particular, B-Raf$^{V600E}$, B-Raf$^{V600K}$, B-Raf$^{V600R}$, B-Raf$^{V600E2}$, B-Raf$^{V600D}$-alterations were frequently described (Bello et al., 2013).

### 3.2.2 BCC and SCC in normal and immunosuppressed persons

BCCs represent the most frequent skin tumors and generally develop at sites that are strongly exposed to sunlight, therefore, severe sunburns during childhood and adolescence increase the risk of BCC development. BCCs grow locally invasive and cause massive tissue destruction but metastasize rarely (< 0.1%). The second most frequent skin tumors are SCCs (Boukamp, 2005). Like in BCCs, the development strongly correlates to UV-irradiation (Cadet et al., 2005; de Gruijl, 1999). Since the SCC-incidence increases with age and the tumor surrounding skin provides evidence for chronic sun exposure, cumulative UV-exposure seems to be a crucial factor in tumor development and progression. Besides sun exposure, chronic exposure to arsenic, heat, X, gamma rays or HPV infections are discussed to cause SCC. The metastasis potential of cutaneous SCCs is generally low (1%) (Boukamp, 2005), but they are capable of local expansion, lymph node metastasis and distant metastasis (Euvrard et al., 2003). This implies that SCC is mostly associated with a low mortality rate (de Gruijl, 1999). However, in immunosuppressed persons, e.g. after organ transplantation, SCC is the most common cancer type, occurring 65-250 times more frequently compared to the general population. The incidence even increases with the duration of immunosuppressive therapy. Moreover, SCCs in immunosuppressed patients grow rapidly, are more aggressive, recur more frequently and show an increased metastasis potential of 5-8% (Euvrard et al., 2003).

### 3.2.3 Multistep process of cSCC development

As proposed by Hanahan and Weinberg, tumorigenesis in human reflects a multistep process driven by several genetic alterations transforming normal cells into tumor cells (Hanahan and Weinberg, 2000). The development of squamous cell carcinomas is also believed to be a multistep process, arising from actinic keratoses (AK), Bowen's disease also known as carcinoma *in situ* (CIS) or keratoacanthoma (KA) (Boukamp, 2005; Burnworth et al., 2007). Evidence for the progression of AK to cutaneous SCC (cSCC) is provided by genetic studies reporting that AKs have a similar karyotypic profile as cSCCs, but lack some degree of complexity, which is consistent with an earlier stage in tumor development (Ashton et al., 2003). KAs are also genetically incomplete, likely still controlled by the environment and may further develop into invasive cSCCs (Burnworth et al., 2007) (Fig. 2).

In agreement with the dependence of cSCC-development on cumulative UV exposure, these tumors demonstrate the highest mutation rate of all cancers (Durinck et al., 2011) and consequently, display a complex genetic background with large cytogenetic heterogeneity. Common chromosomal losses for cSCCs are 3p, 4q, 5q, 8p, 9p, 13q, 15, 17p, while common gains are 3q, 4p, 7q, 8q, 9q, 11q, 14q, 17q, Xq (Boukamp, 2005). The genetic aberrations in cSCCs seem to be a prerequisite for altered cellular functions contributing to carcinogenesis. One example for a characteristic and well-investigated aberration in cSCCs are mutations in the gene coding for p53 (TP53). TP53 shows UV-specific mutations in about 50% of all cSCCs, which impair its function to mediate cell cycle arrest in G1-phase, repair damage or finally induce apoptosis. p53 mutations are supposed to represent the first step in the course of skin carcinogenesis by destabilizing the genome, as lack of functional p53 allows the transmission of non-lethal chromosomal damage to daughter cells (Boukamp, 2005; Brash, 2006; Brash et al., 1996). Furthermore, NOTCH1 and NOTCH2 were also identified to be mutated at an

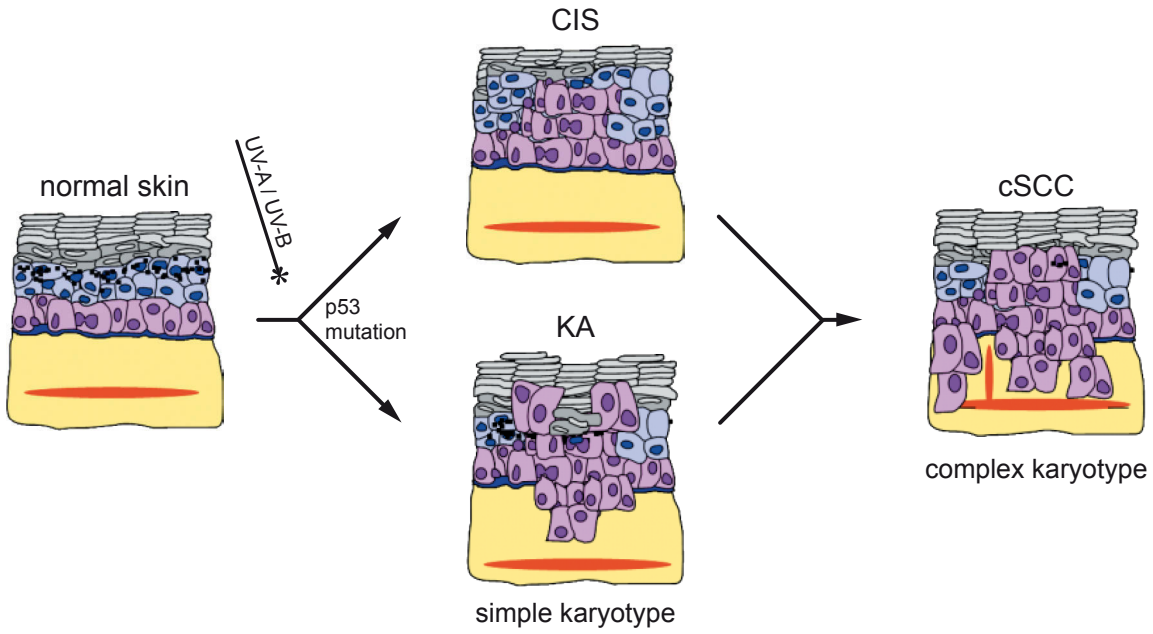


Figure 2 | **Progression model of squamous cell carcinoma.**
Cutaneous squamous cell carcinoma (cSCC) derives from transformed keratinocytes, which is believed to be a multistep process. Cumulative UV irradiation causes specific mutations that inactivate p53 and cause additional genetic alterations further driving tumorigenic transformation. In course of skin carcinogenesis, carcinoma *in situ* (CIS) is a pre-invasive stage of SCCs. Keratoacanthoma (KA) represents a benign cutaneous squamous neoplasia. Both are genetically incomplete cSCCs that are likely to develop into invasive cSCCs with highly complex karyotypes (modified from Boukamp 2005/ Burnworth *et al.*, 2007).

early stage of cSCC development and are also detected in a high percentage tumors. In normal cells, Notch receptors transduce signals in response to ligands on neighboring cells regulating development through cell fate determination, growth and survival (Durinck et al., 2011; South et al., 2014; Wang et al., 2011). Another example for a frequent aberration in cSCCs is the amplification of chromosome 11q13, which was associated with overexpression of Cyclin D1 in KAs and cSCCs. Cyclin D1 together with the Cyclin-dependent kinases 4 and 6 are essential in cell cycle progression during G1/S-phase. Accordingly, enhanced expression of this gene was reported to increase proliferation but also to disturb tissue homeostasis *in vitro* (Burnworth et al., 2007; Burnworth et al., 2006; Utikal et al., 2005). In contrast, mutations in the GTPase Harvey RAS viral oncogene (H-Ras) that are likely caused by UV-radiation represent less frequent alterations. As mutations of this gene are found in only 5-15% of cSCCs, its contribution to skin cancer development is controversially discussed. Besides H-Ras, the GTPase neuroblastoma RAS viral oncogene (N-Ras) and Kirsten RAS viral oncogene (K-Ras) are also members of the Ras-family. These oncogenes encode small GTP-binding proteins, which transduce mitogenic signals, thereby playing a central role in regulating cell proliferation and apoptosis (Barbacid, 1987; Boukamp, 2005). In cSCCs, mutations in H-Ras seem to be an early event, since these were already described in precancerous lesions such as KAs. Thus, H-Ras likely exerts its oncogenic potential only in cooperation with other genetic changes that manifested in a step-wise fashion (Boukamp et al., 1995; Boukamp et al., 1990).

### 3.2.4 Role of the tumor microenvironment in cSCC formation

Besides the multistep tumor progression model that is driven by the accumulation of genetic alterations (Hanahan and Weinberg, 2000), it was hypothesized that the tumor surrounding tissue, the tumor stroma, plays an additional role in the carcinogenesis of keratinocytes. The normal stroma provides the connective tissue framework and consists of a specific ECM as well as cellular components like fibroblasts, leukocytes and blood-vessel cells (Mueller and Fusenig, 2002, 2004) (Fig. 3a). During tumor progression, tumor and stromal cells are in an intensive cross-talk with each other through cell-cell interaction or the secretion of soluble factors (Mueller and Fusenig, 2004). Such factors involve chemokines, a subfamily of cytokines, which are structurally related small signaling molecules (Rollins, 1997). Chemokines are secreted in response to signals like pro-inflammatory cytokines and mediate the chemoattraction of especially inflammatory cells in a paracrine manner. Moreover, chemokines play a role in other biological functions including cell proliferation, migration, angiogenesis and protease induction, which demonstrates their pro-tumorigenic potential (Bergers and Benjamin, 2003; Coussens and Werb, 2002; Deshmane et al., 2009; Gillitzer and Goebeler, 2001). On the other hand, cancer cells themselves can alter their surrounding stroma to a permissive and supportive environment by secreting stroma-modulating factors like interleukins (ILs), granulocyte-macrophage colony-stimulating factors (CSFs), Transforming growth factor-beta (TGF-beta) or Vascular endothelial growth factor (VEGF) (Mueller and Fusenig, 2004).

Tumor and stromal cells are also capable of secreting proteases like matrix metalloproteases (MMPs), which are capable of remodeling and degrading ECM and BM. The MMP family consists of over 24 zinc-dependent enzymes that are usually induced in wound-edge basal keratinocytes at positions of disrupted BM. This MMP expression allows keratinocytes to migrate across the dermal or provisional

matrix in order to repair damaged skin. However, MMPs also play a key role in virtually every step of tumorigenesis. They promote tumor cell invasion, stimulate blood vessel infiltration, metastasis, and release numerous growth factors by ECM degradation (Bergers et al., 2000; Brooks et al., 1996; Giannelli et al., 1997; Kalluri, 2003; Lynch and Matrisian, 2002; Mueller and Fusenig, 2004; Rohani et al., 2014). Therefore, it is not surprising that MMP expression is elevated in nearly all solid tumors, including breast, colon, pancreas and melanoma, which is often correlated with decreased survival (Egeblad and Werb, 2002).

The release of growth factors by tumor cells can activate stromal cells such as fibroblasts, smooth-muscle cells and adipocytes that in turn secrete paracrine factors involved in tumorigenesis (Kalluri, 2003; Lynch and Matrisian, 2002; Mueller and Fusenig, 2004). Moreover, these factors allow transdifferentiation of fibroblasts into myofibroblasts. These cells show a spindle-shaped morphology and share characteristics of fibroblasts and smooth-muscle cells. In association with cancer cells, myofibroblasts are also known as carcinoma-associated fibroblasts (CAFs). The presence of this cell type in the tumor stroma has been observed in many cancer types, such as breast, prostate and skin cancer. CAFs were often associated with tumor growth, onset of invasion and metastasis. The secretion of MMPs is frequently involved in later stages of tumor progression (Egeblad and Werb, 2002; Mishra et al., 2011; O-Charoenrat et al., 2001). Additionally, growth factors and cytokines such as Hepatocyte growth factor (HGF), VEGF or chemokine (C-C motif) ligand 2 (CCL2) further activate tumor as well as stroma and recruit inflammatory

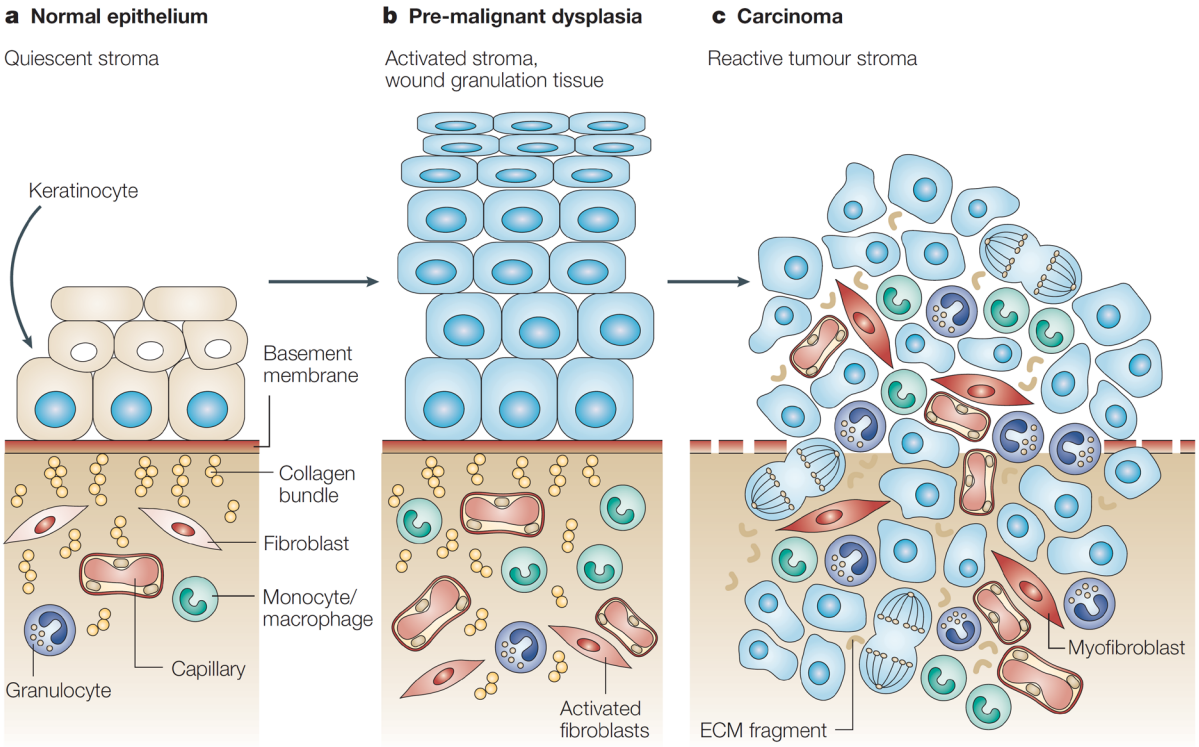


Figure 3 | **Tumor microenvironment and cSCC development.**

**a** | A normal epithelium is composed of keratinocytes in the epidermis that are separated by the basement membrane (BM) from the dermal or stromal compartment. The latter is composed of collagen, fibroblasts, blood vessels and a few leukocytes. **b** | During transition to pre-malignant dysplasia, differentiation of keratinocytes is disturbed, leading to a hyperplastic epithelium with an intact BM. Fibroblasts become activated and the number of macrophages increases. **c** | Further progression to a carcinoma is associated with an increase in inflammatory cells and angiogenesis resulting in a high number of leaky tumor vessels. Fibroblasts differentiate into myofibroblasts (known as carcinoma-associated fibroblasts, CAFs) resulting in the expression of growth factors, matrix components and proteases like MMPs that degrade ECM components such as Collagen. Following BM degradation, tumor cells invade the underlying dermis (adopted from Mueller and Fusenig 2004).

cells (Fig. 3b-c). Thus, genetic alterations in combination with a tumor-supportive microenvironment seem to mediate initiation, progression and invasive growth of SCCs (Kalluri and Zeisberg, 2006; Mueller and Fusenig, 2004; Orimo et al., 2001).

## 3.3 Signaling pathways in cSCC progression

As cSCC demonstrates a high genetic complexity arising from a mutation rate of approximately 1 mutation per 30 kbp coding sequence (Durinck et al., 2011), definite driver events or signaling pathways involved in carcinogenesis remain largely elusive. In many diseases, signaling cascades are inappropriately regulated and contribute to carcinogenesis. Accordingly, deregulated Wnt signaling has been observed in numerous cancer types (Klaus and Birchmeier, 2008), such as colorectal cancer, hepatocellular carcinoma, leukemia or hair follicle tumors (Clevers, 2006; Vermeulen et al., 2010). The fact that cSCCs show frequent amplifications of the chromosomes 7q, 8q, 11q, or 17q (Burnworth et al., 2006; Popp et al., 2002; Popp et al., 2000) that carry genes of the Wnt signaling pathway like Wnt ligands or Frizzled receptors, points to a role of deregulated Wnt signaling also in cSCC development and/ or progression. Besides canonical Wnt signaling, additional pathways are likely to be involved in cSCC tumorigenesis. Deregulation of MAPKs has been reported for a wide range of diseases including different types of human cancer (Mebratu and Tesfaigzi, 2009). In melanoma, especially the Ras-Raf-MEK-ERK MAPK pathway is frequently mutated and essential for tumorigenesis (Heidorn et al., 2010). As a novel melanoma therapy specific B-Raf inhibitors are used. Unexpectedly, this led to the development of cSCCs as adverse effect, suggesting an involvement of the Ras-Raf-MEK-ERK MAPK pathway also in SCCs progression (Bollag et al., 2010).

### 3.3.1 The canonical Wnt signaling pathway

The highly conserved Wnt/Beta-catenin signaling pathway plays a crucial role in virtually every aspect of embryonic development of all animal species and controls homeostatic self-renewal in a wide range of adult tissues. In particular, this pathway regulates proliferation, migration, cell fate determination and organogenesis (Clevers, 2006; Klaus and Birchmeier, 2008; Logan and Nusse, 2004; Reya and Clevers, 2005; Watt and Collins, 2008). In skin, the Wnt pathway is involved in development and maintenance of hair follicles (Gat et al., 1998) as well as in epidermal bulge stem cell renewal and linage selection (Watt et al., 2006). Moreover, the canonical and non-canonical Wnt pathways are critical in cutaneous wound repair (Fathke et al., 2006). The central player of the signal transduction is the protein Beta-catenin, which is an additional component of adherens junctions in epithelia. There, it is an essential and highly stable binding partner for the cytoplasmic tail of E-cadherin (Peifer et al., 1992).

In absence of Wnt ligands, cytoplasmic Beta-catenin is recruited to a destruction complex. This complex consists of Adenomatous polyposis coli (APC), Axins as well as Casein kinase 1 alpha (CK1-alpha) and Glycogen synthase kinase-3 beta (GSK-3 beta). Subsequently, Beta-catenin is N-terminally phosphorylated by both kinases, ubiquitinated by Beta-transducin repeat-containing protein (Beta-TrCP) and finally proteasomally degraded. As consequence, cytoplasmic Beta-catenin levels are low and Wnt pathway target genes are not expressed (Fig. 4a). Canonical Wnt signaling is initiated by Wnt

ligands released from signaling cells that lead to the formation of a trimeric complex with Frizzled (Fz) transmembrane receptors and Low-density lipoprotein receptor-related protein 5/ 6 (LRP-5/ -6) co-receptors in target cells. Thereafter, LRP-5/ 6 are phosphorylated by GSK-3 beta, CK1-alpha and possibly other yet not identified kinases. Dishevelled (DSH) is recruited to Fz at the plasma membrane and polymerizes with other DSH molecules. These events serve as mediators to tether Axin molecules to the plasma membrane, which finally inactivate the destruction complex. As consequence, cytoplasmic Beta-catenin is stabilized, translocates into the nucleus and forms a transcriptionally active complex with LEF/ TCF transcription factors by replacing the protein Groucho. This complex interacts with co-activators like B-cell CLL/ lymphoma 9 protein (Bcl-9), Pygopus or CREB-binding protein (CBP)

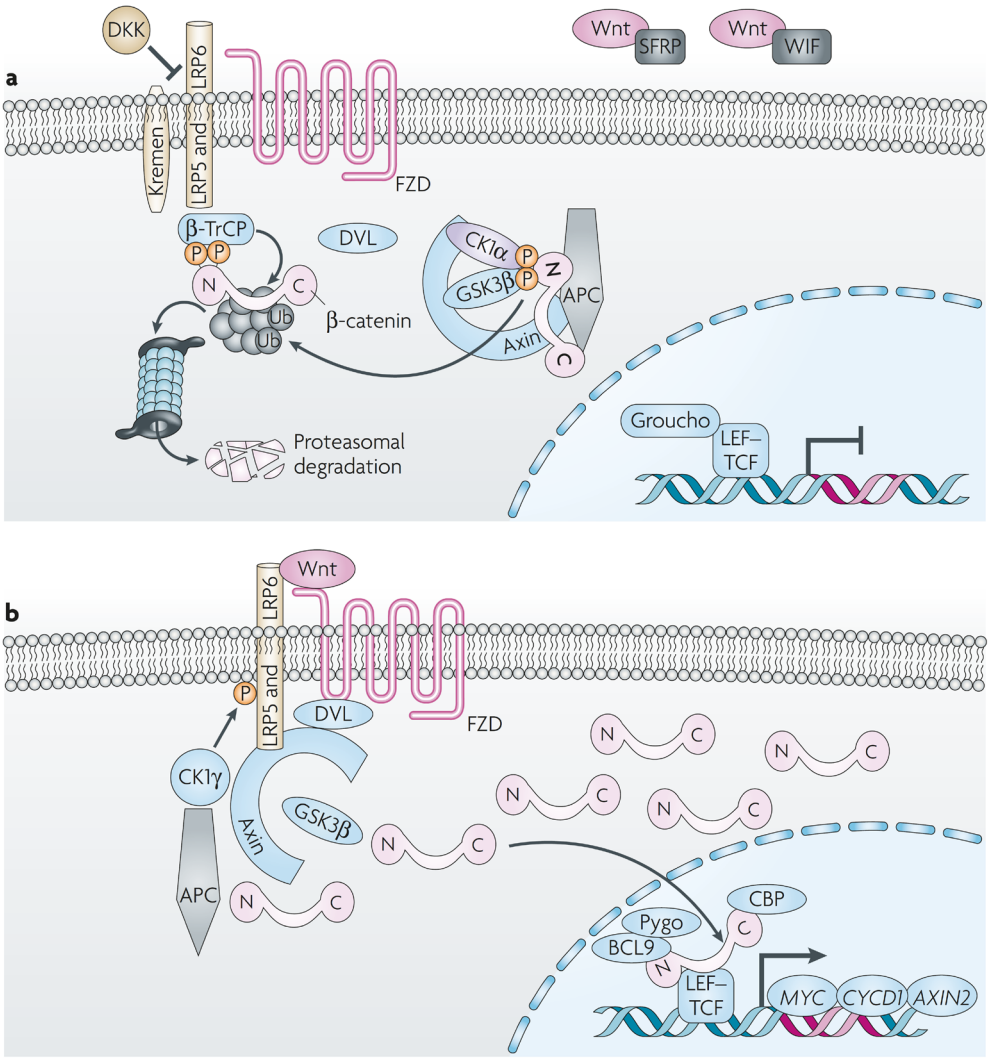


Figure 4 | **The canonical Wnt/Beta-catenin signaling pathway.**

**a** | In absence of Wnt ligands or in presence of inhibitors like Dickkopf (DKK), Beta-catenin is recruited into the destruction complex, consisting of Adenomatous polyposis coli protein (APC), Axins and two kinases: Following N-terminal phosphorylation by Casein kinase I isoform alpha (CKI-alpha) as well as by Glycogen synthase kinase-3 beta (GSK-3 beta) and subsequent ubiquitylation by Beta-transducin repeat-containing protein (beta-TrCP), Beta-catenin is proteasomally degraded. The co-repressor Groucho ensures transcriptional repression of Wnt target genes by binding to Lymphoid enhancer-binding factor (LEF)-T-cell factor (TCF) transcription factors. **b** | In the presence of Wnt ligands, Low-density lipoprotein receptor-related protein 5 (LRP-5) and LRP6 are phosphorylated by CKI-gamma and GSK-3 beta. Dishevelled (DSH/ DVL) proteins are recruited to the plasma membrane and interact with Frizzled (Fz/ FZD) receptors and further Dishevelled molecules. Interaction of Axin with phosphorylated LRP-5, LRP-6 and the Dishevelled polymer inactivates the destruction complex. This stabilizes Beta-catenin, which forms a transcriptionally active complex with LEF and TCF by displacing Grouchos in the nucleus. B-cell CLL/ lymphoma 9 protein (Bcl-9), Pygopus and CREB-binding protein (CBP) serve as co-activators, while MYC, CYCD1 (Cyclin D1), MMPs and AXIN2 are direct target genes (adopted from Klaus and Birchmeier 2008).

in order to mediate gene expression of Wnt target genes (Fig. 4b). A large number of Wnt/Beta-catenin target genes have been identified and include players of the pathway itself like AXIN2, providing positive- and negative feedback controls during signaling. Additional direct Wnt target genes include MYC, CYCD1 (Cyclin D1), different MMPs as well as angiogenic factors like VEGF, pointing to a direct role of this pathway in carcinogenesis. However, most of the target genes are not universal but rather tissue and cell type specific (Clevers, 2006; Klaus and Birchmeier, 2008).

### 3.3.2 Wnt/Beta-catenin signaling in cSCC development and progression

By analyzing 32 human cSCCs and in agreement with other laboratories (Brasanac et al., 2005; Doglioni et al., 2003; Liu et al., 2008; Lyakhovitsky et al., 2004; Malanchi et al., 2008; Papadavid et al., 2001; Papadavid et al., 2002), we could detect nuclear Beta-catenin, a hallmark for Wnt pathway activity, in cSCC tumor cells *in situ*. Interestingly and different from studies performed by others, we could detect nuclear Beta-catenin also in cells of the surrounding tumor stroma (Fig. 5b), while normal skin was negative (Fig. 5a, c, e). These cells were positive for the mesenchymal marker Vimentin and stained negative for the epidermal Keratin-14 (Fig. 5d) as well as for the leukocyte marker CD45 (Fig. 5f). This argued that the Beta-catenin-positive stromal cells are likely fibroblasts. Besides the direct effect of the Wnt signaling pathway on tumor cells, this observation suggested an additional indirect effect through fibroblasts. These stromal cells may be activated by Wnt as well and thus, contribute to cSCC progression in a paracrine manner (Wischermann, 2009).

This hypothesis was further substantiated by functional studies *in vitro*. We could show that fibroblasts are more sensitive to Wnt-3a stimulation compared to the spontaneously immortalized and non-tumorigenic HaCaT keratinocytes. Moreover, global gene expression analysis revealed that Wnt-3a stimulation of dermal fibroblasts results in the upregulation of cytokines including Interleukin-8 (IL-8/ CXCL-8) and C-C motif chemokine 2 (CCL-2/ MCP-1) as well as of ECM remodelers like MMP-1 (Fig. 5g). Thus, IL-8, CCL-2 and MMP-1 might be involved in development or progression of cSCCs (Sobel, Tham et al., 2015). While MMP-1 can directly influence invasion by degrading ECM and BM components (Lynch and Matrisian, 2002), the upregulation of the cytokines IL-8 and CCL-2 suggested a Wnt-induced cross-talk between stromal fibroblasts and HaCaT keratinocytes. IL-8, a member of the CXC chemokine subfamily, is known to be expressed by leukocytes, fibroblasts, endothelial and different tumor cells. Upon secretion, this chemokine plays an important role in inflammation, chemoattraction and angiogenesis but most importantly in tumor growth and metastasis (Li et al., 2005; Waugh and Wilson, 2008). It was also shown that IL-8 stimulates proliferation of cultured keratinocytes (Steude et al., 2002; Tuschil et al., 1992). CCL-2 belongs to the CC chemokine subfamily and is secreted by a variety of cells including epithelial, endothelial, smooth-muscle, meningeal, astrocyte, microglial cells, fibroblasts as well as tumor cells (Conti and Rollins, 2004; Deshmane et al., 2009). However, the major cell types secreting CCL-2 are monocytes and macrophages (Yoshimura et al., 1989). It regulates migration and infiltration of different leukocytes but was shown to also increase proliferation of endothelial cells. There is evidence that IL-8 and CCL-2 act in tumor-stroma communication in several malignancies (Mishra et al., 2011). Moreover, both factors belong to the IL-6-induced cytokine network promoting malignant tumor growth in the HaCaT skin carcinogenesis model (Lederle et al., 2011). In order to understand the contribution of Wnt/Beta-catenin in cSCC tumorigenesis, it was crucial to study the role

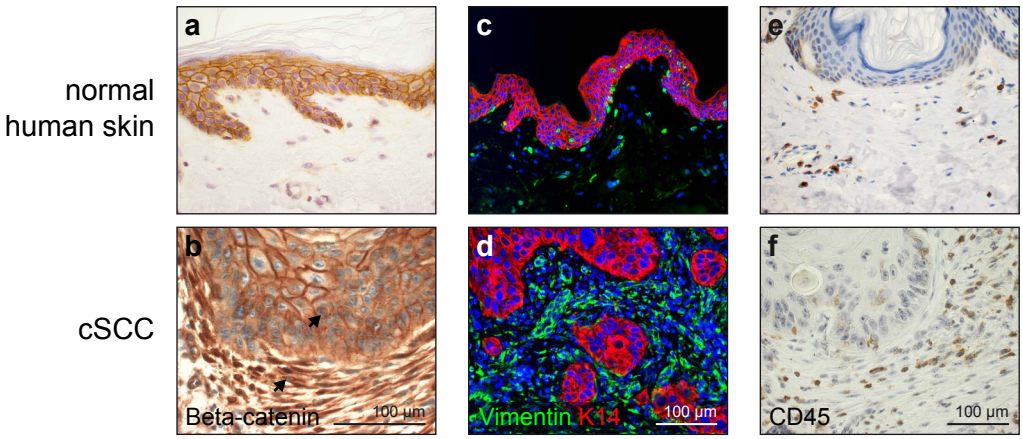


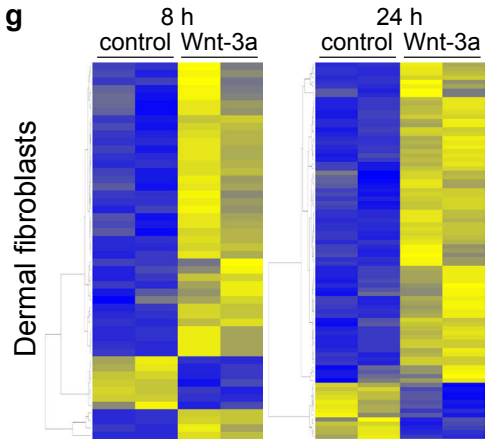


| Gene | Symbol | NCBI Ref. Seq. | Fold Change 8 h | Fold Change 24 h |
|---|---|---|---|---|
| ***Wnt pathway genes*** | | | | |
| axin2 | AXIN2 | NM_004655 | 4.2 | 1.7 |
| adenomatosis polyposis coli down-regulated 1 | APCDD1 | NM_153000 | 2.5 | 2.5 |
| ***Cytokines*** | | | | |
| interleukin 8 | IL8 | NM_000584 | 33.6 | 3.1 |
| chemokine (C-C motif) ligand 2 (CCL2) | CCL2 | NM_002982 | 11.6 | 4.2 |
| chemokine (C-X-C motif) ligand 6 | CXCL6 | NM_002993 | 6.9 | 2.7 |
| chemokine (C-X-C motif) ligand 10 | CXCL10 | NM_001565 | 4.8 | 3.2 |
| chemokine (C-C motif) ligand 8 | CCL8 | NM_005623 | 2.8 | 1.8 |
| interleukin 32 | IL32 | NM_0010126 | --- | 1.8 |
| ***Remodeling of ECM/ Cytoskeleton*** | | | | |
| tumor necrosis factor, alpha-induced protein 6 | TNFAIP6 | NM_007115 | 4.8 | 2.2 |
| podoplanin | PDPN | NM_0010066 | 1.9 | 2.0 |
| matrix metallopeptidase 1 | MMP1 | NM_002421 | --- | 2.5 |

Figure 5 | **Nuclear Beta-catenin is found in stromal fibroblasts of human cSCCs and direct Wnt-3a stimulation of NHDF induces cytokines and matrix modulation factors in fibroblasts.**

**a, b** | Beta-catenin IHC (brown) of normal human skin shows Beta-catenin staining at the plasma membrane of keratinocytes, but not in fibroblasts (a). In SCCs, Beta-catenin was additionally detected in nuclei of tumor cells (upper arrow) as well as of cells within the tumor-stroma (lower arrow, b). **c, d** | IIF for Vimentin (green) and Keratin-14 (K14, red) identified the majority of cells within the ECM of normal skin (c) and the tumor-stroma (d) as mesenchymal cells. **e, f** | CD45 IHC (brown) showed no accumulation of inflammatory cells within the ECM of normal skin (e) or the tumor-stroma (f). **g** | NHDF were stimulated with Wnt-3a (100 *ng/ml*) for 8 and 24 h. Global gene expression analyses followed by hierarchical cluster analyses revealed 50 (8 h) and 87 (24 h) differentially expressed genes (yellow/upregulation, blue/downregulation). Wnt/Beta-catenin regulated genes were summarized in functionally related groups: direct Wnt target genes (AXIN2, APCDD1), cytokines (IL8, CCL2, CXCL6, CXCL10, CCL8, IL32) and ECM/cytoskeleton remodeling genes (TNFAIP6, PDPN, MMP1) (modified from Sobel, Tham *et al.* 2015).

of IL-8, CCL-2 and MMP-1 in more detail.

### 3.3.3 Ras-Raf-MEK-ERK MAP kinase pathway

Besides Wnt/Beta-catenin the Ras-Raf-MEK-ERK MAPK pathway might also be involved in cSCC progression. This highly conserved signaling cascade regulates cell responses to environmental cues (Marshall, 1995) regulating cell proliferation, differentiation, senescence and apoptosis (Heidorn et al., 2010). In general, extracellular stimuli such as cytokines, mitogens, hormones, oxidative stress or heat induce the signaling cascade by interacting with receptor complexes. These receptors include receptor tyrosine kinases (RTKs) like Epithelial growth factor receptor (EGFR), Mast/stem cell growth factor receptor Kit (c-Kit) or G protein-coupled receptors. Downstream signaling from RTKs is mediated

by the Ras-activating guanine nucleotide exchange factor Son of sevenless (SOS). The GDP to GTP conversion leads to the activation of the small guanine nucleotide binding protein Ras, which initiates MAPK signaling through the kinase Raf. Subsequently, this serine/ threonine kinase phosphorylates and thereby activates the kinase MEK that further phosphorylates the kinase ERK, leading to the activation of downstream transcription factors (Chang et al., 2003; Mebratu and Tesfaigzi, 2009). However, the pathway is more complex, as there are three Ras (H-Ras, K-Ras and N-Ras), three Raf (A-Raf, B-Raf, C-Raf/ Raf-1), two MEK (MEK1, MEK2) and two ERK (ERK1, ERK2) proteins with non-redundant function. In addition, the MAP kinase pathway is not linear. In normal cells, B-Raf forms homodimers or heterodimers with C-Raf in a Ras-dependent manner initiating downstream signaling via MEK and ERK (Heidorn et al., 2010). Moreover, cross-talks between this pathway and the Phosphatidylinositol 4,5-bisphosphate 3-kinase (PI3K)-Phosphatidylinositol 3,4,5-trisphosphate 3-phosphatase and dual-specificity protein phosphatase (PTEN)-Akt pathway occur at multiple levels (Vultur et al., 2011; Zaravinos et al., 2009) (Fig. 6).

In malignant melanoma (MM) mutations in KIT, NRAS and especially BRAF were detected in either 3-5%, 15-20% or 30-70% of tumors (Davies et al., 2002; Dong et al., 2003; Heidorn et al., 2010; Libra et al., 2005; Tap et al., 2010). Among different BRAF mutations, the substitution of glutamic acid to valine at position 600 (B-Raf$^{V600E}$, T to A missense transversion at nucleotide 1799) accounts for about 90% of B-Raf mutations. As consequence, the auto-inhibitory state of B-Raf is prevented allowing

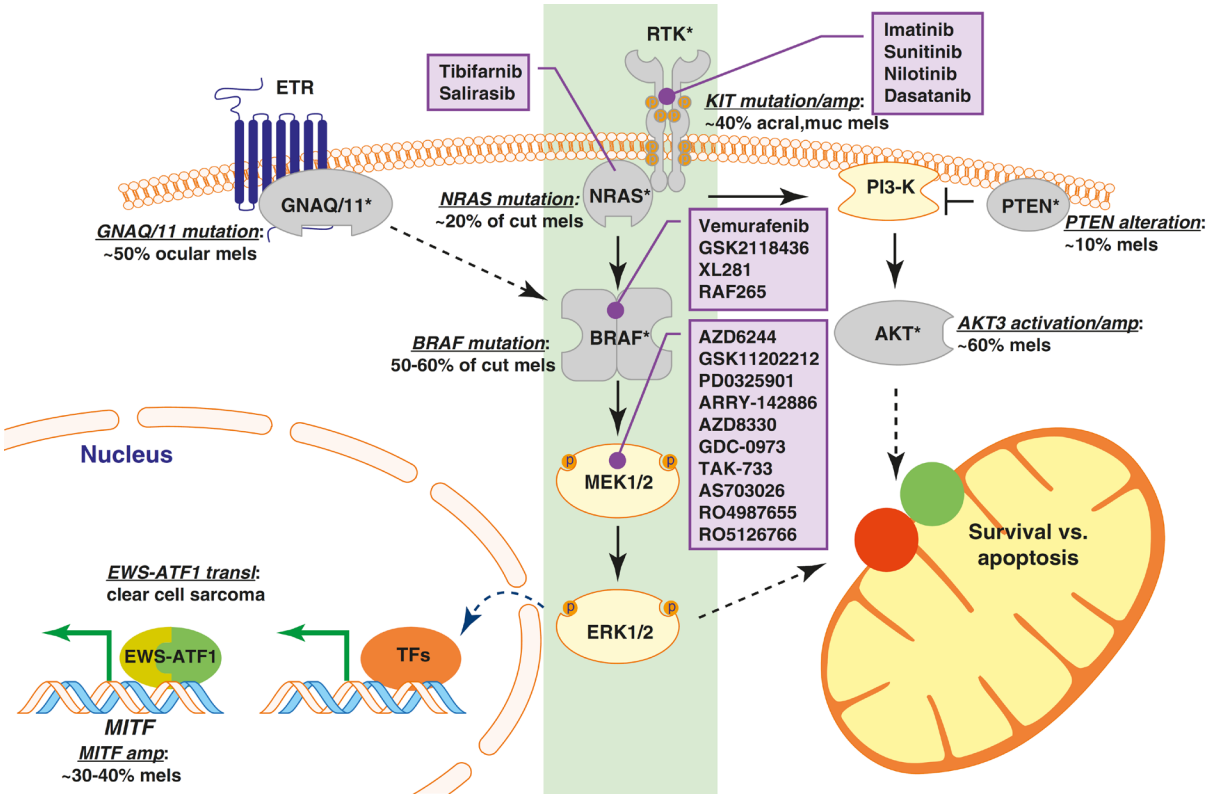


Figure 6 | **Ras-Raf-MEK-ERK signaling, key mutations and therapeutical targets in melanoma.**

Extracellular stimuli such as cytokines, mitogens, hormones, oxidative stress or heat induce the signaling cascade by interacting with receptor complexes including the receptor tyrosine kinases (RTKs) Epithelial growth factor receptor (EGFR), Mast/stem cell growth factor receptor Kit (c-Kit) or G protein-coupled receptors. RTK-activity leads to downstream signaling via Ras-activating guanine nucleotide exchange factor Son of sevenless (SOS) and Ras. Subsequently, Ras stimulates MAPK signaling through Raf, MEK and ERK leading to the activation of transcription factors (TFs) and gene regulation. Cross-talks between Ras-Raf-MEK-ERK signaling and the PI3K-PTEN-Akt pathway occur at multiple levels. Especially the Ras-Raf-MEK-ERK pathway is frequently associated with mutations in cancer. BRAF is the most commonly activated oncogene in melanomas, followed by NRAS and KIT. Drugs with a potential therapeutic impact on melanoma are listed in the purple boxes (adopted from Ji *et al.* 2012).

B-Raf signaling as monomeric protein with a 500-fold increased activity, thus constitutively stimulating MEK-ERK signaling (Heidorn et al., 2010). This prevents apoptosis and induces cell cycle progression (Libra et al., 2005) demonstrating the need for inhibitors targeting different components of the pathway (Fig. 6).

### 3.3.4 B-Raf kinase inhibitors in therapy of malignant melanoma

Since melanomas highly depend on Ras-Raf-MEK-ERK pathway activity, the inhibition of B-Raf represented an attractive target for small molecule inhibitors (Vultur et al., 2011). Two very promising and highly selective ATP-competitive B-Raf$^{V600E}$-inhibitors are Vemurafenib/ PLX4032 (Plexxikon, Roche) and Dabrafenib/ GSK2118436 (GlaxoSmithKline). During clinical trials of B-Raf$^{V600E}$-mutant melanoma patients, both inhibitors showed superior response rates of 50% (Bollag et al., 2010; Flaherty et al., 2010; Menzies et al., 2012; Robert et al., 2011). Compared to the former standard care, chemotherapy with Dacarbazine, Vemurafenib and Dabrafenib increased progression free survival (PFS) from 1.6-2.7 to 6.9 months and overall survival (OS) from 9.7-15.6 to either 13.6 or 18.2 months in Phase III clinical trials (Queirolo et al., 2015). Intriguingly, responses to Vemurafenib were seen at all sites of metastatic disease, including liver, small bowel and bone (Menzies et al., 2012). While treatment of tumors harboring B-Raf$^{V600E}$ resulted in many cases in partial or complete tumor regression, no tumor regression was observed in cells carrying B-Raf$^{wild\text{-}type}$. This rendered both B-Raf inhibitors as promising treatment strategy exclusively for B-Raf mutant melanomas. In contrast, traditional approaches or broad-spectrum kinase inhibitors like Sorafenib (Nexavar, Bayer) showed disappointing results in melanoma therapy, likely due to the non-specific broad-spectrum kinase inhibitory activity and the associated toxicity (Vultur et al., 2010, 2011). Therefore, Vemurafenib was approved by the FDA for the treatment of malignant melanoma in 2011 and is sold as Zelboraf, while Dabrafenib was approved in 2013 and is traded as Tafinlar (Press releases by FDA in August 2011 and May 2013). Besides MM, Vemurafenib was also employed to treat patients suffering from B-Raf$^{V600E}$ mutant stage IV non-small-cell lung cancer (Peters et al., 2013) and in combination with the chemotherapeutic Vinblastine to treat ganglioglioma (Rush et al., 2013).

However, as melanomas develop resistance against Vemurafenib within 2-18 months after onset of treatment, major research efforts focus on the mechanism of resistance development (Molina-Arcas and Downward, 2012). In order to prevent reactivation of Ras-Raf-MEK-ERK signaling and subsequent resistance, novel therapies combining B-Raf inhibitors like Vemurafenib or Dabrafenib with the MEK inhibitors Cobimetinib/ GDC-0973 (Roche) or Trametinib/ GSK1120212 (GlaxoSmithKline), respectively, are employed in clinics. In particular, Phase III trials combining Vemurafenib + Cobimetinib or Dabrafenib + Trametinib improved PFS from 6.9 months, achieved with B-Raf inhibitor mono-therapy, to either 9.9 or 9.3/ 11.4 months (Queirolo et al., 2015).

### 3.3.5 Adverse effects by kinase inhibitors targeting B-Raf

During clinical trials of specific B-Raf$^{V600E}$-inhibitors adverse effects such as fatigue, photosensitivity, rashes, hair loss, joint pain, abnormal liver function, gastrointestinal problems but mainly cutaneous adverse effects including KAs and cSCCs were monitored (Flaherty et al., 2010). KAs and cSCCs

occurred within a median time of 8 weeks in 4-31% of MM patients treated with Vemurafenib (Anforth et al., 2013). Similarly, Dabrafenib led to the development of 9-19% KAs/ cSCCs in Phase I-III clinical trials (Flaherty et al., 2012; Long et al., 2014). Since both, KAs and cSCCs, are typical UV-induced tumors (Boukamp, 2005), it is not surprising that these carcinomas predominantly occur in sun-exposed areas of the skin. This favors the idea that pre-existing oncogenic mutations potentiate the effects of the kinase inhibitors, rather than leading to a *de novo* development (Bollag et al., 2010). Interestingly and different from sporadic cSCCs, the developing tumors were always well-differentiated. Besides KAs and cSCCs, treatment with both specific B-Raf inhibitors led to the development of verrucous keratosis in 29%, which is histologically characterized as hyperkeratotic papules, and hyperkeratosis in 6-51% of melanoma patients (Anforth et al., 2013; Anforth et al., 2015). Recently performed safety-evaluations of Vemurafenib on either 3,222 or 675 treated melanoma patients showed the development of KAs and cSCCs in 14-29% and hyperkeratosis in 19% of patients (Larkin et al., 2014b; McArthur et al., 2014). Hyperkeratotic mucosal lesions and one case of oral SCC upon treatment with specific B-Raf inhibitors was also described (Vigarios et al., 2015). In addition, one case report describes a MM patient developing chronic myelomonocytic leukemia (CMML) after 11 days of Vemurafenib therapy. In particular, ERK-signaling was highly activated in N-Ras$^{G12R}$-mutant monocytes leading to an expansion of this population (Callahan et al., 2012). Besides haematopoietic tumor growth, a case of a MM patient receiving Vemurafenib experienced rapid growth of a pre-existing K-Ras$^{Q61L}$-mutant pancreatic adenocarcinoma as well as subsequent hepatic metastases (Grey et al., 2014). The development of new primary cutaneous melanomas in patients receiving either Vemurafenib or Dabrafenib was also observed. Interestingly, all melanocytic lesions were B-Raf$^{wild\text{-}type}$ (Zimmer et al., 2012). Taken together, these observations suggest that B-Raf-inhibitors are not only affecting B-Raf mutant melanocytes.

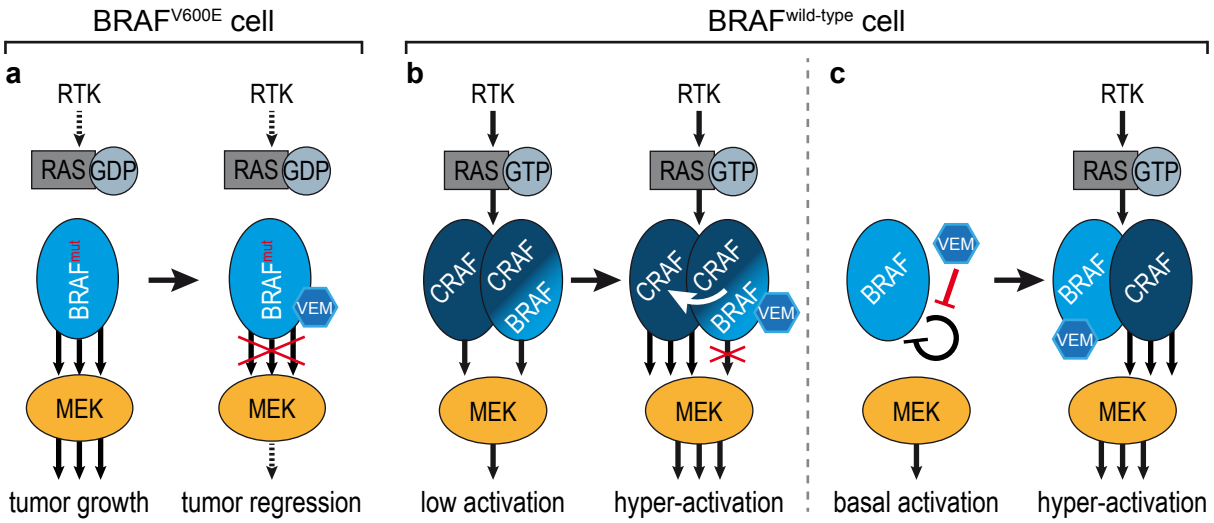


Figure 7 | **Vemurafenib induced block and hyper-activation of MEK-ERK signaling.**

**a |** Melanoma cells rely on ERK-activity for tumor growth. The specific B-Raf inhibitor Vemurafenib (VEM) was designed to binds mutant B-Raf$^{V600E}$ proteins as ATP-competitive inhibitor, abrogate downstream signaling via MEK-ERK and thereby prevent tumor growth. **b, c |** In B-Raf$^{wild\text{-}type}$ cells, Vemurafenib was hypothesized to cause a paradoxical MEK-ERK hyper-activation. Besides B-Raf$^{wild\text{-}type}$ status, both hypothesized models require Ras activity either by Ras mutation or upstream signaling through receptor tyrosine kinases (RTKs). One proposed mechanism by Poulikakos *et al.* (2010) suggests a low local concentration of the specific B-Raf inhibitor as third requirement leading to a stochastic Vemurafenib binding of only one Raf protein in a C-Raf-C-Raf homodimer or C-Raf-B-Raf heterodimer. Subsequently, a conformational change of the bound Raf subunit hyper-actives the second (b). The second proposed mechanism by Heidorn *et al.* and Hatzivassiliou *et al.* (2010) suggests that a specific B-Raf inhibitor resolves the auto-inhibitory state of B-Raf, allowing increased Raf dimer formation in a Ras-dependent manner, which mediates MEK-ERK hyper-activation (c).

In search for mechanisms leading to the described cutaneous adverse effects in melanoma therapy, it was suggested that the same small molecule inhibitors, which efficiently block mutant B-Raf signaling (Fig. 7a) may also lead to a paradoxical activation of this pathway in B-Raf$^{wild\text{-}type}$ cells. As second requirement, both currently hypothesized models require Ras activity resulting from a Ras mutation or activation of upstream pathway components like RTKs (Hatzivassiliou et al., 2010). The first proposed mechanism suggests a low local concentration of a specific B-Raf inhibitor as third requirement. As consequence, the inhibitor stochastically binds and blocks only one Raf protein of a C-Raf-C-Raf homodimer or C-Raf-B-Raf heterodimer. This leads to a conformational change of the bound subunit that trans-activates the second subunit of the complex and causes pronounced downstream signaling. Consequently, a high local B-Raf inhibitor concentration would lead to a block of both Raf subunits within a dimer preventing further downstream signaling (Fig. 7b). According to this hypothesis, a low drug-bioavailability of a B-Raf inhibitor in skin could be the reason for the paradoxical MEK-ERK activation by Vemurafenib (Poulikakos et al., 2010). The second proposed mechanism claimed that a specific B-Raf inhibitor rather resolves the B-Raf auto-inhibitory state allowing Raf dimer formation in a Ras-dependent manner, than acting on the already formed dimer itself (Hatzivassiliou et al., 2010; Heidorn et al., 2010) (Fig. 7c). The outcome of both models is a so called B-Raf inhibitor induced MEK-ERK hyper-activation leading to increased proliferation and transformation of melanoma cells. However, additional mutations may also play a role in tumorigenesis (Robert et al., 2011). This indicates that the development of adverse cutaneous effects actually depends on the RAS-RAF-MEK-ERK pathway, arguing for specific rather than off-target effects by the B-Raf inhibitors.

## 3.4 Aim of the study

The prevalence of cSCCs is constantly increasing worldwide especially in elderly or immunosuppressed transplant recipients, whereas the mechanism of tumor initiation and progression are not yet fully understood. In this thesis, I aimed to investigate two distinct signaling pathways regarding their role in cSCC development. First, the role of Wnt/Beta-catenin activated dermal fibroblasts was further analyzed, as this was identified in a subset of human cSCCs. Second, the effect of the B-Raf$^{V600E}$ inhibitor Vemurafenib and particularly the relevance of Ras-Raf-MEK-ERK MAPK signaling in cSCC progression, observed in treated melanoma patients, was dissected. Besides a direct effect of Vemurafenib on keratinocytes, a stromal modulation changing the fibroblasts' secretome may drive keratinocyte tumorigenesis, as well. To address these questions, experiments were conducted using primarily the HaCaT skin carcinogenesis progression models in monolayer cultures as well as in 3D OTCs resembling human skin. This allowed the analysis of interactions between tumor and stromal cells through direct interactions or soluble factors. Thus, the following questions were the basis for the present study.

(1) Are the Wnt-3a induced cytokines IL-8 and CCL-2 as well as the matrix remodeling factor MMP-1 also expressed in OTCs? What is their effect on epithelial morphology and carcinogenesis?

(2) Is Vemurafenib induced MEK-ERK hyper-activation also observed in B-Raf$^{wild\text{-}type}$ keratinocytes and dermal fibroblasts? What is the impact of Vemurafenib or Ras-Raf-MEK-ERK signaling on epithelial morphology and tumorigenesis?

(3) Are identified mechanisms also found in human primary cSCC samples *in situ*?

# 4. Materials and Methods

## 4.1 Materials

### 4.1.1 Technical equipment

Table 2 | **Technical equipment.**

| Type | Name | Company |
|---|---|---|
| Centrifuges | Centrifuge 5415 R | Eppendorf, Cologne, Germany |
| | Centrifuge 5417 R | Eppendorf, Cologne, Germany |
| | Heraeus Labofuge 400 | Thermo Fischer Scientific, Fermont, USA |
| Cell culture | Casy Cell Counter | Schärfe System GmbH, Reutlingen, Germany |
| | Cell culture incubator | Thermo Fischer Scientific, Fermont, USA |
| | FACSCanto II Flow Cytometer | BD Biosciences, Heidelberg, Germany |
| | FastPrep FP120 | Thermo Fischer Scientific, Fermont, USA |
| Microscopes | AX-70 (Fluorescence images) | Olympus Deutschland, Hamburg, Germany |
| | BX-51 (Brightfield images) | Olympus Deutschland, Hamburg, Germany |
| | Cell Observer (Proliferation images) equipped with Colibri imaging system | Zeiss, Oberkochen, Germany |
| | IX-70 (Cell culture images) | Olympus Deutschland, Hamburg, Germany |
| CCD-Cameras | AxioCam ERc 5s (Cell culture images) | Zeiss, Oberkochen, Germany |
| | AxioCam MRm (Proliferation images) | Zeiss, Oberkochen, Germany |
| | OSIS Color View (Brightfield images) | Olympus Deutschland, Hamburg, Germany |
| | OSIS F View (Fluorescence images) | Olympus Deutschland, Hamburg, Germany |
| | PL60 Digital Camera | Samsung, Schwalbach/ Ts., Germany |
| Software | BD FACSDiva Software 8.0 | BD Biosciences, Heidelberg, Germany |
| | cell^R/ cell^D Imaging Software 3.2 | Olympus Deutschland, Hamburg, Germany |
| | Creative Suite 5 | Adobe Systems, San José, USA |
| | GraphPad Prism 4 | GraphPad Software, La Jolla, USA |
| | Fiji/ ImageJ 2.0.0-rc-23 | http://fiji.sc/wiki/index.php/Fiji |

| | | |
|---|---|---|
| | FlowJo v10.0.7 | FlowJo, Ashland, OR, USA |
| | LightCycler 480 Software 1.5.0 SP3 | Roche Applied Sciences, Mannheim, Germany |
| | ZEN 2012 (blue edition) | Zeiss, Oberkochen, Germany |
| Miscellaneous | Cryostat Cryotome | Leica, Wetzlar, Germany |
| | Fluoroskan Ascent | Thermo Fischer Scientific, Fermont, USA |
| | LightCycler 480 Instrument II | Roche Applied Sciences, Mannheim, Germany |
| | MCK Software (M-FISH analysis) | Leica, Wetzlar, Germany |
| | Microtome | Leica, Wetzlar, Germany |
| | Mini-PROTEAN Tetra Cell | Bio-Rad, Munich, Germany |
| | Mini Trans-Blot Module | Bio-Rad, Munich, Germany |
| | Multiskan FC Microplate Photometer | Thermo Fischer Scientific, Fermont, USA |
| | NanoDrop ND-1000 | Thermo Fischer Scientific, Fermont, USA |
| | Peltier Thermal Cycler | MJ Research, San Francisco, USA |
| | PowerPac HC | Bio-Rad, Munich, Germany |

### 4.1.2 Chemicals and materials

Table 3 | **Chemicals and materials.**

| Name | Company |
|---|---|
| 5'Brom-2'-desoxyuridin/ 5'-Brom2'-Desoxycytidin (BrdU) | Sigma-Aldrich, Taufkirchen, Germany |
| 6-well, 24-well and 96-well plates (flat bottom) | Nunc, Wiesbaden, Germany |
| Acrylamide / Bis-Solution (40%, 37.5:1) | Bio-Rad, Munich, Germany |
| Agarose | Biozym, Hessisch Oldendorf, Germany |
| Alkaline Phosphatase/ Horseradish Peroxidase Block | BioFX Laboratories, Owings Mills, MD, USA |
| Amersham ECL Rainbow Molecular Weight Markers | GE Healthcare, Munich, Germany |
| BEMCOT M-3II | Asahi Kasei, Tokyo, Japan |
| BioCoat Deep Well Plates (6-well) | BD Biosciences, Heidelberg, Germany |
| Bovine Serum Albumin (BSA) | Jackson Immuno Research, Suffolk, UK |
| Cell Culture dishes (6, 10, 15 cm) | Falcon, Heidelberg, Germany |
| Cell Lifter | Corning, Amsterdam, Netherlands |
| Cell Strainer (70 µm) | BD Falcon, Franklin Lakes, NJ, USA |
| Colcemid (KaryoMAX) | Life Technologies, Frederick, MD, USA |
| Eosin G | Roth, Karlsruhe, Germany |
| Eukitt - Non aqueous mounting medium | Sigma-Aldrich, Taufkirchen, Germany |
| Fluorescent Mounting Medium | Dako Cytomation, Hamburg, Germany |
| Haematoxylin | Roth, Karlsruhe, Germany |
| Hank's balanced salt solution | Biochrom, Berlin, Germany |
| Hoechst 33258, pentahydrate (bis-benzimide) (500 *µg/mL*) | Life Technologies, Frederick, MD, USA |
| Lambda DNA-Hind III Ladder | Fermentas, St. Leon-Rot, Germany |
| Medical X-ray film | FujiFilm, Düsseldorf, Germany |
| Microscopic slides (Histobond) | Marienfeld, Lauda-Königshofen, Germany |
| Microscopic slides (Superfrost Plus) | Thermo Fisher Scientific, Waltham, MA, USA |
| Nitroblue tetrazolium chloride/ 5-bromo-4-chloro-3-indolyl phosphate substrate tablets | Roche Applied Sciences, Mannheim, Germany |
| Nitrocellulose membrane (Protran BA 85) | Whatman, Dassel, Germany |

| | |
|---|---|
| PBS/ PBS$^{+}$ (with $MgCl_2$, $CaCl_2$) | Serva Electrophoresis, Heidelberg, Germany |
| PEFA-Block | Serva Electrophoresis, Heidelberg, Germany |
| Pepsin | Sigma-Aldrich, Taufkirchen, Germany |
| Pepstatin | Serva Electrophoresis, Heidelberg, Germany |
| Polycarbonate membrane filter inserts (0.4 µm pore HD, PET track-etched membrane) | Falcon, Heidelberg, Germany |
| Ponceau S, ATX | Sigma-Aldrich, Taufkirchen, Germany |
| Propidium iodide (PI, 80 *mg/mL*) | Sigma-Aldrich, Taufkirchen, Germany |
| Specialized fixative for anatomy and histology | MORPHISTO, Frankfurt a. M., Germany |
| SYBR Green | Life Technologies, Frederick, MD, USA |
| SYBR Safe DNA Gel Stain | Life Technologies, Frederick, MD, USA |
| T7-RNA polymerase | Roche Applied Sciences, Mannheim, Germany |
| TEMED | Roth, Karlsruhe, Germany |
| ThinCerts, 12 well, 0.4 µm, translucent | Greiner Bio-One, Frickenhausen, Germany |
| ThinCert-Plate 12-well | Greiner Bio-One, Frickenhausen, Germany |
| Tissue Tek | Sakura Finetek, Zoeterwoude, Netherlands |
| TRIzol Reagent | Life Technologies, Frederick, MD, USA |

Further basic chemicals were purchased from AppliChem (Darmstadt, Germany), Merck (Darmstadt, Germany), Roth (Karlsruhe, Germany) or Sigma-Aldrich (Taufkirchen, Germany).

Table 4 | **Buffers and solutions.**

| Name | Composition | Application |
|---|---|---|
| Blocking buffer | 3% (w/v) BSA in $PBS^+$ + 0.02% (w/v) Sodium azide | IIF |
| Blocking buffer | 2% (w/v) Milk powder (blocking grade), 0.1% (v/v) Tween 20 in PBS | WB |
| Blocking solution | 0.5% (v/v) Triton X-100 in 3% (w/v) BSA (IgG-free, in $PBS^+$) | WM |
| Loading dye, DNA (3x) | 4 *M* Urea, 50 *mM* EDTA, 50% (w/v) Sucrose, 0.1% (w/v) Bromophenol blue | AGE |
| Loading dye, Protein (5x) | 3.75 *mM* Tris (pH 6.8), 50% (v/v) Glycerol, 350 *mM* SDS, 10% (v/v) beta-Mercaptoethanol, pinch of Bromophenol blue | SDS-PAGE |
| Lower gel buffer | 1.5 *M* Tris (pH 8.8), 14 *mM* SDS | SDS-PAGE |
| RIPA buffer | 10 *mM* Tris-HCl (pH 7.2), 150 *mM* NaCl, 5 *mM* EDTA, 1% (v/v) Triton X-100, 0.1% (w/v) SDS, 1% (w/v) Sodium deoxycholate | Protein extraction |
| RIPA lysis buffer | 0.2 *U/mL* Aprotinin, 1 *ng/µL* Leupeptin, 0.1 *ng/mL* Pepstatin A and 50 *nM* PEFA-Block, diluted in RIPA buffer | Protein extraction |
| Running buffer | 10% (v/v) Tris-Glycine (10x), 0.1% (w/v) SDS | SDS-PAGE |
| SDS-PA collection gel (12%) | 3.75% (v/v) Glycerol, 25% (v/v) Lower gel buffer, 30% (v/v) Acrylamide/ Bis Solution (40%), 0.05% (w/v) APS, 0.05% (v/v) TEMED | SDS-PAGE |
| SDS-PA stacking gel (2.8%) | 25% (v/v) Upper gel buffer, 7.8% (v/v) Acrylamide/ Bis Solution (40%), 0.05% (w/v) APS, 0.2% (v/v) TEMED | SDS-PAGE |
| SSC buffer (20x) | 3 *M* NaCl, 300 *mM* Trisodium citrate, pH 7.0 | ISH, M-FISH |
| TBE pH 8.3 (10x) | 890 *mM* Tris, 890 *mM* Boric acid, 32 *mM* EDTA | AGE |
| Transfer buffer | 10% (v/v) Tris-Glycine (10x), 20% (v/v) Methanol | WB |
| Tris-Glycine Solution (10x) | 330 *mM* Tris, 1.9 *M* Glycine | SDS-PAGE, WB |
| Upper gel buffer | 0.5 *M* Tris (pH 6.8), 14 *mM* SDS | SDS-PAGE |
| Wash buffer | 0.1% (v/v) Tween 20 in PBS | WB |
| Wash buffer 1 | 0.2% (v/v) Tween 20 in $PBS^+$ | WM |
| Wash buffer 2 | 0.2% (v/v) Tween 20 in PBS | WM |

AGE: Agarose gel electrophoresis, IIF: Indirect immunofluorescence, ISH: *In situ* hybridization, M-FISH: Multiplex-fluorescence *in situ* hybridization, SDS-PAGE: SDS-Polyacrylamide gel electrophoresis, WB: Western-Blot, WM: Whole-mount IIF

### 4.1.3 Kits

Table 5 | **Kits.**

| Name | Company |
|---|---|
| Amersham ECL Advance Western Blotting Detection Kit | GE Healthcare, Munich, Germany |
| DIG-RNA Labeling Kit | Roche Applied Sciences, Mannheim, Germany |
| EnzChek Gelatinase/Collagenase Assay Kit | Life Technologies, Frederick, MD, USA |
| FITC Annexin V Apoptosis Detection Kit I | BD Pharmingen, Erembodegem, Belgium |
| LightCycler 480 Probes Master | Roche Applied Sciences, Mannheim, Germany |
| Pierce BCA Protein Assay Kit | Thermo Fischer Scientific, Fermont, USA |
| qBiomarker Somatic Mutation PCR Array, Human Skin Cancers | QIAGEN, Hilden, Germany |
| QIAamp DNA Mini Kit | QIAGEN, Hilden, Germany |
| QIAshredder | QIAGEN, Hilden, Germany |
| Quantikine Human CCL2 / MCP-1 Immunoassay | R&D Systems, Wiesbaden, Germany |
| Quantikine Human IL-8 Immunoassay | R&D Systems, Wiesbaden, Germany |
| Quantikine Human Pro-MMP-1 Immunoassay | R&D Systems, Wiesbaden, Germany |
| Quantikine Human Total MMP-3 Immunoassay | R&D Systems, Wiesbaden, Germany |
| Quantikine Human Total MMP-9 Immunoassay | R&D Systems, Wiesbaden, Germany |
| REAL EnVision Detection System Peroxidase/ DAB+, Rabbit/ Mouse | Dako, Glostrup, Denmark |
| RevertAid H Minus First Strand cDNA Synthesis kit | Thermo Fischer Scientific, Fermont, USA |
| RNase A (20 *mg/mL*, Cell cycle analysis) | Life Technologies, Frederick, MD, USA |
| RNase A (17,500 U, DNA isolation) | QIAGEN, Hilden, Germany |
| RNase-free DNase Set (RNA isolation) | QIAGEN, Hilden, Germany |
| RNeasy Mini Kit | QIAGEN, Hilden, Germany |

### 4.1.4 Primer and probes

The following primers were used for quantitative RT-PCR (qRT-PCR) with an adequate probe from the Universal Probe Library (UPL, Roche).

Table 6 | **qRT-PCR primer and probes.**

| Gene | Primer sequences (5'-3') | UPL # | Efficiency | Cell type |
|---|---|---|---|---|
| alphaSMA | ccctgaagtacccgatagaaca (fwd)<br>ggcaacacgaagctcattg (rev) | 9 | 1.94 | Fibroblasts |
| AXIN2 | cagccattcaggaactaccc (fwd)<br>gaaggtgtgtggaggaaagg (rev) | 3 | 1.93<br>1.99 | Fibroblasts<br>Keratinocytes |
| CCL2 | agtctctgccgcccttct (fwd)<br>gtgactggggcattgattg (rev) | 40 | 1.97 | Fibroblasts |
| CDKN1A | tcactgtcttgtacccttgtgc (fwd)<br>ggcgtttggagtggtagaaa (rev) | 32 | 1.94<br>1.99 | Fibroblasts<br>Keratinocytes |
| CSF2 | tctcagaaatgtttgacctcca (fwd)<br>gcccttgagcttggtgag (rev) | 1 | 2.00 | Fibroblasts |
| CXCL10 | gaaagcagttagcaaggaaaggt (fwd)<br>gacatatactccatgtagggaagtga (rev) | 34 | 2.00 | Fibroblasts |
| CXCL12 | gctggtcctcgtgctgac (fwd)<br>gcatgggcatctgtagctc (rev) | 13 | 1.86 | Fibroblasts |
| EGFR | ctatgtgcagaggaattatgatcttt (fwd)<br>gggcaatgaggacataacca (rev) | 79 | 2.00 | Keratinocytes |
| FGF7 | aagggacccaagagatgaaga (fwd)<br>cctttgattgccacaattcc (rev) | 59 | 2.00 | Fibroblasts |
| FGF10 | gaaggagaactgcccgtaca (fwd)<br>ggcaacaactccgatttctact (rev) | 80 | 2.00 | Fibroblasts |
| FLG | ggactctgagaggcgatctg (fwd)<br>tgctcccgagaagatccat (rev) | 38 | 1.98 | Keratinocytes |
| GAPDH | agccacatcgctcagacac (fwd)<br>gcccaatacgaccaaatcc (rev) | 60 | 1.93<br>1.97 | Fibroblasts<br>Keratinocytes |
| HGF | cagcatgtcctcctgcatc (fwd)<br>tcttttcctttgtccctctgc (rev) | 15 | 1.99 | Fibroblasts |
| IL1A | ggttgagtttaagccaatcca (fwd)<br>tgctgacctaggcttgatga (rev) | 6 | 2.00<br>1.98 | Fibroblasts<br>Keratinocytes |
| IL1B | tacctgtcctgcgtgttgaa (fwd)<br>tctttgggtaatttttgggatct (rev) | 78 | 1.94<br>1.97 | Fibroblasts<br>Keratinocytes |
| IL6 | gatgagtacaaaagtcctgatcca (fwd)<br>ctgcagccactggttctgt (rev) | 40 | 1.70 | Fibroblasts |
| IL8 | agacagcagagcacacaagc (fwd)<br>atggttccttccggtggt (rev) | 72 | 1.97 | Fibroblasts |
| IVL | acccatcaggagcaaatgaa (fwd)<br>agctcgacaggcaccttct (rev) | 16 | 2.00 | Keratinocytes |
| KRT10 | ccatcgatgaccttaaaaatcag (fwd)<br>cgcagagctacctcattctcata (rev) | 64 | 2.00 | Keratinocytes |
| MMP1 | gctaacctttgatgctataactacga (fwd)<br>tttgtgcgcatgtagaatctg (rev) | 7 | 1.94<br>1.98 | Fibroblasts<br>Keratinocytes |

| | | | | |
|---|---|---|---|---|
| MMP3 | cagtttgctcagcctatcca (fwd)<br>tcacatctttttcgaggtcgt (rev) | 58 | 2.00<br>2.00 | Fibroblasts<br>Keratinocytes |
| MMP9 | gaaccaatctcaccgacagg (fwd)<br>gccacccgagtgtaaccata (rev) | 6 | 1.89<br>1.70 | Fibroblasts<br>Keratinocytes |
| MMP14 | caggaatgaggatctgaatgg (fwd)<br>ccgaggggtcactggaat (rev) | 45 | 2.00<br>2.00 | Fibroblasts<br>Keratinocytes |
| SNAI2 | tggttgcttcaaggacacat (fwd)<br>gcaaatgctctgttgcagtg (rev) | 7 | 1.95 | Keratinocytes |
| TGFA | cccagattcccacactcag (fwd)<br>acgtacccagaatggcagac (rev) | 38 | 2.00<br>1.99 | Fibroblasts<br>Keratinocytes |
| TGFB1 | gcagcacgtggagctgta (fwd)<br>cagccggttgctgaggta (rev) | 72 | 1.98<br>2.00 | Fibroblasts<br>Keratinocytes |
| TGFB3 | aagaagcgggctttggac (fwd)<br>gcgcacacagcagttctc (rev) | 38 | 2.00<br>1.93 | Fibroblasts<br>Keratinocytes |

Primers were synthesized by Sigma-Aldrich (Taufkirchen, Germany).

### 4.1.5 Antibodies

Table 7 | **Primary antibodies.**

| Specificity | Species | Dilution | Company | Cat. -No. | Application |
|---|---|---|---|---|---|
| Akt, phospho (Thr308) | Rabbit | 1:1,000 | Cell Signaling | 9275 | WB |
| alpha-SMA | Mouse | 1:100 | Sigma-Aldrich | A2547 | IIF |
| BrdU | Mouse | 1:5 | BD Biosciences | 347580 | WM + IIF |
| Cadherin-1 | Mouse | 1:20 | Progen | 10028 | IIF |
| Cleaved Collagen C1,2C | Rabbit | 1:100 | IBEX Pharmaceuticals | 50-1035 | IIF |
| Collagen IV | Rabbit | 1:100 | Progen | 10760 | IIF |
| Collagen VII | Mouse | 1:400 | Sigma-Aldrich | C6805 | IIF |
| ERK1/2 | Rabbit | 1:2,000 | Cell Signaling | 9102 | WB |
| ERK1/2, phospho (Thr202/ Tyr204) | Mouse | 1:2,000 | Cell Signaling | 9106 | WB |
| ERK1/2, phospho (Thr202/ Tyr204) | Rabbit | 1:400 | Cell Signaling | 4370 | IHC |
| Filaggrin | Mouse | 1:200 | Acris Antibodies | AM00245 | IIF |
| GAPDH | Mouse | 1:50,000 | Merck Millipore | MAB374 | WB |
| Integrin beta-4 | Rat | 1:1,000 | BD Pharmingen | 33691A | IIF |
| Keratin-10 | Mouse | 1:20 | Progen | 11414 | IIF |
| Keratin-14 | Mouse | 1:50 | R&D Systems | MAB3164 | IIF |
| Keratin-14 | Rabbit | 1:1,000 | Biolegend | PRB-155P | IIF |
| Ki67 | Rabbit | 1:300 | Abcam | ab15580 | IIF |
| MEK1/2 | Mouse | 1:1,000 | Cell Signaling | 4694 | WB |
| MEK1/2, phospho (Ser217/ Ser221) | Rabbit | 1:1,000 | Cell Signaling | 9154 | WB |
| MMP-1 | Rabbit | 1:100 | Sigma-Aldrich | M3940 | IIF |
| p38 alpha | Mouse | 1:2,000 | Cell Signaling | 9217 | WB |
| p38, phospho (Thr180/ Tyr182) | Rabbit | 1:1,000 | Cell Signaling | 9211 | WB |
| Vimentin | Mouse | 1:100 | Progen | 61013 | IIF |
| Wnt-3 | Rabbit | 1:100 | Abcam | ab32249 | IIF |

IHC: Immunohistochemistry, IIF: Indirect immunofluorescence, WB: Western-Blot,
WM: Whole-mount IIF

Table 8 | **Secondary antibodies.**

| Specificity | Species | Conjugate | Dilution | Company | Cat. -No. |
|---|---|---|---|---|---|
| Digoxigenin (DIG) | Sheep | Horseradish peroxidase | 1:300 | Roche Applied Sciences | 11207733910 |
| Mouse-IgG | Goat | Alexa-488 (IIF) | 1:600 | Life Technologies | A11029 |
| Mouse-IgG | Goat | Cy3 (IIF) | 1:500 | Jackson ImmunoResearch | 115-165-205 |
| Rabbit-IgG | Goat | Cy3 (WM) | 1:600 | Dianova | 111-165-144 |
| Rat-IgG | Donkey | Cy3 (IIF) | 1:500 | Dianova | 712-166-153 |
| Mouse-IgG | Donkey | Horseradish peroxidase | 1:40,000 | Dianova | 715-035-150 |
| Rabbit-IgG | Donkey | Horseradish peroxidase | 1:40,000 | Dianova | 711-035-152 |

### 4.1.6 Cell culture supplements, media and solutions

Table 9 | **Cell culture supplements.**

| Supplement | Company |
|---|---|
| 2-Phospho-L-Ascorbic Acid, trisodium salt | Sigma-Aldrich, Taufkirchen, Germany |
| Anti-human CCL-2/ MCP-1 Neutralizing Antibody (#MAB279/ nCCL-2) | R&D Systems, Wiesbaden, Germany |
| Anti-human IL-8 Neutralizing Antibody (#MAB208/ nIL-8) | R&D Systems, Wiesbaden, Germany |
| Celastrol | Cayman Chemical, Ann Arbor, MI, USA |
| Cholera toxin | Sigma-Aldrich, Taufkirchen, Germany |
| Cobimetinib/ GDC-0973 (COBI) | Adooq Bioscience, Irvine, CA, USA |
| DermaLife K Medium Complete Kit | Lifeline Cell Technology, Frederick, MD, USA |
| DMEM (Dulbecco's Modified Eagle's Medium) DMEM:F12, 1:1 Mixture | Lonza, Verviers, Belgium |
| Dimethyl Sulfoxide (DMSO) | Sigma-Aldrich, Taufkirchen, Germany |
| EDTA (0.05% (w/v) in PBS + 1 *µL/mL* Phenol red) | Serva Electrophoresis GmbH |
| Fetal Bovine Serum (FBS); Lot, 41Q7791K | Gibco, Auckland, New Zealand |
| Fetal Bovine Serum (FBS) GOLD, Lot: A15112-1936 | GE Healthcare, Munich, Germany |
| Fetal Bovine Serum (FBS) GOOD, Lot: P132307 | PAN-Biotech, Aidenbach, Germany |
| Human recombinant CCL-2/ MCP-1 | R&D Systems, Wiesbaden, Germany |
| Human recombinant EGF | Life Technologies, Frederick, MD, USA |
| Human recombinant FGF-Basic | Life Technologies, Frederick, MD, USA |
| Human recombinant IL-8 | R&D Systems, Wiesbaden, Germany |
| Human recombinant TGF-alpha | R&D Systems, Wiesbaden, Germany |
| Human recombinant TGF-beta-1 | Life Technologies, Frederick, MD, USA |
| Hydrocortisone | Sigma-Aldrich, Taufkirchen, Germany |
| Insulin | Sigma-Aldrich, Taufkirchen, Germany |

| | |
|---|---|
| Mouse recombinant Wnt-3a | R&D Systems, Wiesbaden, Germany |
| Penicillin/ Streptomycin (10,000 *U/mL* / 10,000 *µg/mL*) | Biochrom, Berlin, Germany |
| Penicillin/ Streptomycin/ Fungizone (500 *µg/mL*, 500 *µg/mL*, 1.25 *µg/mL*) | Lonza, Verviers Belgium |
| Tissucol Kit 1.0 | Baxter, Deerfield, IL , USA |
| Trasylol (Aprotinin, 10,000 *U/mL*) | Bayer, Leverkusen, Germany |
| Trypsin (0.1% in PBS + 1 *µL/mL* Phenol red) | Roche Applied Sciences, Mannheim, Germany |
| Vemurafenib/ PLX4032/ RG7204 (VEM) | ChemieTek, Indianapolis, USA |

Table 10 | **Cell culture media and solutions.**

| **Name** | **Composition** |
|---|---|
| Growth medium | DMEM with 10% FBS and 1% (v/v) Penicillin/ Streptomycin |
| $FAD_{complete}$ | DMEM + DMEM F-12 (1:1) with 5% (v/v) FBS, 1% (v/v) Penicillin/ Streptomycin, 24 *ng/mL* Adenine, 0.1 nM Cholera toxin, 1 *ng/mL* EGF, 0.4 *µg/mL* Hydrocortisone, 5 *µg/mL* Insulin |
| FDM medium | DMEM + DMEM F-12 (1:1) with 10% (v/v) FBS, 1% (v/v) Penicillin/ Streptomycin/ Fungizone, 200 *µg/mL* 2-Phospho-L-Ascorbic Acid, 2.5 *ng/mL* EGF, 5 *ng/mL* FGF-Basic, 5 *µg/mL* Insulin, 1 *ng/mL* TGF-beta-1 |
| Freezing Medium | Adequate medium with 20% FBS and 10% (v/v) Glycerol |
| rFAD | DMEM + DMEM F-12 (1:1) with 10% (v/v) FBS, 1% (v/v) Penicillin/ Streptomycin, 200 *µg/mL* 2-Phospho-L-Ascorbic Acid, 0.1 *nM* Cholera toxin, 0.4 *µg/mL* Hydrocortisone |
| Trypsin/ EDTA | NHEK: 0.40% Trypsin/ 0.05% (w/v) EDTA<br>HaCaT: 0.05% Trypsin/ 0.05% (w/v) EDTA<br>NHDF: 0.10% Trypsin/ 0.05% (w/v) EDTA |

### 4.1.7 Cells and cell lines

The parental HaCaT cells (Boukamp et al., 1988), H-Ras$^{G12V}$ transfected benign tumorigenic HaCaT-RAS A-5 and malignant tumorigenic HaCaT-RAS II-4 cells were generated (Boukamp et al., 1982; Mueller and Fusenig, 1999) and routinely cultivated in the laboratory. In addition, the squamous cell carcinoma cell lines SCL-I (Boukamp et al., 1982), SCL-II (Tilgen et al., 1983), SCC-12, SCC-13 (Rheinwald and Beckett, 1981), MET-1 and MET-4 (Proby et al., 2000) were cultivated. Normal human epidermal keratinocytes (NHEK) and normal human dermal fibroblasts (NHDF) were derived from human explant cultures of either epidermis or de-epidermized dermis in a routinely performed method (Maas-Szabowski et al., 2003; Schoop et al., 1999). B-Raf$^{V600E}$-mutant A375 melanoma cells were also cultivated. All cells and cell lines were tested for mycoplasma contamination every two weeks (Venor GeM Mycoplasma Detection Kit; Minerva Biolabs, Berlin, Germany). The purity of cells was validated using the Multiplex Cell Contamination Test by Multiplexion (Heidelberg, Germany), as described (Schmitt and Pawlita, 2009). No Mycoplasma, SMRV and interspecies contamination were detected. HaCaT cells were authenticated using Multiplex Cell Authentication by Multiplexion (Heidelberg, Germany), as described (Castro et al., 2013).

Table 11 | **Origin of normal keratinocytes and fibroblasts.**

| Name | Donor | Body site | Isolation date |
|---|---|---|---|
| NHEK 1 | female, 23 years | Breast | 26.04.2004 |
| NHEK 2 | female, 40 years | Abdomen | 10.03.2008 |
| NHEK 3 | female, 41 years | Abdomen | 02.09.2010 |
| NHEK 4 | female, unknown age | Breast | 20.10.2005 |
| NHDF 1 | female, 23 years | Abdomen | I-04.04.2007 |
| NHDF 2 | female, 22 years | Breast | 08.02.1996 |
| NHDF 3 | male, 21 years | Rump | 09.03.1995 |

## 4.2 Methods

### 4.2.1 Maintenance of cells

Keratinocytes and A375 melanoma cells were cultivated in an incubator at 37 °C with 95% humidity and 5% $CO_2$ pressure (normoxia), while NHDF were incubated at 37 °C with 95% humidity, 5% $CO_2$ and 5% $O_2$ pressure (hypoxia).

NHEK were cultivated in DermaLife K medium complete. 7 days after thawing, cells were rinsed in EDTA, detached using 0.4% Trypsin/ EDTA for 3-5 min and used for subsequent experiments. NHDF were grown in growth medium and were spilt every 7-14 days in a ratio of 1:3. Therefore, cells were rinsed with EDTA and incubated for 3-5 min in 0.1% Trypsin/ EDTA.

Non-tumorigenic HaCaT, benign-tumorigenic HaCaT-RAS A-5, malignant-tumorigenic HaCaT-RAS II-4 and A375 melanoma cells were routinely cultivated in growth medium (see Table 10, 4.1.6), which was replaced every 2-3 days. Cells were spilt either after 7 days at a ratio of 1:12 (A-5, II-4 and A375) or after 10 days at a ratio of 1:10 (HaCaT). In particular, cells were rinsed in EDTA and incubated for 10 min with fresh EDTA. 0.05% Trypsin/ EDTA was added for 3-5 min to detach the keratinocytes and the Trypsin-activity was stopped with two volumes of growth medium. The cSCC cells lines SCL-I, SCL-II, MET-1 and MET-4 cells were cultivated in growth medium, SCC-12 and SCC-13 cells in $FAD_{complete}$ (see Table 10, 4.1.6). cSCC cell lines were split every 7 days, as described for HaCaT-RAS A-5 cells.

#### 4.2.1.1 Freezing and thawing of cell stocks

For freezing, cells at 80% confluence were trypsinized, as described above, centrifuged for 5 min at 1,000 rpm and resuspended in freezing medium (see Table 10, 4.1.6) at a concentration of $2x\ 10^6$ cells/ mL. 1 mL aliquots were transferred into cryo-tubes placed in 2-propanol containing cryo-boxes for controlled freezing (1 °C/min). The cells were pre-cooled for 1 hour at 4 °C and transferred to -80 °C storage over night. Finally, the cell stocks were stored in the gas phase of liquid nitrogen.

To thaw cells, cryo-tubes containing cells were incubated at 37 °C and the suspension was added to a culture dish containing the appropriate growth medium. The medium was replaced after 1-2 days.

#### 4.2.1.2 Harvesting of cells

Cells were trypsinized as described (see 4.2.1) and the suspension was centrifuged for 5 min at 1,000 rpm. The pellet was resuspended in 1 mL PBS and centrifuged again for 5 min at 3,200 rpm. The supernatant was removed and the pellet was stored at -80 °C (harvest by trypsinization). Alternatively, cells were washed twice in PBS at 4 °C, detached in 1 mL PBS using a Cell Lifter (Corning) and transferred to a reaction tube. After centrifugation for 5 min at 3,200 rpm, the supernatant was removed and the pellet was stored at -80 °C (harvest by detachment).

### 4.2.1.3 Stimulation of cells with different agents

Cells were stimulated with the following agents in the corresponding culture medium: human recombinant CCL-2 (100 *ng/mL*), Celastrol (2.2-8.8 $\mu M$ in DMSO), Cobimetinib/ GDC-0973 (COBI, 0.01-1 $\mu M$ in DMSO), DMSO (0.01-0.5%), human recombinant EGF (2-10 *ng/mL*), human recombinant IL-8 (10 *ng/mL*) and Vemurafenib/ PLX4032 (VEM, 0.01-50 $\mu M$ in DMSO). Depending on each solvent, either the appropriate medium or DMSO (0.01-0.5%) in the appropriate medium was used as controls. Medium containing the stimulatory factors was replaced as indicated.

### 4.2.1.4 Continuous cell stimulation

Long-term effects of Vemurafenib on HaCaT and HaCaT-RAS A-5 cells were investigated by continuous treatment with Vemurafenib for 9 weeks or 5 weeks, respectively. Therefore, 5x $10^5$ cells were seeded per 10 cm tissue culture plate and treated either with growth medium and DMSO (0.05%) as controls or with 1 $\mu M$ and 5 $\mu M$ Vemurafenib. The factors were replaced by medium change every 2-3 days. HaCaT and HaCaT-RAS A-5 cells were split every 7 days, were counted using the Casy Cell Counter and 5x $10^5$ cells per 10 cm tissue culture plate and treatment condition were seeded. Cell number was plotted and the morphology was documented using the Olympus IX-70 microscope.

Toxicity and cellular changes were quantified by FACS-based cell cycle (see 4.2.3) and apoptosis assay 24 h after the last Vemurafenib stimulation (see 4.2.4) as well as by multiplex fluorescence *in situ* hybridization (M-FISH) analysis. The latter was performed by Prof. Dr. Anna Jauch of the Institute of Human Genetics at the Heidelberg University Hospital (see 4.2.7). Moreover, RNA was isolated from 4 weeks + 8 h and 8 weeks + 8 h continuously treated HaCaT cells (see 4.2.13.1) to analyze relative gene expression of target genes by qRT-PCR (see 4.2.13.3 and 4.2.13.4).

## 4.2.2 SYBR Green cell proliferation assay

NHEK, HaCaT and HaCaT-RAS A-5 cells were seeded in 24-well plates at a density of $10^4$ cells in 500 $\mu L$ DermaLife K medium complete (NHEK) or growth medium (HaCaT, A-5) per well and incubated for 24 h before treatment. For CCL-2 and IL-8 proliferation assays, HaCaT cells were starved for 72 h in growth medium supplemented with only 2% FBS. For quantification of cell numbers, a standard plate was additionally prepared with 1x, 2x, 3x, 5x, 7x and 10x $10^4$ cells per well in triplicates. 12 h later, the standard plate as well as a seeding control were harvested by removing the medium and storing the plates at -20 °C. Then, cells were stimulated (4 wells per condition and time point) with either recombinant human CCL-2, IL-8, a combination of both, recombinant human EGF or with Vemurafenib while DMSO treatment served as control, diluted in the corresponding pre-treatment medium. Cells were continuously stimulated for 24-72 h without changing the medium and at each time point, one plate was harvested as described for the standard plate.

To determine the total cell number per well, the frozen plates were thawed and incubated with SYBR Green (1:2,500) in 0.1% (v/v) Triton X-100 diluted in PBS for 1 h in the dark. Thereafter, the fluorescence

was measured at 485 nm with Fluoroskan Ascent (Thermo Fischer Scientific). The total cell number was calculated using the standard plate as a reference in which a given fluorescence intensity was correlated to a defined cell number. Each experiment was repeated at least twice and the mean was plotted. The Two-way ANOVA + Bonferroni posttest, comparing each condition to the control treated cells over time, was used to determine statistically significant differences.

### 4.2.3 Cell cycle analysis by FACS

Effects of stimulation on the cell cycle progression were assessed by staining the DNA content of lysed cells using propidium iodide (PI), which was subsequently quantified by FACS analysis. Therefore, cells were harvested by trypsinization (see 4.2.1.2) 24 h or 48 h after control, DMSO or Vemurafenib (1 *µM*/ 5 *µM*) treatment. Each cell pellet was washed once in cold PBS and fixed while vortexing by slowly adding 400 µL 70% (v/v) ethanol in dd$H_2O$ per $10^6$ cells. After >1 h incubation at 4 °C, PBS (4 °C) was added followed by centrifugation for 5 min at 3,200 rpm, 4 °C to remove the ethanol. PBS washing was repeated when required. Cell pellets were resuspended in PBS (4 °C) and incubated with 50 *µg/mL* RNase A for 30 min at 37 °C. Thereafter, 500 *µg/mL* PI was added to stain the DNA for 10 min, before analysis by flow cytometry at a flow rate of approx. 150 events/sec employing a FACSCanto II (BD). Unstained cells were included into the analysis as controls and to set the voltage of forward (FSC) and side scatter (SSC) using the BD FACSDiva Software (PI-filter: 616/ 26 nm). Data was plotted by using FlowJo.

### 4.2.4 Apoptosis analysis by FACS

Toxicity upon stimulation of cells with Vemurafenib was assessed by performing a FACS-based apoptosis assay according to the FITC Annexin V Apoptosis Detection Kit I (BD Pharmingen) to detect early and late apoptotic cells. It relies on the principle that early apoptotic cells lose membrane asymmetry allowing FITC labeled Annexin V to bind the membrane phospholipid phosphatidylserine, usually located at the inner plasma membrane leaflet of a viable cell. Late apoptosis is additionally detected by PI that enters cells due to a damaged plasma membrane. Celastrol, which is known to induce apoptosis in HaCaT cells (Zhou et al., 2011), was used as positive control.

After control, DMSO, Celastrol or Vemurafenib treatment for 24 h or 48 h, cells were harvested by trypsinization (see 4.2.1.2), washed once in PBS (4 °C) and resuspended in the supplied binding buffer at a concentration of $10^6$ cells/mL. 100 µL cell suspension was mixed with 5 µL FITC Annexin V and 5 µL PI solution, vortexed and incubated for 15 min at room temperature (RT) in the dark. Then, 400 µL binding buffer was added and the samples were analyzed by flow cytometry using a FACSCanto II (BD). Unstained as well as FITC Annexin V or PI single stained cells were included into the analysis to set the voltage of forward (FSC) and side scatter (SSC) and to perform compensation using the BD FACSDiva Software (FITC-filter: 530/ 30 nm, PI-filter: 616/ 26 nm). Data was plotted using FlowJo and statistically significance was calculated by Two-way ANOVA + Bonferroni posttest comparing each treatment to the corresponding control.

### 4.2.5 Preparation and maintenance of organotypic co-culture (OTC) models

In this study three different organotypic co-culture models were used depending on the raised research question (Fig. 8). Generation, maintenance, stimulation and harvest are described in the following paragraphs.

#### 4.2.5.1 Generation and maintenance of OTCs

*(a) Collagen-based organotypic culture (colOTC)*

Organotypic co-cultures based on collagen as dermal equivalent and scaffold were prepared following the method of Schoop and co-workers (Schoop et al., 1999). Accordingly, Collagen type I gels with embedded NHDF 3 were prepared on ice by mixing 8 volumes of a rat Collagen type I solution (5 *mg/mL* in 0.1% (v/v) acetic acid, 4 °C; isolated from rat tails) with 1 volume 10x Hank's buffered saline. After neutralization with 5 *M* NaOH, NHDF were trypsinized (see 4.2.1) and resuspended at 5x $10^5$ cells/mL in FBS. 3.5 mL of the resulting mixture was poured into polycarbonate membrane filter inserts (0.4 µm pore HD, PET track-etched, Falcon) placed in BioCoat Deep Well Plates (6-well, BD Biosciences). The gels were polymerized for 1 h at 37 °C. Subsequently, glass rings (Technical Infrastructure, DKFZ Heidelberg) were gently placed on top of the gels and incubated for additional 15-20 min at 37 °C. Thereafter, the released liquid was aspirated and growth medium supplemented with 200 *µg/mL* 2-phospho-L-ascorbic acid was added into each well plus filter insert to ensure equilibration of the gels over night at 37 °C. The next day, HaCaT cells were trypsinized (see 4.2.1), singularized using a 70 µm cell strainer and $10^6$ cells were seeded on top of each dermal equivalent. Therefore, the medium within the ring was removed and 1 mL of the HaCaT cell suspension ($10^6$ cells/mL) was added into the ring. After 18-24 h of submersed cultivation, cells that did not adhere and the medium with the glass rings were carefully removed in order to allow air-exposed growth of the keratinocytes (air-lift). During the first week of cultivation, OTCs were incubated in growth medium supplemented with 200 *µg/mL* 2-phospho-L-ascorbic acid, 2 *ng/mL* human recombinant EGF and 2 *ng/mL* human recombinant TGF-alpha. Thereafter, OTCs were cultured in growth medium supplemented with 2-phospho-L-ascorbic acid only, which was replaced every 2-3 days until harvesting the cultures after 2-4 weeks (Fig. 8a).

*(b) Scaffold-based organotypic culture (scaOTC)*

Organotypic co-cultures based on the cellulose material BEMCOT M-3II (Asahi Kasei) as physical scaffold and fibroblasts embedded in a Fibrin matrix as dermal equivalent were prepared following the method of Böhnke and co-workers (Boehnke *et al.*, in preparation). For the use in 6-well cell culture inserts, circular M-3II pieces with diameter of 22 mm were prepared using a punch and sterilized by autoclaving between two microscopic slides. The scaffolds were inserted onto polycarbonate membrane filter inserts (0.4 µm pore HD, PET track-etched, Falcon) placed in 6-well plates (Nunc). NHDF 1 were trypsinized (see 4.2.1) and 7.5x $10^5$ cells resuspended in 375 µL FBS were mixed with 375 µL Thrombin in PBS (10 *I.E./mL*, Tissucol Kit 1.0, Baxter) per OTC and filled into the M-3II-containing insert. Fibrinogen (Tissucol Kit 1.0, Baxter) was dissolved in 10 mL PBS, pH 7.0 resulting in an 8 *mg/*

*mL* Fibrinogen solution. 375 µL Fibrinogen solution was diluted with 375 µL PBS per culture and additionally added into the filter insert to produce a gel with embedded fibroblasts (final concentrations: 2.5 *I.E./mL* Thrombin, 2 *mg/mL* Fibrinogen). For the clotting reaction, dermal equivalents were incubated for 30 min in the incubator. Subsequently, glass rings (Technical Infrastructure, DKFZ Heidelberg) were gently placed on top. Liquid on the gel was removed before adding the pre-culture medium consisting of growth medium supplemented with 200 *µg/mL* 2-phospho-L-ascorbic acid and 1 *ng/mL* human recombinant TGF-beta-1 for 7 days submersed cultivation. One day before seeding keratinocytes, the inserts were placed in BioCoat Deep Well Plates (6-well, BD Biosciences) and the medium was shifted to growth medium with 200 *µg/mL* 2-phospho-L-ascorbic acid and Trasylol (500 *U/mL*, Bayer) to prevent degradation of the gel. HaCaT cells were trypsinized (see 4.2.1), singularized using a 70 µm cell strainer and $10^6$ cells were seeded on top of the dermal equivalent. Therefore, the medium within the ring was removed and 1 mL of the HaCaT cell suspension ($10^6$ cells/mL) was seeded. After 18-24 h of submersed cultivation, cells that did not adhere and the medium with the glass rings were carefully removed in order to allow air-exposed growth of the keratinocytes (air-lift). During the first week of culture, OTCs were incubated in growth medium supplemented with 200 *µg/mL* 2-phospho-L-ascorbic acid, 500 *U/mL* Trasylol, 2 *ng/mL* human recombinant EGF and 2 *ng/mL* human recombinant TGF-alpha. Thereafter, OTCs were cultured in growth medium supplemented 2-phospho-L-ascorbic acid and Aprotinin only, which was replaced every 2-3 days until harvesting the cultures after 4-9 weeks (Fig. 8b).

### *(c) Fibroblast-derived matrix-based organotypic culture (fdmOTC)*

Organotypic co-cultures based on a fibroblast-derived matrix (fdm) as dermal equivalent and scaffold were prepared following the method of Berning and co-workers (Berning et al., 2015). Therefore, ThinCerts (0.4 µm, translucent) 12-well filter inserts (Greiner Bio-One) were placed in ThinCert-Plates 12-well (Greiner Bio-One) and 5 mL FDM medium (see Table 10, 4.1.6) was added to the bottom well. NHDF 1 were trypsinized (see 4.2.1), resuspended at $10^6$ cells/mL in FDM medium. 500 µL of the resulting suspension was added to each filter insert (1$^{st}$ NHDF seeding). After 2-3 days each, this procedure was repeated for a 2$^{nd}$ and 3$^{rd}$ NHDF seeding of 5x $10^5$ cells per filter insert. To generate a fibroblast-derived matrix, submersed cultivation was continued for four weeks with medium changes every 2-3 days (insert: 0.5 mL, bottom well: 5 mL). The day before seeding keratinocytes, medium was replaced by rFAD (see Table 10, 4.1.6). NHEK 2, HaCaT, HaCaT-RAS A-5 were trypsinized accordingly (see 4.2.1), singularized using a 70 µm cell strainer and resuspended at 0.5x $10^6$ cells/mL in rFAD medium. 500 µL of the resulting suspension was seeded onto the fdm within the filter insert. After 4-5 days of submersed cultivation, the medium within the filter inserts was removed in order to allow air-exposed growth of the keratinocytes (air-lift). During the first week of cultivation, OTCs were incubated in rFAD medium supplemented with 2 *ng/mL* human recombinant EGF and 2 *ng/mL* human recombinant TGF-alpha. Thereafter, OTCs were cultured in rFAD only, which was replaced every 2-3 days until harvesting the cultures after 3-7 weeks (Fig. 8c).

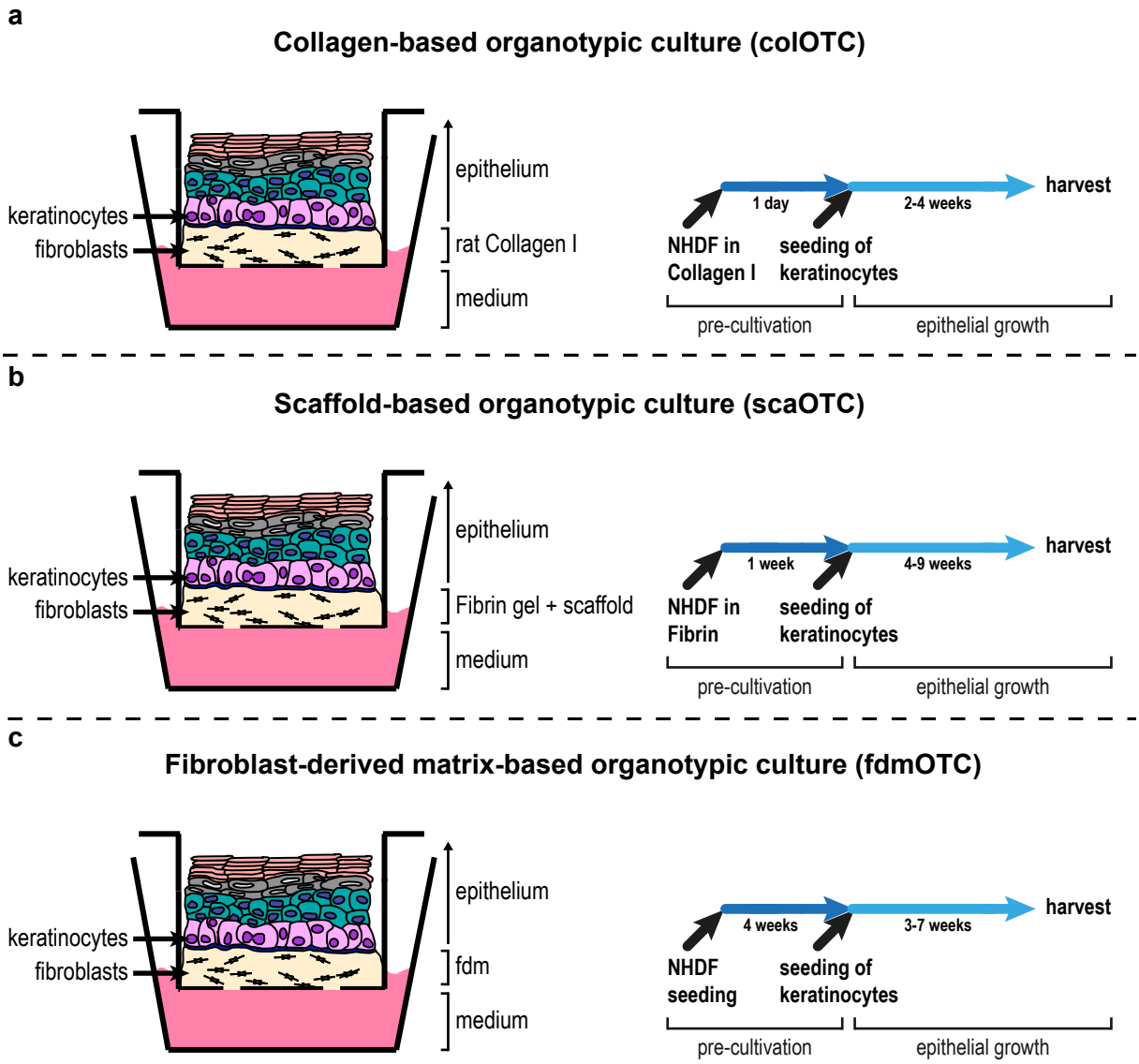


Figure 8 | **Organotypic culture models.**
To resemble human skin *in vitro*, organotypic cultures (OTCs) were generated by embedding fibroblasts in a matrix forming the dermal equivalent. Keratinocytes that are seeded on top and grown air-exposed form a multilayered stratifying epithelium. OTCs differ in the employed keratinocytes, the composition of the dermal equivalent and the scaffold. **a |** colOTCs base on Collagen type I with embedded fibroblasts as dermal equivalent and scaffold. They require a short pre-incubation time of 1 day, before seeding keratinocytes and last for 4 weeks. **b |** scaOTCs base on Cellulose as physical scaffold and fibroblasts embedded in a Fibrin matrix as dermal equivalent. They require a medium pre-incubation time of 1 week, before seeding keratinocytes and are stable for more than 9 weeks. **c |** fdmOTCs base on a fibroblast-derived matrix (fdm) as dermal equivalent and scaffold. They require a long pre-incubation of 4 weeks allowing the fibroblasts to build a matrix, before seeding keratinocytes. These OTCs are stable for more than 7 weeks.

### 4.2.5.2 Stimulation of OTCs

OTCs were stimulated with the following agents in the corresponding culture medium: Cobimetinib/ GDC-0973 (COBI, 0.01-1 $\mu M$ in DMSO), Vemurafenib/ PLX4032 (VEM, 0.01-50 $\mu M$ in DMSO) or recombinant mouse Wnt-3a (100 $ng/mL$). In order to block the effects of either CCL-2 or IL-8, OTCs were treated with anti-human CCL-2 neutralizing antibody (nCCL-2, 4 $\mu g/mL$) and anti-human IL-8 neutralizing antibody (nIL-8, 1 $\mu g/mL$). Depending on each solvent, either the appropriate medium or DMSO (0.01-0.5%) in the appropriate medium was used as control. Medium containing the stimulatory factors was replaced every 2-3 days.

colOTCs were stimulated directly after air-lift with Wnt-3a and anti-human CCL-2/ IL-8 neutralizing antibodies for 2-4 weeks, while scaOTC were grown in for 2 weeks after air-lift allowing epithelial growth. Thereafter, scaOTCs were stimulated with Vemurafenib for 2-7 weeks. Similarly, fdmOTC were grown for 2 weeks after air-lift in rFAD before stimulating with Cobimetinib and/ or Vemurafenib for 1-5 weeks. Only Wnt-3a treatment of fdmOTCs was started immediately after air-lift and was continued for 4 weeks.

#### 4.2.5.3 Harvest and processing of OTCs

OTCs were incubated with BrdU (65 $\mu M$) for 5 h prior to harvest in order to label proliferating cells. Thereafter, OTCs were taken off the membrane and cut for further processing according to the following.

*(a) Paraffin embedding*

One quarter of each OTC was fixed over night using specialized fixative for anatomy and histology (Morphisto). Afterwards, the samples were subjected to dehydration in increasingly concentrated ethanol solutions and were transferred to xylene prior to paraffin embedding. Sections of formalin-fixed paraffin-embedded (FFPE) colOTCs, scaOTCs or fdmOTCs were cut with 5 µm, 5 µm or 7 µm in diameter, respectively, using a microtome (Leica). Sections were mounted on uncoated microscope slides and were dried at 37 °C for 2 days.

*(b) Cryo-conservation*

One quarter to half of the OTCs was mounted in Tissue Tek, frozen in the gas phase of liquid nitrogen and then stored at -80 °C. For immunofluorescence staining of colOTCs, scaOTCs or fdmOTCs, 7 µm cryo-sections were cut at -26 to -28 °C with a cryostat microtome (Leica) and were mounted on Histobond microscopic slides (Marienfeld). These slides were air-dried and stored at -80 °C.

*(c) Whole-mount preparation*

The epithelium of a quarter of an colOTC was peeled off the dermal equivalent using forceps, while fdmOTCs were not separated as these cultures are translucent. Each OTC was transferred into PBS and fixed in 3.7% (v/v) formaldehyde in PBS for 2 h at RT. After washing 3x in PBS, the epithelium was stored at 4 °C in PBS containing 0.02% (w/v) sodium azide until further antibody staining.

*(d) RNA isolation of fdmOTCs*

For RNA expression analysis comparing gene regulation in the dermal equivalent vs. the epithelium, one quarter of an fdmOTC was incubated with 1 *mg/mL* Dispase II (Roche) for 120 min at 37 °C to digest the BM component Collagen IV. This treatment allowed separating dermal equivalent from

epidermis. Each sample was transferred to a 2 mL screw cap tube containing 1 mL TRIzol Reagent (Life Technologies). Subsequently, the tissue was homogenized using a FastPrep FP120 (Thermo Fischer Scientific) for 2-3x 30 sec at speed 6.0 and further stored at -80 °C. For the subsequent RNA-isolation from OTCs see 4.2.13.2.

*(e) Conditioned medium*

The medium of OTCs was harvested 48 h after medium change. Following centrifuged for 1 min at 3,200 rpm to remove cell debris, conditioned medium was stored at -20 °C until subsequent analysis by ELISA (see 4.2.15).

## 4.2.6 Histology staining of OTC sections

Prior to H/E staining, the FFPE and dried sections (prepared as described in 4.2.5.3a) were deparaffinized by immersion in xylene, followed by stepwise rehydration in graded ethanol solutions of decreasing concentration (100%, 96%, 80% and 70% ethanol) and finally immersed in distilled $H_2O$. Subsequently, sections were stained with haematoxylin and eosin. A 5% (v/v) HCl in 70% (v/v) ethanol bath as well as extended washing steps ensured the removal of excess dye before dehydration of the sections in graded ethanol solutions and xylene. The stained sections were mounted with Eukitt mounting medium (Sigma-Aldrich) and were analyzed using an Olympus BX-51 microscope equipped with a OSIS Color View CCD camera and the accompanying cell^D software (Olympus).

## 4.2.7 Multiplex fluorescence *in situ* hybridization (M-FISH) analysis

To investigate whether continuous Vemurafenib treatment leads to cell selection or additional chromosomal aberrations, M-FISH analysis was performed in collaboration with Prof. Dr. Anna Jauch at the Institute of Human Genetics of the Heidelberg University Hospital. To prepare metaphase spreads, continuously treated HaCaT cells (5 weeks, see 4.2.1.4) were split and when reaching a high proliferation rate, they were arrested in metaphase by incubation with 0.27 *µg/mL* Colcemid (KaryoMAX, Life Technologies) in growth medium for 4 h, 37 °C. Subsequently, HaCaT cells were trypsinized (see 4.2.1), slowly mixed with 15 mL KCl solution (75 *mM*), 37 °C and incubated for 15-20 min in order to lyse the cells by the osmotic pressure. The nuclei were fixed by 3x centrifugation for 10 min at 1,500 rpm, removal of the supernatant and slowly adding 15 mL of a 75% (v/v) methanol/ 25% (v/v) acetic acid solution, 4 °C. Finally, nuclei were resuspended in 0.5-1 mL of 75% (v/v) methanol/ 25% (v/v) acetic acid solution and dripped onto microscopic slides. For RNA and protein digestion, slides were washed in 2x SSC buffer, incubated in 100 *µg/mL* RNase A in 2x SSC buffer for 30-60 min at 37 °C, washed 3x 5 min in 2x SSC buffer and incubated in a 75 *µg/mL* Pepsin (Sigma)/ 0.01 M HCl solution for 10 min at 37 °C. Slides were washed 2x 5 min in PBS, incubated in a 50 *mM* $MgCl_2$/ PBS solution for 5 min, fixed in 1% (v/v) formaldehyde/ 50 *mM* $MgCl_2$/ PBS for 10 min and washed for 5 min in PBS. DNA was dehydrated in graded ethanol solutions of increasing concentration (70%, 90% and 100% ethanol) for 3 min each and was finally air-dried. DNA was denatured in 70% (v/v) formamide/ 2x SSC for 100 min at 75 °C and

dehydrated in graded ethanol solutions of increasing concentration (70%, 90% and 100% ethanol) for 2 min each.

According to Geigl and co-workers (Geigl et al., 2006), seven whole chromosome painting probes, conjugated with DEAC, FITC, Cy3, TexasRed, Cy5, Biotin dUTP or DIG-dUTP, were mixed with 50% (v/v) formamide in 2x SSC and Cot1-DNA. The probes were denatured for 7 min at 75 °C, pre-annealed for 20 min at 37 °C and finally added to the denatured metaphase preparations for hybridization (48 h at 37 °C). Thereafter, slides were washed 2x 5 min in 2x SSC buffer at RT, 2x 7 min in 0.2 % (v/v) SSC/ 0.2% (v/v) Tween-20 solution at 56 °C and 1x 5 min in 4x SSC/ 0.2% (v/v) Tween-20. To detect the Biotin and DIG labeled chromosome probes, indirect immunofluorescence was performed according to the following. Slides were blocked in 3% (w/v) bovine serum albumin (BSA) in 2x SSC buffer for 30 min at 37 °C and were briefly washed in 4x SSC/ Tween-20 solution. The following antibodies were diluted in 1% (w/v) BSA in 4x SSC buffer/ 0.2% (v/v) Tween-20 and added to the slides for 45 min at 37 °C. Primary antibody-step: anti-Streptavidin Alexa-750 (Life Technologies, S21384), secondary antibody-step: anti-Avidin (Vector, BA-300) and anti-Digoxin (Sigma, D7782), third antibody-step: anti-rabbit IgG-Cy5.5 (Calbiochem, 401311) and anti-Streptavidin Alexa-750 (Life Technologies S21384). After the incubation, washing steps were performed 3x 5 min in 4x SSC buffer/ 0.2% (v/v) Tween-20 at 45 °C. Subsequently, slides were incubated with 10 $\mu M$ Biotin in 4x SSC/ 0.2% (v/v) Tween-20 for 10 min at 37 °C, washed 5 min in 4x SSC/ 0.2% (v/v) Tween-20, incubated with 0.2 *mg/mL* DAPI (4',6-diamidino-2-phenylindole) diluted in 2xSSC and mounted. Images were taken using highly specific microscope filters (Chroma Technology, Brattleboro, VT, USA) and were analyzed using Leica MCK Software.

### 4.2.8 *In situ* hybridization

Cryo-conserved samples of human cSCCs and skin without any pathological changes were obtained from several individual donors (approved by the Ethics Commission of University of Heidelberg, Germany; #422005 07.03.2005). For *in situ* hybridization a 245 bp cDNA probe of the WNT2 coding 3'-end (nucleotide position 2473-2717) and a 261 bp cDNA probe of the WNT3 coding 3'-end (nucleotide position 1214-1474) were generated by PCR and cloned into a pCR2.1 vector for synthesis of a specific probe by using T7-RNA polymerase (Roche). As positive control, a specific probe of the KRT14 3′-coding region of 380 bp was used. For Digoxigenin (DIG)-labeling of the cRNA probe, the DIG-RNA labeling Kit (Roche) was used following the instructions of the manufacturer. To detect IL8 and CCL2 mRNA, DIG labeled probes were designed and ordered from Exiqon (IL8: 5'-AGGTAAGATGGTGGCTAATACT-3', CCL2: 5'-ACACTAGTACCATGAAAGATA-3'). After denaturation of cryo-conserved sections of human skin and cSCCs at 90 °C, pre-hybridization with 2x SSC/ 50% formamide and hybridization with the probe was performed at 42 °C over night. Washing was performed at 50 °C including RNase A digestion. For detection, an Alkaline phosphatase-labeled anti-DIG antibody (Roche) was used. For blocking internal tissue phosphatases, samples were treated with 0.2 *mg/mL* Levamisole for 30 min. For the color substrate reaction of the phosphatase, Nitroblue tetrazolium chloride/5-bromo-4-chloro-3-indolyl phosphate substrate tablets (Roche) were used. Positive (Keratin-14) and negative controls (hybridization buffer; sense probes) were included. Samples were analyzed using a BX-51 microscope equipped with an OSIS Color View CCD camera and the accompanying cell^D software (Olympus).

## 4.2.9 Immunohistochemistry (IHC)

To investigate ERK activation in OTCs, phospho-ERK1/2 was stained by immunohistochemistry (IHC) following the REAL EnVision Detection System Peroxidase/ DAB+, Rabbit/ Mouse (Dako). FFPE OTC sections (see 4.2.5.3a) on Superfrost Plus microscopic slides (Thermo Fischer Scientific) were deparaffinized and rehydrated by 2x 5 min xylene, 3 min 95% (v/v) ethanol, 3 min 70% (v/v) ethanol and $dH_2O$ incubation. Antigen retrieval was performed in target retrieval solution (1:10 in $ddH_2O$, Dako) for 20 min at 80 °C followed by 20 min at RT and 5 min in PBS. The sections were further incubated with Peroxidase Block (BioFX Laboratories) for 20 min at RT and were washed 3x 5 min with PBS. Phospho-ERK1/2 antibody (Cell Signaling; see Table 7, 4.1.5) was diluted in 3% BSA and the solution was incubated on the sections for 90 min at RT. Thereafter, slides were washed 3x 5 min in $PBS^+$. Control slides were included which were only incubated with BSA. Afterwards, the sections were incubated with EnVision HRP Rabbit/ Mouse (Dako) for 30 min at RT and were subsequently washed 3x 5 min in $PBS^+$. For detection, DAB+ Chromogen was diluted in DAB+ Buffer (1:50, Dako) and added to the sections for 10 min. Then, sections were rinsed in $dH_2O$ and counterstained by incubation in haematoxylin for 5 min followed by rinsing in $dH_2O$ for 10 min. Slides were dehydrated by 3 min 70% (v/v) ethanol, 3 min 100% (v/v) ethanol, 3 min xylene and were mounted using Eukitt mounting medium (Sigma-Aldrich). Images were taken using the AX-51 microscope equipped with a OSIS Color View CCD camera and the accompanying cell^D software (Olympus Microscopy).

## 4.2.10 Indirect immunofluorescence (IIF)

In this study different IIF-protocols were performed as described below. A list of primary and secondary antibodies is given in Table 7+8 (see 4.1.5).

*(a) Immunofluorescence of OTC cryo-sections*

After briefly washing the cryo sections (see 4.2.5.3b) in $dH_2O$, sections were fixed in 80% (v/v) methanol for 5 min at 4 °C followed by acetone dehydration for 2 min at -20 °C. Air-dried sections were blocked with Blocking buffer (see Table 4, 4.1.2) for 20 min at RT followed by incubation with the primary antibody (see Table 7, 4.1.5), diluted in Blocking buffer, for 1 h at 37 °C + 1 h at RT or alternatively for 30 min at 37 °C + over night at 4 °C. After washing for 5 min in 0.1% (v/v) Triton X-100/ $PBS^+$ solution and 2x 5 min in $PBS^+$, sections were incubated with fluorochrome-conjugated secondary antibodies (see Table 8, 4.1.5) + 5 *µg/mL* Hoechst 33258 (Life Technologies), diluted in Blocking buffer, for 30 min at 37 °C and 30 min at RT. After washing for 5 min in 0.1% (v/v) Triton X-100/ $PBS^+$ solution and 2x 5 min in $PBS^+$, slides were briefly immersed in $dH_2O$ and mounted using Fluorescent Mounting Medium (Dako).

Sections were analyzed employing an Olympus AX-70 fluorescence microscope equipped with a OSIS F View CCD camera and the accompanying cell^R software (Olympus). Images were processed with Adobe Photoshop CS5. For proliferation analysis after BrdU or Ki67 staining complete sections were imaged using a Cell Observer fluorescence microscope equipped with a AxioCam MRm and the

accompanying ZEN software (Zeiss). The number of BrdU/ Ki67-positive keratinocytes was determined with Fiji software and expressed relative to the corresponding BM length as determined by Collagen VII co-staining (proliferation index). The proliferation index was plotted as mean of 2 sections per OTC of 2-3 individual cultures. Statistical significance was calculated by performing a One-way ANOVA + Dunnett's Multiple Comparison Test that compared each treatment modality to the corresponding control.

*(b) Immunofluorescence of OTC whole-mount preparations*

Whole-mount samples (prepared and fixed as described in 4.2.5.3c) were incubated during the whole procedure in 24-well plates with the basal cell layer floating on top of 200 µL liquid. All steps were carried out at RT on a horizontal shaker (70-100 rpm). To quantify proliferation by BrdU-staining, samples were treated with 2 *M* HCl for 25 min followed by washing in Wash buffer 1 (see Table 4, 4.1.2) for 4x 10 min. Thereafter, samples were blocked with Blocking solution (see Table 4, 4.1.2) for 1 h at 100 rpm. Samples were incubated with anti-BrdU antibody over night at RT and 70 rpm. The 24-well plate was additionally sealed with Parafilm (Pechiney Plastic Packaging). On day 2, samples were washed in Wash buffer 2 for 5x 45 min at 100 rpm. Then, samples were incubated with anti-mouse IgG-Cy3 antibody + 5 *µg/mL* Hoechst 33258, diluted in 0.5% Triton X-100/ PBS solution, over night at RT and 70 rpm. Again, plates were sealed with Parafilm. On day 3, samples were washed in Wash buffer 2 for 5x 45 min. Afterwards, the samples were placed on microscopic slides with the basal cell layer facing away from the glass. The whole-mounts were embedded with Fluorescent Mounting Medium and analyzed using a Cell Observer fluorescence microscope equipped with a AxioCam MRm and the accompanying ZEN software (Zeiss). Each whole-mount was entirely imaged and the number of all cells (Hoechst positive) and BrdU-positive cells was determined with Fiji to calculate the percentage of proliferation. The mean proliferation of 5,000 cells per data point and OTC was plotted. Statistical significance was calculated by performing a One-way ANOVA + Dunnett's Multiple Comparison Test that compared each treatment modality to the corresponding control.

### 4.2.11 *In situ* zymography (Gelatinase assay)

To visualize *in situ* MMP-activity, the quenched fluorescin-labeled DQ-gelatin (EnzChek Gelatinase/ Collagenase Assay Kit, Life Technologies) was employed. Upon cleavage of the Gelatin substrate, quenching is released and fluorescence signals can be visualized. Therefore, 10x Gelatinase assay buffer was prepared according to the manufacturer's protocol: 0.5 *M* Tris-HCl, 1.5 *M* NaCl, 50 *mM* $CaCl_2$, 2 *mM* sodium azide, pH 7.6. Cryostat sections of OTCs (see 4.2.5.3b) were incubated in 1x Gelatinase assay buffer supplemented with 50 *µg/mL* DQ-gelatin and 5 *µg/mL* Hoechst 33258 for 60 min at RT. Sections were washed 2x 5 min in PBS and subsequently fixed in 80% (v/v) methanol for 5 min at 4 °C followed by acetone dehydration for 2 min at -20 °C. Air-dried sections were mounted using Fluorescent Mounting Medium (Dako) and immediately examined employing an Olympus AX-70 fluorescence microscope equipped with a OSIS F View CCD camera and the accompanying cell^R software (Olympus). Fluorescence was documented using equal exposure times for all sections.

### 4.2.12 Mutation analysis of genomic DNA

To analyze genomic DNA of keratinocytes representing different stages of skin carcinogenesis for frequently occurring mutations, DNA was isolated from cultured cells and the quality was confirmed by NanoDrop spectroscopic measurement as well as by Agarose gel electrophoresis. Thereafter, a somatic mutation PCR array was performed using a LightCycler 480 Instrument II (Roche).

#### 4.2.12.1 Isolation of genomic DNA

Cell pellets of 5x $10^6$ cells, prepared by trypsinization as described (see 4.2.1.2), were lysed and processed with the QIAamp DNA Mini Kit (QIAGEN) including Protease plus RNase A digestion according to the manufacturer's instructions. Elution of the genomic DNA was performed with 200 µL nuclease free water (QIAGEN) and the concentration was determined with a NanoDrop ND-1000 spectrophotometer (Thermo Fischer Scientific). The quality was confirmed by measuring the OD260/OD280 (approx. 1.8) and OD260/OD230 (approx. 1.7) by a NanoDrop ND-1000. DNA integrity was confirmed by Agarose gel electrophoresis. DNA was stored at -80 °C.

#### 4.2.12.2 Agarose gel electrophoresis of genomic DNA

Genomic DNA quality can be assessed by detecting DNA fragments larger than 2 kb in length with some fragments greater than 10 kb. This was analyzed by separating the genomic DNA according to the size using Agarose gel electrophoresis. Therefore, 1% (w/v) agarose was solubilized in 1x TBE (see Table 4, 4.1.2) and boiled with 0.01% (v/v) SYBR Safe DNA gel stain, allowing detection of the DNA. 500 ng of each isolation was mixed with DNA loading dye (3x, see Table 4, 4.1.2), loaded onto the polymerized agarose gel in 1x TBE and separated at 100 V (constant). Lambda DNA-Hind III Ladder (4 µL per lane) was used as marker. DNA fragments as well as the ladder were visualized by irradiation at 254 nm. For all DNA isolations, DNA integrity was confirmed.

#### 4.2.12.3 Somatic mutation PCR array

The Human Skin Cancer qBiomarker Somatic Mutation PCR Array (QIAGEN) allows profiling of the 78 most frequent somatic mutations in human skin cancer samples. The array includes mutations within the following genes: BRAF, CDKN2A, CTNNB1, FGFR3, GNAQ, HRAS, KIT, KRAS, NRAS, PIK3CA, PTCH1, PTEN, RB1, SMO, LKB1/STK11 and TP53. The kit was used to characterize mutations in HaCaT and HaCaT-RAS II-4 cells as well as in the SCC cell lines SCL-I, SCL-II, SCC-12, SCC-13, MET-1 and MET-4. NHEK 1 (see Table 11, 4.1.7) that do not show any somatic mutation in the analyzed set of genes was used to normalize the assay.

After quality and integrity control, 3 µg genomic DNA per cell type and 96-well plate was used for the PCR reaction using a LightCycler 480 Instrument II (Roche) according to the manufacturer's protocol with the following settings: initial heating for 10 min at 95 °C and 40 cycles composed of 15 sec at 95

°C (ramp rate: 1 °C/sec), 60 sec at 60 °C (ramp rate: 1 °C/sec). Fluorescence was measured after each cycle. The crossing point (CP) of each gene in a given sample that identifies the cycle number at which the fluorescence signal rises above a certain threshold fluorescence was obtained using the Second Derivative Maximum method with High Confidence setting of the LightCycler 480 Software (Roche). The assay was performed in duplicates per analyzed cell line (n=2) and the mutational characterization was performed using the supplied Data Analysis Template Excel Sheet (QIAGEN).

### 4.2.13 Gene expression analysis

For investigating gene expression in monoculture cells as well as in organotypic cultures, RNA was isolated and transcribed to cDNA. Quantitative PCR allowed relative gene expression analysis by comparing target gene expression normalized to the house-keeping gene GAPDH in treated vs. untreated cells or OTCs.

#### 4.2.13.1 RNA-isolation from cultured cells

Cell pellets, prepared by trypsinization (see 4.2.1.2), were lysed and processed with the QIAshredder Kit (QIAGEN), according to the manufacturer's instructions. Thereafter, RNA isolation was performed using the RNeasy Mini Kit (QIAGEN) with an additional DNase digestion (RNase free DNase Set, QIAGEN). Elution of RNA was performed with 35 µL RNase-free water. The concentration was determined with a NanoDrop ND-1000 spectrophotometer (Thermo Fischer Scientific) and the quality was confirmed by measuring an OD260/OD280 > 2.0. RNA was stored at -80 °C until further use for reverse transcription.

#### 4.2.13.2 RNA-isolation from OTCs

Each epidermal or dermal tissue homogenized in TRIzol Reagent (see 4.2.5.3d) was thawed and centrifuged for 10 min at 12,000 rpm to remove remaining cell debris or ECM. The supernatant was mixed with 0.2 mL chloroform (Roth) for 15 sec and incubated for 2-3 min at RT. After centrifugation for 15 min at 12,000 rpm, 4 °C the upper aqueous phase was carefully transferred to a fresh tube. RNA was precipitated by adding 500 µL isopropyl alcohol per 600 µL transferred solution, incubation for 10 min at RT and centrifugation for 10 min at 12,000 rpm, 4 °C. The pellet was washed with 1 mL of 75% (v/v) ethanol, precipitated by centrifugation for 10 min at 9,000 rpm, 4 °C, air-dried and dissolved in nuclease-free water. The concentration was determined with a NanoDrop ND-1000 spectrophotometer (Thermo Fischer Scientific) and the quality was confirmed by measuring an OD260/OD280 > 2.0. RNA was stored at -80 °C until further use for reverse transcription.

### 4.2.13.3 Reverse Transcription

cDNA synthesis was performed with the RevertAid H Minus First Strand cDNA Synthesis Kit (Thermo Fischer Scientific). In particular, 4 µg total RNA was transcribed in a 40 µL reaction mix according to the manufacturer's instructions: RNA was mixed with RNase free water ad 22 µL + 2 µL oligo $(dT)_{18}$ primer (1 *µg/µL*), followed by incubations for 5 min at 65 °C and 5 min at 4 °C. Afterwards, 8 µL reaction buffer (5x), 4 µL dNTP mix (10 *mM*), 2 µL RiboLock Ribonuclease Inhibitor (10 *U/µL*) and 2 µL RevertAid H Minus M-MuLV Reverse Transcriptase (200 *U/µL*) were added. The reverse transcription was carried out at 42 °C for 1 h and was stopped by heating to 70 °C for 10 min. cDNA was further stored at -20 °C for real-time PCR.

### 4.2.13.4 Real-time/ quantitative RT-PCR (qRT-PCR)

Quantitative RT-PCR (qRT-PCR) allows the relative quantification of mRNA expression. Therefore, the Universal Probe Library (UPL) system (Roche) was used and qRT-PCR was performed in a 96-well plate based LightCycler 480 Instrument II (Roche) according to the manufacturer's instructions. The primers were designed using the UPL tool (www.universalprobelibrary.com; for primers and probes see Table 6, 4.1.4). Each reaction consisted of a 15 µL mix in nuclease free water containing 10 µL LightCycler 480 master (2x), 0.4 *µM* forward and reverse primers (stock: 10 *µM*) and 0.1 *µM* UPL-probe (stock: 10 *µM*). 50 ng cDNA in 5 µL RNase free water was added after the reaction mix into each well. A negative control containing water instead of cDNA was performed for each primer pair and every qRT-PCR was performed in technical duplicates. The reaction was incubated in a PCR 96-well TW-MT Plate, white (Biozym) that was sealed with Adhesive Clear qPCR Seals (Biozym), centrifuged at 2,000 rpm for 1 min and run according to the following: After a pre-incubation for 10 min at 95 °C, 45 cycles were carried out, each consisting of 10 sec at 95 °C (ramp rate 4.4 °C/sec), 30 sec at 60 °C (ramp rate 2.2 °C/sec) and 1 sec at 72 °C (ramp rate 4.4 °C/sec). Fluorescence was measured after each cycle. To verify the quality of the primer/ probe combination and the efficiency of the PCR reaction, standard curves were performed for each primer pair using a dilution series of 100, 20, 4, 0.80 and 0.16 ng pooled cDNA for each target cell type.

For relative quantification, the gene of interest (target) and the housekeeping gene GAPDH (reference) were compared for each control and stimulated sample. For this calculation, the CP of each gene in a given sample that identifies the cycle number at which the fluorescence signal rises above certain threshold fluorescence, was obtained using the Second Derivative Maximum method of the LightCycler 480 Software (Roche). With these CP values the ratio of the relative gene expression of control vs. treated sample, normalized to the housekeeping gene GAPDH, was calculated using the formula proposed by Pfaffl (Pfaffl, 2001). Data was displayed using linear or logarithmic scales, whereas the corresponding control was always set to one.

## 4.2.14 Protein expression and phosphorylation analysis

To determine protein expression as well as the activity of signaling pathways by phosphorylation

analysis of key proteins, total protein was isolated from control or treated cells and quantified by protein assay. Proteins were separated according to their size by SDS-Polyacrylamide gel electrophoresis (SDS-PAGE) and protein of interest levels were analyzed by Western-Blot using specific primary and secondary antibodies (see Table 7+8, 4.1.5).

### 4.2.14.1 Protein extraction

Thawed cell pellets harvested by detachment (see 4.2.1.2) were resuspended on ice in 150-200 µL freshly prepared RIPA lysis buffer (see Table 4, 4.1.2) and further incubated for 30 min at 4 °C. In order to pellet cell debris, the suspension was centrifuged for 20 min at 14,000 rpm, 4 °C. The protein-containing supernatant was transferred to a fresh tube and stored at -80 °C.

### 4.2.14.2 Protein assay

To determine the total protein concentration of the different extractions the Pierce BCA Protein Assay Kit (Thermo Fischer Scientific) was used according to the manufacturer's protocol. The lysates were diluted 1:10 with $ddH_2O$ to a total volume of 60 µL and 25 µL was added in technical duplicates to a 96-well plate (flat bottom). In addition, a BSA standard, ranging from 0-2,000 *µg/mL* total protein, was included. 200 µL of the supplied reaction mix was added to each protein dilution. After 30 min incubation at 37 °C, the optical density was determined at 595 nm using a Multiskan FC Microplate Photometer (Thermo Fischer Scientific). The protein concentration of the cell lysates was calculated according to the BSA standard curve.

### 4.2.14.3 SDS-PAGE

Total protein lysates were separated according to the size of individual proteins by SDS-PAGE. Therefore, discontinuous 10% SDS-PA gels were polymerized using the Mini-PROTEAN Tetra Cell system (Bio-Rad). 30 µg total protein per lane of each lysate was mixed with Protein loading dye (5x, see Table 4, 4.1.2), boiled for 5 min at 95 °C and loaded onto the SDS-PA gels. Rainbow Molecular Weight Marker (Full-Range, GE Healthcare) was loaded to estimate the corresponding molecular size. The protein samples were separated in a chamber filled with Running buffer (see Table 4, 4.1.2) at 200 V (constant) using a PowerPac HC (Bio-Rad) power supply until the dye front reached the end of the gel.

### 4.2.14.4 Western-Blot

SDS-PA gels were blotted on Nitrocellulose membrane (Whatman) using a Mini Trans-Blot Module wet transfer device (Bio-Rad) according to the manufacturer's instructions. Accordingly, the membrane was activated in $ddH_2O$, followed by incubation in Transfer buffer (see Table 4, 4.1.2). Blotting was performed in the device filled with Transfer buffer for 2.5 h at 48 V (constant) using a PowerPac HC

(Bio-Rad) power supply. When completed, Ponceau staining of the membrane was used to confirm the transfer.

The membrane was blocked in Blocking buffer (see Table 4, 4.1.2) for 90 min at RT on a rotating shaker. Then, the membrane was rinsed twice in PBS before incubation with the appropriate primary antibody (see Table 7, 4.1.5) diluted in 3% (w/v) BSA/ 0.1% (v/v) Tween 20 in PBS with 0.02% (w/v) sodium azide over night at 4 °C. Afterwards, unbound antibody was removed by washing 3x 10 min in Wash buffer (see Table 4, 4.1.2). The secondary antibody (see Table 8, 4.1.5) was diluted in Blocking buffer and incubated on the membrane for 45-60 min at RT on an rotating shaker. Again, unbound antibody was removed by incubation with Wash buffer for 3x 10 min at RT. The secondary antibodies were visualized using Amersham ECL Advance Western Blotting Detection Kit (GE Healthcare) with a 1:10 dilution of the substrate solution in $ddH_2O$. The signals were detected on Medical X-ray film (FujiFilm). All antibody incubations were performed on a rotating shaker, whereas an orbital shaker at 250 rpm was utilized for the washing steps.

### 4.2.15 Enzyme-linked immunosorbent assay (ELISA)

To study the protein levels of CCL-2, IL-8, pro MMP-1, MMP-3 and MMP-9 in conditioned medium, the ELISA Kits Quantikine Human CCL-2/ MCP-1, Quantikine CXCL-8/ IL-8, Quantikine Human Pro-MMP-1, Quantikine Human MMP-3 and Quantikine Human MMP-9 Immunoassay (all R&D Systems) were used. Conditioned medium was collected from treated OTCs (see 4.2.5.3e). The ELISAs were performed as described in the manufacturer's protocol. Supernatants were diluted when necessary in the supplied solution. A Multiskan FC Microplate Photometer (Thermo-Scientific) was used to perform the readout at 450 nm with enabled background subtraction at 620 nm. Protein concentrations were calculated according to a standard curve of recombinant protein that was included in each kit. Statistical significance was calculated by performing a One-way ANOVA + Dunnett's Multiple Comparison Test or Two-way ANOVA + Bonferroni posttest, which both compare each treatment modality to the corresponding controls.

### 4.2.16 Statistics

Depending on the obtained data One-way or Two-way Analysis of variance (ANOVA) was performed with or without posttest as indicated in the corresponding method section or figure legend.

# 5. Results

In order to study skin carcinogenesis, different human cell lines and cultivation systems have been identified that display cancer progression and were employed to study the effects of Wnt/Beta-catenin and specific B-Raf inhibitors on the development of cSCC. A model for functional studies bases on the HaCaT keratinocytes, which were obtained by culturing keratinocytes of a healthy, 62 year-old donor under low calcium and elevated temperature allowing the spontaneous transformation. HaCaT cells are immortal but remain non-tumorigenic upon injection into immunodeficient mice. HaCaT cells also show chromosomal alterations that are characteristic for SCCs, such as loss of 3p, 9p and gain of 3q (Boukamp et al., 1988; Boukamp et al., 1997) as well as UV-B type-specific mutations in both alleles of the p53 gene (Lehman et al., 1993). Despite the unlimited growth potential, they form a structured and fully differentiated epidermis on nude mice and thereby, express differentiation state specific keratins and other markers. These properties render HaCaT cells as early stage model of skin carcinogenesis (Boukamp et al., 1988; Ryle et al., 1989). Transfection of the parental HaCaT cells with H-Ras$^{G12V}$ led to the generations of benign-tumorigenic HaCaT-RAS A-5 and malignant-tumorigenic HaCaT-RAS II-4 cells, representing two further steps in skin cancer progression (Boukamp et al., 1990; Mueller and Fusenig, 1999). Moreover, cross-talk between keratinocytes and fibroblasts, spacial distribution and the cellular environment are also crucial aspects to investigate that were considered when developing different 3D organotypic co-culture models (OTCs).

## 5.1 Wnt/Beta-catenin signaling in cSCC development and progression

Wnt/Beta-catenin activation is well-known in tumorigenic keratinocytes of cSCC. However, we could additionally detect nuclear Beta-catenin, a hallmark for Wnt pathway activity, in fibroblasts surrounding the tumor, suggesting a role for stromal Wnt/Beta-catenin activation in cSCC progression. Furthermore, global gene expression analysis of Wnt-3a stimulated NHDF revealed a strong upregulation of the cytokines IL-8 and CCL-2 as well as of the matrix remodeling factor MMP-1 (Sobel, Tham et al., 2015). Thus, potential roles of the NHDF-derived factors IL-8, CCL-2 and MMP-1 on cSCC development and/or progression were investigated in monolayer cultures as well as in 3D OTCs.

### 5.1.1 Wnt-3a induces IL-8 and CCL-2 expression in colOTCs

To analyze the effects of Wnt-3a as well as of IL-8 and CCL-2 in a 3D environment, collagen-based organotypic cultures (colOTCs) were employed (Schoop et al., 1999). Therefore, NHDF were embedded into a Collagen type I gel and seeded into filter inserts forming a dermal equivalent. Subsequently, HaCaT cells were seeded on top of the dermal equivalents and were grown air-exposed, forming a multi-layered stratified epithelium (see 4.2.5). Wnt-3a stimulation (100 *ng/mL*) for 2 and 4 weeks was performed though the culture medium. In addition to Wnt-3a, neutralizing antibodies targeting IL-8 (nIL-8) and CCL-2 (nCCL-2) were used to specifically inhibit effects of these cytokines.

To ask whether IL-8 and CCL-2 are indeed secreted in Wnt-3a stimulated colOTCs, conditioned medium was harvested over the entire culture time and analyzed by immunoassays. IL-8 protein level increased

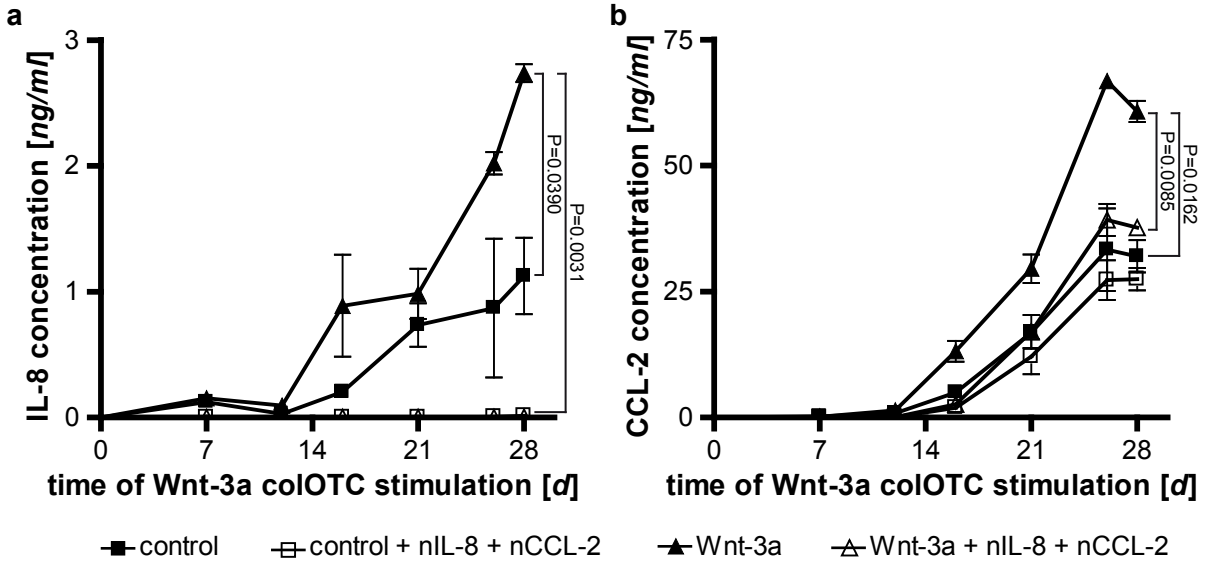


Figure 9 | **Wnt-3a leads to IL-8 and CCL-2 secretion in colOTCs.**

colOTCs were prepared by seeding HaCaT cells on top of a dermal equivalent, consisting of NHDF embedded in a Collagen type I matrix. HaCaT colOTCs were stimulated with Wnt-3a (100 *ng/mL*) for 4 weeks through the culture medium. In addition, neutralizing antibodies targeting IL-8 (nIL-8, 1 *mg/mL*) and CCL-2 (nCCL-2, 4 *mg/mL*) were used to specifically inhibit effects of these cytokines. Conditioned medium was analyzed by ELISAs for IL-8 (**a**) and CCL-2 (**b**). Both cytokines were significantly increased in Wnt-3a stimulated cultures. The addition of nIL-8 and nCCL-2 to Wnt-3a treated OTCs caused a significant reduction of IL-8 and CCL-2 levels in Wnt-3a colOTCs. [n=2, mean ± SD, Two-way ANOVA + Bonferroni posttest]

with time in Wnt-3a treated cultures to 2.7 *ng/mL* on day 28 (Fig. 9a). CCL-2 levels reached a maximum of 61 *ng/mL* at day 24 (Fig. 9b). Although IL-8 and CCL-2 protein levels were increasing in control cultures as well, Wnt-3a treatment caused a significant increase of both cytokines (IL-8: P=0.039, CCL-2: P=0.016). Interestingly, the cytokines became measurable after 7 days of OTC cultivation compared to a direct expression in monoculture NHDF (Sobel, Tham et al., 2015). Since IL-8 and CCL-2 are probably highly expressed in NHDF upon Wnt-3a stimulation also in 3D, this finding suggested that both cytokines are retained in the ECM of colOTCs at the early time points, before becoming measurable in the culture medium. Furthermore, control and Wnt-3a cultures were additionally treated with neutralizing antibodies. As result, IL-8 was completely eliminated in the medium of both culture types (P=0.003, Fig. 9a), whereas CCL-2 levels were slightly reduced in control, but significantly decreased in Wnt-3a cultures by nCCL-2 treatment (P=0.009, Fig. 9b).

After 2 weeks of cultivation, histological analysis revealed a thin HaCaT cell epithelium without terminal differentiation. Stimulation with Wnt-3a or treatment with neutralizing antibodies (nIL-8, nCCL-2) did not alter the epithelial morphology (Fig. 10 a-d). After 4 weeks, all epithelia increased in thickness and showed some differentiating layers. As control colOTCs (Fig. 10e) were comparable to cultures treated with nIL-8 and nCCL-2, demonstrated that the neutralizing antibodies neither altered epithelial growth and differentiation nor caused major toxicity (Fig. 10f). Importantly, by stimulating OTCs with Wnt-3a for 4 weeks, HaCaT cells grew invasively into the underlying dermal equivalent (Fig. 10g). This was prevented by additional treatment of Wnt-3a cultures with both neutralizing antibodies (Fig. 10h) suggesting that IL-8 and CCL-2 facilitate invasion in some areas of colOTCs.

To analyze differentiation and invasion in more detail, indirect immunofluorescence was performed to investigate the late differentiation marker Filaggrin, expressed from stratum granulosum to stratum corneum in normal skin (Watt, 1989) as well as integrity proteins of the BM. Since Filaggrin expression

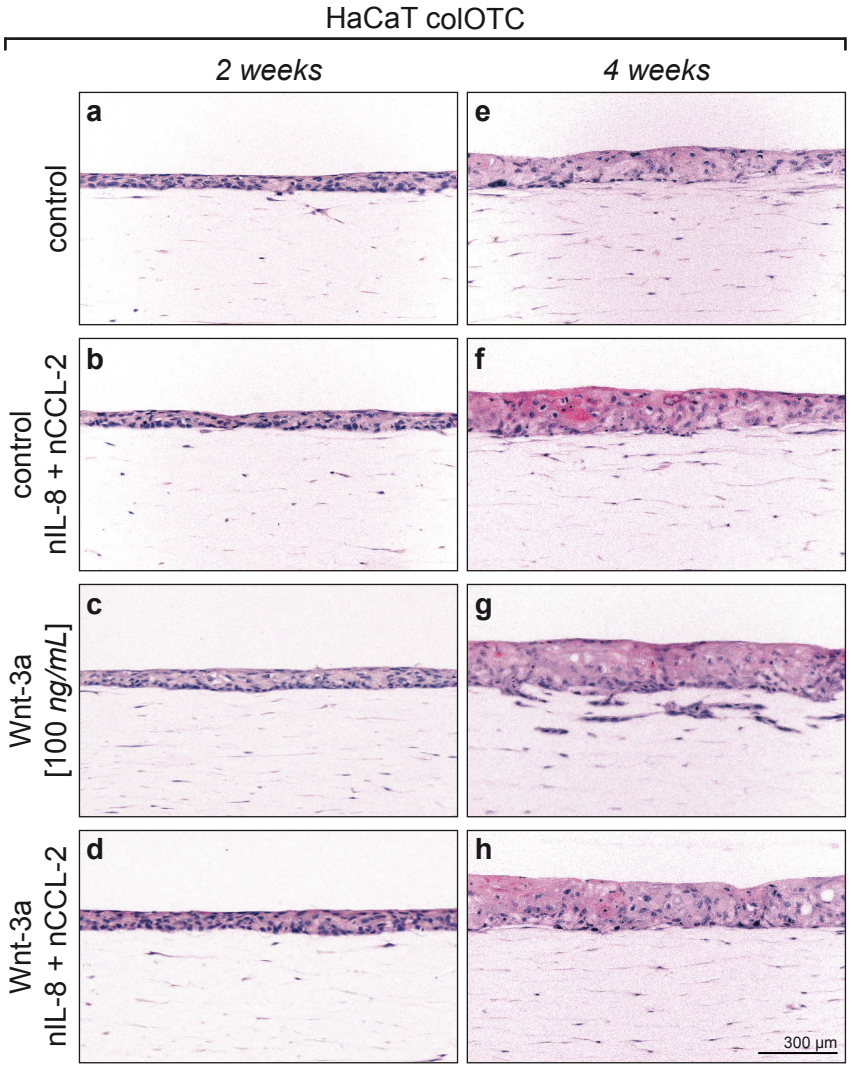


Figure 10 | **Invasion in HaCaT colOTCs is triggered by Wnt-3a induced IL-8 and CCL-2.**
colOTCs were prepared by seeding HaCaT cells on top of a dermal equivalent, consisting of NHDF embedded in a Collagen type I matrix. OTCs were stimulated with Wnt-3a (100 *ng/mL*) through the culture medium. In addition, neutralizing antibodies targeting IL-8 (nIL-8, 1 *mg/mL*) and CCL-2 (nCCL-2, 4 *mg/mL*) were used to specifically inhibit effects of these cytokines. FFPE sections were stained with haematoxylin/ eosin to analyze the morphology. **a-d** | After 2 weeks, cultures revealed a thin undifferentiated HaCaT cell epithelium (a). Treatment with neutralizing antibodies (b), Wnt-3a (c) or both (d) did not alter the epithelial morphology. **e-h** | After 4 weeks, control (e) and nIL-8 + nCCL-2 treated cultures (f) showed some stratified layers. Stimulation with Wnt-3a led to invasive growth of HaCaT cells (g), which was prevented by the addition of nIL-8 and nCCL-2 (h). [n=2]

and localization was not changed by any treatment after 4 weeks, terminal differentiation did not seem to be altered. However, more differentiation markers should be analyzed to clearly answer this question (Fig. 11a-c). The BM separates dermis from epidermis and is composed of many proteins including lamins, HSPGs and collagens, but especially of Collagen IV. Keratinocytes adhere to the BM by cell surface proteins like Integrin (Kalluri, 2003). An Integrin beta-4 and Collagen IV staining between dermis and HaCaT epithelium revealed a continuous BM in control cultures (Fig. 11a, d). Interestingly, Wnt-3a stimulation led to reduction of both, Integrin beta-4 and Collagen IV, suggesting that this may have caused invasive growth in some areas of the HaCaT colOTCs (Fig. 11b, e). Neutralizing of IL-8 and CCL-2 in Wnt-3a treated cultures led to a similar BM as observed in control cultures (Fig. 11c, f). This suggested that the invasive phenotype actually correlates with IL-8 and CCL-2 expression.

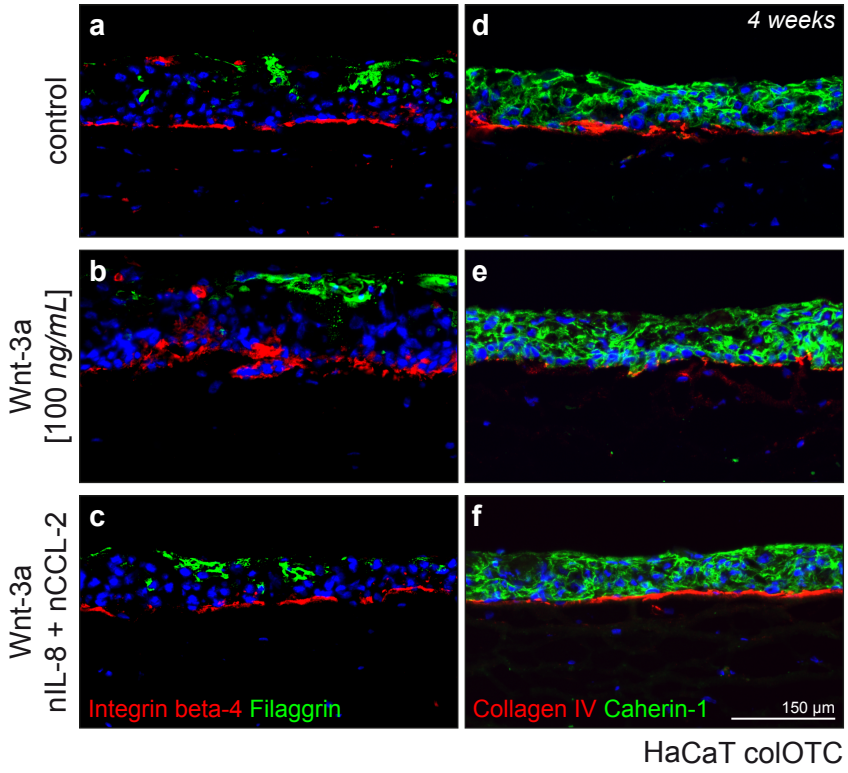


Figure 11 | **IL-8 and CCL-2 do not affect HaCaT cell differentiation, but reduce BM proteins.**
colOTCs were prepared by seeding HaCaT cells on top of a dermal equivalent, consisting of NHDF embedded in a Collagen type I matrix. HaCaT colOTCs were stimulated with Wnt-3a (100 *ng/mL*) through the culture medium. In addition, neutralizing antibodies targeting IL-8 (nIL-8, 1 *mg/mL*) and CCL-2 (nCCL-2, 4 *mg/mL*) were used to specifically inhibit effects of these cytokines. Cryo-sections of 4 week-old cultures were fixed to analyze differentiation and BM integrity by immunofluorescence. **a-c** | Expression and localization of the late differentiation marker Filaggrin (green) was not altered by any treatment. [n=2] **a-f** | Staining for the BM markers Integrin beta-4 (red) and Collagen IV (red) showed a continuous BM in control cultures, while Cadherin-1 (green) served as epithelial marker (a, d). Wnt-3a stimulation caused a reduction of Integrin beta-4 and Collagen IV (b, e), whereas additional treatment with nIL-8 and nCCL-2 resembled the BM staining of control cultures (c, f). [n=2]

## 5.1.2 IL-8 and CCL-2 increase HaCaT cell proliferation

Although both, IL-8 and CCL-2 are described to trigger proliferation in various cell types (Mishra et al., 2011; Steude et al., 2002; Tuschil et al., 1992), the effect of these chemokines on keratinocytes remains largely elusive. Therefore, I asked whether Wnt-3a induced levels of both cytokines also increase proliferation of HaCaT cells in colOTCs after 2 weeks. To quantify proliferation, the thymidine analogue BrdU was added to the OTCs prior to harvest for 5 h and thereafter, epithelial whole-mounts of OTCs were prepared by physically separating the epidermis from the dermal equivalent. BrdU staining of the entire whole-mount by immunofluorescence (Fig. 12a) revealed either 13% or 19% BrdU-positive HaCaT cells in control or nIL-8 + nCCL-2 treated colOTCs. Wnt-3a stimulation significantly increased proliferation to 31% ($P<0.001$). Most importantly, this increase was prevented by co-treatment with the neutralizing antibodies, keeping HaCaT cell proliferation at the control rate of 19% ($P<0.001$, Fig. 12b). As both cytokines were simultaneously neutralized within the culture medium, either IL-8, CCL-2, or the combination of both was directly responsible for increased HaCaT proliferation in colOTCs.

To answer which factor induced HaCaT cell proliferation, stimulation with each cytokine or the combination of both was repeated in HaCaT cell proliferation in monolayer cultures. Proliferation was quantified employing the SYBR Green cell proliferation assay. As positive control, 10 *ng/mL* of the

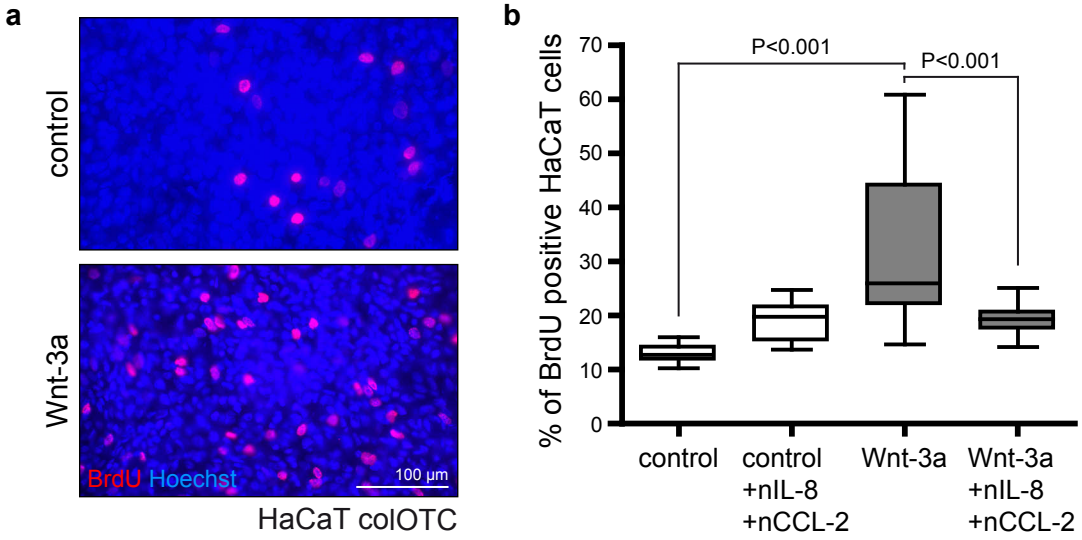


Figure 12 | **Wnt-3a leads to IL-8 and CCL-2-dependent increased HaCaT cell proliferation in 3D.**
colOTCs were prepared by seeding HaCaT cells on top of a dermal equivalent, consisting of NHDF embedded in a Collagen type I matrix. HaCaT colOTCs were stimulated with Wnt-3a (100 *ng/mL*) through the culture medium. In addition, neutralizing antibodies targeting IL-8 (nIL-8, 1 *mg/mL*) and CCL-2 (nCCL-2, 4 *mg/mL*) were used to specifically inhibit effects of these cytokines. **a** | Proliferation was assessed in epithelial whole-mounts prepared by peeling the epithelium from the dermal equivalent of 2 week-old OTCs. The fixed whole-mounts were analyzed by immunofluorescence staining for BrdU (red) and nuclei (blue). **b** | Wnt-3a stimulated OTCs significantly increased proliferation of basal HaCaT cells compared to controls. Depletion of IL-8 and CCL-2 with neutralizing antibodies prevented this Wnt-3a effect. [n=2, box plot with median, One-way ANOVA + Dunnett's Multiple Comparison Test]

known mitogen EGF (Dhillon et al., 2007) led to a significant increase in HaCaT cell proliferation compared to unstimulated cells (P<0.001). Moreover, stimulation of HaCaT cells with 10 *ng/mL* IL-8 or 100 *ng/mL* CCL-2 for 24–72 h, representing the protein levels determined in OTCs, caused an even stronger increase in proliferation (P<0.001). Interestingly, combining both factors did not further increase proliferation suggesting that a maximal stimulation of HaCaT cells was reached already by each individual factor (Fig. 13). This, clearly showed that IL-8 and CCL-2 are potent and atypical mitogens for keratinocytes that directly affected HaCaT cell growth in monolayer cultures and OTCs.

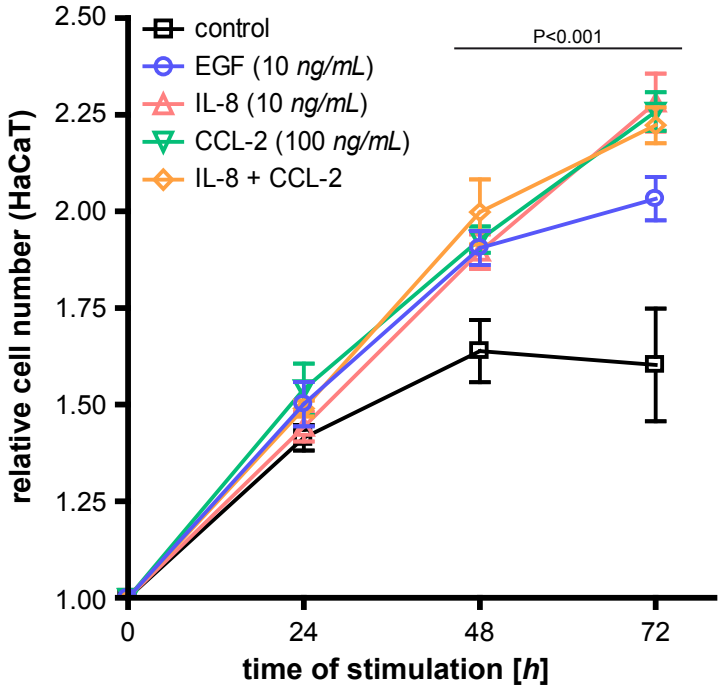


Figure 13 | **IL-8 and CCL-2 directly increase HaCaT cell proliferation.**
HaCaT cell monolayer cultures were stimulated with human recombinant EGF (10 *ng/mL*), IL-8 (10 *ng/mL*), CCL-2 (100 *ng/mL*) or a combination of IL-8 and CCL-2 for 24-72 h. Proliferation was quantified by SYBR Green cell proliferation assay. Stimulation with the known mitogen EGF led to a significantly elevation, while IL-8, CCL-2 or the combination of both even further increased HaCaT cell proliferation. [n=2, mean ± SEM, Two-way ANOVA + Bonferroni posttest]

## 5.1.3 Wnt-3a induces MMP expression in colOTCs

Another Wnt-3a target gene identified by global gene expression analysis in NHDF was MMP1. MMPs are responsible for the degradation of the ECM, a process required for tumor cell invasion (Lynch and Matrisian, 2002) and thus, are crucial in preparing a permissive tumor stroma. Several MMPs were shown to be direct Wnt target genes (Brabletz et al., 1999; Lowy et al., 2006; Takahashi et al., 2002). As we found MMP1 to be upregulated in Wnt-3a-treated NHDF (Sobel, Tham et al., 2015), I investigated whether MMP1 triggered invasive growth of non-tumorigenic HaCaT cells. First, the expression of pro MMP-1 was analyzed by immunoassay of conditioned colOTC medium. As result, pro MMP-1 accumulated over the cultivation period of 4 weeks in HaCaT control colOTCs, reaching a maximum of 1,005 *ng/mL*. At the same time, Wnt-3a stimulation significantly increased secretion of pro MMP-1 to 1,320 *ng/mL* (P=0.033, Fig. 14a). Using DQ-Gelatin *in situ* zymography to directly assay for active MMPs in colOTCs sections, demonstrated a low gelatinolytic activity (green) in the dermal equivalents of controls, while Wnt-3a-treatment caused an increased MMP-activity (Fig. 14b, c). Additionally, Wnt-3a-treated OTCs stained strongly with an antibody that specifically detects Collagenase-cleaved Collagen type I and II compared to control cultures (Figs. 14e, f), thus, confirming an active matrix degradation by MMP-1. Importantly, IL-8 and CCL-2 neutralization in Wnt-3a stimulated cultures reduced neither pro MMP-1 levels, which was still significantly increased (1,554 *ng/mL* after 4 weeks) compared to control cultures (P=0.006, Fig. 14a), nor MMP-activity (Fig. 14d) or levels

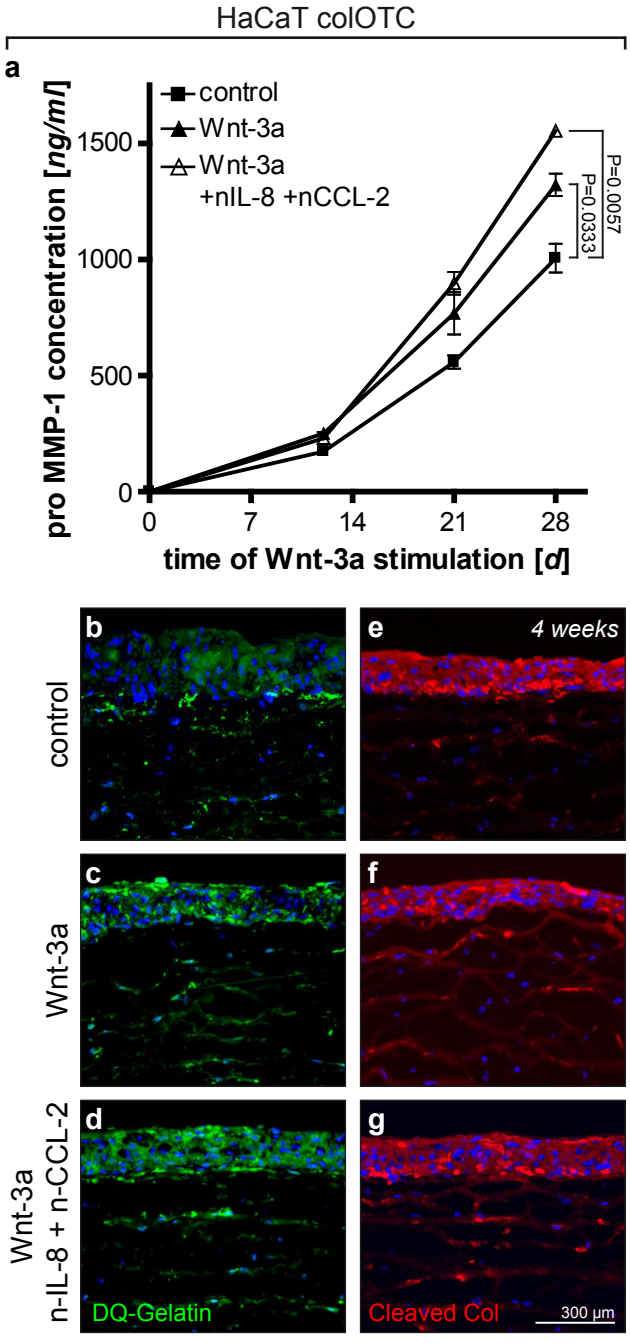


Figure 14 | **Wnt-3a causes pro MMP-1 secretion and MMP-activity in HaCaT colOTCs.**
HaCaT colOTCs were stimulated with Wnt-3a (100 *ng/mL*) through the culture medium. In addition, neutralizing antibodies targeting IL-8 (nIL-8, 1 *mg/mL*) and CCL-2 (nCCL-2, 4 *mg/mL*) were used to specifically inhibit effects of these cytokines. **a** | Conditioned medium was analyzed by ELISA for pro MMP-1 protein levels during 28 days of cultivation. Wnt-3a treatment significantly increased pro MMP-1 secretion compared to controls. Wnt-3a effects on pro MMP-1 were not altered by depletion of IL-8 and CCL-2. [n=2, mean ± SD, Two-way ANOVA + Bonferroni posttest] **b-d** | *In situ* zymography to analyze MMP-activity in 4 week-old cryo-conserved HaCaT colOTCs revealed only weak gelatinolytic activity (green) in control OTCs (b). Stimulation with Wnt-3a strongly increased gelatinolytic activity (c), which was not reduced by IL-8 and CCL-2 neutralization (d). [n=3]. **e-g** | In agreement, immunofluorescence for collagen cleavage products in 4 week-old cultures demonstrated a strong accumulation of cleaved collagen (red) only in sections of Wnt-3a-treated cultures (f), but not in untreated OTC sections (e). This was not altered by nIL-8 and nCCL-2 (g). [n=2]

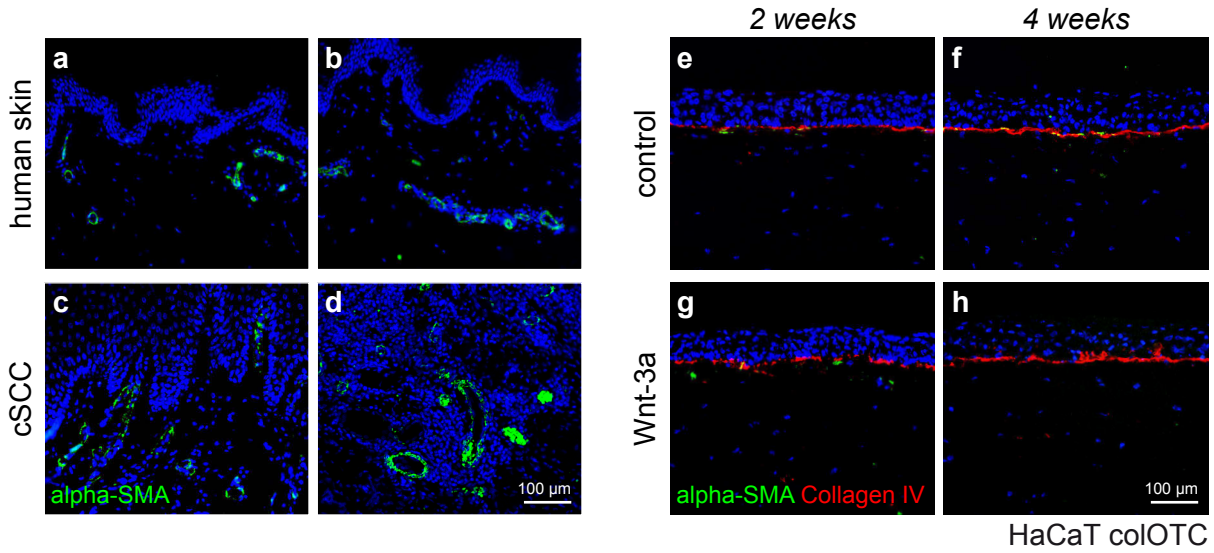


Figure 15 | **Myofibroblasts are not present in Wnt 3a-treated OTCs or cSCC.**
**a-d** | Immunofluorescence staining for the myofibroblast marker alpha smooth muscle actin (alpha-SMA, green) revealed pericytes surrounding blood vessels in sections of normal human skin (a, b) and human cSCCs cryo-sections (c, d). **e-h** | Immunofluorescence co-staining of alpha-SMA (green) with the BM marker Collagen IV (red) in 2 and 4 week-old fixed cryo-sections did not show myofibroblasts in control (e, f) and Wnt-3a-stimulated OTCs (g, h).

of Collagen cleavage (Fig. 14g). Importantly, these findings did not reflect the invasive behavior of HaCaT cells in colOTCs, which was dependent on increased IL-8 and CCL-2 levels (Fig. 10), but demonstrated that MMP upregulation is a direct effect of Wnt-3a.

Since the presence of myofibroblasts or CAFs within the tumor stroma was frequently associated with tumor progression (Mishra et al., 2011), I asked whether myofibroblasts or CAFs play a role in tumorigenesis *in vivo* or in invasion of colOTCs. By immunofluorescence staining of sections with the myofibroblast marker alpha-Smooth muscle actin (alpha-SMA) signals relating to blood vessels were detected in normal human skin (Fig. 15a, b) and human cSCCs (Fig. 15c, d). However, neither *in vivo* nor in control (Fig. 15e, f) or Wnt-3a stimulated colOTCs (Fig. 15g, h) alpha-SMA positive stromal cells were detected, arguing that CAFs do not play a role in MMP secretion and HaCaT cell invasion or human cSCC progression.

Taken together, these findings argue for two distinct mechanisms. On one hand, Wnt/Beta-catenin activation of NHDF led to MMP expression, secretion and activation, which is frequently involved in an invasive phenotype. On the other hand, invasion of HaCaT cells grown on colOTCs was clearly dependent on Wnt-3a induced and NHDF secreted IL-8 and CCL-2. However, both mechanisms may also work in concert.

### 5.1.4 Wnt-3a stimulation of fdmOTCs leads to invasion of HaCaT-RAS A-5 cells

In order to confirm the observed invasive phenotype, fibroblast-derived matrix OTCs (fdmOTCs) as a more stable OTC model that is not prone to self-degradation was employed. After 4 weeks of fdmOTCs growth, HaCaT cells formed a well-differentiated parakeratotic epithelium (Fig. 16a, b). Under these more stringent conditions, however, neither control nor Wnt-3a stimulated HaCaT fdmOTCs showed invasive growth (Fig. 16c, d). Besides non-tumorigenic HaCaT cells, the invasive behavior of H-Ras$^{G12V}$-

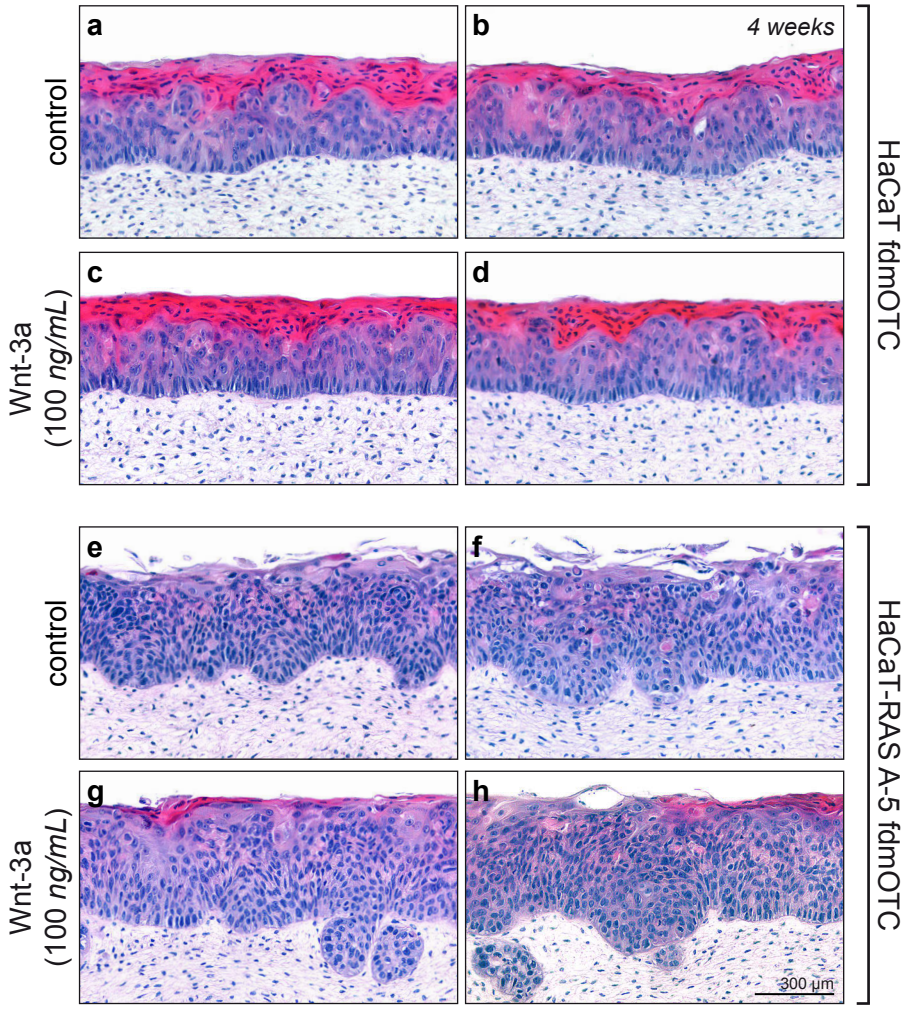


Figure 16 | **Wnt-3a causes invasion of HaCaT-RAS A-5, but not of HaCaT cells in fdmOTCs.**

fdmOTCs were prepared by allowing NHDF to build an ECM before seeding HaCaT or HaCaT-RAS A-5 cells, resulting in a stable OTC model that is not prone to self-degradation. fdmOTCs were stimulated with Wnt-3a (100 *ng/mL*) through the culture medium for 4 weeks. FFPE sections were stained with haematoxylin/ eosin to analyze the morphology. **a-d** | Non-tumorigenic HaCaT cells formed a well-differentiated parakeratotic epithelium (a, b). Under the fdmOTC conditions, Wnt-3a stimulated did not induce invasive growth (c, d). **e-h** | Benign-tumorigenic HaCaT-RAS A-5 cells formed a more hyperplastic epithelium showing low levels of terminal differentiation (e, f). Wnt-3a stimulation increased differentiation and invasion into the dermal equivalent (g, h). [n=3]

transfected benign-tumorigenic HaCaT-RAS A-5 cells was also analyzed. HaCaT-RAS A-5 fdmOTCs formed a more hyperplastic epithelium showing less terminal differentiation as HaCaT fdmOTCs (Fig. 16e, f). When stimulating these cultures with Wnt-3a, HaCaT-RAS A-5 cell differentiation was slightly increased. Most importantly, cells grew invasively into the dermal equivalent (Fig. 16g, h), showing that Wnt-3a led to invasion of benign-tumorigenic keratinocytes only in fdmOTCs. Thus, whether exclusively benign-tumorigenic or also non-tumorigenic cells grew invasively strongly depended on the stability of the employed OTC model.

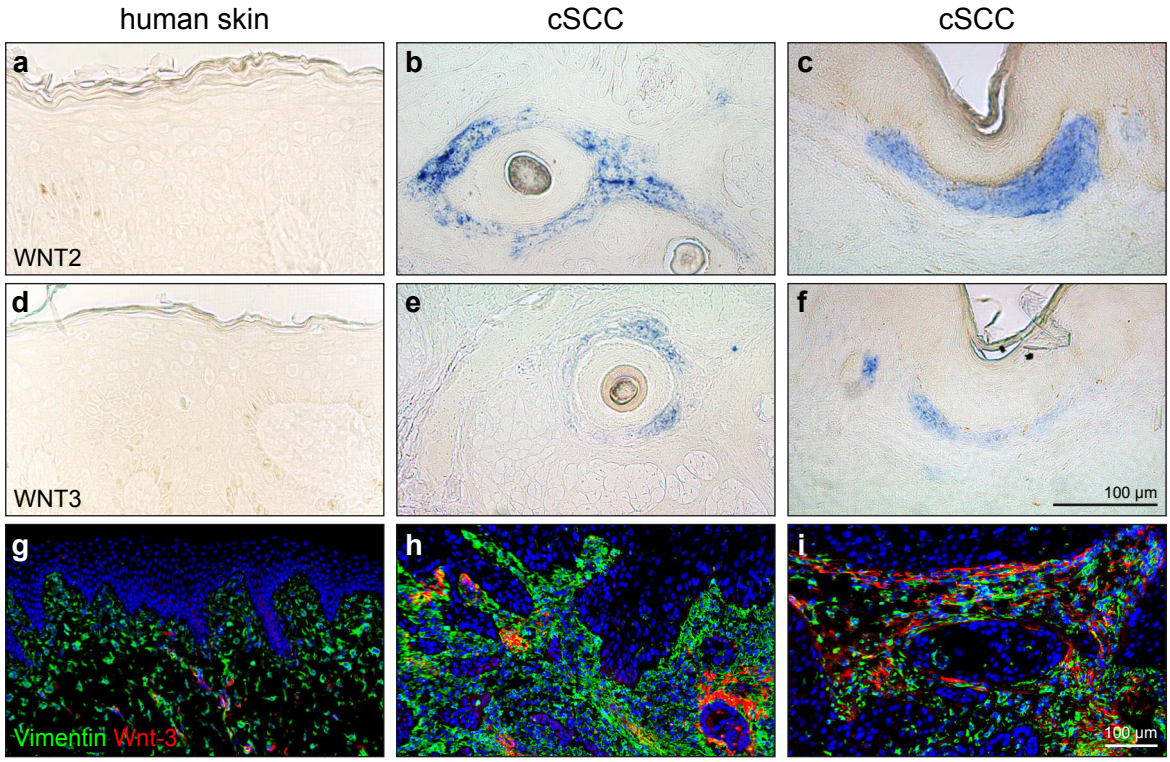


Figure 17 | **WNT2 and WNT3 are expressed in Wnt/Beta-catenin positive cSCC.**

Wnt/Beta-catenin positive cryo-conserved cSCC sections were analyzed for the presence of Wnt ligands **a-f** | *In situ* hybridization revealed WNT2 (b, c) and WNT3 (e, f) in the tumor-stroma of some cSCCs (blue), but not in normal skin (a, d). **g-i** | Immunofluorescence confirmed an increased Wnt-3 (red) expression within the Vimentin (green) positive tumor stroma (h, i) compared to normal skin (g).

### 5.1.5 Wnt ligands, IL-8, CCL-2 and MMP-1 in Beta-catenin positive cSCCs

To determine the relevance of these findings, the expression of Wnt ligands as well as of the Wnt/Beta-catenin induced factors IL-8, CCL-2 and MMP-1 was investigated in human primary cSCCs. First, WNT2 and WNT3 mRNA expression was analyzed by *in situ* hybridization. While normal skin was generally negative for WNT2 and WNT3 transcripts (Fig. 17a, d), cSCCs showed focal WNT2 and WNT3 mRNA expression (blue) within the tumor-stroma (Fig. 17b-c, e-f). In agreement, Wnt-3 protein could not be detected by immunofluorescence in normal skin (Fig. 17g), but was stained positive within the Vimentin positive cSCC stroma (Fig. 17h, i). This demonstrated that Wnt ligands are present in the stroma of some Wnt/Beta-catenin activated cSCCs.

Second, *in situ* hybridization for IL8 and CCL2 in normal human skin, revealed strong signals of both cytokines in sebaceous glands and hair follicles (blue, Fig. 18a, d). When analyzing the cSCC sections, high levels of both IL8 and CCL2 were additionally expressed within the tumor stoma (Fig. 18b-c, e-f), arguing that both cytokines are indeed expressed in some Wnt/Beta-catenin positive tumors and most likely act in concert. Third, high stromal MMP-1 levels (Fig. 18g, h) and MMP-cleaved collagen (Fig. 18i, j) could also be confirmed by immunofluorescence in cSCCs *in situ*, thereby supporting that MMP-1 is also expressed *in vivo* and contributes to matrix degradation and remodeling.

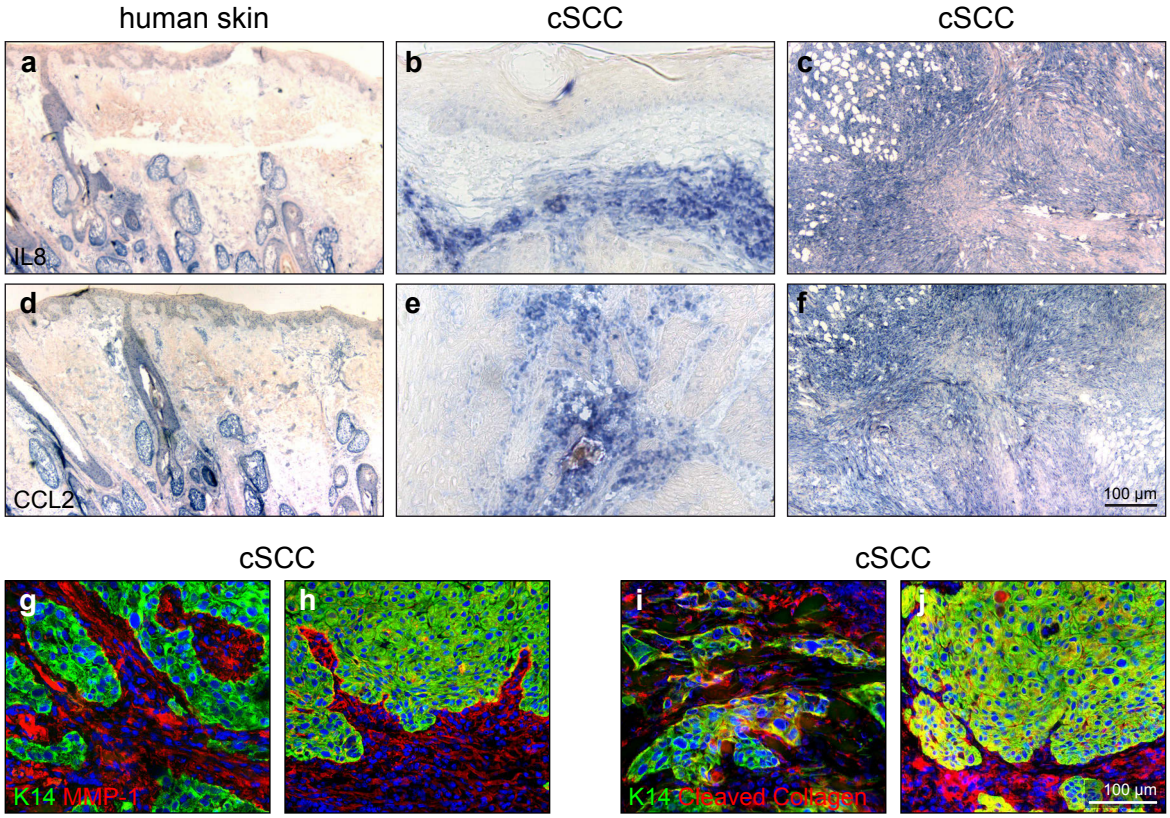


Figure 18 | **Effector genes IL8, CCL2 and MMP1 are expressed in Wnt/Beta-catenin positive cSCC.**

Wnt/Beta-catenin positive cryo-conserved cSCC sections were analyzed for the expression of the Wnt-3a induced genes IL8, CCL2 and MMP1. **a-f** | *In situ* hybridization showed high amounts of IL8 (b, c) and CCL2 (e, f) in the tumor-stroma of some cSCCs (blue) compared to normal skin (a, d). **g-j** | Immunofluorescence demonstrated a strong accumulation of MMP-1 (red) within the Keratin-14 (K14, green)-negative tumor stroma (g, h). Staining for MMP-cleaved collagen (red) confirmed MMP activity within the K14 (green)-negative cSCC stroma (i, j).

## 5.2 The B-Raf inhibitor Vemurafenib in cSCC progression

Besides the canonical Wnt signaling pathway, additional pathways may play a role in cSCC development and progression. It was recently described in melanoma therapy using the specific B-Raf$^{V600E}$ inhibitor Vemurafenib (VEM) that cSCCs represent a frequently observed and early adverse effect. Moreover, it was hypothesized that a paradoxical MEK-ERK MAPK hyper-activation by Vemurafenib in BRAF wild-type melanoma cells also represents the mechanism underlying cSCC development (Halaban et al., 2010; Hatzivassiliou et al., 2010). Thus, Vemurafenib-induced and Ras-Raf-MEK-ERK MAPK pathway dependent or independent effects could drive keratinocyte transformation, as well.

### 5.2.1 HaCaT and SCC cell lines does not reveal BRAF mutations

In order to determine the importance of activating BRAF and RAS mutations in cSCCs as well as to identify a suitable model system for the analysis of Vemurafenib induced cutaneous effects, frequent somatic mutation were analyzed. Besides the HaCaT carcinogenesis progression model, cSCC cell lines isolated directly from human tumors were included. The MET1-4 cell lines were isolated from the primary cSCC, two recurrences and a metastasis of the same patient (Proby et al., 2000). These cells carry a number of cSCC characteristic chromosomal changes and mutations except for TP53, thus allowing to study p53-independent mechanisms in skin carcinogenesis and metastasis (Boukamp, 2005; Popp et al., 2000). Moreover, SCL-I (Boukamp et al., 1982), SCL-II (Tilgen et al., 1983), SCC-12, SCC-13 (Rheinwald and Beckett, 1981) that were also isolated from primary human cSCCs display later stages in carcinogenesis.

The PCR-based array allowed the analysis of 78 frequently reported somatic mutations in human skin cancer within the genes BRAF, CDKN2A, CTNNB1, FGFR3, GNAQ, HRAS, KIT, KRAS, NRAS, PIK3CA, PTCH1, PTEN, RB1, SMO, LKB1/STK11 and TP53. NHEK of a young donor and from a sun-protected body site that unlikely carry any of the listed mutations were used to normalize the PCR array. When analyzing parental non-tumorigenic HaCaT cells as well as malignant tumorigenic HaCaT-RAS II-4 cells, the known TP53 mutations p.H179Y and p.R282W could be detected, confirming the specificity of the assay. The third known TP53 mutation p.281 was not included in the assay and thus, not detected (Lehman et al., 1993). Besides TP53 mutations, HaCaT-RAS II-4 cells also showed the expected HRAS mutation p.G12V (Boukamp et al., 1990), but no additional common mutation. The SCC cell lines SCL-I and SCL-II have the known TP53 mutations p.197$^{STOP}$ and p.N132K, respectively. SCC-12 cells have the TP53 mutation p.V216G and the HRAS mutation p.G12L, which were also not part of the employed array. In SCC-13 cells the TP53 mutation p.E258K could be confirmed (Popp et al., 2002) and a so-far unpublished HRAS mutation p.G12D was identified. Surprisingly, MET-1 cells originating from a primary SCC did not show any mutation, while MET-4 cells established from a lymph node metastasis of the same tumor showed an unknown CDKN2A (p16) mutation p.W110* (Table 12).

Thus, HaCaT, SCL-I and SCL-II cells showed TP53 mutations only while HaCaT-RAS II-4, SCC-12 and SCC-13 harbor additional HRAS mutations. The MET-1 and MET-4 cells had neither TP53 nor RAS mutations but MET-4 showed a so-far unknown CDKN2A (p16) mutation. Most importantly, all cell lines were negative for the typical BRAF mutations and only some revealed RAS mutations, thus

Table 12 | **Mutation analysis of HaCaT variants and SCC cell lines.**

| | TP53 (p53) | | HRAS | | CDKN2A (p16) | |
|---|---|---|---|---|---|---|
| | Base change | Amino acid change | Base change | Amino acid change | Base change | Amino acid change |
| **HaCaT** (immortalized) | c.535C>T<br>c.844C>T | [4]p.H179Y<br>[3]p.281<br>[4]p.R282W | - | - | - | - |
| **HaCaT A-5** (benign) | c.535C>T<br>c.844C>T | [3]p.H179Y<br>[3]p.281<br>[3]p.R282W | c.35G>T | [3]p.G12V | - | - |
| **HaCaT II-4** (malignant) | c.535C>T<br>c.844C>T | [4]p.H179Y<br>[3]p.281<br>[4]p.R282W | c.35G>T | [4]p.G12V | | |
| **SCL-I** (moderate differentiation) | c. C>T | [1]p.197$^{STOP}$ | - | - | - | - |
| **SCL-II** (low differentiation) | c. T>G | [1]p.N132K | - | - | - | - |
| **SCC-12** (high differentiation) | c. T>G | [1]p.V216G | c. CC>TT | [1]p.G12L | - | - |
| **SCC-13** (high differentiation) | c.772G>A | [2]p.E258K | c.35G>A | p.G12D | - | - |
| **MET-1** (primary SCC) | - | - | - | - | - | - |
| **MET-4** (metastasis) | - | - | - | - | c.330G>A | p.W110* |

[1]Adopted from, [2]confirmed by Popp *et al.*, 2002/ [3]Adopted from, [4]confirmed by Lehmann *et al.* 1993 or Boukamp *et al.* 1990/ newly detected mutation.

showing that especially BRAF mutations are in contrast to melanoma not involved in cSCC development. Having shown that TP53 but not BRAF mutations are frequently found in cSCCs, non-tumorigenic HaCaT cells displaying this genotype were chosen as model system to study Vemurafenib effects on keratinocytes cells. As benign-tumorigenic HaCaT-RAS A-5 and malignant-tumorigenic HaCaT-RAS II-4 cells showed an additional RAS mutation, these cells allowed studying the involvement of Ras in Vemurafenib induced cSCCs.

### 5.2.2 MEK-ERK signaling can be stimulated in HaCaT and HaCaT-RAS II-4 cells

Furthermore, we asked whether a normal activation of the Ras-Raf-MEK-ERK MAPK pathway by EGFR stimulation is possible in HaCaT and HaCaT-RAS II-4 cells. Therefore, cells were staved for 40 h in growth medium without FBS and stimulated with either the specific EGFR-inducer EGF (2 *ng/mL*) or FBS (10%)-containing growth medium. Subsequent activation of MEK, ERK and the related MAPK p38 as well as of the adjacent PI3K-PTEN-Akt pathway by phosphorylation was analyzed by Western-Blot.

In HaCaT cells, stimulation with EGF led to a strong phosphorylation of MEK1/2 and ERK1/2 already after 15 min and lasted for more than 60 min compared to the baseline after starvation (0 min). Importantly, total MEK and ERK protein levels remained unchanged. Stimulation with growth medium + FBS also caused MEK1/2 and ERK1/2 phosphorylation after 15 min, but showed a weaker and shorter effect on Ras-Raf-MEK-ERK pathway activation compared to EGF stimulation. A weak increase in phosphorylated p38 was also noted after 45-60 min of stimulation, while phosphorylated Akt was not reproducibly affected (Fig. 19a). A longer treatment showed that both, EGF and FBS stimulated MEK/ ERK, but not p38 MAPK phosphorylation for more than 6 h (Fig. 19b).

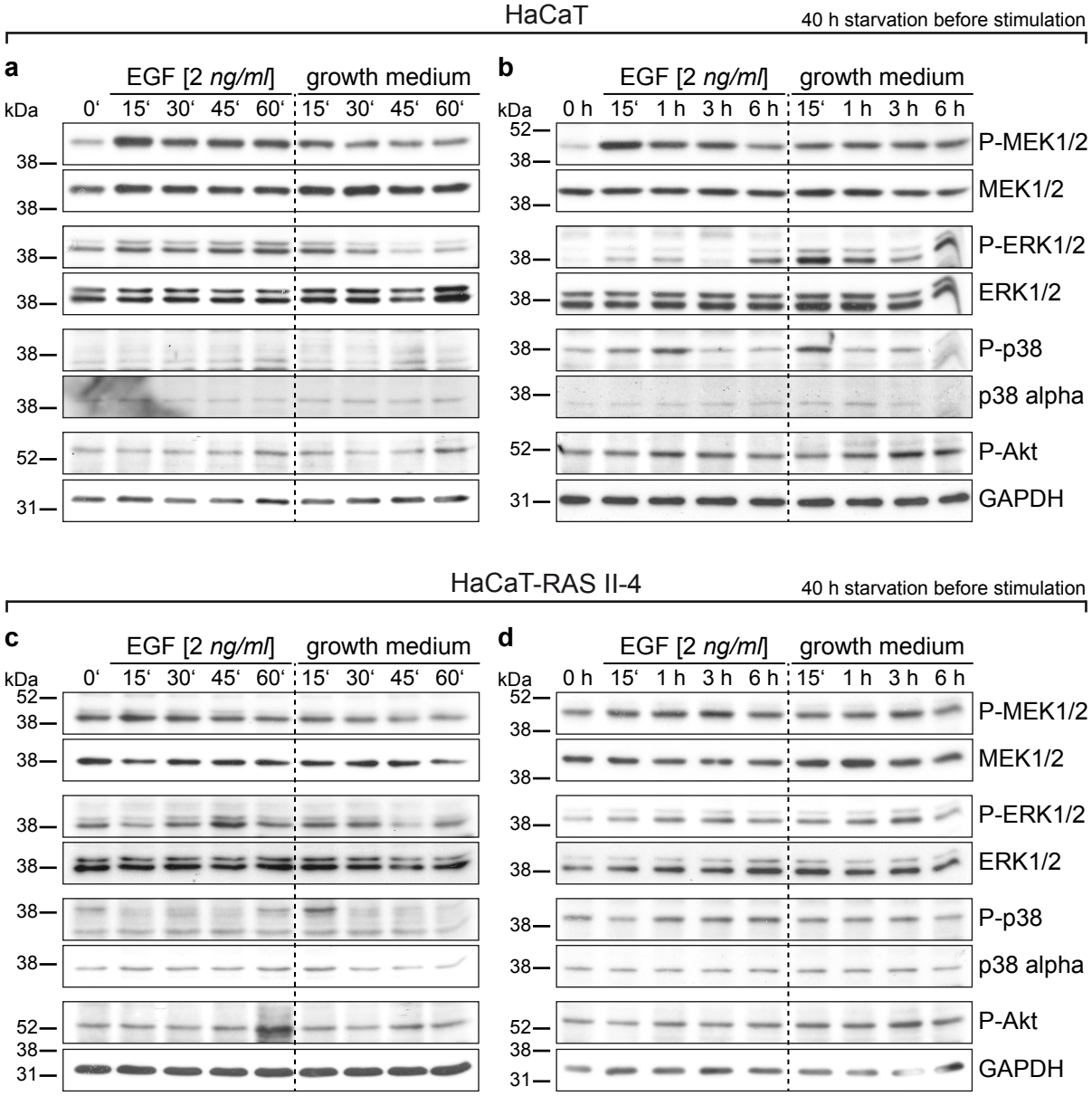


Figure 19 | **EGF and FBS stimulate MEK-ERK signaling in HaCaT and HaCaT-RAS II-4 cells.**

HaCaT and HaCaT-RAS II-4 cells were staved for 40 h in growth medium without FBS and stimulated with either the EGFR ligand EGF (2 *ng/mL*) or FBS (10%)-containing growth medium. MEK, ERK, p38 MAPK and PI3K-PTEN-Akt pathway activation was monitored over 6 h by Western-Blot. **a, b** | In HaCaT cells, EGF and FBS stimulation caused a strong MEK-ERK phosphorylation after 15 min (a) that was observed for more than 6 h (b), while total MEK and ERK protein levels remained unchanged. A weak but not reproducible increase in phosphorylated p38 and Akt was also noted (a, b). **c, d** | In HaCaT-RAS II-4 cells, the baseline MEK-ERK activation was increased compared to HaCaT cells. EGF or FBS stimulation caused MEK and ERK phosphorylation after 15 min (c) that remained increased until reaching 3 h (d) and was not as strong as in HaCaT cells. [n=2]

In HaCaT-RAS II-4 cells, the baseline MEK-ERK activation was increased compared to HaCaT cells. By stimulation with either EGF or growth medium + FBS, MEK and ERK phosphorylation was also observed after 15 min and remained increased until reaching 3 h. Again, phosphorylated p38 was slightly increased after stimulation and phosphorylated levels of Akt remained unchanged (Fig. 19c, d). Thus, EGF and FBS stimulated EGFR as well as downstream signaling to MEK1/2 and ERK1/2 in HaCaT and at lower levels also in HaCaT-RAS II-4 cells.

### 5.2.3 Treatment of HaCaT cells with the B-Raf inhibitor Vemurafenib does not cause toxicity

In order to study Vemurafenib on keratinocytes, toxicity was assessed by apoptosis assay. Vemurafenib is generally solubilized in DMSO and was used in different studies on melanoma cells at a concentration of 0.01-50 $\mu M$, while it is commonly at 1 $\mu M$ for the investigation of signaling pathways in cell culture (Comin-Anduix et al., 2010; Søndergaard et al., 2010; Yu et al., 2011). To determine apoptosis, HaCaT cells were stimulated for 24 and 48 h with 1, 10 or 50 $\mu M$ Vemurafenib or the corresponding DMSO concentrations 0.01, 0.1 or 0.5% (v/v) as control. After trypsinization, FITC-labeled Annexin V binding to the phospholipid phosphatidylserine at the outer cell membrane layer identified early apoptosis, while PI that entered the cell marked late apoptotic/ dead cells. Staining was analyzed by FACS for each cell, plotted (Fig. 20a) and quantified accordingly. Celastrol, a known inducer of apoptosis in HaCaT cells (Zhou et al., 2011), was used as positive control. Compared to untreated control cells, Celastrol induced a minor increase in overall apoptosis from 13.1 to 16.9% apoptotic cells at 2.2 $\mu M$ and a significant increase to 77.4% at 8.8 $\mu M$ after 24 h of treatment ($P<0.01$). In contrast, increasing DMSO or Vemurafenib concentrations induced apoptosis after neither 24 h (Fig. 20b) nor 48 h of treatment (Fig. 20c). Thus, 0.01-5 $\mu M$ Vemurafenib could be used for subsequent experiments.

### 5.2.4 Vemurafenib long-term stimulation does not alter apoptosis but causes partial G1/G0 phase arrest of HaCaT cells

Since short-term hyper-activation of MEK-ERK signaling in HaCaT cells did not show any toxicity, I asked whether such an effect is observed in continuously stimulated HaCaT cells. For this reason, HaCaT cells were cultivated in growth medium and growth medium supplemented with 0.5% (v/v) DMSO, 1 $\mu M$ or 5 $\mu M$ Vemurafenib for 9 weeks. As cells reached confluency under control conditions after 7 days, all conditions were split every week and $0.5 \times 10^6$ cells were routinely reseeded per 10 cm culture dish and condition. (Fig. 21a). After 5 weeks of continuous treatment, HaCaT cells were stimulated for another 24 h to determine apoptosis. FACS analysis revealed an overall apoptosis rate of 15% in DMSO treated HaCaT cells. In contrast, apoptosis was significantly increased to 90% by treating the same cells for 24 h with 8.8 $\mu M$ Celastrol confirming the specificity of the assay ($P<0.05$). Treatment for 5 weeks + 24 h with either 1 $\mu M$ or 5 $\mu M$ Vemurafenib did not result in significant changes in HaCaT cell apoptosis compared to DMSO treated cells (Fig. 21b, c).

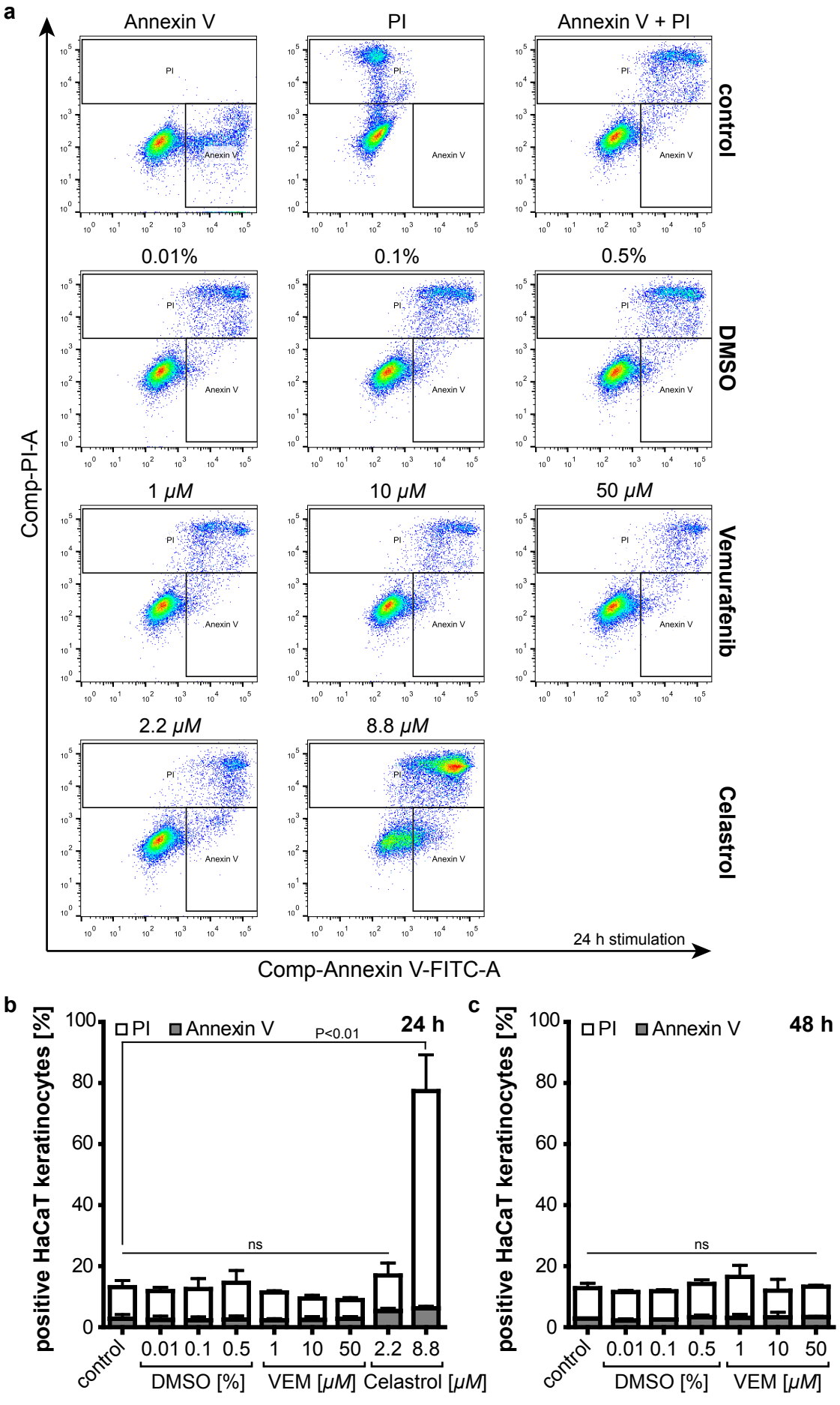
a
Annexin V
PI
Annexin V + PI
control
0.01%
0.1%
0.5%
DMSO
1 μM
10 μM
50 μM
Vemurafenib
2.2 μM
8.8 μM
Celastrol
Comp-PI-A
Comp-Annexin V-FITC-A
24 h stimulation
b
positive HaCaT keratinocytes [%]
PI
Annexin V
P<0.01
24 h
ns
control
0.01 0.1 0.5
DMSO [%]
1 10 50
VEM [μM]
2.2 8.8
Celastrol [μM]
c
positive HaCaT keratinocytes [%]
PI
Annexin V
48 h
ns
control
0.01 0.1 0.5
DMSO [%]
1 10 50
VEM [μM]

Figure 20 | **Vemurafenib does not induce apoptosis in HaCaT cells.**

Vemurafenib induced toxicity was assessed by apoptosis assay. HaCaT monolayer cultures were stimulated for 24 and 48 h with 1, 10 or 50 *µM* Vemurafenib, solubilized in DMSO, or the corresponding DMSO concentration of 0.01, 0.1 or 0.5% (v/v) as control. Celastrol (2.2 *µM*, 8.8 *µM*), as known inducer of apoptosis in HaCaT cells, served as positive control. Trypsinized HaCaT cells were stained with FITC-labeled Annexin V marking early apoptotic cells and PI detecting late apoptotic/ dead cells. **a** | FACS-based single cell analysis was plotted according to FITC and PI fluorescence. **b, c** | Quantification revealed a minor elevation in overall apoptosis by 2.2 *µM* and a significant increase by 8.8 *µM* Celastrol after 24 h, compared to untreated control cells. Increasing DMSO or Vemurafenib concentrations did not significantly increase apoptosis after 24 h (b) or 48 h (c). [n=2, mean ± SEM, Two-way ANOVA + Bonferroni posttest]

To determine whether cell cycle progression was altered by continuous Vemurafenib stimulation in HaCaT cells, a cell cycle measurement was performed after 5 or 9 weeks. Therefore, HaCaT cells were fixed and the cell cycle phases were distinguished according to the DNA content of each cell by FACS analysis (Fig. 22a). After 5 weeks + 24 h, control and DMSO treated HaCaT cells showed approx. 44% G1/G0, 35% S and 18.0% G2 phase. By 1 *µM*/ 5 *µM* Vemurafenib stimulation, G1/G0 phase was

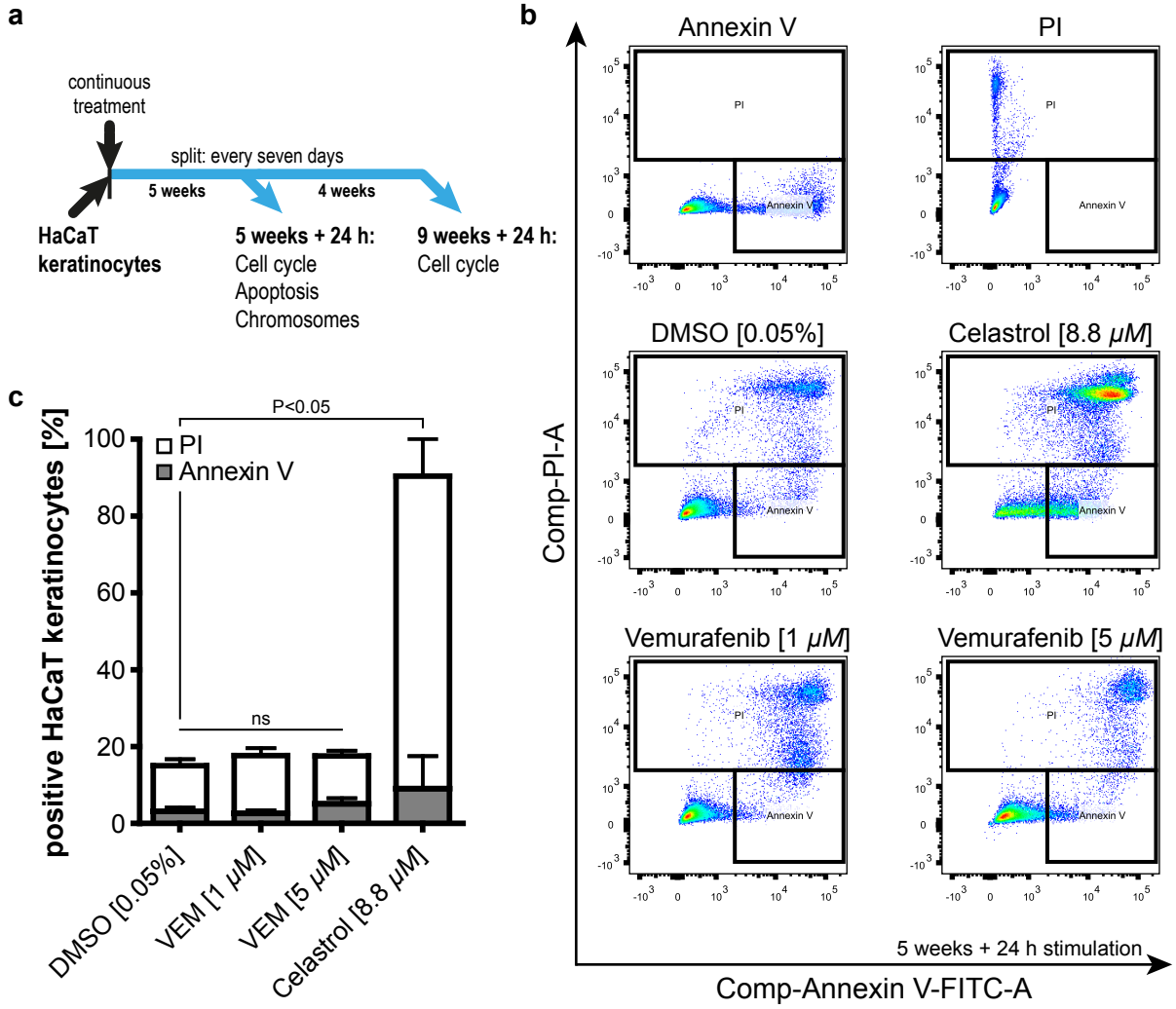


Figure 21 | **Vemurafenib long-term treatment of HaCaT cells does not induce apoptosis.**

Vemurafenib induced toxicity in long-term treated HaCaT monolayer cultures was assessed by apoptosis assay. **a** | HaCaT cells were continuously stimulated for 9 weeks with 0.05% (v/v) DMSO, 1 *µM* or 5 *µM* Vemurafenib. As cells reached confluency every 7 days, they were trypsinized and 0.5x $10^6$ cells were reseeded per 10 cm culture dish. **b** | After 5 weeks, HaCaT cells were treated for another 24 h accordingly and stained with FITC-labeled Annexin V marking early apoptotic cells and PI detecting late apoptotic/ dead cells. FACS-based single cell analysis was plotted for FITC and PI fluorescence. **c** | Quantification of control cells treated for 24 h with Celastrol (8.8 *µM*), as known inducer of apoptosis in HaCaT cells, revealed a significant increase in apoptosis, compared to control cells. Treatment for 5 weeks + 24 h with either 1 *µM* or 5 *µM* Vemurafenib did not result in significant changes in HaCaT cell apoptosis. [n=2, mean ± SEM, Two-way ANOVA + Bonferroni posttest]

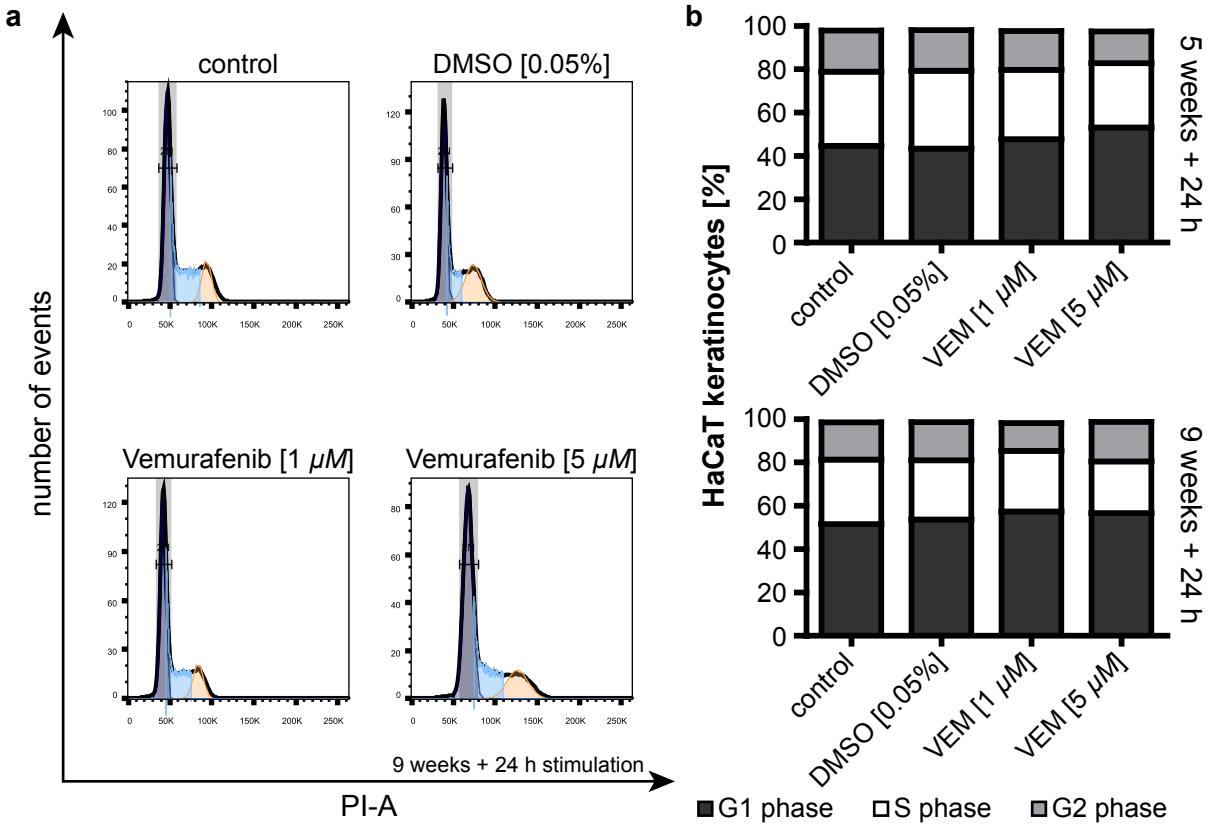


Figure 22 | **Vemurafenib rather inhibites than accelerates cell cycle progression of HaCaT cells.**
Vemurafenib induced toxicity of long-term treated HaCaT monolayer cultures was assessed by cell cycle analysis. HaCaT cells were continuously stimulated for 9 weeks with 0.05% (v/v) DMSO, 1 *μM* or 5 *μM* Vemurafenib. As cells reached confluency every 7 days, they were trypsinized and 0.5x $10^6$ cells were reseeded per 10 cm culture dish. **a** | After 5 or 9 weeks, HaCaT cells were treated for another 24 h accordingly, were fixed and stained with PI. As the PI intensity per cell relates to the DNA content, a FACS analysis allowed distinguishing the cell cycle phases G1/ G0, S and G2. **b** | After 5 weeks + 24 h or 9 weeks + 24 h, 1 *μM* or 5 *μM* Vemurafenib stimulation led to a shift from G2 or S to G1/G0 phase when compared to control and DMSO treated HaCaT cells. This suggested inhibited rather than accelerated cell cycle progression of HaCaT cells. [n=1 for each time point]

increased to 47.8/ 53.1%, whereas S phase was decreased to 31.9/ 29.7% and also G2 phase cells were not altered/ reduced to 18.0/ 14.6%. After 9 weeks + 24 h, control and DMSO treated HaCaT cells showed approx. 52% G1/G0, 29% S and 17.0% G2 phase. By 1 *μM*/ 5 *μM* Vemurafenib stimulation, G1/ G0 phase also was increased to 57.4/ 56.6%, whereas S phase was decreased to 28.0/ 23.8% and also G2 phase cells were reduced/ slightly increased to 12.8/ 18.2%. Thus, the cell cycle quantification revealed a small shift from G2 or S to G1/G0 phase after 5 and 9 weeks of Vemurafenib treatment (Fig. 22b), suggesting that Vemurafenib rather inhibited than accelerated cell cycle progression of HaCaT cells. However, this demonstrated that neither short-term nor long-term treatment with 1-5 *μM* Vemurafenib induced toxicity on HaCaT cells.

### 5.2.5 Vemurafenib abrogates MEK-ERK signaling in B-Raf-mutant melanoma cells but causes hyper-activation in B-Raf wild-type keratinocytes

To test the efficacy of the B-Raf inhibitor Vemurafenib at a concentration of 1 *μM*, I stimulated B-Raf p.V600E mutant A375 melanoma cells. Western-Blot analysis of phosphorylated MEK1/2 and ERK1/2 revealed high levels of both proteins at baseline in this tumor cell line, accounting to the

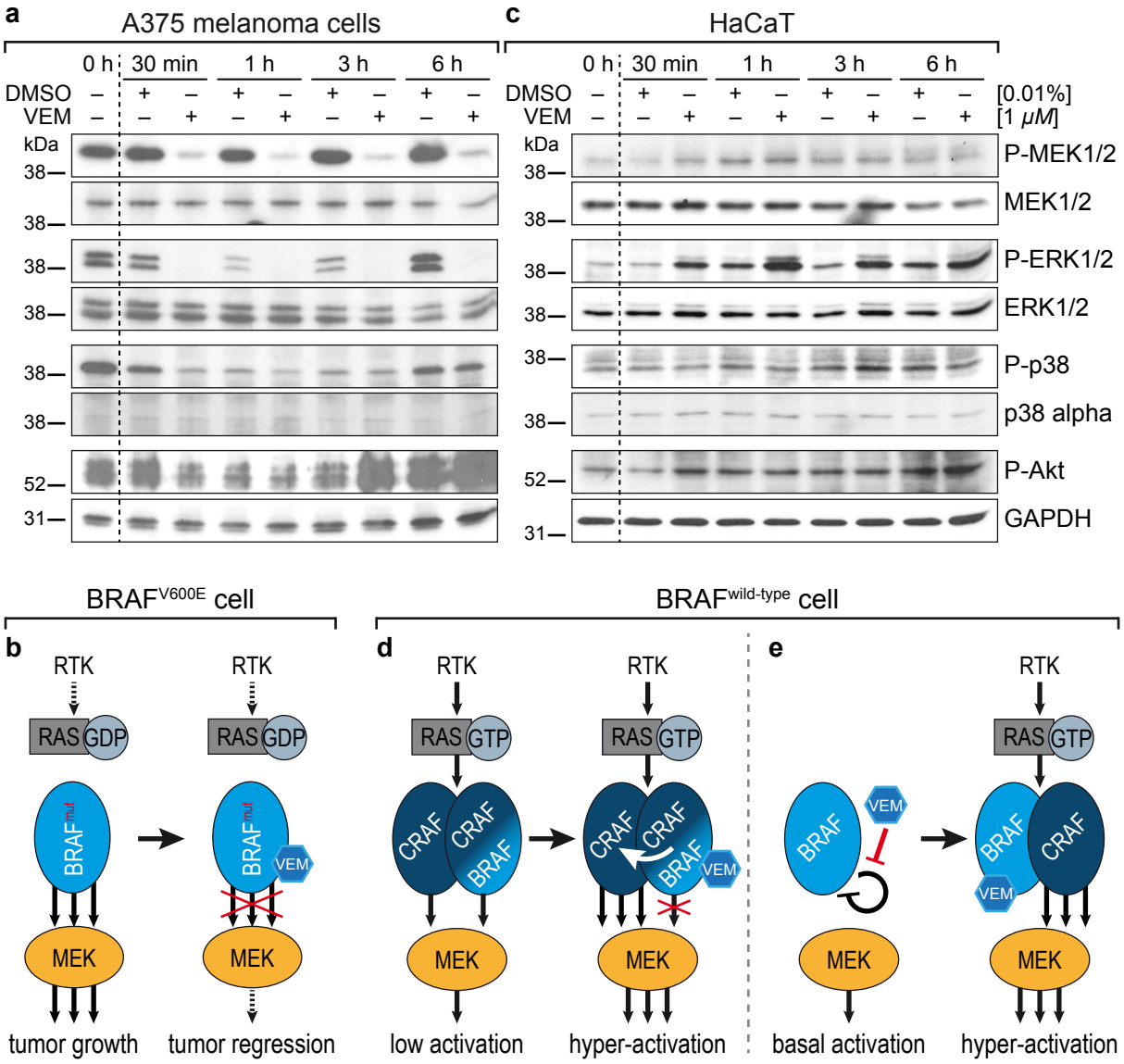


Figure 23 | **MEK-ERK signaling is blocked by Vemurafenib in mutant, but hyper-activated in wild-type B-Raf cells.**

B-Raf$^{V600E}$-mutant A375 melanoma cells and B-Raf$^{wild\text{-}type}$ HaCaT cells were stimulated with 1 *μM* or 0.01% (v/v) DMSO as control in FBS-containing growth medium for 6 h. MEK, ERK, p38 MAPK and PI3K-PTEN-Akt pathway activation was monitored by Western-Blot. **a, b** | A375 cells demonstrated high MEK and ERK levels at baseline due to mutant B-Raf signaling. By Vemurafenib, both phosphorylated proteins were strongly reduced for more than 6 h compared to treatment with DMSO. The corresponding total protein was not altered. p38 and Akt did not show Vemurafenib specific effects (a). This confirmed that Vemurafenib abrogates downstream signaling by monomeric B-Raf$^{V600E}$ (b). [n=2] **c-f** | HaCaT cells demonstrated a low basal MEK-ERK activity. When stimulated with Vemurafenib, levels of phosphorylated MEK and ERK were increased after 30 min for more than 6 h. p38 and Akt activation accounted to fresh growth medium (c). Accordingly, B-Raf$^{wild\text{-}type}$, both hypothesized models require a Ras mutation or receptor tyrosine kinases (RTKs) signaling (d, e). Poulikakos (2010) suggested a low Vemurafenib concentration as third requirement that blocks and conformationally alters one Raf subunit leading hyper-activation of the second (d). Alternatively, Heidorn and Hatzivassiliou (2010) proposed that Vemurafenib resolves the B-Raf auto-inhibitory state allowing Ras-dependent dimer formation and MEK-ERK hyper-activation (e). [n=2]

constitutively active mutant B-Raf signaling. When adding Vemurafenib, both phosphorylated proteins were strongly reduced for more than 6 h compared to treatment with 0.01% (v/v) DMSO, as expected. The corresponding total protein load was not altered. The increase in phosphorylation of MEK, ERK, p38 and Akt between 1-6 h likely accounted to the addition of new growth medium, which activated these pathways irrespective of the treatment. Comparable effects were also observed in subsequent Western-Blot experiments. However, phosphorylated p38 and Akt were not reproducibly affected by

Vemurafenib (Fig. 23a). This shows that a concentration of 1 µM Vemurafenib is indeed sufficient to specifically block downstream signaling from monomeric B-Raf$^{V600E}$ to MEK and ERK in A375 melanoma cells (Fig. 23b).

In contrast to A375 cells, HaCaT cells showed a low basal MEK-ERK activation. When stimulating HaCaT cells with Vemurafenib, levels of phosphorylated MEK and especially ERK increased as soon as after 30 min and persisted for more than 6 h reaching a maximum after 1 h post treatment. Again, the related signaling pathways p38 and Akt were activated over time under both conditions, which accounted to pathway stimulation by growth medium rather than being a Vemurafenib-specific effect (Fig. 23c). As suggested by the pathway hyper-activation hypothesis initially described in BRAF$^{wild\text{-}type}$ melanoma cells, Vemurafenib leads to pathway activation rather than inhibition (Hatzivassiliou et al., 2010) also in BRAF$^{wild\text{-}type}$ HaCaT cells. Accordingly, upon upstream activity via EGFR or Ras and a low Vemurafenib concentration only one subunit of the B-Raf/B-Raf or B-Raf/C-Raf dimer is stochastically blocked leading to conformational changes that likely hyper-activated the second subunit (Poulikakos et al., 2010) (Fig. 23d). An alternatively hypothesis suggests the release of the B-Raf auto-inhibitory state by Vemurafenib leading to increased downstream signaling through MEK and ERK, as well (Hatzivassiliou et al., 2010; Heidorn et al., 2010) (Fig. 23e).

To test whether Vemurafenib itself is capable of hyper-activating MEK-ERK signaling or requires upstream activity through EGFR or Ras, HaCaT cells were starved in medium without FBS for 48 h and stimulated with 1 *µM* Vemurafenib only or in combination with 2 *ng/mL* EGF for 1 and 3 h. Compared to DMSO treatment, Vemurafenib caused a weak, while EGF stimulation mediated a strong MEK-ERK phosphorylation after 1 h that further increased and was maintained for more than 3 h. Combined stimulation with Vemurafenib and EGF further increased MEK and ERK phosphorylation above the levels of each individual stimulation. p38 MAPK and Akt revealed some activation, which could not be reproducibly linked to EGF or Vemurafenib. This argued that B-Raf upstream activity increases the hyper-activation effect of Vemurafenib also in HaCaT keratinocytes (Fig. 24a). Thereafter, effects of higher Vemurafenib concentrations on HaCaT cells in growth medium were investigated by adding 1, 10 or 50 *µM* Vemurafenib to the cells for 1 or 3 h. Compared to 0.5% (v/v) DMSO, 1 *µM* Vemurafenib led to ERK activation after 1 and 3 h. 10 *µM* Vemurafenib mediated a strongly increased ERK phosphorylation after 1 h, which was not maintained at 3 h. Even more interesting, 50 *µM* led to a reduced response at 1 h compared to 10 *µM*, which was also not maintained for 3 h. Again, neither p38 nor Akt phosphorylation were reproducibly affected (Fig. 24b). This suggested that Vemurafenib concentrations between 10 and 50 *µM* lead to the binding of both subunits of a Raf dimer, thus, preventing signaling through MEK and ERK. Therefore, Vemurafenib concentrations below 10 *µM* were used in the subsequent experiments.

As Vemurafenib induced MEK-ERK hyper-activation in HaCaT cells, I asked whether BRAF$^{wild\text{-}type}$ NHEK, HaCaT-RAS A-5 and HaCaT-RAS II-4 cells respond also with pathway activation. Again, keratinocytes were stimulated with either 1 *µM* Vemurafenib or 0.01% (v/v) DMSO in growth medium for 6 h. Two different normal keratinocytes, NHEK 1 and NHEK 2, responded with increased levels of phosphorylated MEK and ERK after 30 min with a peak at 1 h of Vemurafenib stimulation, compared to the corresponding control at each time point. Importantly, total MEK and ERK protein levels remained unchanged (Fig. 25a, b). Even H-Ras$^{G12V}$ transfected and benign-tumorigenic HaCaT-RAS A-5 cells responded similarly to Vemurafenib with ERK phosphorylation after 30 min and a maximum level after 1 h (Fig. 25c). HaCaT-RAS II-4 cells showed a strong MEK and ERK phosphorylation after 30 min

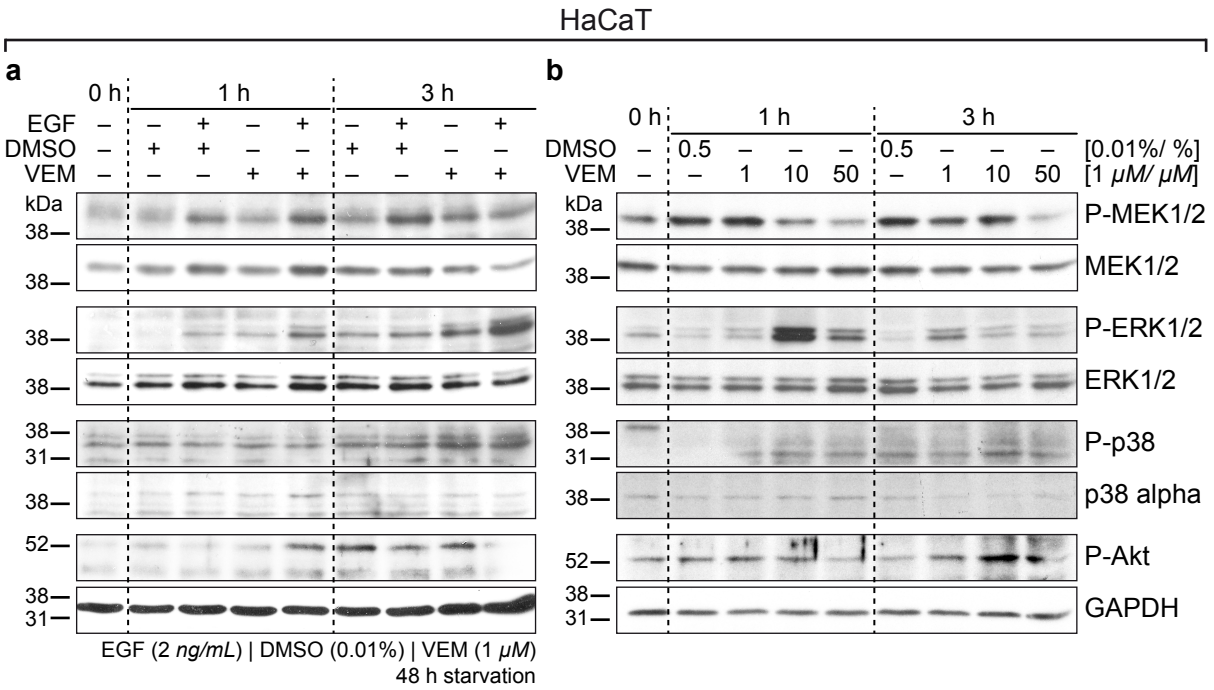


Figure 24 | **MEK-ERK activation is increased by EGF, but not by high Vemurafenib concentrations.**
**a** | HaCaT cells were starved for 48 h and stimulated by either 1 *μM* Vemurafenib only or in combination with 2 *ng/mL* EGF for 1-3 h. MEK, ERK, p38 or Akt-activation were analyzed by Western-Blot. Compared to DMSO treatment, Vemurafenib caused a weak and EGF stimulation a strong MEK-ERK phosphorylation after 1 h that increased and persisted for more than 3 h. Combined stimulation further increased MEK and ERK phosphorylation above the individual level. p38 MAPK and Akt revealed some not reproducible regulation. [n=2] **b** | Effects of higher Vemurafenib concentrations were analyzed by adding 1, 10 or 50 *μM* Vemurafenib in growth medium to HaCaT cells for 1 or 3 h. Compared to 0.5% (v/v) DMSO, 1 *μM* Vemurafenib led to a higher ERK activation after 1 and 3 h. 10 *μM* Vemurafenib led to an increased ERK phosphorylation after 1 h, which was not maintained at 3 h, while 50 *μM* caused a reduced response at 1 h and no detectable effect after 3 h. Neither p38 nor Akt phosphorylation were reproducibly affected. [n=2]

of treatment that was maintained for more than 6 h at a similar level (Fig. 25d). In case of control and Vemurafenib, MEK, ERK p38 and Akt phosphorylation increased over time due to pathway activation by fresh growth medium, whereas only MEK and ERK were also reproducibly hyper-activated by Vemurafenib (Fig. 25a-d). Taken together, Vemurafenib abrogated signaling through MEK and ERK in B-Raf$^{V600E}$ mutant A375 cells, but increased MEK-ERK signaling in all analyzed B-Raf$^{wild\text{-}type}$ keratinocytes irrespective of RAS mutations or the stages in skin carcinogenesis. Moreover, pathway upstream activity and Vemurafenib concentration below 10 μM seemed to promote a solid response in HaCaT cells.

## 5.2.6 MEK-ERK hyper-activation does not increase proliferation of keratinocytes

Activation of MEK-ERK signaling was frequently linked to increased cell proliferation (Dhillon et al., 2007). As Vemurafenib mediated MEK-ERK hyper-activation in keratinocytes, this may subsequently lead to increased cell proliferation. Therefore, NEHK, HaCaT and HaCaT-RAS A-5 cells were stimulated with different Vemurafenib concentrations or 0.05% (v/v) DMSO. Since B-Raf upstream activity was found to increase Vemurafenib induced MEK-ERK hyper-activation, keratinocytes were cultured and stimulated in growth medium. A subsequent SYBR Green-based cell proliferation assay revealed for NHEK cultured in Derma Life a normal growth behavior with slow proliferation onset during 0-24

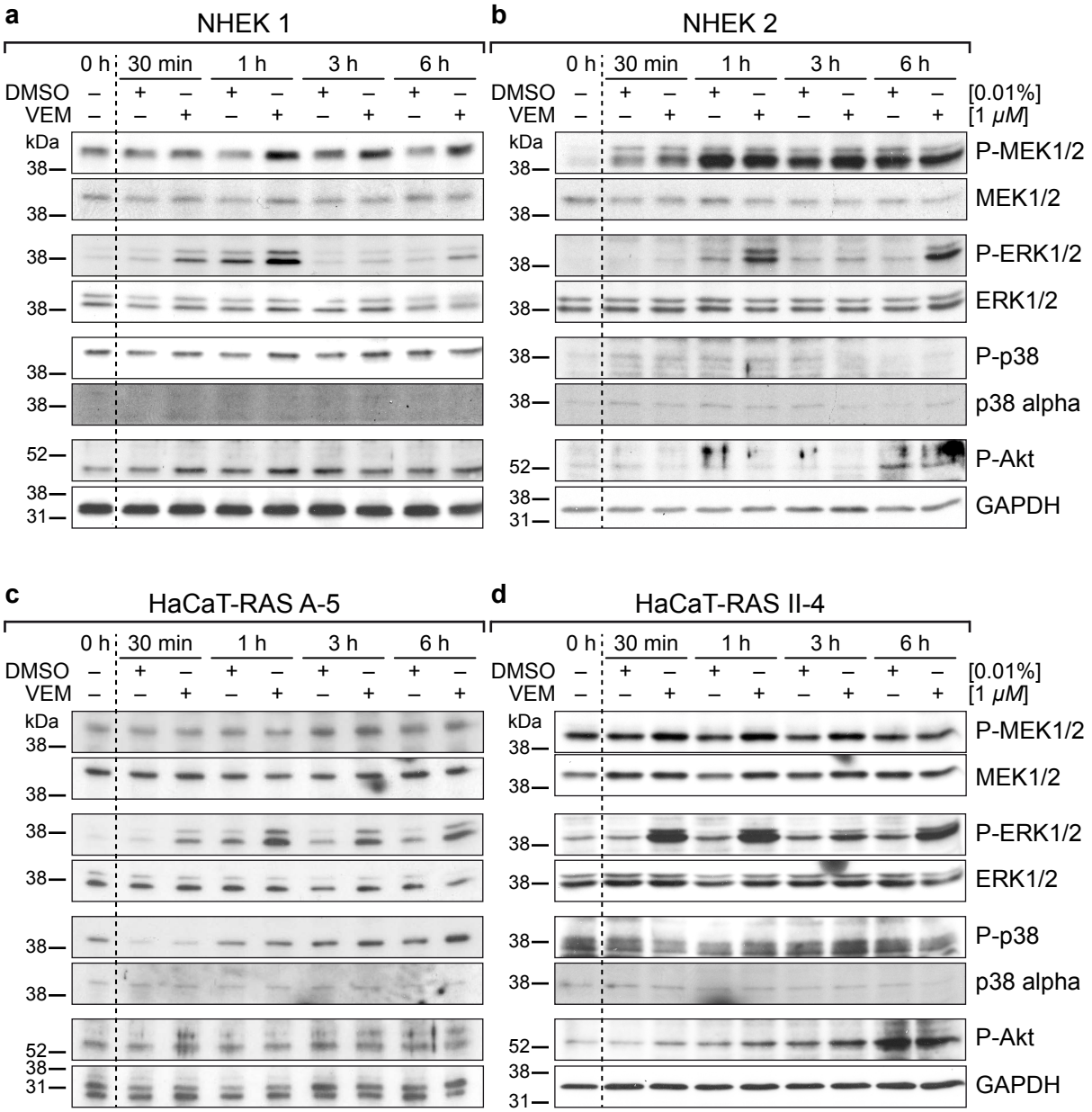


Figure 25 | **Vemurafenib triggers MEK-ERK hyper-activation in NHEK and HaCaT-RAS cells.**

Keratinocytes were stimulated with either 1 *μM* Vemurafenib or 0.01% (v/v) DMSO in growth medium for 6 h and MEK, ERK, p38 or Akt-activation were analyzed by Western-Blot. **a, b** | Two different normal keratinocytes, NHEK 1 (a) and NHEK 2 (b), responded to Vemurafenib with increased levels of phosphorylated MEK and ERK after 30 min compared to controls, whereas total MEK and ERK protein levels remained unchanged. Other signaling pathways were not affected by Vemurafenib. [n=1 per NHEK donor] **c, d** | HRAS transfected HaCaT-RAS A-5 (c) and HaCaT-RAS II-4 cells (d) responded to Vemurafenib with ERK phosphorylation after 30 min that was maintained for more than 6 h (d). MEK, ERK p38 and Akt phosphorylation increased due to growth medium replacement. [n=2]

h that increased to a hyper-proliferative growth between 24-72 h. Stimulation with either DMSO, 0.1 and 0.01 *μM* Vemurafenib did not show an effect on NHEK proliferation as initial cell numbers of 7,300 cells at 0 h generally increased to approx. 20,000 cells after 24 h, to approx. 60,000 cells after 48 h and to 90,000 cells after 72 h. In contrast, stimulation with 1 *μM* or 5 *μM* Vemurafenib led to a dose-dependent and significant inhibition of growth ($P<0.05$). Treatment with 1 *μM* revealed a maximal cell number of approx. 14,000 cells after 48 h, while 5 μM Vemurafenib prevented growth of NHEK (Fig. 26a). HaCaT cells grew generally slower than NHEK by reaching approx. 47,000 cells after 72 h under control conditions. The lag-phase between 0-24 h was also observed, however, growth kept similar kinetics thereafter without showing a hyper-proliferative phase. Moreover, 1 *μM* or 5 *μM* did

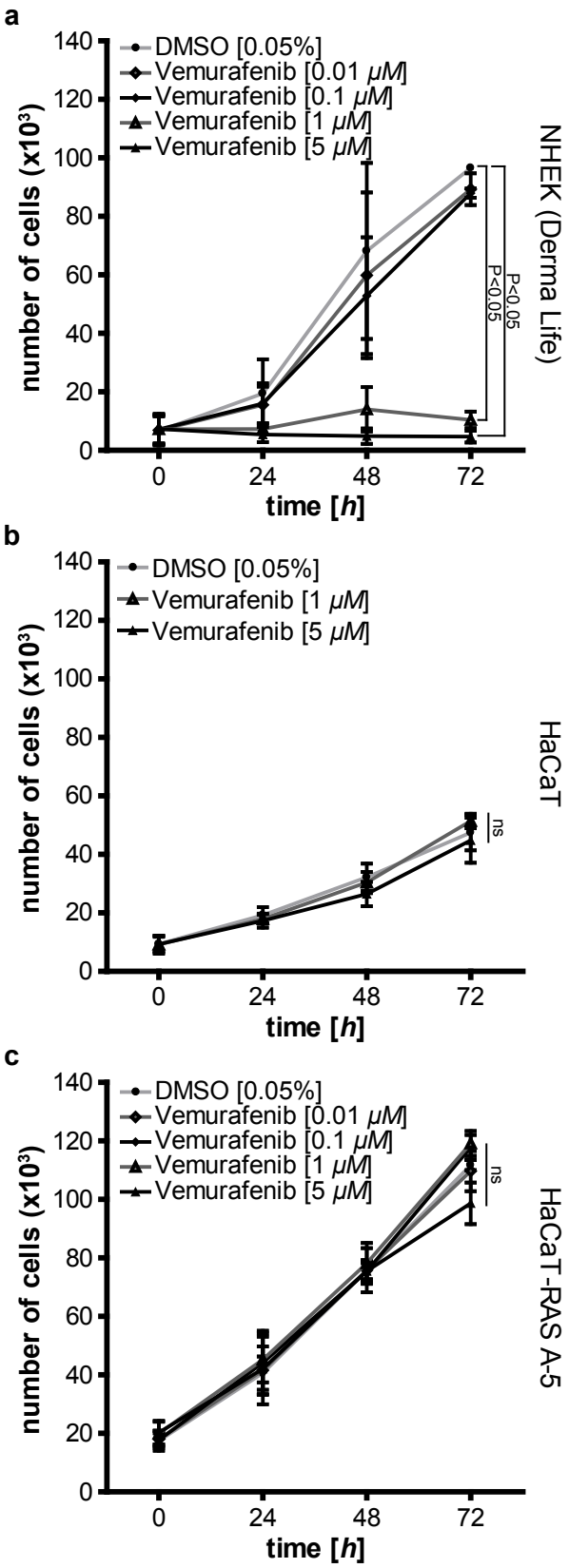


Figure 26 | **Vemurafenib does not increase proliferation in keratinocytes.**

Keratinocytes were stimulated using different Vemurafenib concentrations or 0.05% (v/v) DMSO. After 0-72 h, cells were lysed and incubated with a SYBR Green solution that stained DNA. Cell number was determined by correlating the fluorescence measurement of each well to a standard plate with defined cell counts. **a** | NHEK in Derma Life showed a normal growth behavior with slow proliferation during 0-24 h and hyper-proliferative growth between 24-72 h. Stimulation with either DMSO, 0.01 and 0.1 *µM* Vemurafenib did not show an effect on growth. Stimulation with 1 *µM* or 5 *µM* Vemurafenib led to a dose-dependent and significant inhibition of growth. [n=2] **b** | HaCaT cells grew slower than NHEK and did not show a hyper-proliferative phase. 1 *µM* or 5 *µM* did not affect the growth. [n=2] **c** | HaCaT-RAS A-5 cells demonstrated hyper-proliferation directly after seeding. Compared to DMSO treatment, 0.01, 0.1, 1 or 5 *µM* Vemurafenib did alter the growth kinetics. [n=2, mean ± SD, Two-way ANOVA + Bonferroni posttest]

not affect this growth rate (Fig. 26b). HaCaT-RAS A-5 cells did not show a lag-phase, but hyper-proliferative growth already between 0-24 h, which was continued with similar kinetics. Under DMSO treatment, HaCaT-RAS A-5 cells grew to approx. 111,000 cells within 72 h of cultivation. Similarly to HaCaT cells 1 or 5 *µM* Vemurafenib did alter the growth kinetics showing comparable cell numbers at each time point compared to control cells. To ask whether low Vemurafenib concentrations lead to an increased proliferative response by binding only one subunit of a B-Raf/ C-Raf dimer, HaCaT-RAS A-5 cells were stimulated with 0.01 and 0.1 *µM* Vemurafenib. However, none Vemurafenib concentration revealed significant changes in proliferation (Fig. 26c). Thus, Vemurafenib-induced hyper-activation did not lead to elevated cell proliferation in NHEK, HaCaT and HaCaT-RAS A-5 cells, but rather prevented growth of NHEK at higher concentrations.

### 5.2.7 Long-term Vemurafenib treatment leads to increased keratinocyte differentiation

KAs and cSCCs occurred within a median time of 8 weeks melanoma patients treated with Vemurafenib (Anforth et al., 2013). Since short-term treatment with Vemurafenib leads to MEK-ERK hyper-

activation, but did not increase proliferation of keratinocytes, I asked whether similar as *in vivo* a continuous stimulation is required cause downstream effects. Therefore, HaCaT/ HaCaT-RAS A-5 cells were cultivated in growth medium and growth medium supplemented with 0.05% (v/v) DMSO, 1 *µM* or 5 *µM* Vemurafenib for 9 or 5 weeks, respectively, and cell numbers were monitored. As cells reached confluency under control conditions after 7 days, all conditions were split every week and 0.5x $10^6$ cells were routinely reseeded per 10 cm culture dish and condition.

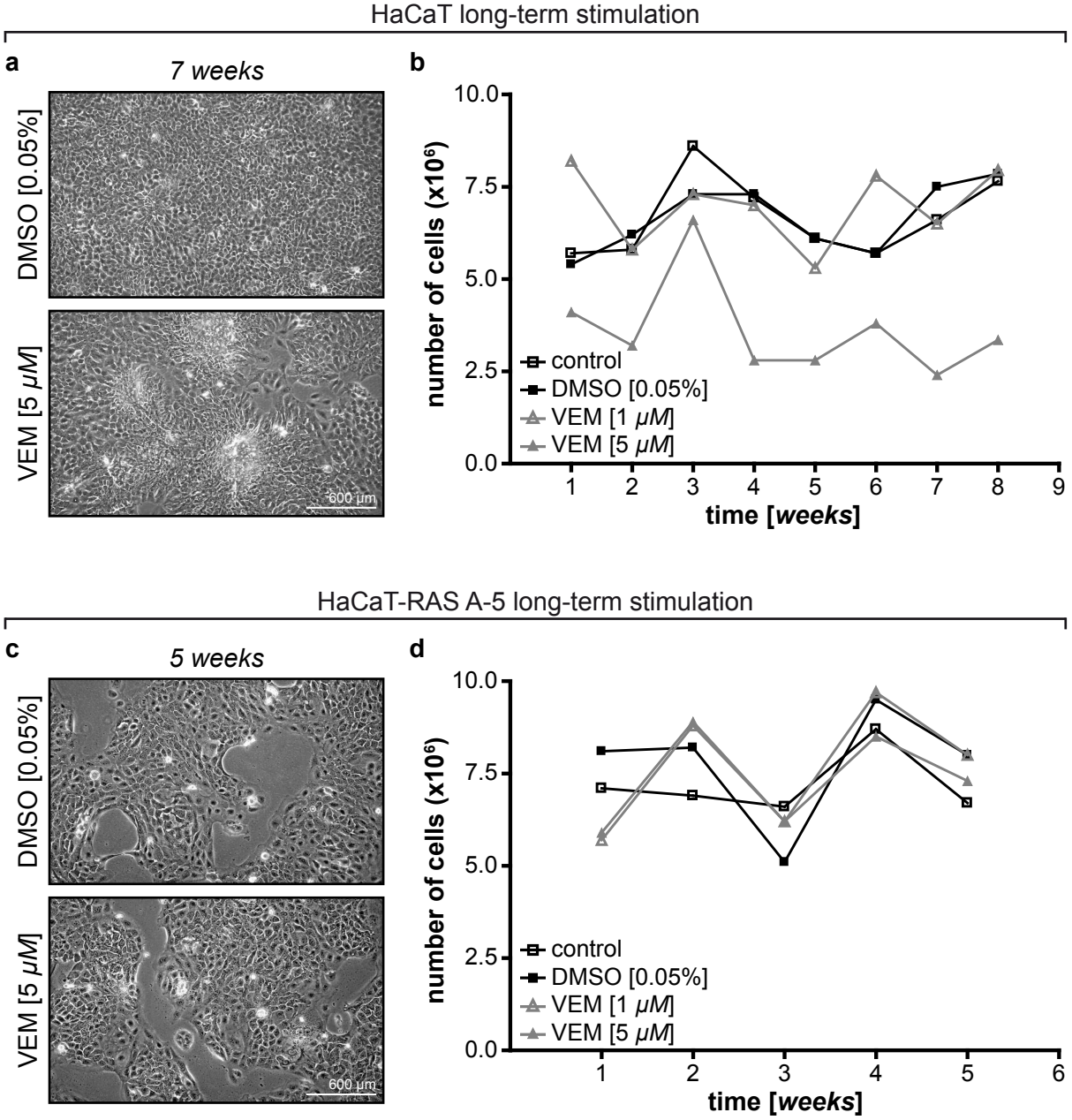


Figure 27 | **Continuous Vemurafenib stimulation increases differentiation rather than proliferation.**

HaCaT or HaCaT-RAS A-5 cells were cultivated in growth medium supplemented with 0.05% (v/v) DMSO, 1 *µM* or 5 *µM* Vemurafenib for either 9 or 5 weeks. As cells reached confluency under control conditions every 7 days, cells were trypsinized and 0.5x $10^6$ cells were reseeded per 10 cm culture dish and condition. **a, b** | After 7 weeks, light microscopic evaluation of HaCaT cells revealed that 5 *µM* Vemurafenib leads to earlier and increased differentiation compared to DMSO treated cells (a). This was also reflected by the cell numbers as control, DMSO and 1 *µM* stimulated cells were comparable, while 5 *µM* Vemurafenib decreased the cell numbers (b). [n=1] **c, d** | After 5 weeks, light microscopic evaluation of HaCaT-RAS A-5 revealed smaller differences in differentiation between DMSO and Vemurafenib treated cells compared to HaCaT cells (c). The cell numbers were comparable among all cultivation conditions (d). [n=1]

A light microscopic evaluation of 7 weeks continuously stimulated HaCaT cells revealed that 5 $\mu M$ Vemurafenib leads to earlier and increased differentiation compared to DMSO treated cells (Fig. 27a). Interestingly, this was also reflected in the cell numbers obtained after the weekly split of the HaCaT cells. Control, DMSO and 1 $\mu M$ Vemurafenib stimulated cells revealed similar numbers of 6.8x $10^6$ cells per 10 cm dish and week, thus, demonstrating a similar proliferation rate. In contrast, 5 $\mu M$ Vemurafenib reduced the cell number to 3.5x $10^6$ cells per 10 cm dish (Fig. 27b), arguing that Vemurafenib triggers differentiation in combination with a reduced proliferation in HaCaT cells. To determine whether Vemurafenib also affects differentiation of HaCaT-RAS A-5, these cells were cultivated for 5 weeks in growth medium and in growth medium containing 0.05% (v/v) DMSO, 1 µM or 5 µM Vemurafenib. A morphological analysis by light microscopy revealed smaller differences in differentiation between DMSO and Vemurafenib treated HaCaT-RAS A-5 cells compared to HaCaT cells. However, a tendency towards accelerated differentiation through Vemurafenib was generally observed (Fig. 27c). Throughout the different conditions, a mean cell number of 7.5x $10^6$ per 10 cm dish was determined after each week (Fig. 27d), showing that HaCaT-RAS A-5 proliferation was not affected by Vemurafenib at all.

Taken together, Vemurafenib long-term stimulation of HaCaT cells did not cause increased proliferation, but rather led to an accelerated differentiation. In contrast, HaCaT-RAS A-5 cell numbers did not change by any treatment, which was also reflected in a weaker acceleration of differentiation. Importantly, cSCCs induced by Vemurafenib in melanoma cells were also described to be well-differentiated (Anforth et al., 2013; Anforth et al., 2015), which may be resembled by accelerated differentiation of HaCaT cells.

### 5.2.8 Vemurafenib caused genetic selection of HaCaT cells

As cSCCs are observed in Vemurafenib treated patients within weeks, prolonged exposure of keratinocytes could lead to either genotoxicity or the selection of a subclone that both may facilitate tumorigenesis. Accelerated differentiation of HaCaT monolayer cultures was only observed after several weeks of continuous exposure to Vemurafenib also implying a selection of a HaCaT cells. To address this question, HaCaT cells were continuously treated with 0.05% (v/v) DMSO, 1 $\mu M$ or 5 $\mu M$ Vemurafenib and subjected to a multiplex fluorescence *in situ* hybridization (M-FISH) analysis performed in cooperation with Prof. Dr. Anna Jauch (Heidelberg University Hospital). Interestingly, the Vemurafenib treated HaCaT cells remained genetically very similar to the control (DMSO) cells. Comparison of numerical aberrations for the individual chromosomes demonstrated a very similar profile with only a few deviations. When specifically comparing the aberration profile of the control cells with that of Vemurafenib treated HaCaT cells, it became obvious that Vemurafenib rather favored the selection of a preexisting subpopulations instead of novel aberrations. In particular, we detected a Vemurafenib dose-dependent gain of i(1q) carrying genes like S100, RASSF5, MAPKAPK2, TP53BP, WNT3A and WNT9A. Second, HaCaT cells showed a loss of i(17p) containing genes including TP53, MAP2K4, MAPK7 and RASD1. Third, we observed a dose-dependent translocation of (2)t(2;8) leading to a gain of MYC (Fig. 28). Thus, these data suggest that a potential mechanism of Vemurafenib in keratinocytes may be selection of preexisting subpopulations with a genetic makeup prone for tumorigenicity. Whether Vemurafenib is selecting for specific changes has yet to be determined.

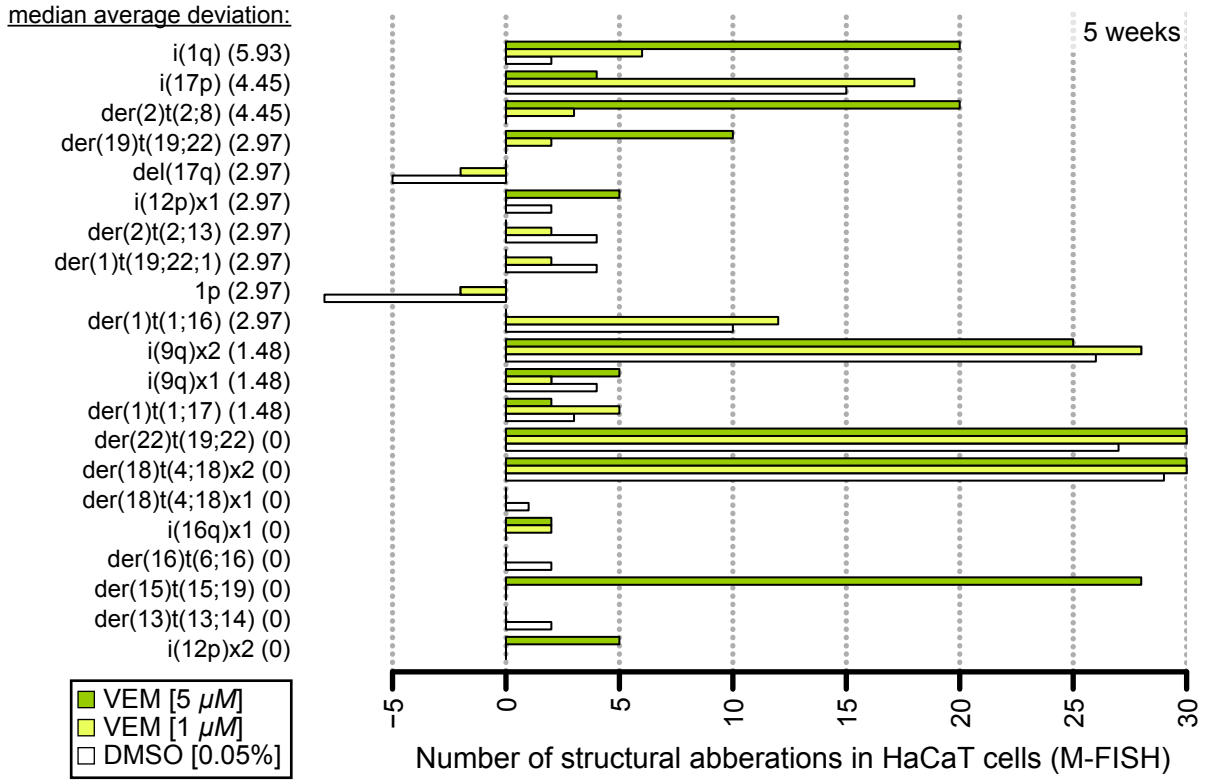


Figure 28 | **Vemurafenib mediates genetic selection of HaCaT cells.**

HaCaT cells were continuously treated with 0.05% (v/v) DMSO, 1 *μM* or 5 *μM* Vemurafenib for 5 weeks and subjected to a multiplex fluorescence *in situ* hybridization (M-FISH) analysis. Vemurafenib treated HaCaT cells remained genetically similar to the control, although Vemurafenib favored the selection of a preexisting subpopulation showing gain of i(1q), loss of i(17p) and dose-dependent translocation of (2)t(2;8) leading to a gain of MYC. [n=1]

## 5.2.9 Vemurafenib stimulation of scaOTCs increases HaCaT cell differentiation

In monolayer cultures, I could detect that Vemurafenib robustly hyper-activated MEK-ERK signaling in $BRAF^{wild\text{-}type}$ keratinocytes reflecting different stages in skin carcinogenesis. However, besides increased differentiation and a genetic selection pressure triggered by Vemurafenib, downstream effects explaining SCC progression remained elusive. The 3D organization may also be crucial for Vemurafenib induced carcinogenesis. Therefore, scaffold-based organotypic cultures (scaOTCs) were employed providing optimal growth and differentiation conditions for keratinocytes through the interaction with NHDF embedded in a Fibrin matrix. These cultures are stable for several months, allowing a longer follow-up of Vemurafenib stimulation compared to colOTCs. After one week submersed pre-cultivation, HaCaT cells were seeded on top of the dermal equivalent and grown air-exposed, forming a multi-layered stratified epithelium (Fig. 29a). To investigate the consequences under *in vivo*-like conditions, epithelial growth and stratification was allowed for 2 weeks to mimic the situation in patient's skin before treatment with Vemurafenib. As the Vemurafenib half-life in MM patients was assessed to be 51.6 h (Funck-Brentano et al., 2015), medium containing Vemurafenib or DMSO was replaced every 2-3 days. After 2 weeks (w 2+2), 4 weeks (w 2+4) or 7 weeks (w 2+7) of treatment, cultures were harvested (Fig. 29b). A macroscopic evaluation of these cultures showed that control cultures (Fig. 29c, d) were comparable to DMSO cultures after 2+4 weeks (Fig. 29e, f), implying that DMSO does not influence growth and differentiation of keratinocytes. In contrast, scaOTCs treatment with 1 *μM* (Fig. 29g, h) or 5 *μM* Vemurafenib (Fig. 29i, j) implied increased differentiation, but caused a dose-dependent loss in vitality of HaCaT cells.

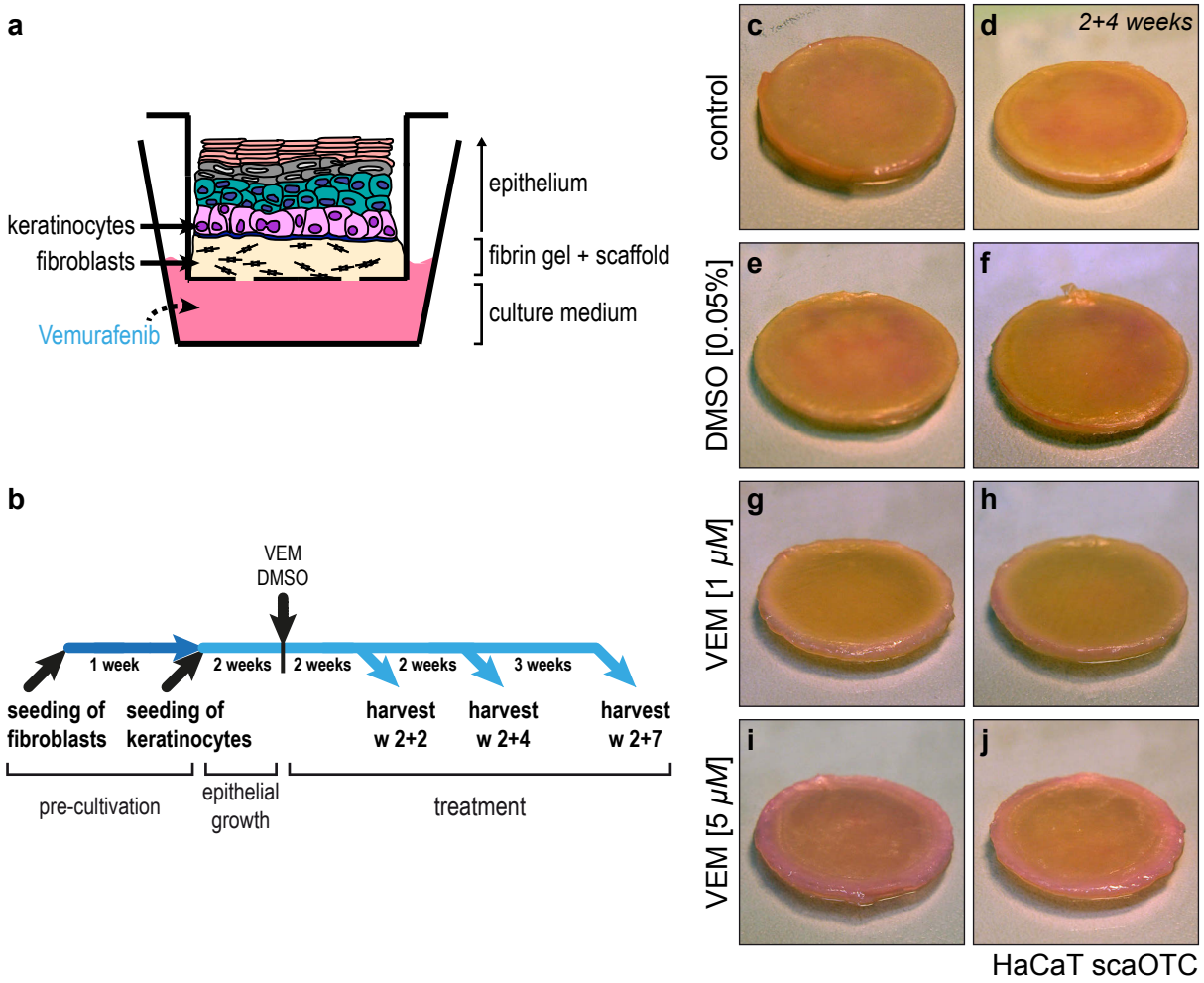


Figure 29 | **Stimulation of HaCaT scaOTCs with Vemurafenib.**

**a, b** | scaOTCs consisted of a Cellulose scaffold and a Fibrin matrix with embedded NHDF, which formed the dermal equivalent. After 1 week submersed pre-cultivation of NHDF, HaCaT cells were seeded and grown air-exposed. Epithelial growth and stratification was allowed for 2 weeks to mimic the *in vivo* situation before treatment with 0.05% (v/v) DMSO, 1 *µM* or 5 *µM* Vemurafenib for another 2, 4 or 7 weeks. **c-j** | A macroscopic evaluation after 2+4 weeks showed that controls (c, d) were comparable to DMSO cultures (e, f). scaOTCs treated with 1 *µM* (g, h) or 5 *µM* Vemurafenib (i, j) revealed increased differentiation and a dose-dependent loss in vitality of HaCaT cells. [n=2]

Histological analysis of the scaOTCs demonstrated that HaCaT cells formed a multilayered and rather disorganized epithelium revealing parakeratotic stratification from 2+2 to 2+4 weeks under control conditions (Fig. 30a, e). After 2+7 weeks, 2 viable basal cell layers remained with numerous cornfield layers on top (Fig. 30i). 0.05% (v/v) DMSO did not affect growth and morphology of keratinocytes under these 3D conditions, showing that DMSO treated cultures could serve as proper control for Vemurafenib cultures (Fig. 30b, f, j). Treatment with 1 *µM* Vemurafenib accelerated terminal differentiation of HaCaT cells as early as after 2 weeks compared to DMSO or control cultures (Fig. 30c). This effect was also observed at later harvest points (2+4, 2+7 weeks/ Fig. 30g, k) and comparable when treating the cultures for 2+2 or 2+4 weeks with 5 *µM* Vemurafenib (Fig. 30d, h). Viable basal cells could be observed under each condition even after 2+7 weeks of cultivation. Importantly, treatment for 2+7 weeks with 5 µM Vemurafenib caused an early invasion phenotype (Fig. 30l). Taken together, this first study confirmed in an *in vivo*-like environment the absence of toxic effects, but accelerated differentiation triggered by Vemurafenib in HaCaT cells. In addition, Vemurafenib may favor invasive growth of HaCaT cells, which required further investigations.

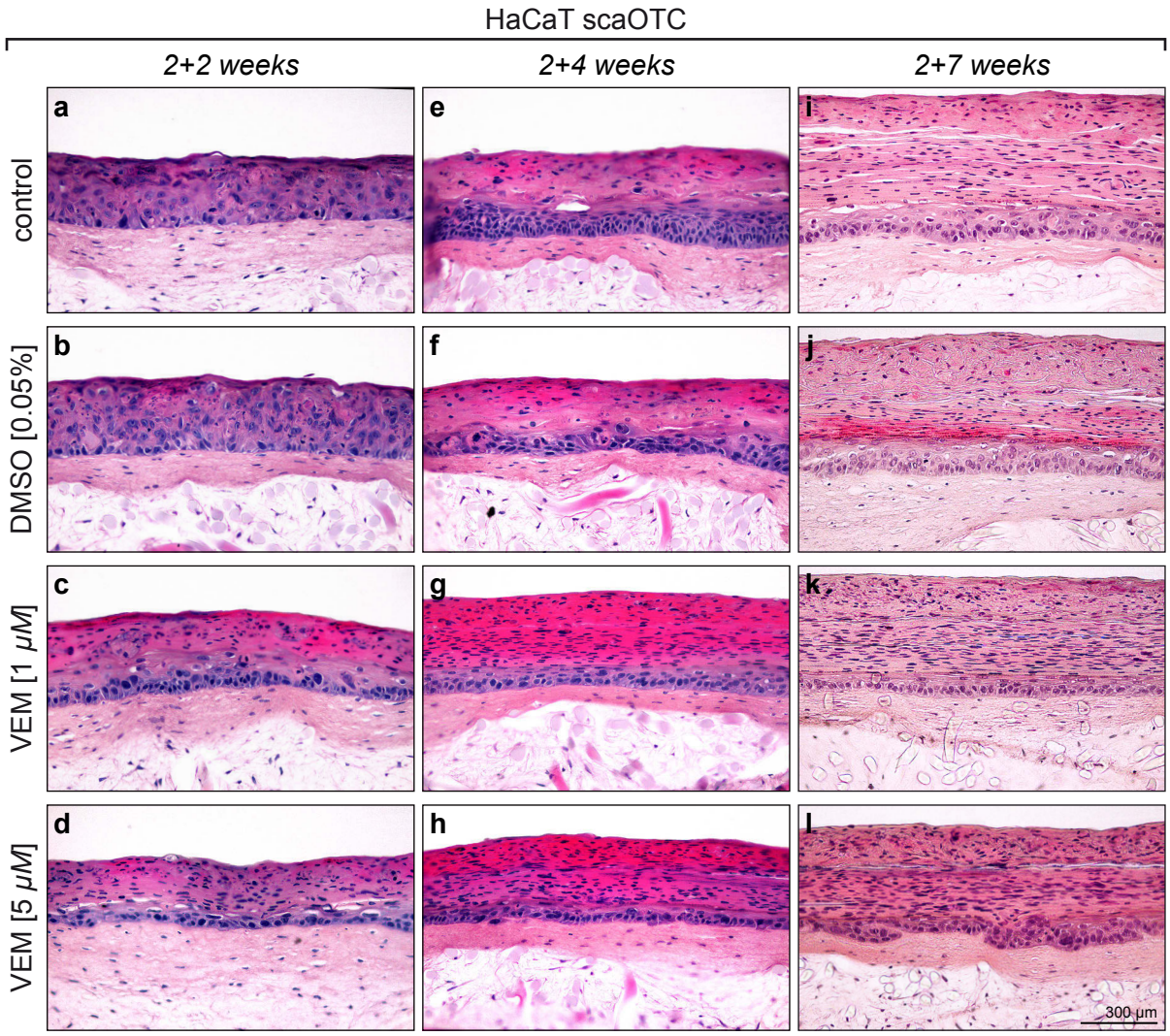


Figure 30 | **Vemurafenib accelerates terminal differentiation of HaCaT scaOTCs.**
scaOTCs consisted of a Cellulose scaffold and a Fibrin matrix with embedded NHDF, which formed the dermal equivalent. HaCaT cells were seeded on top and grown air-exposed. Epithelial growth and stratification was allowed for 2 weeks to mimic the *in vivo* situation before treatment with 0.05% (v/v) DMSO, 1 *µM* or 5 *µM* Vemurafenib. FFPE sections were stained with haematoxylin/ eosin to analyze the morphology. **a, e, i** | After 2+2 to 2+4 weeks, control cultures revealed a multilayered and disorganized epithelium with parakeratotic stratification (a, e). After 2+7 weeks, two viable basal cell layers remained with numerous cornfield layers (i). **b, f, j** | DMSO did not affect growth and morphology of HaCaT cells. **c, g, k** | Treatment with 1 *µM* Vemurafenib accelerated terminal differentiation of HaCaT cells after at each time point compared to the control. **d, h, l** | The accelerated differentiation was confirmed by 5 *µM* Vemurafenib (d, h, l). After 2+7 weeks, 5 *µM* Vemurafenib caused an early invasion phenotype (l). [n=2]

## 5.2.10 Vemurafenib stimulation of fdmOTCs

Since especially keratinocyte invasion is highly dependent on its environment and scaOTCs used in the first 3D experiments do not provide an ECM composition and height perfectly suited for invasion studies, the fibroblast-derived matrix-based organotypic cultures (fdmOTCs) were employed for subsequent experiments. This model makes use of a ECM secreted by NHDF that additionally shows increased vertical space to monitor invasive behavior of keratinocytes (Berning et al., 2015) (Fig. 31a). In order to generate fdmOTCs, NHDF were cultivated submersed for 4 weeks in FDM medium to generate the fibroblast-derived matrix. Afterwards, keratinocytes displaying different stages in skin carcinogenesis were also grown air-exposed on top for 2 weeks to resemble the pre-treatment situation in patients. Thereafter, stimulation with 1 *µM*, 5 *µM* Vemurafenib or 0.05% (v/v) DMSO was performed for 1 (2+1

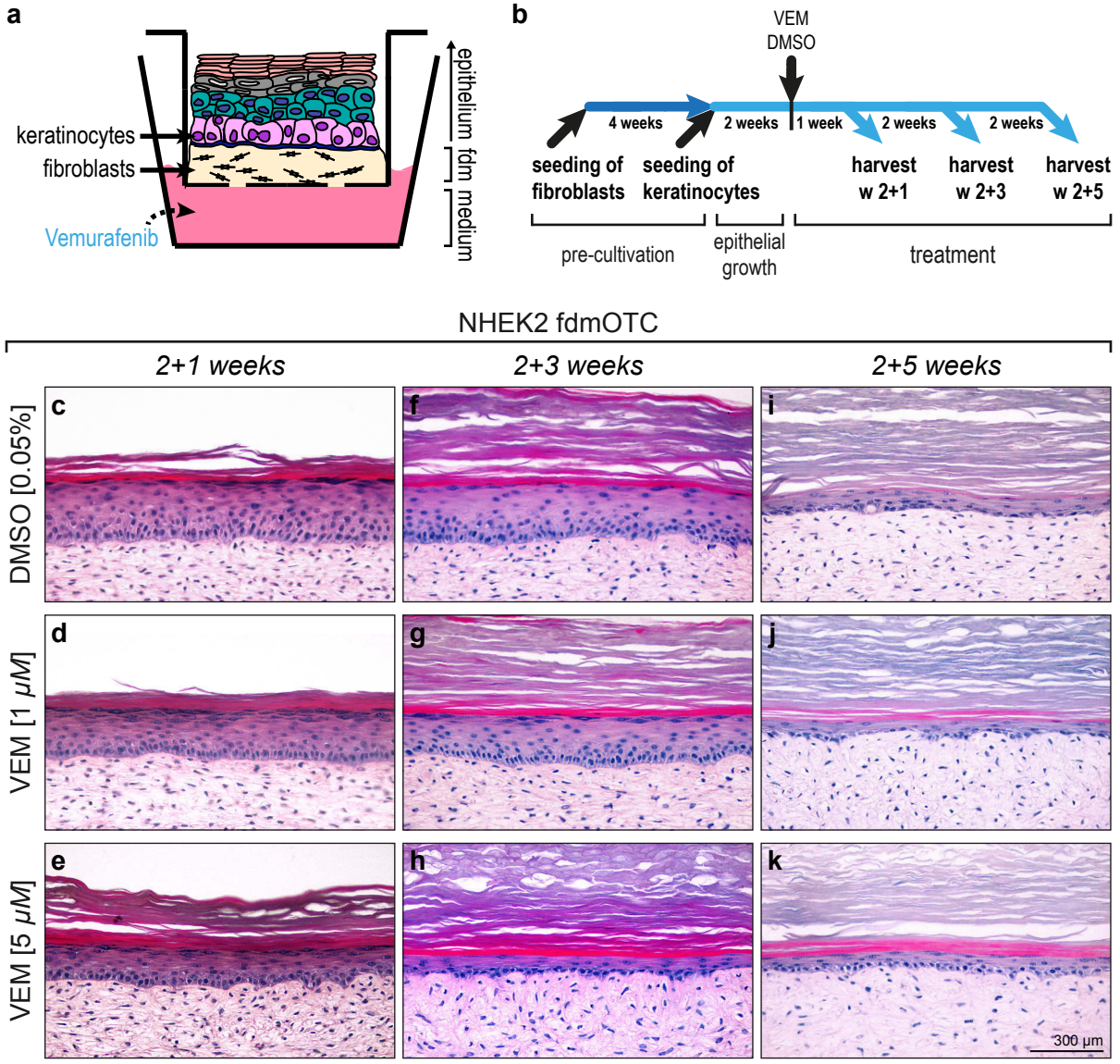


Figure 31 | **Vemurafenib accelerates terminal differentiation of NHEK fdmOTCs.**

**a, b** | fdmOTCs were prepared by NHDF cultivation for 4 weeks to generate a fibroblast-derived matrix (fdm), before keratinocyte seeding. The fdmOTC model makes use of an ECM secreted by NHDF that is more stable and shows increased vertical space to monitor invasive behavior (a). Epithelial growth and stratification was allowed for 2 weeks to mimic the *in vivo* situation and thereafter, cultures were treated with 0.05% (v/v) DMSO, 1 *µM* or 5 *µM* Vemurafenib for another 1, 3 or 5 weeks (b). FFPE sections were stained with haematoxylin/ eosin to analyze the morphology. **c, f, i** | After 2+1 weeks, NHEK fdmOTCs revealed an organized, hyperplastic, orthokeratotic, well-stratified epithelium (c). After 2+3 weeks, basal cells were organized, but the number of layers was reduced together with an accumulation of stratum corneum (f), which was more pronounced after 2+5 weeks (i). This demonstrated the typical shift from a hyperplastic to a homeostatic epithelium. **d, g, j** | Treatment with 1 *µM* Vemurafenib slightly increased differentiation. **e, h, k** | Stimulation with 5 *µM* Vemurafenib further reduced vital layers and led to an accumulation of stratum corneum already after 2+1 weeks (e). [n=2]

weeks), 3 (2+3 weeks) and 5 weeks (2+5 weeks), since Vemurafenib effects on scaOTCs were already observed after 2 and 4 weeks (Fig. 31b).

### 5.2.10.1 Vemurafenib stimulates differentiation and invasion of keratinocytes

NHEK fdmOTCs formed an organized but hyperplastic, well-stratified and orthokeratotic epithelium after 2+1 weeks of DMSO treatment (Fig. 31c). After 2+3 weeks, the basal cells were still organized

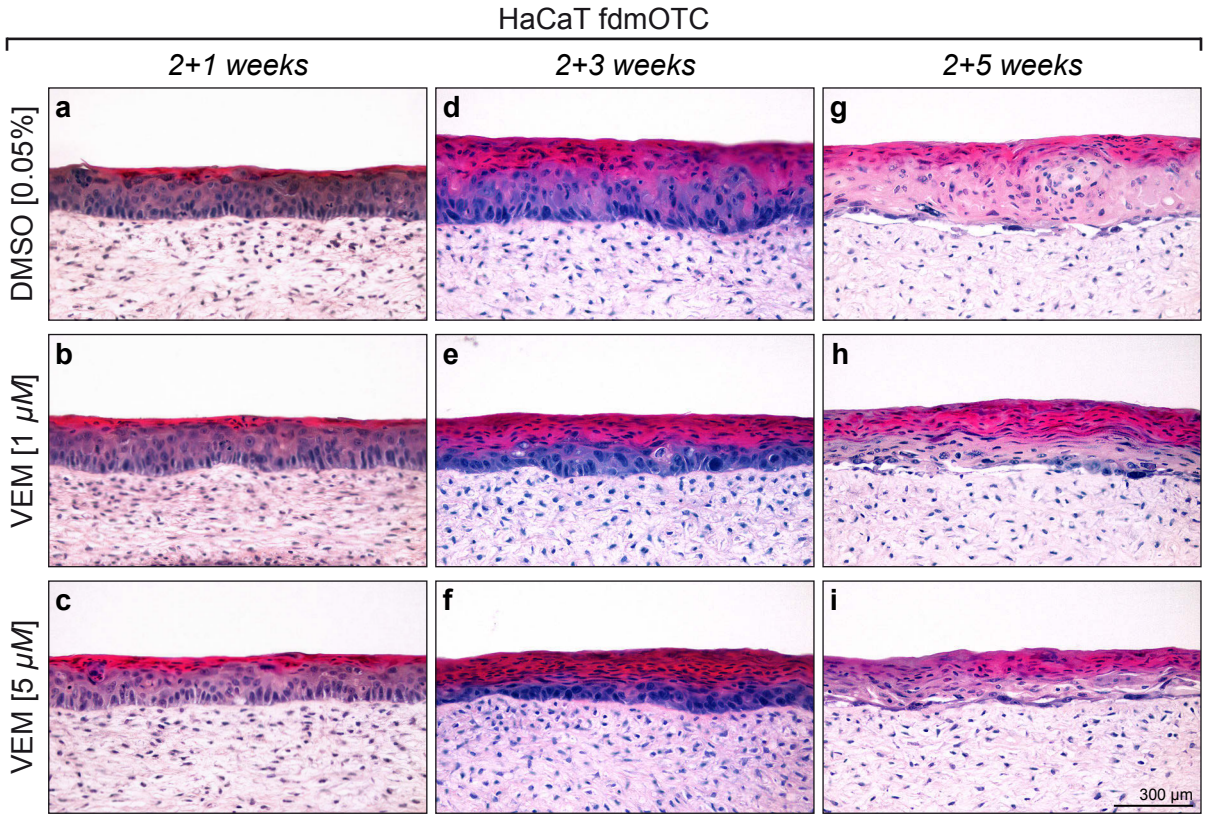


Figure 32 | **Vemurafenib accelerates terminal differentiation of HaCaT fdmOTCs.**

fdmOTCs were prepared by NHDF cultivation for 4 weeks to generate a fibroblast-derived matrix (fdm), before HaCaT cell seeding. Epithelial growth and stratification was allowed for 2 weeks to mimic the *in vivo* situation and thereafter, cultures were treated with 0.05% (v/v) DMSO, 1 *µM* or 5 *µM* Vemurafenib for another 1, 3 or 5 weeks. FFPE sections were stained with haematoxylin/ eosin to analyze the morphology. **a, d, g** | After 2+1 weeks, HaCaT fdmOTCs cultures showed a multi-layered, parakeratotic and slightly cornified epithelium (a). Differentiation improved by 2+3 weeks (d), which also prevented long-term regeneration of the cultures after 2+5 weeks (g). **b, e, h** | Treatment with 1 *µM* Vemurafenib showed no change after 2+1 weeks (b), but led to a reduction in vital layers and increased HaCaT cell differentiation after 2+3 weeks (e). Long-term regeneration was prevented as only differentiated layers remained after 2+5 weeks (h). **c, f, i** | 5 *µM* Vemurafenib caused elevated differentiation after 2+1 weeks (c), which further increased at cost of vital layers by 2+3 weeks (f). After 2+5 weeks, terminal differentiation of all vital HaCaT cell layers was observed (i). [n=2]

but a reduction in the number of vital layers together with an accumulation of stratum corneum were observed. This displayed the typical shift from a hyperplastic to a homeostatic epithelium that is also found in wounded normal skin (Fig. 31f). The progression towards a homeostatic epithelium could be followed until 2+5 weeks (Fig. 31i). Treatment with 1 *µM* Vemurafenib did not reveal morphological changes of the epithelium compared to control cultures. However, due to the large stratum corneum in control cultures, small effects on differentiation could likely not be visualized (Fig. 31d, g, j). Stimulation of NHEK with 5 *µM* Vemurafenib led to a reduction in vital layers and an accelerated accumulation of stratum corneum already after 2+1 weeks (Fig. 31e, h, k). A vital epithelium was preserved under all conditions, confirming that Vemurafenib did not hinter long-term regeneration of NHEK (Fig. 31i, j, k).

HaCaT fdmOTCs showed a multi-layered but little cornified and parakeratotic epithelium after 2+1 weeks (Fig. 32a). Differentiation improved by 2+3 weeks (Fig. 32d), however, long-term regeneration was hampered by terminal differentiation of the cultures. After 2+5 weeks, barely a vital HaCaT cell could be observed below the differentiated layers (Fig. 32g). Treatment with 1 *µM* Vemurafenib showed a similar morphology compared to DMSO treated cultures after 2+1 weeks (Fig. 32b). However, after

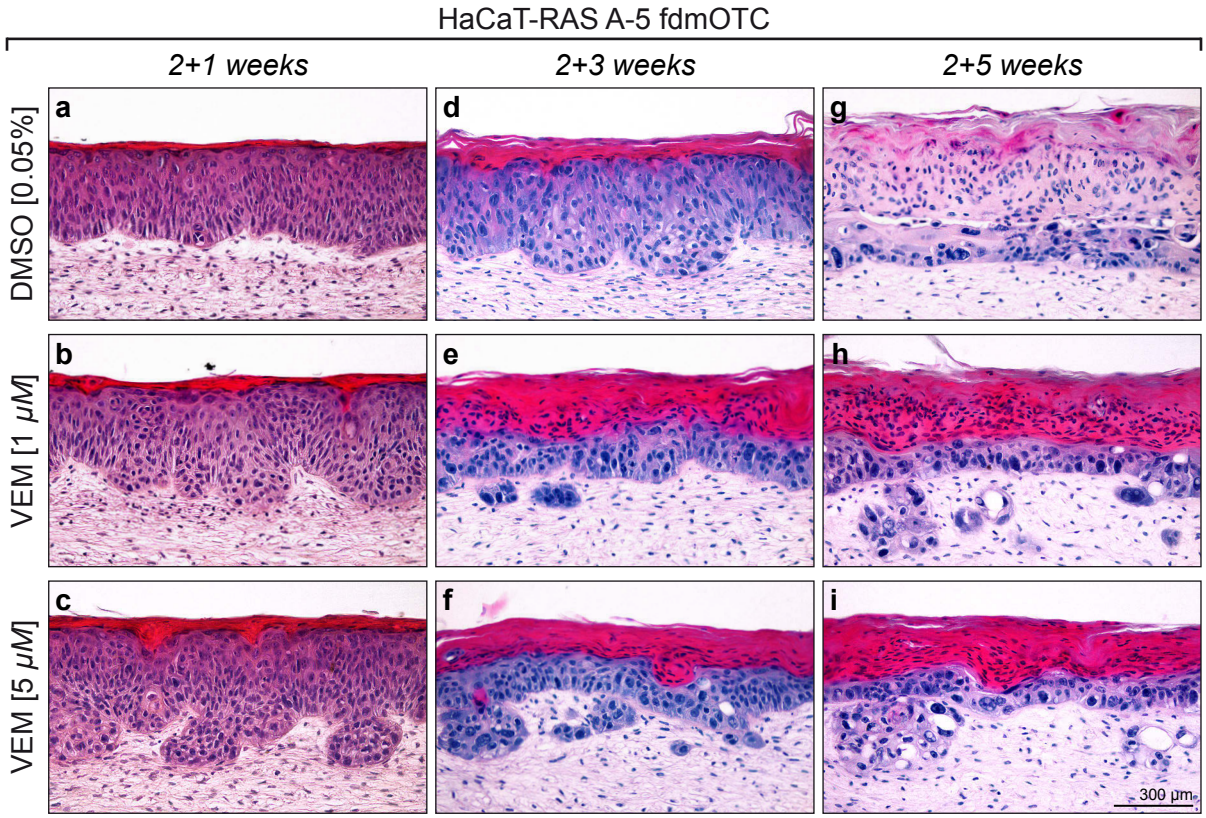


Figure 33 | **Vemurafenib causes differentiation and invasion of HaCaT-RAS A-5 fdmOTCs.**
fdmOTCs were prepared by NHDF cultivation for 4 weeks to generate a fibroblast-derived matrix (fdm), before HaCaT-RAS A-5 cell seeding. Epithelial growth and stratification was allowed for 2 weeks to mimic the *in vivo* situation and thereafter, cultures were treated with 0.05% (v/v) DMSO, 1 *µM* or 5 *µM* Vemurafenib for another 1, 3 or 5 weeks. FFPE sections were stained with haematoxylin/ eosin to analyze the morphology. **a, d, g** | After 2+1 weeks, HaCaT-RAS A-5 fdmOTCs established a multilayered hyper-proliferative and orthokeratotic epithelium (a). After 2+3 weeks, the epithelium showed less organization and increased differentiation with a discrete stratum corneum (d). At 2+5 weeks, the epithelium showed parakeratosis and became atrophic (g). **b, e, h** | Treatment with 1 *µM* Vemurafenib caused accelerated differentiation after 2+1 weeks (b), which was still observed after 2+3 weeks, although a shift orthokeratosis to parakeratosis was observed (e). A highly cornified but vital epithelium was detected after 2+5 weeks (h). 1 *µM* Vemurafenib also caused HaCaT-RAS A-5 cell invasion into the dermal equivalent. After 2+1 weeks, early invasive buds were observed (b) leading to complete invasive growth after 2+3 weeks (e). **c, f, i** | Treatment with 5 µM Vemurafenib led to similar effects, including accelerated differentiation and, a shift from orthokeratosis to parakeratosis (c, f, i). 5 *µM* Vemurafenib also caused HaCaT-RAS A-5 cell invasion into the underlying dermal equivalent (f, i). [n=2]

2+3 weeks of treatment, Vemurafenib caused a reduction in vital layers together with an increase in HaCaT cell differentiation (Fig. 32e). Similar to DMSO treated cultures, long-term regeneration was prevented as only differentiated layers remained after 2+5 weeks (Fig. 32h). 5 *µM* Vemurafenib already mediated increased differentiation after 2+1 weeks (Fig. 32c), which subsequently increased at cost of vital layers by 2+3 weeks (Fig. 32f). After 2+5 weeks, long-term regeneration was prevented by terminal differentiation of all vital HaCaT cell layers (Fig. 32i).

HaCaT-RAS A-5 fdmOTCs established a multilayered hyper-proliferative and orthokeratotic epithelium after 2+1 weeks with more cell layers as observed in NHEK and HaCaT fdmOTCs (Fig. 33a). After 2+3 weeks, the epithelium showed less organization and increased differentiation with a discrete stratum corneum (Fig. 33d). However, after 2+5 weeks, the epithelium showed parakeratosis and became atrophic leaving only some vital cells within the basal layers (Fig. 33g). Treatment with 1 *µM* Vemurafenib already caused accelerated differentiation revealing a orthokeratotic epithelium after 2+1 weeks (Fig. 33b). After 2+3 weeks, accelerated differentiation was still observed leading

to large amounts of terminally differentiated layers, however, revealing a shift from orthokeratosis to parakeratosis (Fig. 33e). Especially after 2+5 weeks, a highly cornified epithelium and still vital parakeratotic HaCaT-RAS A-5 epithelium was observed (Fig. 33h). Treatment with 5 µM Vemurafenib led to similar effects, including accelerated differentiation, a shift from orthokeratosis to parakeratosis as well as the generation of a highly differentiated, but vital epithelium after 2+5 weeks (Fig. 33c, f, i). Besides that, both, 1 $\mu M$ and 5 $\mu M$ Vemurafenib treatment caused HaCaT-RAS A-5 cell invasion into the underlying dermal equivalent. After 2+1 weeks of treatment, early invasive buds were observed leading to complete invasive growth after 2+3 weeks. Interestingly, signs of atrophy were observed after 2+5 weeks at invasion sites (Fig. 33e, h, f, i).

Taken together, treatment with Vemurafenib led to an accelerated differentiation accompanied by a reduction of vital layers in all analyzed keratinocytes. Importantly, Vemurafenib stimulation of benign-tumorigenic HaCaT-RAS A-5 cells caused invasive growth together with an improved viability after 2+5 weeks.

### 5.2.10.2 Vemurafenib mediates ERK hyper-activation in fdmOTCs

To correlate the observed accelerated differentiation, but especially the invasion of HaCaT-RAS A-5 cells to a potential Vemurafenib induced MEK-ERK hyper-activation also OTCs, sections of HaCaT and HaCaT-RAS A-5 fdmOTCs were analyzed for ERK phosphorylation by immunohistochemistry (IHC). DMSO treated HaCaT and HaCaT-RAS A-5 cultures showed some cytoplasmic ERK phosphorylation (brown) with a tendency for basal keratinocytes after 2+3 weeks (Fig. 34a, c). At the same time, Vemurafenib treatment (5 $\mu M$) strongly increased ERK phosphorylation in all vital layers of the HaCaT epithelium and demonstrated activation in the underlying NHDF (Fig. 34b). Moreover, Vemurafenib also induced ERK phosphorylation throughout the HaCaT-RAS A-5 epithelium (Fig. 34d). This showed that Vemurafenib leads to MEK-ERK hyper-activation in BRAF$^{\text{wild-type}}$ keratinocytes as well as in HaCaT and HaCaT-RAS A-5 fdmOTCs, which likely mediated the observed effects in differentiation and invasion.

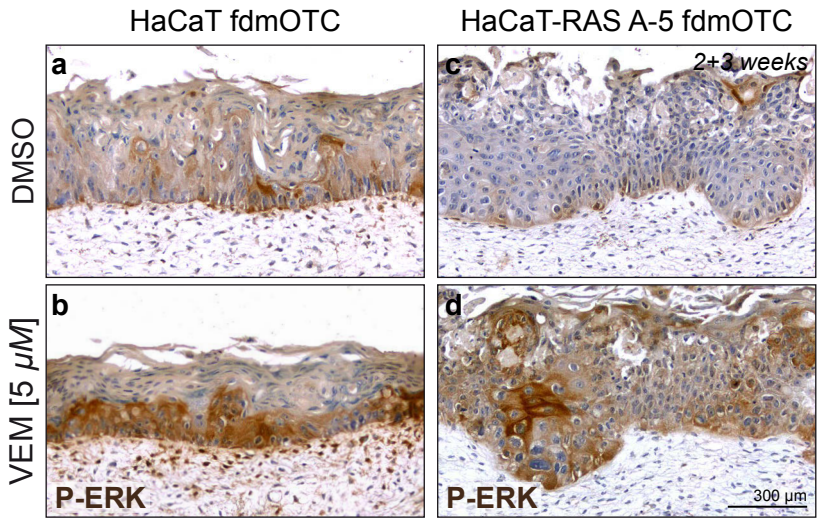


Figure 34 | **Vemurafenib triggers MEK-ERK hyper-activation in fdmOTCs.**
fdmOTCs were prepared by NHDF cultivation for 4 weeks to generate a fibroblast-derived matrix (fdm), before HaCaT or HaCaT-RAS A-5 cell seeding. Epithelial growth and stratification was allowed for 2 weeks to mimic the *in vivo* situation and thereafter, cultures were treated with 0.05% (v/v) DMSO or 5 $\mu M$ Vemurafenib for another 3 weeks. Ras-Raf-MEK-ERK pathway activity was analyzed by performing immunohistochemistry (IHC) for ERK phosphorylation on FFPE fdmOTCs. **a, b** | DMSO treated HaCaT cultures showed some cytoplasmic ERK phosphorylation (brown) after 2+3 weeks (a). Vemurafenib strongly increased ERK phosphorylation, thus pathway activation, in all vital layers and demonstrated activation in the underlying NHDF (b). **c, d** | DMSO treated HaCaT-RAS A-5 cultures showed ERK phosphorylation (brown) in the basal cell layer (c). Vemurafenib induced ERK phosphorylation throughout the epithelium (d). [n=2]

### 5.2.10.3 Differentiation but not proliferation is accelerated by Vemurafenib fdmOTCs

Although MEK-ERK activation is commonly coupled to growth (Dhillon et al., 2007), proliferation was not detected in monolayer cultures. As 3D organization and interaction with NHDF may be crucial mediators, proliferation upon Vemurafenib treatment was assessed in 2+3 week-old fdmOTCs. Therefore, NHEK as well as TP53 and HRAS-mutant HaCaT-RAS A-5 cultures as two opposing cell types were stained by immunofluorescence for the proliferation marker Ki67. Staining for the BM marker Collagen VII revealed the epidermal-mesenchymal border and allowed calculating a proliferation index that correlates the number of proliferating cells to the corresponding BM length. As result, NHEK cultures showed some basal proliferation without major differences in Ki67 staining between DMSO (Fig. 35a), 1 $\mu M$ (Fig. 35b) or 5 $\mu M$ Vemurafenib treated cultures (Fig. 35c). Quantification showed a proliferation index of approx. 4.1 irrespective of the treatment condition (Fig. 35g). HaCaT-RAS A-5 fdmOTCs generally showed suprabasal Ki67-positive cells (Fig. 35d), which may account to the slightly increased proliferation index of 5.6 compared to NHEK cultures (Fig. 35g). Upon Vemurafenib stimulation (1 $\mu M$ or 5 $\mu M$), HaCaT-RAS A-5 cells revealed accumulations of proliferative cells at invasion sites demonstrating that proliferation is not homogeneously distributed over the entire culture (Fig. 35e,

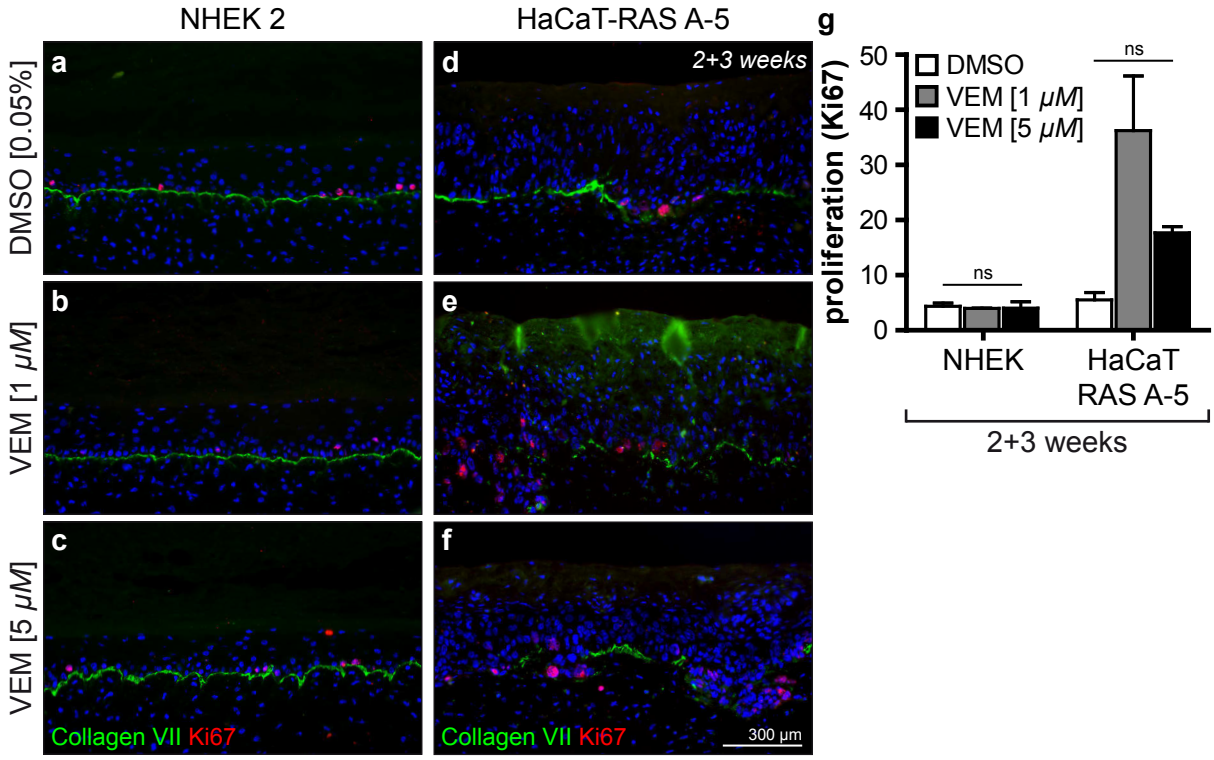


Figure 35 | **Keratinocyte proliferation is not induced by Vemurafenib in fdmOTCs.**
fdmOTCs were prepared by NHDF cultivation for 4 weeks to generate a fibroblast-derived matrix (fdm), before keratinocyte seeding. Epithelial growth and stratification was allowed for 2 weeks to mimic the *in vivo* situation and thereafter, cultures were treated with 0.05% (v/v) DMSO, 1 $\mu M$ or 5 $\mu M$ Vemurafenib for another 3 weeks. To assess proliferation, cryo-conserved and fixed sections of NHEK 2 and HaCaT-RAS A-5 cultures were stained for the proliferation marker Ki67 and the BM component Collagen VII by immunofluorescence. **a-f** | NHEK cultures showed some basal proliferation without major differences in Ki67 staining between DMSO (a), 1 $\mu M$ (b) or 5 $\mu M$ Vemurafenib treated cultures (c). HaCaT-RAS A-5 fdmOTCs generally showed suprabasal Ki67-positive cells (d). Vemurafenib stimulation led to the accumulation of proliferative cells at invasion sites (e, f). **g** | Co-staining with Collagen VII allowed calculating a proliferation index by correlating the number of proliferating cells to the BM length. Neither HaCaT nor HaCaT-RAS A-5 cells revealed significant differences in the proliferative index upon Vemurafenib. [n=2, mean ± SEM, One-way ANOVA + Dunnett's Multiple Comparison Test]

f). Therefore, 1 $\mu M$ and 5 $\mu M$ Vemurafenib increased the proliferation index to either 36.3 or 17.7. However, none of these results revealed significant differences in proliferation (Fig. 35g).

In order to confirm the increased differentiation upon Vemurafenib as observed in histological staining, 2+3 week-old fdmOTC cryo sections were analyzed for differentiation markers by immunofluorescence. Staining was performed for the early differentiation marker Keratin-10, expressed in the stratum spinosum up to the stratum corneum, as well as for the late differentiation marker Filaggrin, expressed from stratum granulosum to stratum corneum in human skin. NHEK control fdmOTCs revealed Keratin-10 in all epithelial layers besides the stratum basale as expected for normal cells (Fig. 36a). Treatment with 1 $\mu M$ or 5 $\mu M$ Vemurafenib even increased the number of the differentiated layers (Fig. 36b, c). HaCaT cells showed Keratin-10 staining only in the uppermost epidermal layers confirming a low differentiation profile, as described by histology (Fig. 36d). 1 $\mu M$ and 5 $\mu M$ Vemurafenib increased tissue organization and the number of Keratin-10 positive cell layers, thus differentiation (Fig. 36e, f). Compared to HaCaT cultures, HaCaT-RAS A-5 control fdmOTCs showed increased differentiation (Fig. 36g). Again, Vemurafenib seemed to improve tissue organization revealing a more organized suprabasal distribution of Keratin-10 positive cell layers, while invasive buds were not stained. Although Vemurafenib treated HaCaT-RAS A-5 cultures showed accelerated differentiation in the histological sections, this effect could not be confirmed by Keratin-10 immunofluorescence. Control and treated cultures showed a similar Keratin-10 expression. However, the Keratin-10 positive layers may be more compact in Vemurafenib cultures compared to the control (Fig. 36h, i).

Furthermore, the late differentiation maker Filaggrin was detected in the stratum granulosum and stratum corneum of control NHEK fdmOTCs, as expected for normal cells (Fig. 36j). Treatment with Vemurafenib led to an increased terminal differentiation as determined by the higher number of Filaggrin positive layers (Fig. 36k, l). HaCaT fdmOTCs generally showed very low levels of late differentiation compared to NHEK (Fig. 36m). Vemurafenib treatment led, if at all, to a minor increase in Filaggrin levels compared to DMSO control cultures (Fig. 36n, o). In contrast, HaCaT-RAS A-5 control cultures demonstrated higher Filaggrin levels compared to HaCaT fdmOTCs (Fig. 36p). Vemurafenib slightly increased suprabasal Filaggrin at 1 $\mu M$, which was further increased showing locally elevated concentrations when stimulated with 5 $\mu M$. Invasion sites remained negative also for Filaggrin (Fig. 36q, r). In addition to immunofluorescence staining, NHEK and HaCaT-RAS A-5 fdmOTC epithelia were also separated from the dermal equivalents by Dispase incubation to perform RNA isolation and qRT-PCR analysis of FLG mRNA expression. In NHEK fdmOTCs, 5 $\mu M$ Vemurafenib treatment caused a 2.4-fold increased FLG expression compared to DMSO cultures after 2+1 weeks. Thereafter, FLG expression levels decreased to 0.6-fold after 2+3 weeks. A similar FLG upregulation was also detected in HaCaT-RAS A-5 fdmOTCs, however, showing 0.7-fold regulation after 2+1 weeks, followed by a delayed upregulation of 2.6-fold after 2+3 weeks (Fig. 36s). Together, this confirmed that Vemurafenib directly accelerated differentiation also in fdmOTCs, while keratinocyte proliferation was not altered.

### 5.2.10.4 Gelatinolytic activity is increased by Vemurafenib

The BM was analyzed in fdmOTCs by immunofluorescence staining for the BM component Collagen IV in order to investigate the mechanism of HaCaT-RAS A-5 invasion. In NHEK fdmOTCs, Collagen IV

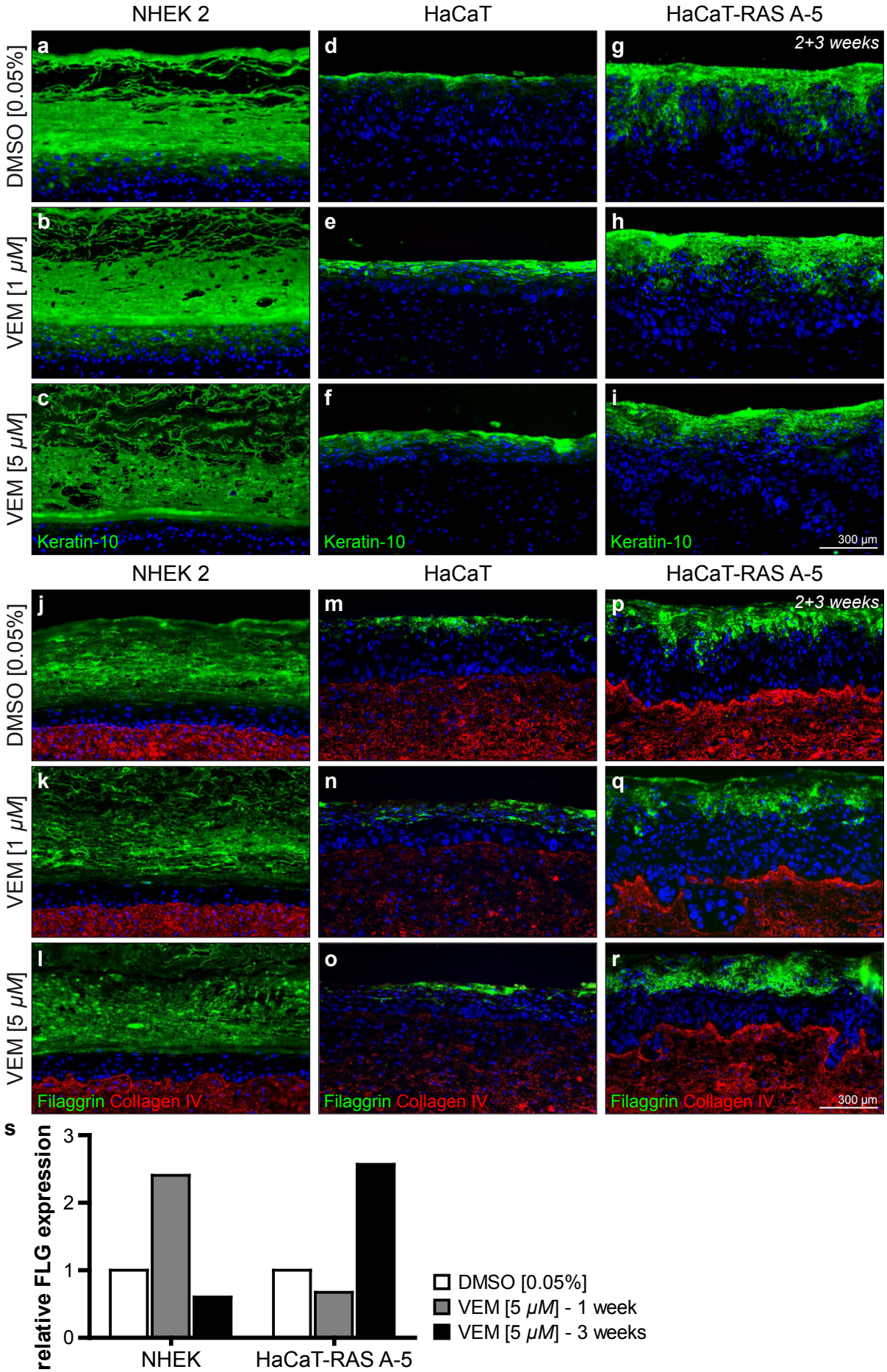
NHEK 2
HaCaT
HaCaT-RAS A-5
DMSO [0.05%]
VEM [1 µM]
VEM [5 µM]
a
b
c
d
e
f
g
h
i
2+3 weeks
Keratin-10
300 µm
j
k
l
m
n
o
p
q
r
Filaggrin Collagen IV
s
relative FLG expression
0
1
2
3
NHEK
HaCaT-RAS A-5
DMSO [0.05%]
VEM [5 µM] - 1 week
VEM [5 µM] - 3 weeks

Figure 36 | **Keratinocyte differentiation is accelerated by Vemurafenib in fdmOTCs.**
fdmOTCs were prepared by NHDF cultivation for 4 weeks to generate a fibroblast-derived matrix (fdm), before NHEK, HaCaT or HaCaT-RAS A-5 cell seeding. Epithelial growth and stratification was allowed for 2 weeks to mimic the *in vivo* situation and thereafter, cultures were treated with 0.05% (v/v) DMSO, 1 *µM* or 5 *µM* Vemurafenib for another 1 or 3 weeks. **a-i** | To analyze keratinocyte differentiation, cryo-sections of 2+3 week-old fdmOTC were fixed and analyzed for differentiation markers by immunofluorescence. In NHEK the early differentiation marker Keratin-10 (green) was detected in all epithelial layers besides the stratum basale, as in normal skin (a). Treatment with 1 *µM* or 5 *µM* Vemurafenib increased the number of the differentiated layers (b, c). HaCaT cells showed Keratin-10 staining only in the uppermost epidermal layers (d). 1 *µM* and 5 *µM* Vemurafenib increased tissue organization and the number of Keratin-10 cell layers (e, f). HaCaT-RAS A-5 control fdmOTCs showed increased differentiation (g). Vemurafenib improved Keratin-10 organization likely leading to differentiated layers with increased density (h, i). [n=2] **j-r** | The late differentiation maker Filaggrin (green) was detected in the stratum granulosum and corneum of control NHEK fdmOTCs (j), while Vemurafenib increased the number of Filaggrin positive layers (k, l). HaCaT fdmOTCs generally showed low terminal differentiation (m). Vemurafenib treatment led to a minor increase in Filaggrin (n, o). HaCaT-RAS A-5 control cultures demonstrated higher Filaggrin levels as HaCaT fdmOTCs (p) and Vemurafenib slightly increased suprabasal Filaggrin in a dose-dependent manner (q, r). The BM component Collagen IV (red) was detected in NHEK fdmOTCs at the BM as well as throughout the dermal ECM (j), remained constant by 1 *µM* (k), but slightly decreased by 5 µM Vemurafenib (l). HaCaT fdmOTCs revealed low Collagen IV levels (m). 1 *µM* and 5 *µM* Vemurafenib treatment caused a reduction (n, o). HaCaT-RAS A-5 cultures revealed a strong Collagen IV signal with an accumulation at the BM (p), which was reduction by Vemurafenib treatment (q, r). [n=2] **s** | NHEK and HaCaT-RAS A-5 fdmOTC epithelia were separated from the dermal equivalents by Dispase incubation and subjected to RNA isolation and qRT-PCR analysis. In NHEK fdmOTCs, 5 *µM* Vemurafenib increased FLG expression at 2+1 weeks, whereas levels declined thereafter. A delayed FLG upregulation was detected in HaCaT-RAS A-5 fdmOTCs showing a downregulation after 2+1 weeks followed by an upregulation after 2+3 weeks. [n=1]

was detected at the BM as well as throughout the dermal ECM after 2+3 weeks (Fig. 36j). Interestingly, Collagen IV levels remained constant by stimulation with 1 *µM* (Fig. 36k), but showed a slight decrease by 5 µM Vemurafenib (Fig. 36l). HaCaT fdmOTCs generally showed lower Collagen IV levels especially directly under the epithelium (Fig. 36m). 1 *µM* and 5 *µM* Vemurafenib treatment caused a reduction in Collagen IV levels compared to DMSO control cultures (Fig. 36n, o). Furthermore, HaCaT-RAS A-5 control cultures revealed a strong Collagen IV signal across the dermal equivalent with an accumulation at the BM (Fig. 36p), which was reduced by Vemurafenib treatment (Fig. 36q, r).

Invasion is commonly associated with MMPs. To determine whether MMP-activity is involved in the observed reduction of Collagen IV in Vemurafenib treated fdmOTCs as well as the invasive phenotype of HaCaT-RAS A-5 cultures, a Gelatinase assay was performed on cryo-sections of invasively growing HaCaT-RAS A-5 fdmOTC. Control HaCaT-RAS A-5 fdmOTCs demonstrated a low fluorescence signal (green) after 2+5 weeks, arguing for an overall weak Gelatinase cleavage and thus, for a low MMP-

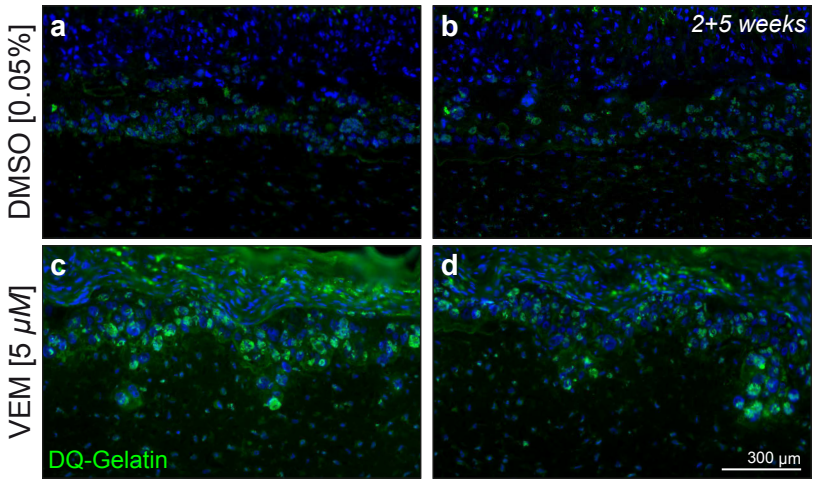


Figure 37 | **Gelatinolytic activity is increased by Vemurafenib in HaCaT-RAS A-5 fdmOTCs.**
fdmOTCs were prepared by NHDF cultivation for 4 weeks to generate a fibroblast-derived matrix (fdm), before HaCaT-RAS A-5 cell seeding. Epithelial growth and stratification was allowed for 2 weeks to mimic the *in vivo* situation and thereafter, cultures were treated with 0.05% (v/v) DMSO or 5 *µM* Vemurafenib for another 5 weeks. An *in situ* zymography was performed on unfixed cryo-section to investigate the MMP-activity. Control cultures demonstrated a low fluorescence signal (green), implying a low MMP-activity (**a, b**). Vemurafenib caused a strong increase in fluorescence signal especially within the invasive areas (**c, d**). [n=2]

activity (Fig. 37a, b). In contrast, Vemurafenib caused a strong increase in fluorescence signal especially within the invasive areas of the HaCaT-RAS A-5 epithelium (Fig. 37c, d). Thus, an elevated MMP-activity upon Vemurafenib correlated with Collagen IV degradation and invasion of HaCaT-RAS A-5 cells.

## 5.2.11 MEK-ERK hyper-activation is mediated by Vemurafenib in NHDF

To investigate whether Vemurafenib triggered the release of paracrine factors by NHDF leading to invasive growth of HaCaT-RAS A-5 cells, we first asked if Vemurafenib indeed hyper-activated MEK-ERK signaling also in NHDF monolayer cultures of two individual donors. Western-Blot analysis revealed increased phosphorylation of MEK and ERK after 30 min Vemurafenib stimulation (1 $\mu M$) that reached a maximal induction after 1-3 h and was subsequently declining. NHDF stimulated with DMSO (0.01%) also showed some increased MEK and ERK phosphorylation, which could be correlated to the addition of fresh growth medium at the time of stimulation. While Akt signaling was not altered, a reproducible p38 phosphorylation was monitored after 30 min of Vemurafenib stimulation. Since MEK, ERK and p38 regulations were similar in both NHDF strains, we excluded donor-specific effects (Fig. 38a, b). Thus, this data demonstrated that Vemurafenib-induced MEK-ERK hyper-activation is not only triggered in BRAF$^{\text{wild-type}}$ keratinocytes, but also in NHDF. As both, keratinocytes and NHDF were activated by Vemurafenib, the observed HaCaT-RAS A-5 invasion could indeed result either from direct keratinocyte stimulation or secreted factors derived from activated NHDF.

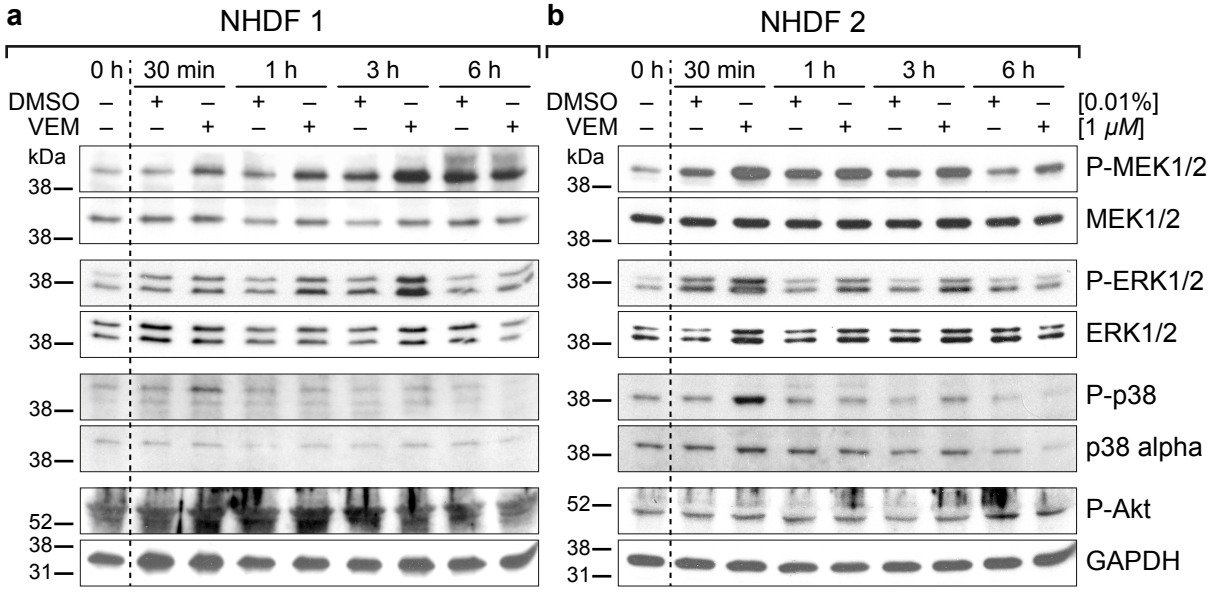


Figure 38 | **Vemurafenib triggers MEK-ERK hyper-activation also in NHDF.**

NHDF monolayer cultures were stimulated with either 1 $\mu M$ Vemurafenib or 0.01% (v/v) DMSO in growth medium for 6 h and MEK, ERK, p38 or Akt-activation were analyzed by Western-Blot. Stimulation of two different normal human dermal fibroblasts, NHEK 1 (**a**) and NHEK 2 (**b**), with DMSO showed some increased MEK and ERK phosphorylation, which could be accounted to the addition of fresh growth medium. Vemurafenib mediated MEK and ERK hyper-phosphorylation after 30 min, which reached a maximum after 1-3 h and subsequently declined. While Akt signaling was not altered, a reproducible p38 phosphorylation was monitored after 30 min of Vemurafenib stimulation. [n=1 per NHDF donor]

## 5.2.12 Vemurafenib activation of NHDF and invasion in fdmOTCs

To address the role of Vemurafenib-activated NHDF on HaCaT-RAS A-5 invasion, NHDF were pre-treated with Vemurafenib for 3 weeks during fdm generation. The treatment was discontinued immediately before seeding of HaCaT-RAS A-5 cells, allowing the accumulation of potential fibroblast-derived factors that may act on the keratinocytes (Fig. 39a). After another 3 weeks, cultures pre-treated with 0.05% (v/v) DMSO showed several undifferentiated cell layers and a BM without signs of invasion (Fig. 39b). Pre-treatment with 1 *µM* or 5 *µM* Vemurafenib did not strongly affect differentiation, as expected, but caused a disorganization of the BM in a dose-dependent manner (Fig. 39c, d). This early invasive phenotype may point either to a role of Vemurafenib activated NHDF or alternatively to Vemurafenib which was retained in the ECM and directly acted on HaCaT-RAS A-5 cells.

In order to determine genes, which are expressed in response to Vemurafenib, NHDF monolayer cultures were stimulated with 1 *µM* or 5 *µM* Vemurafenib for 8 h and 24 h. Subsequently, RNA was subjected to expression analysis for known growth factors (TGFA, TGFB1, TGFB3, IL1A, IL1B, HGF, CSF2, FGF7, FGF10), cytokines of the fibroblast secretome (IL6, IL8, CCL2, CXCL10, CXCL12) and matrix remodeling factors (MMP1, MMP3, MMP9, MMP14). The activation of Wnt/Beta-catenin signaling (AXIN2) or the p21 pathway (CDKN1A) as well as expression of the myofibroblast marker (alphaSMA) were also determined. Normalization was performed using GAPDH as house-keeping gene and fold-changes were expressed by comparing 1 *µM* or 5 *µM* Vemurafenib treatment of NHDF to 0.05% (v/v) DMSO stimulation. To our surprise, none of the genes showed regulation beyond 2-fold after 8 and 24 h (Fig. 40a). As the tissue organization may play a role in gene regulation also in respect to treatment with Vemurafenib, NHDF was allowed to form a dermal equivalent (fdm). After an initial phase of 1 week, NHDF were constantly stimulated with Vemurafenib for another 3 weeks in FDM medium. Compared to monolayer cultures, a few distinct gene regulations were detected including a 3.7-fold downregulation of TGFA by 5 *µM* Vemurafenib as well as a 2.1-fold upregulation of CSF2 by 1 *µM* Vemurafenib. However, in agreement with 2D cultures, I did not observe major gene regulations also in 3D (Fig. 40b).

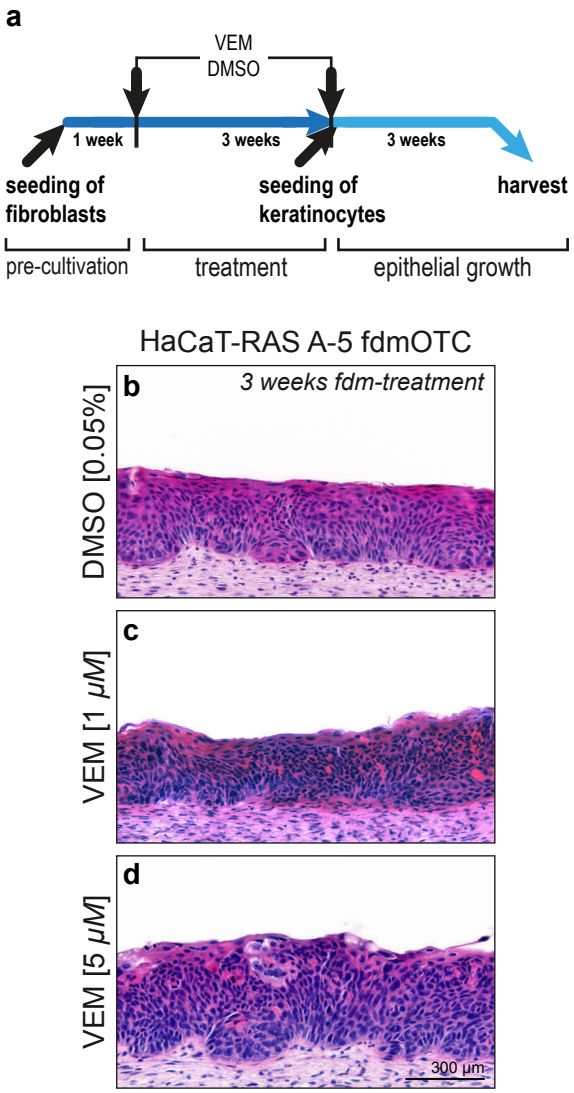


Figure 39 | **fdmOTC pre-treatment with Vemurafenib leads to BM disorganization.**

**a** | fdmOTCs were prepared by NHDF cultivation for 4 weeks to generate a fibroblast-derived matrix (fdm). During the last 3 weeks of fdm generation, NHDF were treated with 0.05% (v/v) DMSO, 1 *µM* or 5 *µM* Vemurafenib, before HaCaT-RAS A-5 cell seeding. Cultivation with growth medium only was performed for another 3 weeks. **b-d** | FFPE and haematoxylin/ eosin stained sections of control cultures showed several undifferentiated cell layers and a BM without signs of invasion (b). Pre-treatment with 1 *µM* or 5 *µM* caused BM disorganization in a dose-dependent manner (c, d). [n=3]

Since TGF-alpha acts as growth factor and is routinely added to fdmOTCs after seeding HaCaT cells, a TGFA downregulation in NHDF can be excluded as reason for invasive growth. Therefore, only CSF2, other faintly regulated or non-investigated factors remained as potential paracrine acting factors inducing HaCaT-RAS A-5 invasion, which requires further investigations.

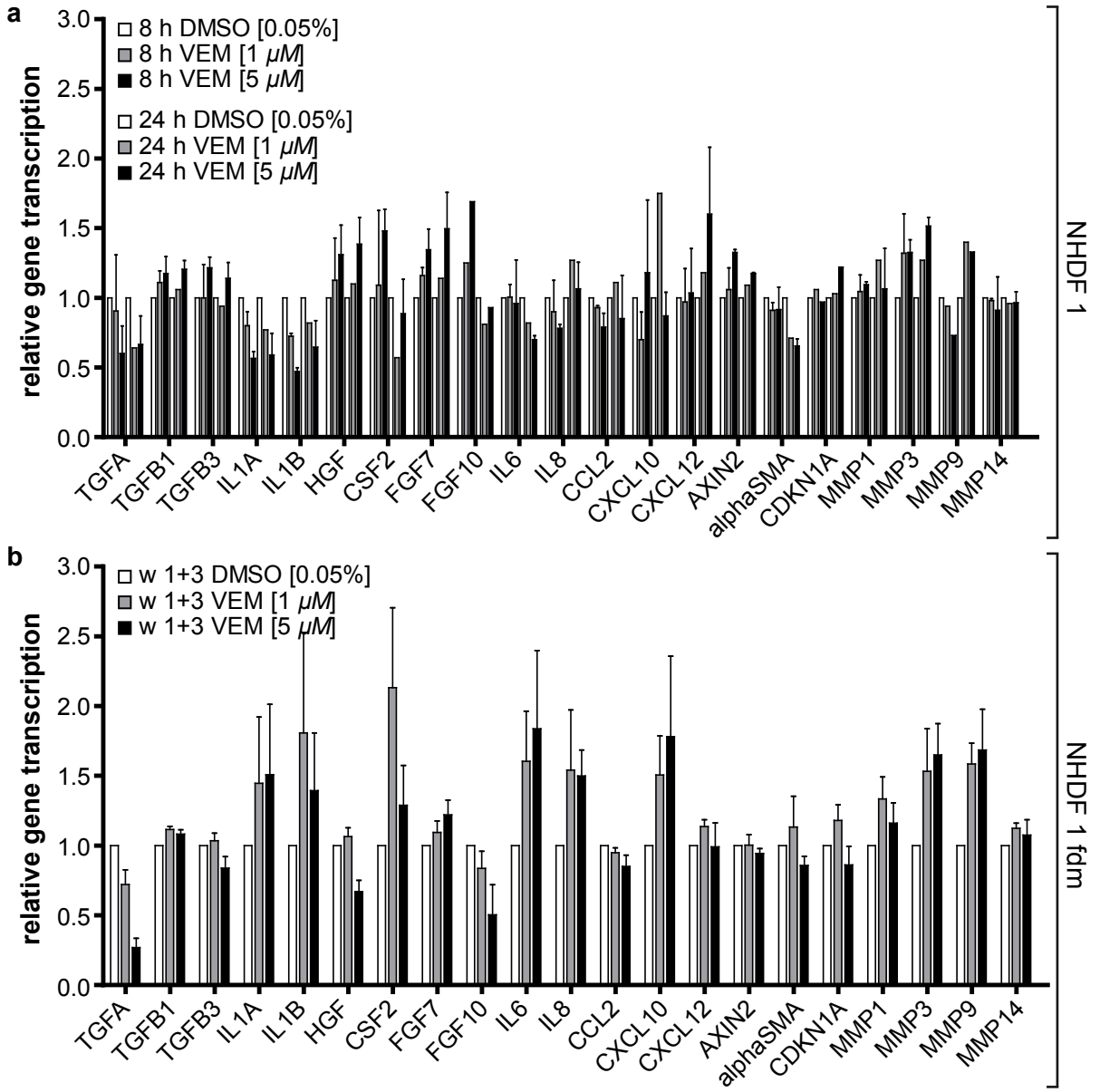


Figure 40 | **Vemurafenib does not regulate gene expression in 2D and 3D cultured NHDF.**

NHDF were stimulated with 0.05% (v/v) DMSO, 1 *μM* or 5 μM Vemurafenib. RNA was subjected to expression analysis for known growth factors (TGFA, TGFB1, TGFB3, IL1A, IL1B, HGF, CSF2, FGF7, FGF10), cytokines of the fibroblast secretome (IL6, IL8, CCL2, CXCL10, CXCL12) and matrix remodeling factors (MMP1, MMP3, MMP9, MMP14). Activation of Wnt/Beta-catenin (AXIN2) or p21 pathways (CDKN1A) and the myofibroblast marker (alphaSMA) were also investigated. Normalization was performed using GAPDH as house-keeping gene and fold-changes were expressed by comparing 1 *μM* or 5 *μM* Vemurafenib treatment of NHDF to DMSO stimulation. **a** | NHDF stimulation in monolayer cultures for 8 and 24 h did not show regulation beyond 2-fold. **b** | NHDF was allowed to form a dermal equivalent (fdm) within 4 weeks, which was constantly stimulated during the last 3 weeks with Vemurafenib or DMSO in FDM medium. Gene expression analysis showed that Vemurafenib led to TGFA downregulation and a minor CSF2 upregulation only. [n=2, mean ± SD]

### 5.2.13 Vemurafenib upregulates MMP1 and MMP3 in keratinocytes

While Vemurafenib caused only minor changes in gene regulation of NHDF, a direct gene regulation in keratinocytes leading invasive growth of HaCaT-RAS A-5 cells became more likely. Similarly to NHDF, NHEK, HaCaT and HaCaT-RAS A-5 cells were stimulated with 1 $\mu M$, 5 $\mu M$ Vemurafenib or DMSO as control in monolayer cultures. RNA was subjected to qRT-PCR for a gene regulation analysis of growth factors (TGFA, TGFB1, TGFB3, IL1A, IL1B), matrix remodeling factors (MMP1, MMP3, MMP9, MMP14) and differentiation-associated genes (KRT10, FLG, IVL). Moreover, activation of Wnt/Beta-catenin (AXIN2) or the p21 pathway (CDKN1A), EGF receptor expression (EGFR) and EMT (SNAI2) were also analyzed. Normalization was performed using GAPDH and fold-changes were expressed by comparing 1 $\mu M$ or 5 $\mu M$ Vemurafenib treatment of keratinocytes to 0.05% (v/v) DMSO stimulation. NHEK upregulated IL1A and IL1B by 2.6 or 2.9-fold, the differentiation marker IVL, expressed in late stratum spinosum and stratum granulosum, by 4.7 or 7.7-fold, FLG by 1.4 or 2.2-fold as well as slightly KRT10 upon 1 $\mu M$ or 5 $\mu M$ Vemurafenib treatment for 24 h, respectively. IVL, FLG and KRT10 upregulation further confirmed the direct role of Vemurafenib in keratinocyte differentiation. In addition, MMP1 and MMP3 were induced by 1 $\mu M$ or 5 $\mu M$ Vemurafenib in a dose-dependent manner already after 8 h by either 2.0 or 4.3-fold and 2.6 or 2.9-fold, but even stronger after 24 h of stimulation leading to 28 or 62-fold MMP1 and 20 or 51-fold MMP3 upregulation, respectively (Fig. 41a).

Also HaCaT cells showed 2.0-2.2-fold upregulation of IL1A and IL1B by Vemurafenib after 8 and 24 h, but in contrast to NHEK no regulation of differentiation genes was detected. Furthermore, 1 $\mu M$ or 5 $\mu M$ Vemurafenib induced MMP1 in a dose-dependent manner by 3.6 or 6.1-fold (8 h) and 3.9 or 5.5-fold (24 h), respectively. MMP3 was also induced reaching 3.2 or 6.4-fold (8 h) and 3.6 or 5.0-fold (Fig. 41b). In HaCaT-RAS A-5 cells 1 $\mu M$ or 5 $\mu M$ Vemurafenib led to a 1.7 or 1.9-fold (8 h) and 2.2 or 2.6-fold (24 h) induction of TGFA, respectively, which was slightly stronger compared to NHEK and HaCaT cells. IL1A was induced by 1.8 or 1.9 (8 h) and 2.3 or 2.5-fold (24 h), while IL1B levels were increased by 1.7 or 1.6-fold (8 h) and 2.6 or 3.0-fold (24 h). No differentiation genes were regulated in HaCaT-RAS A-5 cells. However, MMP1, MMP3 and MMP9 showed a dose-dependent upregulation by 1 $\mu M$ or 5 $\mu M$ Vemurafenib. While MMP9 showed a 1.9 or 2.3-fold regulation only after 24 h, MMP1 was 3.6 or 5.1-fold (8 h)/ 3.8 or 8.6-fold (24 h) and MMP3 3.1 or 5.2-fold (8 h)/ 1.5 or 2.8-fold (24 h) upregulated, respectively (Fig. 41c).

To assess whether Vemurafenib induced gene regulated only temporarily or can be observed over a prolonged time, HaCaT monolayer cultures were continuously stimulated for 4 and 8 weeks. After another 8 h of the corresponding stimulation, HaCaT cells were subjected to qRT-PCR analysis. After 8 weeks + 8 h with 1 $\mu M$ or 5 $\mu M$ Vemurafenib, IL1A was either 2.4-fold or 1.6-fold upregulated. Also MMP1 was 1.8 or 4.6-fold upregulated after 4 weeks, which declined to 1.0 or 2.5-fold regulation after 8 weeks. MMP3 was 2.0 or 18.4-fold upregulated after 4 weeks and the levels remained at 2.3 or 5.3-fold after 8 weeks of stimulation, respectively. In contrast to HaCaT cell short-term stimulation, TGFA showed a 2.0-fold upregulation by 1 $\mu M$ Vemurafenib after 8 weeks. Importantly, levels of the differentiation-associated genes were increased by 5 $\mu M$ Vemurafenib reaching for KRT10 3.4 or 4.2-fold and for FLG 3.6 or 2.5-fold upregulation after 4 or 8 weeks, respectively. In contrast to NHEK monolayer cultures, IVL was not regulated (Fig. 42). Thus, the gene expression data of the keratinocytes confirmed for NHEK a direct and early as well as for HaCaT cells a direct but delayed

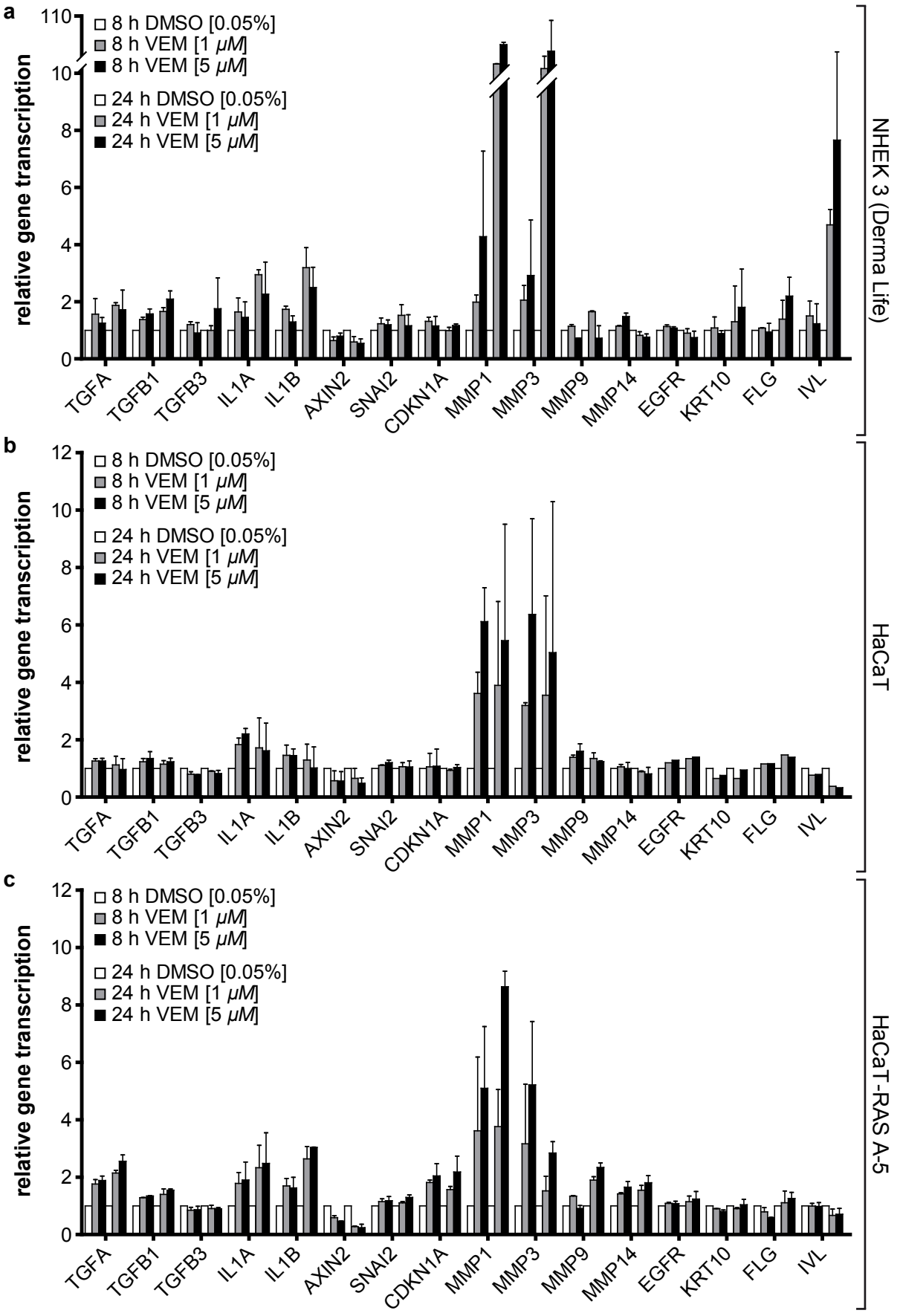
a
b
c
relative gene transcription
8 h DMSO [0.05%]
8 h VEM [1 µM]
8 h VEM [5 µM]
24 h DMSO [0.05%]
24 h VEM [1 µM]
24 h VEM [5 µM]
TGFA
TGFB1
TGFB3
IL1A
IL1B
AXIN2
SNAI2
CDKN1A
MMP1
MMP3
MMP9
MMP14
EGFR
KRT10
FLG
IVL
NHEK 3 (Derma Life)
HaCaT
HaCaT-RAS A-5

Figure 41 | **Vemurafenib shows distinct gene regulation pattern in keratinocytes.**

Keratinocytes were stimulated with 0.05% (v/v) DMSO, 1 *µM*, 5 *µM* Vemurafenib in monolayer cultures for 8 and 24 h. RNA was subjected to qRT-PCR-based gene expression analysis of growth factors (TGFA, TGFB1, TGFB3, IL1A, IL1B), matrix remodeling factors (MMP1, MMP3, MMP9, MMP14) and differentiation-associated genes (KRT10, FLG, IVL). Activation of Wnt/Beta-catenin (AXIN2) or p21 pathway (CDKN1A), EGF receptor expression (EGFR) and EMT (SNAI2) were also investigated. Normalization was performed using GAPDH and fold-changes were expressed by comparing 1 *µM* or 5 *µM* Vemurafenib to DMSO stimulation. **a** | NHEK upregulated IL1A, IL1B, IVL, FLG and KRT10 mostly after 1 *µM* or 5 *µM* Vemurafenib stimulation. In addition, MMP1 and MMP3 were highly induced in a dose-dependent manner after 8 h, but even stronger after 24 h. **b** | HaCaT cells showed some upregulation of IL1A, IL1B, but a major induction of MMP1 and MMP3 by Vemurafenib starting after 8 h. **c** | HaCaT-RAS A-5 cells revealed induction of TGFA, IL1A and IL1B at lower levels. MMP1, MMP3 and MMP9 showed a dose-dependent upregulation by 1 *µM* or 5 *µM* Vemurafenib. [n=2, mean ± SD]

effect of Vemurafenib on keratinocyte differentiation. Furthermore, the induction of MMP1, MMP3 and MMP9 by Vemurafenib was detected in all analyzed keratinocytes, ranging from normal to benign-tumorigenic cells. This rendered these matrix remodeling factors as possible trigger for HaCaT-RAS A-5 cell invasion. As Vemurafenib induced MEK-ERK hyper-activation in all analyzed keratinocytes, the observed gene expression is most likely dependent on this pathway activity.

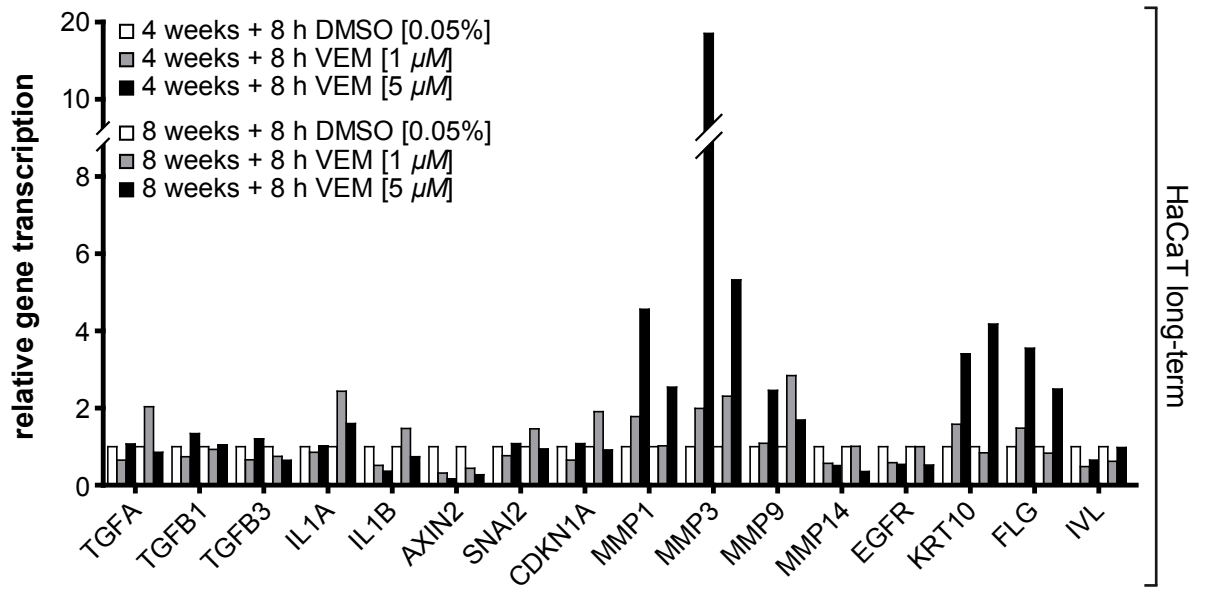


Figure 42 | **Vemurafenib induced gene regulation is maintained in HaCaT cells.**

HaCaT monolayer cultures were continuously stimulated with 0.05% (v/v) DMSO, 1 *µM*, 5 *µM* Vemurafenib for 4 and 8 weeks. After another 8 h corresponding stimulation, RNA was subjected to qRT-PCR-based gene expression analysis of growth factors (TGFA, TGFB1, TGFB3, IL1A, IL1B), matrix remodeling factors (MMP1, MMP3, MMP9, MMP14) and differentiation-associated genes (KRT10, FLG, IVL). Activation of Wnt/Beta-catenin (AXIN2) or p21 pathway (CDKN1A), EGF receptor expression (EGFR) and EMT (SNAI2) were also investigated. As result, IL1A and TGFA were slightly elevated by Vemurafenib only after 8 weeks + 8 h. After 4 and 8 weeks, Vemurafenib upregulated MMP9 and especially MMP1 + MMP3. Expression of the differentiation-associated genes KRT10 and FLG was increased by 5 *µM* Vemurafenib after 4 or 8 weeks + 8 h. [n=1]

## 5.2.14 Cobimetinib prevents MEK-ERK hyper-activation and gene regulation by Vemurafenib

In melanoma patients, the resistance development to the B-Raf$^{V600E}$ inhibitor Vemurafenib is counteracted by additionally administering a MEK inhibitor like Cobimetinib (COBI) (Queirolo et al., 2015). We made use of the co-treatment with Cobimetinib in order to block the Vemurafenib induced MEK-ERK hyper-activation downstream at MEK in order to ask which keratinocyte phenotypes are indeed dependent on MEK-ERK activity.

To determine the Cobimetinib concentration that was sufficient to block the Vemurafenib induced hyper-activation, but without causing major toxicity, monolayer cultures were treated with different Cobimetinib concentrations to analyze effects on MEK and ERK signaling. In particular, HaCaT-RAS A-5 cells were stimulation with 0.15% (v/v) DMSO, 1 $\mu M$ or 5 $\mu M$ Vemurafenib in combination with 0, 0.01, 0.1 or 1 $\mu M$ Cobimetinib for 4 h. Western-Blot analysis revealed ERK phosphorylation by treatment with 1 $\mu M$ and 5 $\mu M$ Vemurafenib compared to DMSO treatment. ERK activation by 1 $\mu M$ Vemurafenib was blocked by adding 0.01 $\mu M$ Cobimetinib. However, this Cobimetinib concentration was not sufficient to prevent ERK phosphorylation in combination with 5 $\mu M$ Vemurafenib. A reduction of this hyper-activation to control levels was achieved by 0.1 $\mu M$ Cobimetinib. Moreover, increasing concentrations of Cobimetinib led to an accumulation of phosphorylated MEK, but not total MEK. This effect was even stronger in combination with Vemurafenib and thus, likely reflected the MEK inhibitor mechanism, which did not allow further ERK phosphorylation by MEK leading to an accumulation of phosphorylated MEK. Hyper-activation of signaling through Vemurafenib further increased this effect (Fig. 43). Since the combination of 5 $\mu M$ Vemurafenib with 0.1 $\mu M$ Cobimetinib completely blocked pathway activation at the level of MEK, this concentration was used for subsequent experiments.

Subsequently, the response of Cobimetinib co-treatment and thereby, the MEK-ERK specificity of Vemurafenib induced gene expression was assessed in HaCaT-RAS A-5 monolayer cultures by qRT-PCR. Normalization was performed using GAPDH and fold-changes were expressed by comparing each treatment to the DMSO control set to one. As shown before (see Fig. 41), Vemurafenib (5 $\mu M$) upregulated the growth factors TGFA, IL1A and IL1B by 2-4-fold (8 or 24 h) compared to the control. The cytokine IL-8 was included in the analysis, as it mediated proliferation of HaCaT cells (see Figs. 12+13 and Sobel, Tham et al. 2015). Also IL8 and was similarly upregulated by Vemurafenib after 8 and 24 h. Importantly, the co-treatment with 0.1 $\mu M$ Cobimetinib caused a downregulation of these genes.

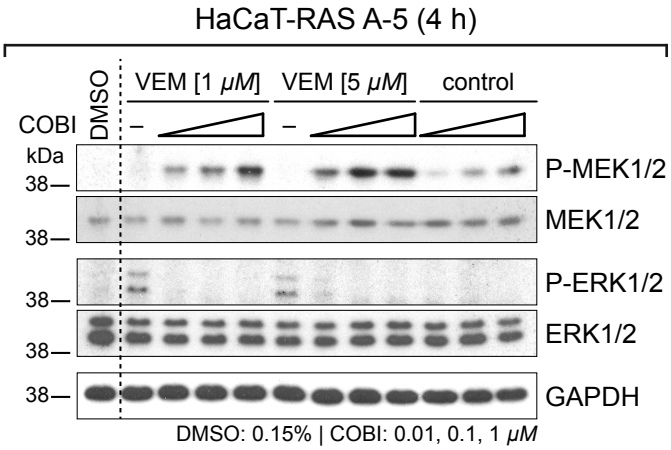


Figure 43 | **Cobimetinib prevents Vemurafenib induced MEK-ERK hyper-activation.**

HaCaT-RAS A-5 cells were stimulation with 0.15% (v/v) DMSO, 1 or 5 $\mu M$ Vemurafenib in combination with 0, 0.01, 0.1 or 1 $\mu M$ Cobimetinib for 4 h. Western-Blot analysis revealed ERK phosphorylation by Vemurafenib treatment. Co-treatment with 0.1 $\mu M$ Cobimetinib prevented Vemurafenib induced ERK phosphorylation. Additionally, Cobimetinib led to an accumulation of phosphorylated MEK, but not total MEK, which was more pronounced with increasing Cobimetinib concentrations or in combination with Vemurafenib. This likely reflected a block in ERK phosphorylation by MEK. [n=1]

Furthermore, inhibition of basal MEK activity by Cobimetinib (0.1 $\mu M$) led to a similar downregulation as the combination treatment. The matrix remodeling factor MMP1 was 3.0 or 2.1-fold upregulated by Vemurafenib after 8 or 24 h, respectively, while Cobimetinib co-treatment caused a downregulation. Furthermore, MMP3 revealed a 6.8-fold upregulation after 8 h, which was downregulated by additionally adding Cobimetinib, while a 2.3-fold downregulation was detected by Vemurafenib treatment after 24 h. MMP9 was either 4.6 or 3.4-fold upregulated by Vemurafenib stimulation after 8 or 24 h, respectively, while Cobimetinib co-treatment prevented this effect. Interestingly, whereas MMP1, MMP3 and MMP9 were regulated by both inhibitors, MMP14 gene expression did not respond to any treatment. Additionally, the differentiation marker KRT10 did not respond to Vemurafenib, but Cobimetinib co-treatment caused a 1.8 or 2.7-fold upregulation after 8 or 24 h, respectively. FLG did not respond to Vemurafenib or Cobimetinib (Fig.44a).

Since NHEK cultured in Derma Life showed a very high MMP1 and MMP3 gene induction upon Vemurafenib, I tested whether this effect depends on calcium level regulating keratinocyte differentiation. Therefore, HaCaT-RAS A-5 cells were shifted for 9 days from FBS and calcium containing growth medium to the defined low-calcium medium Derma Life. This resulted in basal HaCaT-RAS A-5 cells that did not differentiate upon reaching confluency (Fig. 44c). Expression analysis demonstrated that TGFA, IL1A, IL1B and IL8 were upregulated by Vemurafenib, while combination treatment with Cobimetinib resulted in a downregulation comparable to HaCaT-RAS A-5 cells in calcium-containing growth medium. Importantly gene expression of MMP1 (15 or 155-fold), MMP3 (13 or 15-fold) and MMP9 (3.5 or 14-fold) was highly increased by Vemurafenib after either 8 or 24 h. Again, MMP14 expression remained unchanged by any treatment demonstrating that it is not regulated by MEK-ERK MAPK signaling. Cobimetinib also prevented the induction of MMP1, MMP3 and MMP9 and led to a gene downregulation compared to the DMSO control. KRT10 levels were either not altered after 8 h or downregulated by Vemurafenib after 24 h compared to DMSO treated HaCaT-RAS A-5 cells. However, Cobimetinib increased KRT10 by either 4 or 64-fold (8 or 24 h). Similarly, FLG was not altered by Vemurafenib, but 1.6 or 2.1-fold upregulated (8 or 24 h) by Cobimetinib treatment suggesting toxicity related differentiation (Fig. 44b).

A possible reason for the higher induction of especially MMP1 in HaCaT-RAS A-5 cells grown in Derma Life vs. growth medium is a lower basal gene expression in Derma Life. Hence, the relative differences in mRNA levels were calculated between DMSO treated HaCaT-RAS A-5 cells cultured in Derma Life and DMEM+FBS. TGFA, IL1B, MMP3, MMP9 and MMP14 revealed a similar basal expression under both conditions. IL1A was not altered after 8 h, but 34-fold higher expressed in cells grown in Derma Life 24 h after replacing the medium. Although Derma Life generally induces IL1A expression, this difference was not reflected in the regulation by Vemurafenib in Derma Life vs. DMEM+FBS. Importantly, MMP1 demonstrated a 26 or 71-fold lower basal expression in HaCaT-RAS A-5 grown in Derma Life 8 or 24 h post medium-change, respectively (Fig. 44d), thus implying a higher range for Vemurafenib induced gene upregulation.

Taken together, 0.1 $\mu M$ Cobimetinib prevented Vemurafenib-induced MEK-ERK hyper-activation in HaCaT-RAS A-5 cells confirming that the Vemurafenib increased gene expression especially of MMP1, MMP3 and MMP9 was most likely dependent on ERK-activity and specific for keratinocytes.

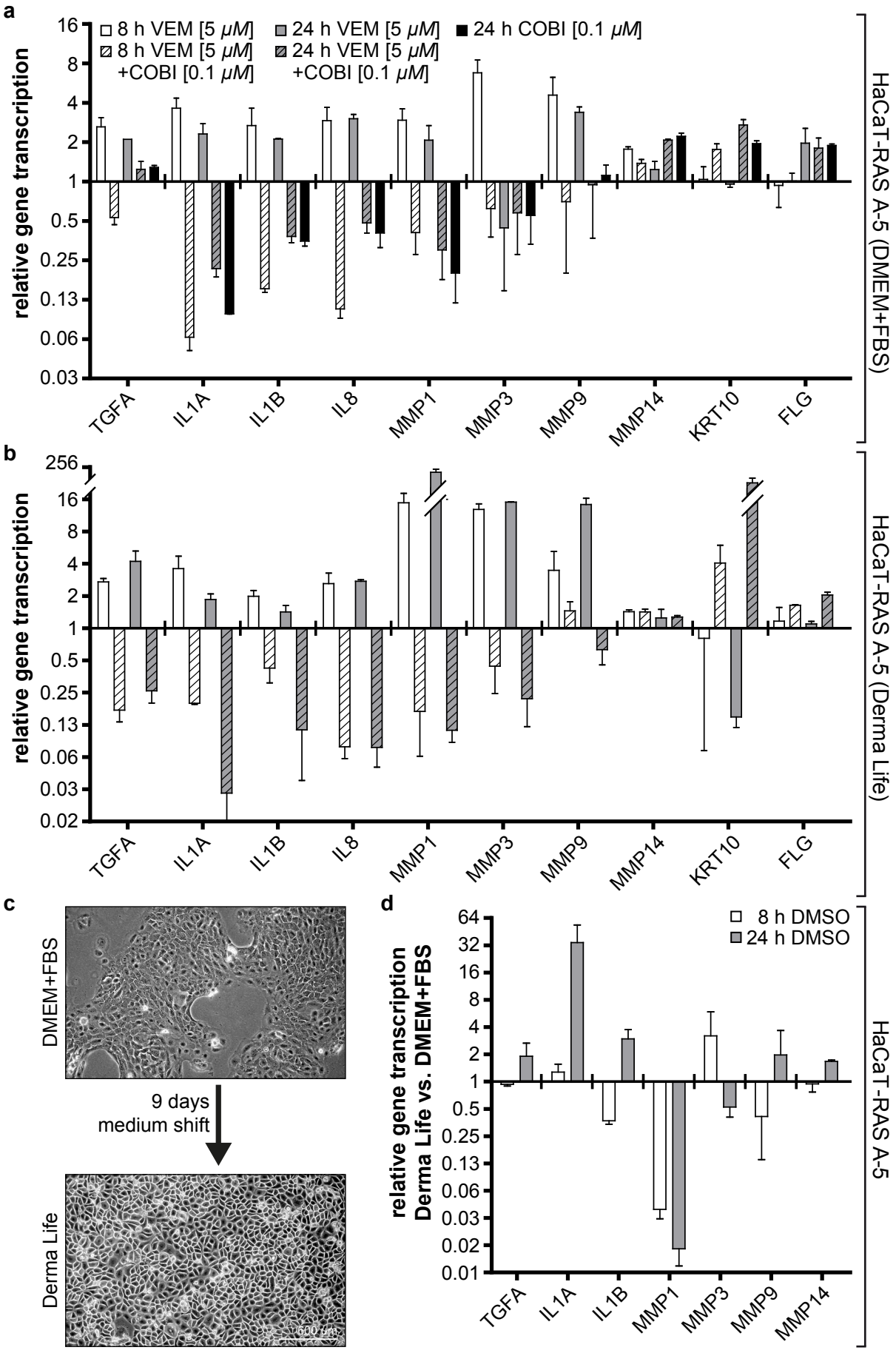
a
8 h VEM [5 µM]
24 h VEM [5 µM]
24 h COBI [0.1 µM]
8 h VEM [5 µM] +COBI [0.1 µM]
24 h VEM [5 µM] +COBI [0.1 µM]
relative gene transcription
16
8
4
2
1
0.5
0.25
0.13
0.06
0.03
TGFA
IL1A
IL1B
IL8
MMP1
MMP3
MMP9
MMP14
KRT10
FLG
HaCaT-RAS A-5 (DMEM+FBS)
b
relative gene transcription
256
16
8
4
2
1
0.5
0.25
0.13
0.06
0.03
0.02
TGFA
IL1A
IL1B
IL8
MMP1
MMP3
MMP9
MMP14
KRT10
FLG
HaCaT-RAS A-5 (Derma Life)
c
DMEM+FBS
9 days
medium shift
Derma Life
d
8 h DMSO
24 h DMSO
relative gene transcription
Derma Life vs. DMEM+FBS
64
32
16
8
4
2
1
0.5
0.25
0.13
0.06
0.03
0.02
0.01
TGFA
IL1A
IL1B
MMP1
MMP3
MMP9
MMP14
HaCaT-RAS A-5

Figure 44 | **Vemurafenib gene regulation depends on ERK-activity in HaCaT-RAS A-5 cells.**
HaCaT-RAS A-5 monolayer cultures were stimulated with 0.06% (v/v) DMSO and 5 *μM* Vemurafenib alone or in combination with 0.1 *μM* Cobimetinib for 8 and 24 h. RNA was subjected to qRT-PCR for a gene expression analysis of growth factors (TGFA, IL1A, IL1B, IL8), matrix remodeling factors (MMP1, MMP3, MMP9, MMP14) and differentiation-associated genes (KRT10, FLG). Normalization was performed using GAPDH and fold-changes were expressed by comparing each treatment to the DMSO control set to one. **a** | All growth factors and matrix remodeling factors were increased by Vemurafenib after 8 and 24 h, while MMP3 was only unregulated after 8 h. Co-treatment with 0.1 *μM* Cobimetinib caused downregulation of these genes compared to DMSO stimulated cells. Inhibition of basal MEK activity by Cobimetinib (0.1 *μM*) led to a similar downregulation. MMP14 was not regulated by any treatment. The differentiation marker KRT10 did not respond to Vemurafenib, but Cobimetinib co-treatment led to an upregulation after 8 or 24 h, while FLG was not regulated. **b, c** | HaCaT-RAS A-5 cells were shifted for 9 days to the low-calcium medium Derma Life, resulting in cells that did not differentiate upon reaching confluency (c). Expression analysis demonstrated that Vemurafenib induced gene regulation was comparable to high-calcium growth medium and combination treatment with Cobimetinib also resulted in a downregulation of these genes. MMP1 was strongly upregulated by Vemurafenib especially in Derma Life, which was turned to a downregulation by combination treatment. KRT10 was downregulated by Vemurafenib, while Cobimetinib highly increased KRT10 after 24 h stimulation. MMP14 and FLG expression remained unchanged (b). **d** | The differential expression between control cultures in Derma Life and DMEM+FBS was calculated 8 and 24 h after replacing the respective medium. TGFA, IL1B, MMP3, MMP9 and MMP14 revealed a similar basal expression, while IL1A was higher expressed in HaCaT-RAS A-5 cells grown in Derma Life after 24 h. MMP1 demonstrated highly increased expression in cells grown in Derma Life after 8 or 24 h, implying a higher range for Vemurafenib induced gene upregulation. [n=2, mean ± SD, normalized to DMSO control, $\log_2$ scale]

## 5.2.15 Vemurafenib and Cobimetinib combination treatment of fdmOTCs

To determine whether the two major Vemurafenib induced phenotypes differentiation and invasion depend on MEK-ERK hyper-activation in fdmOTCs, Cobimetinib was used to abrogate signaling via ERK and thus, restore the epithelial morphology.

### 5.2.15.1 Cobimetinib treatment is tolerated in HaCaT-RAS A-5 fdmOTCs

Toxicity by Cobimetinib was assessed in HaCaT-Ras A-5 cells because they showed major gene regulation as well as strong changes in differentiation and invasion upon Vemurafenib. For this purpose, 2 week-old HaCaT-RAS A-5 fdmOTCs were treated with 0.06% (v/v) DMSO as control, 0.1 *μM* or 1 *μM* Cobimetinib for 3 weeks (Fig. 45a). In control cultures, HaCaT-RAS A-5 cells formed the typical multilayered and hyper-proliferative epithelium with a disorganized BM (Fig. 45b). Treatment with 0.1 *μM* Cobimetinib resembled the control, although the number of epithelial layers was reduced and parts of the epithelium became atrophic (Fig. 45c). Cobimetinib at a concentration of 1 *μM* caused complete atrophy of the epithelium, leaving only few vital cell islands. Interestingly, NHDF appeared to be only slightly affected in their number by Cobimetinib (Fig. 45d), demonstrating that high Cobimetinib concentrations are toxic for epithelial development only. As 0.1 µM Cobimetinib revealed only a limited toxicity and was proven to be sufficient to block ERK hyper-activation as well as Vemurafenib induced gene induction *in vitro*, this concentration was subsequently employed.

### 5.2.15.2 Combination treatment prevents ERK hyper-activation, differentiation and invasion

In order to determine the role of ERK activation as well as the presence of a Ras mutation in Vemurafenib mediated epithelial invasion and differentiation, fdmOTCs with non-tumorigenic HaCaT as well as

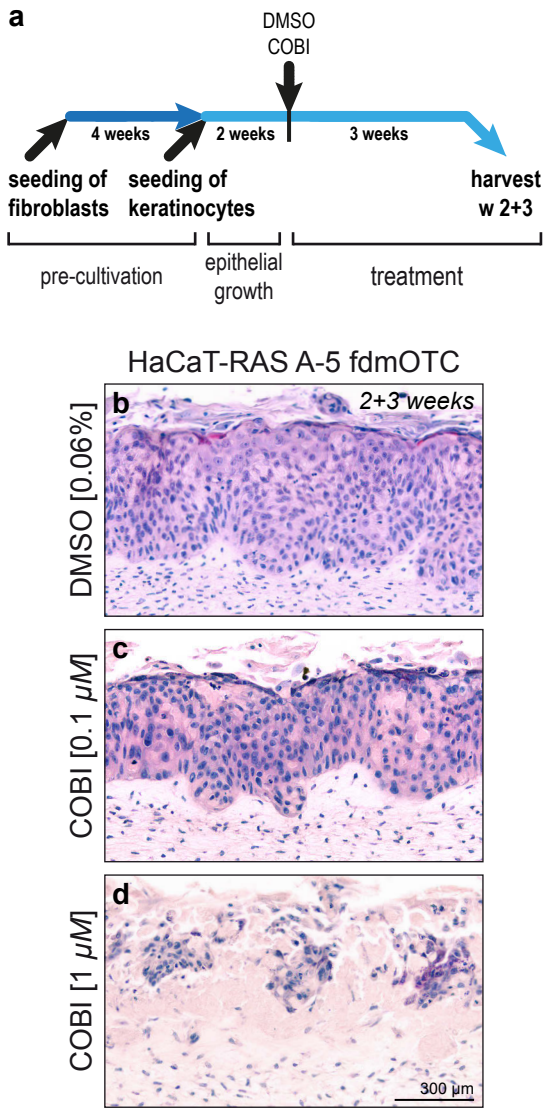


Figure 45 | **High Cobimetinib concentrations cause epithelial atrophy in HaCaT-RAS A-5 fdmOTCs.**

**a** | fdmOTCs were prepared by NHDF cultivation for 4 weeks to generate a fibroblast-derived matrix (fdm), before HaCaT-RAS A-5 cell seeding. Epithelial growth and stratification was allowed for 2 weeks to mimic the *in vivo* situation and thereafter, cultures were treated with 0.06% (v/v) DMSO, 0.1 µM or 1 µM Cobimetinib for another 3 weeks. **b-d** | FFPE sections were stained with haematoxylin/ eosin to analyze the morphology. DMSO treated HaCaT-RAS A-5 cells formed the typical multilayered and hyper-proliferative epithelium with a disorganized BM (b). Treatment with 0.1 *µM* Cobimetinib resembled the control, although the number of epithelial layers was reduced (c). 1 *µM* Cobimetinib caused complete atrophy of the epithelium, leaving only few vital cell islands. NHDF appeared to be only slightly affected by Cobimetinib (d). [n=3]

with H-Ras$^{G12V}$-transfected benign-tumorigenic HaCaT-RAS A-5 cells were prepared. Cultures were grown for 2 weeks to resemble a multilayered and differentiated epithelium before stimulating with either 0.06% (v/v) DMSO, 5 µM Vemurafenib, 0.1 µM Cobimetinib or the combination of both inhibitors for another 1-3 weeks (Fig. 46a, b).

Histological characterization of HaCaT control cultures revealed the generation of a multilayered and disorganized epithelium showing parakeratotic stratification after 2+1 weeks (Fig. 46c). Treatment with Cobimetinib abolished terminal differentiation and reduced the number of cell layers, implying some toxicity (Fig. 46d). As observed earlier, Vemurafenib accelerated differentiation at the cost of vital HaCaT cell layers (Fig. 46e). Co-treatment with Cobimetinib prevented Vemurafenib accelerated differentiation restoring the epithelium of control cultures with fewer differentiation (Fig. 46f). After 2+3 weeks, control cultures further stratified, while reducing the number of vital layers (Fig. 46g). Cobimetinib mono-treatment prevented terminal differentiation, but at the same time caused some atrophy of the epithelium (Fig. 46h). Vemurafenib stimulation further accelerated differentiation of HaCaT cells compared to controls, accompanied by a reduction in vital layers. Basal cells were even more organized compared to controls, but without showing invasive growth (Fig. 46i). The combination treatment prevented Vemurafenib induced differentiation, but caused atrophy that became stronger compared to 2+1 week-old cultures (Fig. 46j). Moreover, IHC was performed to visualize the level of ERK hyper-activation in 2+3 week-old HaCaT fdmOTCs. In control cultures, some basal ERK phosphorylation was observed (brown, Fig. 46k). Cobimetinib led to a complete loss of ERK phosphorylation demonstrating its specificity to inhibit MEK and confirming the employed inhibitor concentration (Fig. 46l). Vemurafenib strongly increased ERK phosphorylation in basal HaCaT cells and NHDF directly underneath the epithelium showing that Vemurafenib mediates MEK-ERK hyper-activation also in fdmOTCs (Fig. 46m). Importantly, Cobimetinib co-treatment reduced ERK phosphorylation below the level of control cultures (Fig. 46n), thus preventing ERK-dependent effects by Vemurafenib.

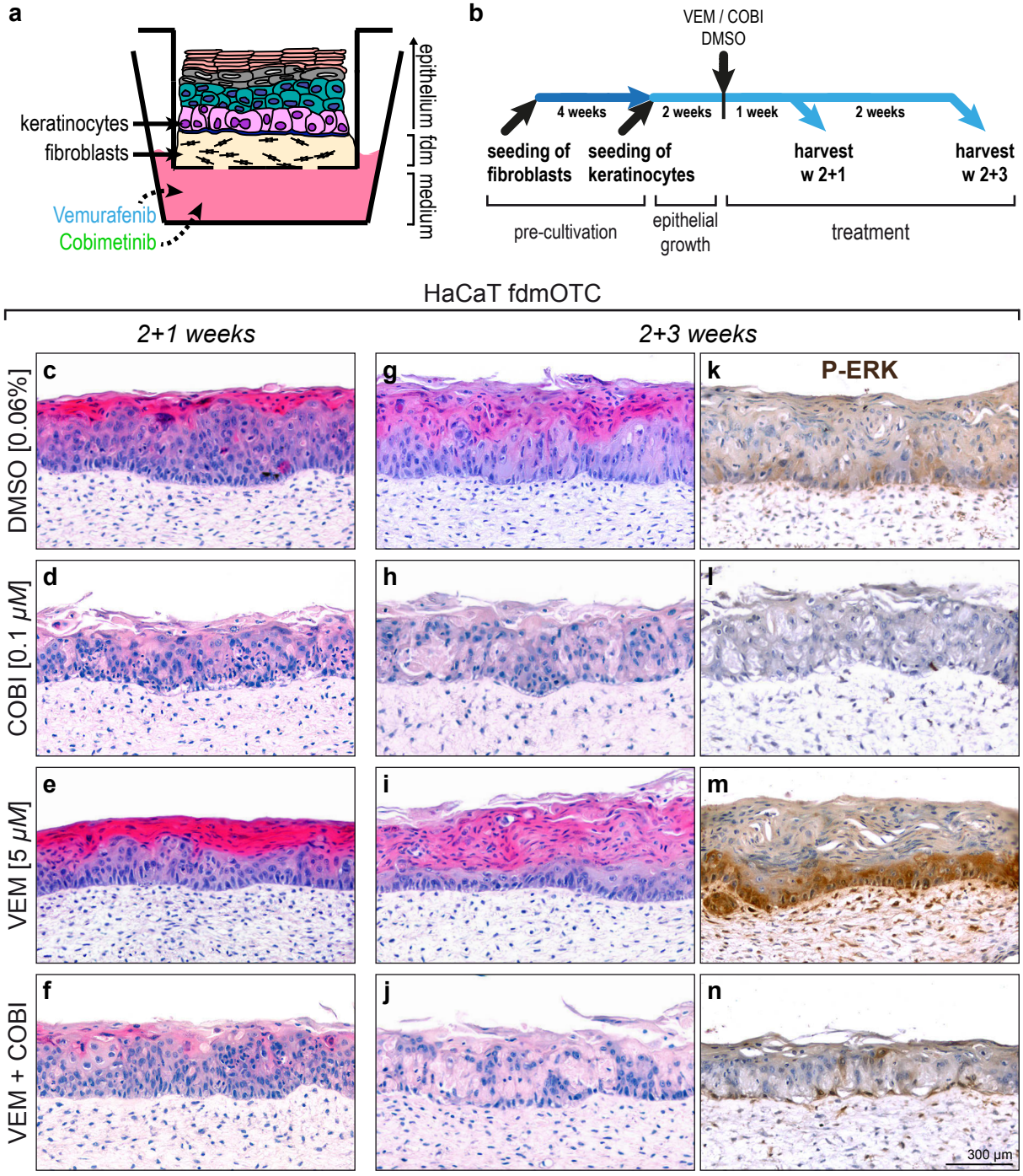


Figure 46 | **Vemurafenib induced differentiation depends on ERK-activity in fdmOTCs.**

**a, b** | fdmOTCs were prepared by NHDF cultivation for 4 weeks to generate a fibroblast-derived matrix (fdm), before keratinocyte seeding (a). Epithelial growth and stratification was allowed for 2 weeks to mimic the *in vivo* situation and thereafter, cultures were treated with 0.06% (v/v) DMSO, 5 µM Vemurafenib, 0.1 µM Cobimetinib or the combination of both inhibitors for another 1 or 3 weeks (b). **c-j** | FFPE sections were stained with haematoxylin/eosin to analyze the morphology. After 2+1 weeks, HaCaT control cultures generated the typical multilayered and disorganized epithelium showing parakeratotic stratification (c). Treatment with Cobimetinib abolished terminal differentiation and reduced the number of cell layers (d). Vemurafenib accelerated differentiation at the cost of vital cell layers (e), while co-treatment with Cobimetinib prevented differentiation (f). After 2+3 weeks, controls further stratified (g). Cobimetinib prevented terminal differentiation and caused some atrophy (h). Vemurafenib stimulation accelerated differentiation and led to increased organization of basal cells (i), which was prevented by Cobimetinib co-treatment (j). [n=3] **k-n** | Immunohistochemistry (IHC) of FFPE sections was performed to visualize ERK phosphorylation in 2+3 week-old HaCaT fdmOTCs. IHC without antibody did not result in any defined signal (not shown). Some basal ERK phosphorylation (brown) was observed in control cultures (k). Cobimetinib led to a complete loss of ERK phosphorylation demonstrating its specificity (l). Vemurafenib strongly increased ERK phosphorylation in basal HaCaT cells and NHDF (m), which was prevented by Cobimetinib co-treatment (n). [n=3]

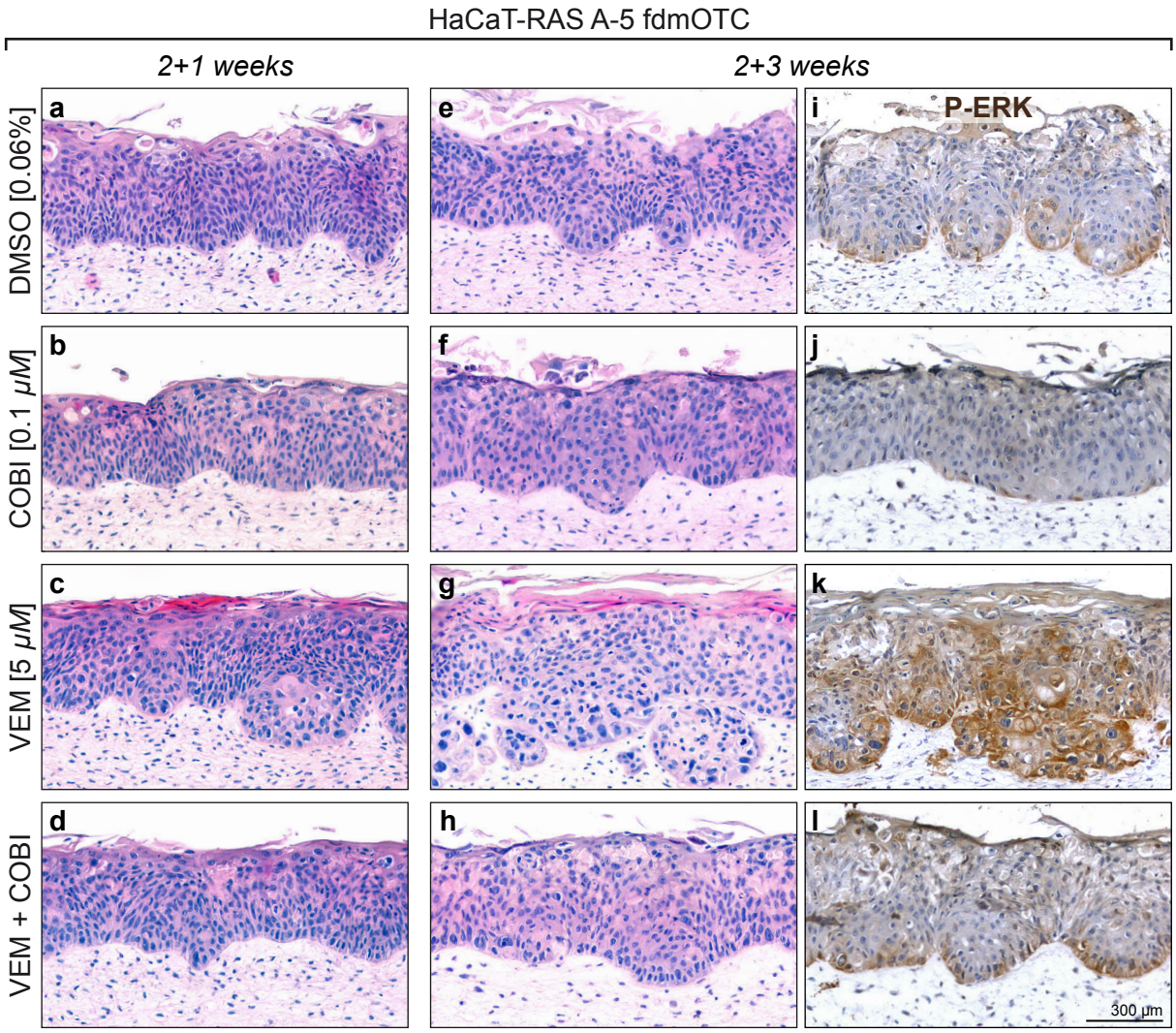


Figure 47 | **Vemurafenib induced differentiation/ invasion depends on ERK-activity in fdmOTCs.** fdmOTCs were prepared by NHDF cultivation for 4 weeks to generate a fibroblast-derived matrix (fdm), before HaCaT-RAS A-5 seeding. Epithelial growth and stratification was allowed for 2 weeks to mimic the *in vivo* situation and thereafter, cultures were treated with 0.06% (v/v) DMSO, 5 µM Vemurafenib, 0.1 µM Cobimetinib or the combination of both inhibitors for another 1 or 3 weeks. **a-h** | FFPE sections were stained with haematoxylin/ eosin to analyze the morphology. After 2+1 weeks, HaCaT-RAS A-5 control fdmOTCs formed the typical multi-layered, disorganized and hyperplastic epithelium lacking cornification (a). Cobimetinib treated cultures resembled controls without showing toxicity (b). Vemurafenib caused terminal differentiation as well as increased basal disorganization (c), but Cobimetinib co-treatment restored the control epithelial morphology (d). After 2+3 weeks, control epithelia (e) and Cobimetinib cultures remained unchanged (f). Vemurafenib stimulated cultures demonstrated increased differentiation and cells grew invasively into the dermal equivalent (g). Both, accelerated differentiation and invasion were prevented by Cobimetinib co-treatment (h). [n=3] **i-l** | Immunohistochemistry (IHC) of FFPE sections was performed to visualize ERK phosphorylation in 2+3 week-old HaCaT-RAS A-5 fdmOTCs. IHC without antibody did not result in any defined signal (not shown). HaCaT-RAS A-5 control fdmOTCs revealed basal ERK phosphorylation (i). Cobimetinib prevented ERK activation (j). Vemurafenib stimulation led to a strong increase in epithelial ERK phosphorylation (k), which was prevented by Cobimetinib, restoring basal ERK activation (l). [n=3]

HaCaT-RAS A-5 control fdmOTCs formed the typical multi-layered, disorganized and hyperplastic epithelium lacking cornification after 2+1 weeks (Fig. 47a). Cobimetinib treated cultures resembled controls without showing toxicity (Fig. 47b). In contrast, Vemurafenib treatment caused terminal differentiation as well as an increased basal disorganization (Fig. 47c). Cobimetinib co-treatment restored the epithelial morphology of controls by preventing both, accelerated differentiation and pre-invasive behavior (Fig. 47d). After 2+3 weeks, HaCaT-RAS A-5 control epithelia were very similar compared to the 2+1 weeks cultures (Fig. 47e). Also Cobimetinib treated cultures remained largely unchanged,

showing only minor toxicity compared to HaCaT cultures (Fig. 47f). Vemurafenib stimulated cultures demonstrated further increased differentiation including the appearance of horn pearls. Moreover, cells grew invasively into the dermal equivalent, which was also described in an earlier experiment after 2+3 weeks of treatment (Fig. 47g). Importantly, accelerated differentiation and even invasion were prevented by Cobimetinib co-treatment (Fig. 47h). When analyzing phosphorylated ERK levels of the different cultures by IHC, HaCaT-RAS A-5 fdmOTCs also showed a basal ERK phosphorylation (Fig. 47i). Cobimetinib completely prevented ERK activation showing its specificity also in HaCaT-RAS A-5 cells (Fig. 47j). In contrast, Vemurafenib stimulation led to a tremendous increase in ERK phosphorylation compared to control cultures that was observed throughout the culture, but especially present at invasive sites (Fig. 47k). Combination treatment with Cobimetinib prevented invasion, and also restored basal ERK activation of control cultures (Fig. 47l).

Taken together, Vemurafenib mediated ERK hyper-activation in HaCaT and HaCaT-RAS A-5 fdmOTCs was retained at basal levels by Cobimetinib co-treatment. Furthermore, Vemurafenib-induced differentiation as well as invasion of HaCaT-RAS A-5 cells was prevented by Cobimetinib co-treatment. This suggested that both phenotypes indeed depend on Vemurafenib induced MEK-ERK activity, whereas the Ras mutation of HaCaT-RAS A-5 cells may be additionally required for invasive growth.

### 5.2.15.3 Keratinocyte differentiation and MMP-activity depends on ERK-signaling

For an in-depth analysis of proliferation, differentiation and invasion in response to Vemurafenib and Cobimetinib treatment, immunofluorescence was performed. First, proliferation was determined by staining for incorporated BrdU in HaCaT and HaCaT-RAS A-5 cultures. Therefore, the number of BrdU-positive cells of entire fdmOTC sections was calculated relative to the corresponding BM length, as measured by Collagen IV staining (proliferation index). In HaCaT fdmOTCs, a proliferation index of 1.8 was determined after 2+3 weeks. Vemurafenib (5 $\mu M$) increased proliferation to 2.9, which was reduced by Cobimetinib (0.1 $\mu M$) co-treatment to 0.7. However, none of these changes were significant. HaCaT-RAS A-5 control cultures revealed a proliferation index of 10.4, confirming the higher basal

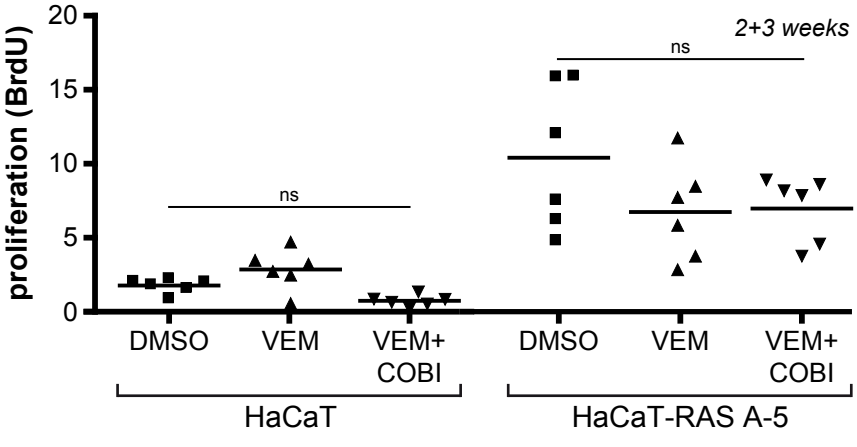


Figure 48 | **Proliferation of keratinocytes is not affected by ERK-activity in fdmOTCs.**

fdmOTCs were prepared by NHDF cultivation for 4 weeks to generate a fibroblast-derived matrix (fdm), before seeding keratinocytes. Epithelial growth and stratification was allowed for 2 weeks to mimic the *in vivo* situation and thereafter, cultures were treated with 0.06% (v/v) DMSO, 5 µM Vemurafenib only or in combination with 0.1 µM Cobimetinib for another 3 weeks. Keratinocyte proliferation was determined by staining cryo-sections for incorporated BrdU and quantified by calculating the number of BrdU-positive cells relative to the BM length, measured by Collagen IV co-staining (proliferation index). Neither in HaCaT nor in HaCaT-RAS A-5 cells, proliferation was significantly altered by Vemurafenib or Cobimetinib compared to control cultures. [n=3, mean, One-way ANOVA + Dunnett's Multiple Comparison Test]

proliferation compared to HaCaT cells. Vemurafenib (5 $\mu M$) or Cobimetinib (0.1 $\mu M$) co-treatment decreased proliferation to either 6.7 or 7.0, but none of the effects were considered significant. This confirmed that Vemurafenib was not affecting proliferation of keratinocytes irrespective of a RAS mutation (Fig. 48).

Second, keratinocyte differentiation upon treatment was investigated by staining for the late differentiation marker Filaggrin. After 2+3 weeks, DMSO stimulated cultures showed low levels of Filaggrin on top of the epithelium (Fig. 49a). Filaggrin signal was increased in Vemurafenib stimulated cultures accounting for the increased differentiation (Fig. 49b). By combination treatment with Cobimetinib, Filaggrin levels were strongly reduced leaving only one positive cell layer on the culture (Fig. 49c). HaCaT-RAS A-5 fdmOTCs also demonstrated only some Filaggrin-positive suprabasal cell layers (Fig. 49d). Vemurafenib led to a tremendous increase in Filaggrin-positive cells layers including the formation of horn pearls within the epithelium, accounting for an accelerated differentiation (Fig. 49e). This observation also correlated with a decrease in HaCaT-RAS A-5 proliferation upon Vemurafenib (see Fig. 48). As observed by histology, the addition of Cobimetinib largely prevented Filaggrin deposition, resembling control cultures (Fig. 49f), thus confirming a ERK-dependent acceleration of HaCaT and HaCaT-RAS terminal differentiation also at a molecular level.

Third, co-staining with the BM maker Collagen IV revealed a strong signal at the BM separating HaCaT cells and NHDF as well as throughout the dermal equivalent. However, Collagen IV staining was altered by neither Vemurafenib nor Cobimetinib co-treatment (Fig. 49a-c). HaCaT-RAS A-5 control

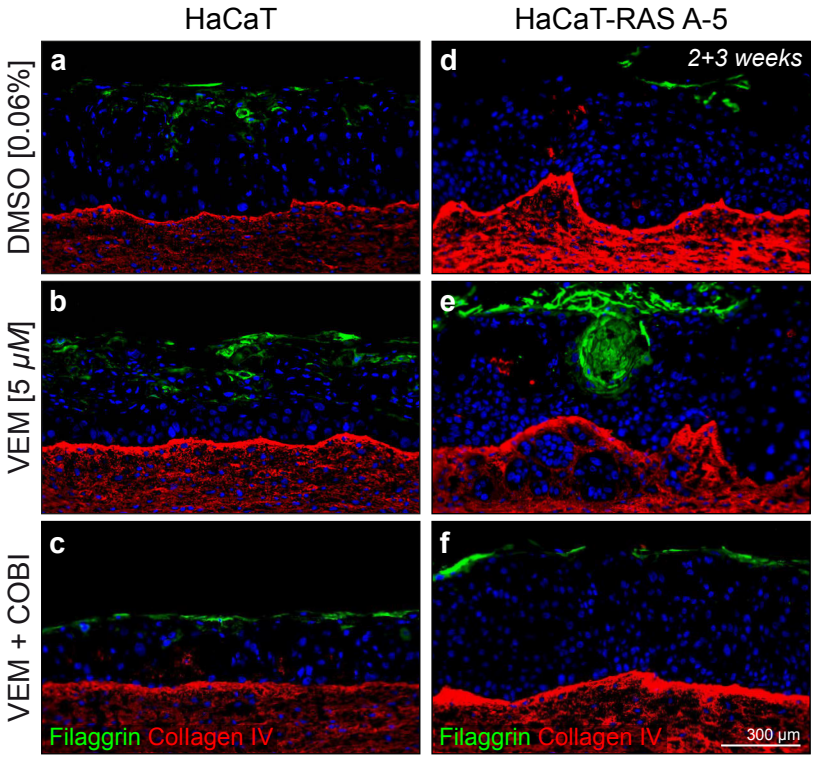


Figure 49 | **Vemurafenib induced accelerated differentiation depends on ERK-activity in fdmOTCs.**

fdmOTCs were prepared by NHDF cultivation for 4 weeks to generate a fibroblast-derived matrix (fdm), before HaCaT or HaCaT-RAS A-5 seeding. Epithelial growth and stratification was allowed for 2 weeks to mimic the *in vivo* situation and thereafter, cultures were treated with 0.06% (v/v) DMSO, 5 µM Vemurafenib only or in combination with 0.1 µM Cobimetinib for another 3 weeks. Immunofluorescence staining of cryo-conserved and fixed sections was performed to investigate terminal differentiation by Filaggrin and BM integrity by Collagen IV expression. **a-c** | HaCaT control cultures showed low levels of Filaggrin (green) (a). Filaggrin signal was increased in Vemurafenib stimulated cultures (b), which was strongly reduced by Cobimetinib combination treatment (c). Staining for Collagen IV (red) in HaCaT cultures revealed a strong signal at the BM and throughout the dermal equivalent (a) that was not altered by Vemurafenib or Cobimetinib (b, c). **d-f** | HaCaT-RAS A-5 control fdmOTCs demonstrated some Filaggrin-positive suprabasal cell layers (d). Vemurafenib led to a strong increase in Filaggrin-positive cells layers (e), which was prevented by Cobimetinib co-treatment (f). HaCaT-RAS A-5 control cultures demonstrated a strong Collagen IV signal throughout the dermal equivalent (d). Vemurafenib slightly decreased overall Collagen IV levels (e) that was restored by Vemurafenib + Cobimetinib co-treatment (f). [n=3]

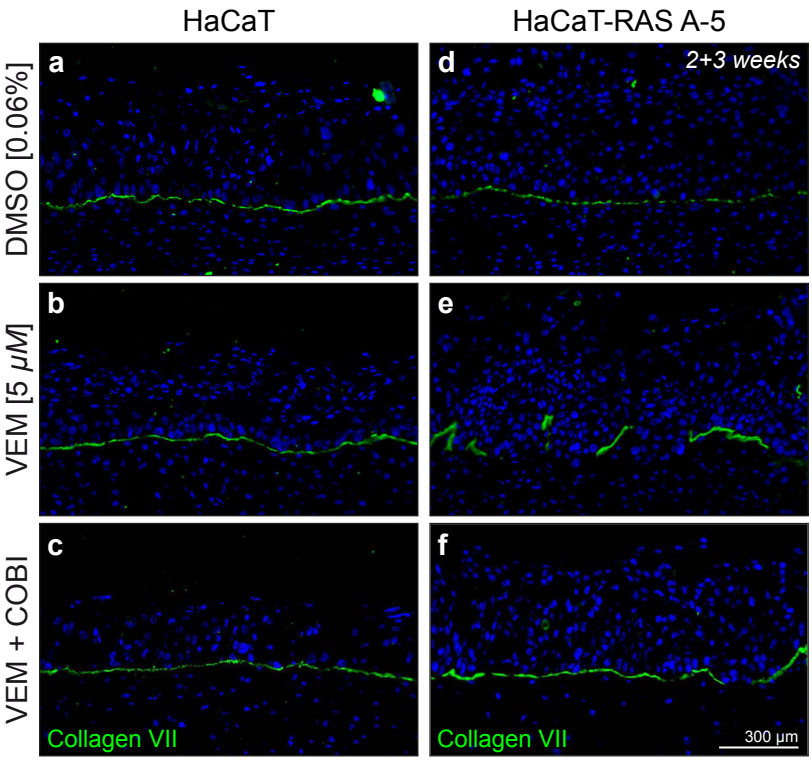


Figure 50 | **Vemurafenib induced ERK-activity results in a disrupted BM of fdmOTCs.** fdmOTCs were prepared by NHDF cultivation for 4 weeks to generate a fibroblast-derived matrix (fdm), before HaCaT or HaCaT-RAS A-5 seeding. Epithelial growth and stratification was allowed for 2 weeks to mimic the *in vivo* situation and thereafter, cultures were treated 0.06% (v/v) DMSO, 5 µM Vemurafenib only or in combination with 0.1 µM Cobimetinib for another 3 weeks. Immunofluorescence staining of cryo-conserved and fixed sections was performed to investigate BM integrity by Collagen VII expression and localization. **a-c** | HaCaT control cultures revealed a continuous Collagen VII pattern (green) at the BM that was not altered by Vemurafenib or Vemurafenib + Cobimetinib. **d-f** | In HaCaT-RAS A-5 control cultures, Collagen VII revealed a continuous staining at the BM (d). Vemurafenib treatment led to discontinuous Collagen VII signals at the BM (e), which was restored to a strong Collagen VII pattern without any disruption by Cobimetinib co-treatment (f). [n=3]

fdmOTCs demonstrated a stronger Collagen IV signal throughout the dermal equivalent (Fig. 49d). By Vemurafenib treatment, a slight decrease in overall Collagen IV levels was observed together with a complete degradation at invasive islands (Fig. 49e). Vemurafenib + Cobimetinib co-treatment revealed a stronger overall Collagen IV staining especially at the BM without any signs of invasion (Fig. 49f). As we detected an ERK-dependent decrease of Collagen IV in some cultures, Collagen VII was analyzed as second BM marker. Immunofluorescence of 2+3 week-old HaCaT control fdmOTCs demonstrated a continuous Collagen VII pattern at the BM that was not altered by Vemurafenib or Vemurafenib + Cobimetinib (Fig. 50a-c). In HaCaT-RAS A-5 control cultures, Collagen VII also revealed a continuous but weaker staining at the BM (Fig. 50d). By Vemurafenib treatment, Collagen VII became a largely discontinuous. This was also observed at sites that did not show single cell invasion (Fig. 50e). In contrast, Cobimetinib co-treatment demonstrated a strong Collagen VII pattern without any BM disruption (Fig. 50f). This showed that Collagen IV and VII degradation is also dependent on ERK activity. Since BM degradation correlated with invasion only in HaCaT-RAS A-5 fdmOTCs, we speculate that the RAS mutation plays in concert with the ERK-activity in mediating tumor progression.

### 5.2.15.4 MMP expression and activation are mediated through on ERK-activity in fdmOTCs

As Vemurafenib-induced MEK-ERK hyper-activation led to MMP1, MMP3 and MMP9 gene expression in monolayer cultured keratinocytes, I asked whether these matrix remodeling factors also correlate with the observed Collagen degradation. Therefore, MMP-1, MMP-3 and MMP-9 secretion was determined in 2+3 week-old cultures by ELISA of 48 h conditioned medium. HaCaT fdmOTCs revealed a basal level

of 9.4 *ng/mL* pro MMP-1, which remained unchanged by Cobimetinib mono-treatment. Vemurafenib (5 *µM*) significantly increased the pro MMP-1 levels to 14.1 *ng/mL* (P<0.05). Furthermore, the combination treatment of 5 µM Vemurafenib and 0.1 µM Cobimetinib led to a significant reduction to 6.1 *ng/mL* pro MMP-1, which is even below the level of control cultures (P<0.01). A MMP-3 concentration of 5.7 *ng/mL* was detected in HaCaT control cultures that was not significantly changed by treatment with any inhibitor. A MMP-9 level of 12.6 *ng/mL* was determined in control fdmOTCs. MMP-9 was significantly downregulated by any treatment, but mainly in the presence of Cobimetinib suggesting a dependence on ERK activity (P<0.01, Fig. 51a).

HaCaT-RAS A-5 control fdmOTCs revealed a pro MMP-1 secretion of 27.1 *ng/mL*, demonstrating a 3-fold higher pro MMP-1 secretion as HaCaT cultures. By Cobimetinib treatment, the levels were significantly decreased to 4.2 *ng/mL* pro MMP-1 (P<0.01). Vemurafenib caused a significant upregulation of pro MMP-1 to 39.2 *ng/mL* (P<0.01). Importantly, combined treatment with Vemurafenib and Cobimetinib led to a significant pro MMP-1 reduction from Vemurafenib stimulated cultures to 17.5 *ng/mL* (P<0.01),

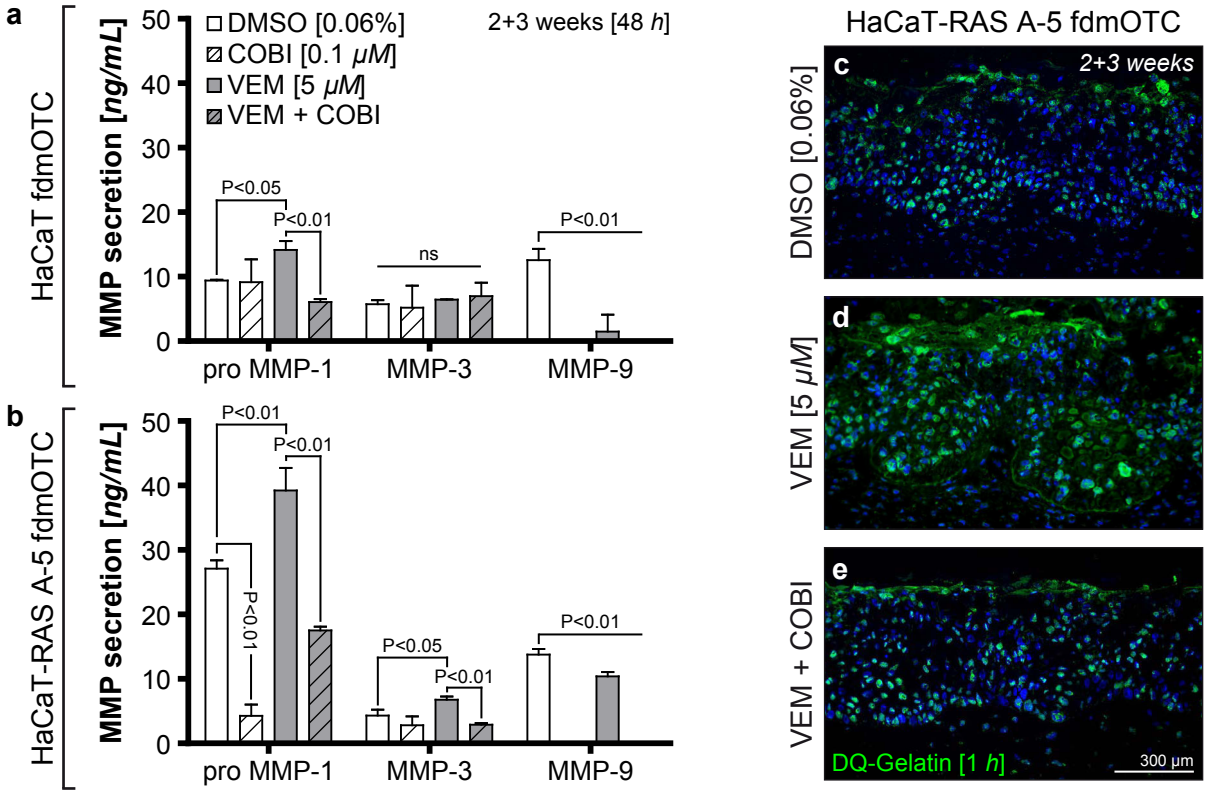


Figure 51 | **ERK-activity causes MMP expression and activation in fdmOTCs.**

fdmOTCs were prepared by NHDF cultivation for 4 weeks to generate a fibroblast-derived matrix (fdm), before HaCaT or HaCaT-RAS A-5 seeding. Epithelial growth and stratification was allowed for 2 weeks to mimic the *in vivo* situation and thereafter, cultures were treated with 0.06% (v/v) DMSO, 5 µM Vemurafenib, 0.1 µM Cobimetinib or the combination of both inhibitors for another 3 weeks. **a, b** | MMP-1, MMP-3 and MMP-9 secretion was determined in 2+3 week-old cultures by ELISA of 48 h conditioned medium. In HaCaT fdmOTCs pro MMP-1 remained unchanged by Cobimetinib mono-treatment. Vemurafenib significantly increased pro MMP-1, which was even reduced below the level of control cultures by Cobimetinib co-treatment. MMP-3 was not significantly altered and MMP-9 was significantly downregulated by any treatment in HaCaT cultures (a). HaCaT-RAS A-5 control fdmOTCs revealed a 3-fold higher pro MMP-1 secretion than HaCaT cultures, which was significantly decreased by Cobimetinib. Vemurafenib significantly upregulated pro MMP-1, which was reduced to control level by Cobimetinib co-treatment. MMP-3 was not altered by Cobimetinib, but it was significantly upregulated by Vemurafenib. Cobimetinib combination treatment caused a significant decrease from Vemurafenib levels. MMP-9 was significantly downregulated by any treatment (b). [n=3, mean ± SD, One-way ANOVA + Dunnett's Multiple Comparison Test] **c-e** | *In situ* zymography to analyze MMP-activity in HaCaT-RAS A-5 fdmOTCs revealed only weak gelatinolytic activity (green) in control cultures (c). Vemurafenib treatment increased fluorescence signals in the epithelium and at invasive sites showing increased MMP-activity (d) that was reduced to the level of control cultures by Cobimetinib co-treatment (e). [n=3]

which did not reach the reduction by Cobimetinib mono-treatment. HaCaT-RAS A-5 cultures secreted 4.3 *ng/mL* MMP-3, which was not altered by Cobimetinib. However, Vemurafenib significantly increased MMP-3 levels to 6.8 *ng/mL* ($P<0.05$). Combination treatment caused again a significant decrease from Vemurafenib levels to 2.9 *ng/mL* MMP-3 ($P<0.01$). Moreover, MMP-9 revealed a basal expression of 13.8 *ng/mL* in control cultures and was significantly downregulated by any treatment but especially by Cobimetinib. As MMP-9 was generally downregulated by treatment, it does not seem to be involved in the invasive phenotype ($P<0.01$, Fig. 51b). Taken together, HaCaT-RAS A-5 fdmOTCs showed higher basal MMP secretion than HaCaT cultures. However, Vemurafenib increased pro MMP-1 secretion in both, confirming the increased MMP1 gene expression of 2D cultures. MMP-3 showed similar levels in both cell types, but was only upregulated by Vemurafenib in HaCaT-RAS A-5 fdmOTCs. Most importantly, co-treatment with Cobimetinib reduced MMP-1 in both cell types and MMP-3 in HaCaT-RAS A-5 cells below the level of control cultures demonstrating that MMP-1 and MMP-3 are direct target genes of ERK signaling.

Since Vemurafenib upregulated MMP-1 and MMP-3 in HaCaT-RAS A-5 fdmOTCs, the activity of MMPs was investigated by a *in situ* zymography. 2+3 week-old control cultures showed a weak epithelial staining (Fig. 51c). Under Vemurafenib treatment, elevated fluorescence signals in the epithelium and at invasive sites corresponded to increased MMP-activity (Fig. 51d). Cobimetinib co-treatment reduced the fluorescence signal approximately to the level of control cultures (Fig. 51e), suggesting that MMP activation was also dependent on ERK signaling in HaCaT-RAS A-5 cultures. Thus, ERK-dependent Collagen degradation as well as MMP expression, secretion and activity correlated with invasive growth of HaCaT-RAS A-5 cells.

# 6. Discussion

The number of cSCC is constantly increasing worldwide (Molho-Pessach and Lotem, 2007). Although the local resection of skin tumors is mostly possible, undetected cSCCs become life threatening as soon as tumor cells metastasize. Aggressive tumor growth and metastasis is particularly observed for immunosuppressed transplant recipients (Euvrard et al., 2003). As mechanisms leading to cSCC initiation and progression are not yet fully understood, the roles of two most likely involved signaling pathways were investigated in detail. First, I characterized a novel Wnt/Beta-catenin dependent fibroblast activation contributing to cSCC progression. Second, as specific B-Raf inhibitors cause cSCC, I investigated the contribution of Vemurafenib and the Ras-Raf-MEK-ERK MAPK pathway in tumor development and progression.

## 6.1 Stromal Wnt/Beta-catenin activation in cSCC progression

Previous studies focused on deregulation of Wnt signaling in cSCC tumor cells (Brasanac et al., 2005; Doglioni et al., 2003; Lyakhovitsky et al., 2004; Malanchi et al., 2008; Papadavid et al., 2002). In addition, we detected Wnt/Beta-catenin activation in stromal fibroblasts and subsequent analyses revealed that deregulation of Wnt signaling in NHDF acted to both, increase epithelial cell proliferation and remodel the adjacent stroma. Thus, aberrant Wnt signaling may not only be important for the autocrine regulation of the tumor cells, but also act in a paracrine fashion within the tumor microenvironment to promote skin carcinogenesis. In particular, Wnt-3a stimulated NHDF to secrete the cytokines IL-8 and CCL-2, which positively affected HaCaT cell proliferation, as well as the matrix remodeling factor MMP-1 that actively degraded ECM and BM, thereby promoting invasive growth of keratinocytes.

### 6.1.1 Activation of stromal Wnt/Beta-catenin signaling

A constitutive activate Wnt/Beta-catenin was already previously reported in chemically induced murine SCCs (Bhatia and Spiegelman, 2005). Wnt pathway activation in the stroma is also not restricted to skin cancer. Sano and co-workers found Wnt-induced signaling within the stroma of human mucinous cystic neoplasms of the pancreas, suggesting a general role of canonical Wnt signaling in tumor development (Sano et al., 2014). How canonical Wnt signaling is induced in tumor cells and stromal fibroblasts is still controversially discussed. Previously, it was shown that fibroblasts secrete R-spondin-2, an activator of the Wnt/Beta-catenin signaling, contributing to epithelial thickening in a skin OTC model for keloid pathology (Chua et al., 2011). Samuel *et al.* showed that a Rho/ROCK pathway-dependent activation of Beta-catenin in mouse skin resulted in epithelial hyper-proliferation and skin thickening. They also found activated ROCK in 90% of human cSCCs (Samuel et al., 2011). Kaler and co-workers provided evidence for macrophage-derived IL-1 beta as a potential inducer of Wnt/Beta-catenin signaling in colon cancer cells *in vitro* (Kaler et al., 2009).

Importantly, nuclear Beta-catenin is not distributed homogeneously in cSCCs (Sobel, Tham et al., 2015) or colon carcinomas. In the latter, it was detected at the invasive front, thereby underlining the importance of the stroma to provide signals for the tumor cells that drive tumor progression (Brabletz

et al., 1998). Similarly, Vermeulen *et al.* observed a high Wnt activity in tumor cells located close to stromal myofibroblasts. They suggested that the myofibroblast-derived HGF is an activator of Wnt/Beta-catenin signaling (Vermeulen et al., 2010). In this study, the expression of WNT2 and WNT3 mRNA as well as of Wnt-3 protein was detected in the microenvironment of a subset of human Beta-catenin positive cSCCs *in situ*, suggesting an alternative mechanism for an activated Wnt pathway in cSCC progression. However, the involvement CAFs was excluded *in vitro* and *in vivo* as we detected myofibroblasts in neither Wnt-3a stimulated colOTCs nor Beta-catenin activated human cSCCs.

### 6.1.2 IL-8 and CCL-2 increase HaCaT cell proliferation

We identified IL-8 and CCL-2 as two candidates for Wnt/Beta-catenin induced paracrine factors by NHDF leading to epithelial proliferation. Accordingly, functional studies of keratinocytes *in vitro* demonstrated that keratinocytes express the receptors for IL-8 and CCL-2 (Sobel, Tham et al., 2015) and showed increased proliferation when stimulated with either IL-8 or CCL-2. In agreement with the literature (Luger and Schwarz, 1990; Michel et al., 1992; Steude et al., 2002; Tuschil et al., 1992), IL-8 caused a significantly increased proliferation in monolayer HaCaT cells. CCL-2 is also known to increase endothelial cell (Okada et al., 2009) and mammary carcinoma cell proliferation (Conti and Rollins, 2004). Both, IL-8 and CCL-2 even led to a comparable response as the known mitogen EGF. Interestingly, co-stimulation with CCL2 and IL-8 did not further increase proliferation over the individual stimulation, arguing that a maximal level of proliferation was reached. In 3D HaCaT colOTCs, Wnt-3a stimulation also elevated IL-8 and CCL-2 levels that went along with a significantly increased HaCaT cell proliferation. Interestingly, besides increased proliferation, Wnt-3a stimulation showed only weak effects on epithelial morphology of HaCaT colOTCs and fdmOTCs. Furthermore, Wnt-3a stimulated colOTC were treated with neutralizing antibodies for CCL-2 and IL-8 in order to specifically prevent effects of both factors. Inhibiting IL-8 and CCL-2 indeed prevented the hyper-proliferative response of the HaCaT cells in Wnt-3a stimulated colOTCs, proving that IL-8 and CCL-2 were responsible for the increased proliferation. Importantly, as we detected a similar expression pattern for IL8 and CCL2 in human Beta-catenin positive cSCCs *in situ*, both chemokines likely stimulate keratinocyte proliferation in concert *in vivo*, as well.

In mouse models, fibroblast-derived CCL-2 was shown to recruit and activate tumor-associated macrophages (TAMs), which further secrete growth-, survival- and angiogenic factors, thereby promoting tumor growth (Condeelis and Pollard, 2006; Lewis and Pollard, 2006). CCL-2 was associated with the recruitment of TAMs also in ovarian-, esophageal- and gastric carcinomas (Negus et al., 1997; Ohta et al., 2002, 2003). In breast cancer, high levels of CCL-2 within the tumor stroma enhanced primary tumor progression as well as metastasis in a macrophage-dependent and independent manner (Hembruff et al., 2010). In the OTC model consisting of NHDF and HaCaT cells only, additional pro-tumorigenic effects by CCL-2 involving the immune system cannot be determined. Thus, an additional activation of the immune system may or may not enhance tumorigenic effects by CCL-2.

### 6.1.3 Stromal Wnt/Beta-catenin activation promotes keratinocyte invasion

Besides the cytokines IL-8 and CCL-2, the ECM remodeling protein MMP-1 was also upregulated in Wnt-3a stimulated monolayer cultures of NHDF. In agreement, Wnt-3a stimulated colOTCs revealed significantly increased pro MMP-1 levels in the conditioned medium, which correlated with elevated gelatinolytic activity and increased levels of cleaved collagen, demonstrating that MMPs were activated upon Wnt-3a stimulation. Importantly, these effects were not altered by IL-8 and CCL-2 neutralization showing an independent regulation of MMP-1 in Wnt-3a stimulated NHDF. Since MMP1 has TCF/LEF promoter binding sites (Clark et al., 2008), expression is probably directly regulated by the Wnt/Beta-catenin pathway. Thus, MMP-1 revealed a similar regulation as MMP7, MMP14 and MT3-MMP, which have already been described to be direct Wnt target genes in many cancer types (Brabletz et al., 1999; Crawford et al., 1999; Lowy et al., 2006; Takahashi et al., 2002). Importantly, MMP-1 and cleaved collagen were also found to be highly elevated in Beta-catenin activated human cSCCs, underlining the relevance of this mechanism for cSCC *in situ*.

High expression of MMP-1 was frequently reported for tumor and stromal cells as well as for many cell lines derived from primary cSCCs (Airola and Fusenig, 2001; Gray et al., 1992; Haider et al., 2006) and MMP-1 activity is well-known for providing a pro-migratory and pro-invasive environment (Kalluri, 2003; Lynch and Matrisian, 2002; Mueller and Fusenig, 2004). By Wnt-3a stimulation of colOTCs, we observed a reduction of the BM component Collagen IV and its epidermal binding protein Integrin beta-4, which went along with invasive growth of HaCaT cells. Importantly, Collagen IV and Integrin beta-4 reduction as well as invasive growth of HaCaT cells was prevented by co-treatment with IL-8 and CCL-2 neutralizing antibodies. As MMP1 is likely a direct Wnt target gene (Clark et al., 2008), pro MMP-1 levels and MMP-activity remained unchanged by neutralizing IL-8 and CCL-2. Thus, an additional BM destructive mechanism relying on IL-8 and CCL-2 expression may cooperate with MMP expression in invasion of HaCaT cells, both relying on Wnt/Beta-catenin activation of NHDF. In order to further analyze invasive growth, fdmOTCs as a more stable OTC invasion model, which is not prone to self-degradation (Berning et al., 2015), were stimulated with Wnt-3a. In this model, invasive growth was only observed in case of the benign-tumorigenic HaCaT-RAS A-5 cells. HaCaT cells could most likely not overcome these more stringent culture conditions. As Wnt-3a activated NHDF increased proliferation and invasion, representing two well-established events in the course of carcinogenesis, regulation of stromal Wnt activity is important to maintain normal skin homeostasis.

Taken together, we detected deregulation of Wnt/Beta-catenin signaling in fibroblasts of the cSCC stroma that triggered the expression of the cytokines IL-8 and CCL-2 as well as of the matrix remodeler MMP-1. These factors acted by stimulating either growth of epithelial HaCaT cells in a paracrine fashion or by remodeling the immediate stromal environment in OTCs, allowing invasive growth of benign-tumorigenic HaCaT-RAS A-5 cells in fdmOTCs. Since both, keratinocyte proliferation and matrix remodeling are prerequisites for tumor progression (Hanahan and Weinberg, 2011), our findings support the role of Wnt regulation in stromal fibroblasts as a crucial mechanism in cSCC progression (Fig. 52).

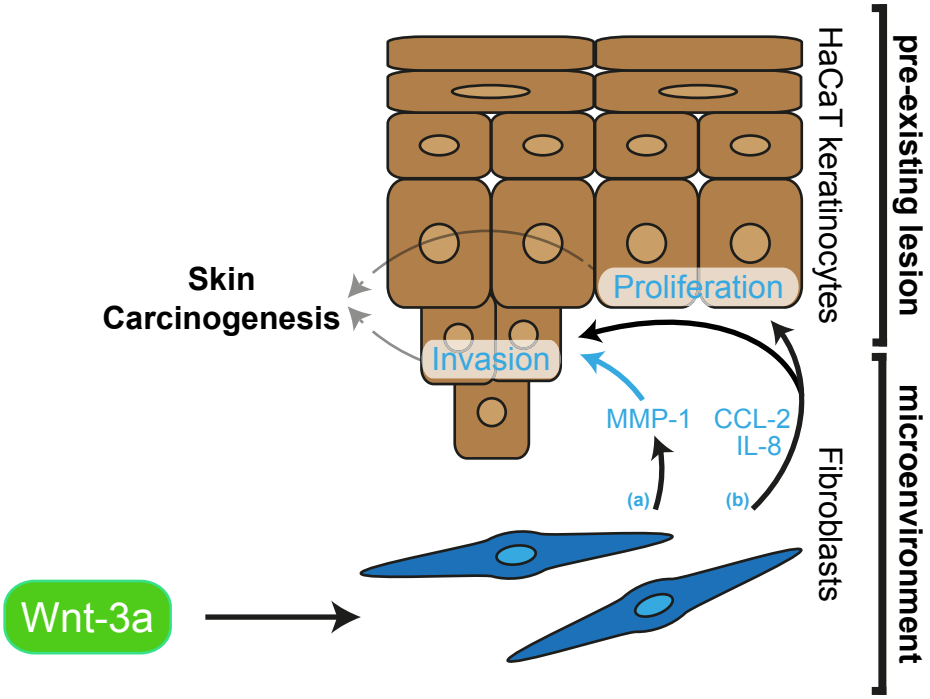


Figure 52 | **Stromal Wnt/Beta-catenin in skin carcinogenesis.**
Deregulated Wnt/Beta-catenin signaling in fibroblasts of the cSCC stroma triggers the expression of the matrix remodeler MMP-1 as well as of the cytokines IL-8 and CCL-2. While MMP-1 remodeled stroma allows invasive growth of benign-tumorigenic HaCaT-RAS A-5 cells in fdmOTCs (**a**), IL-8 and CCL-2 directly increase proliferation of keratinocytes and likely play an additional role in invasive growth (**b**). Since keratinocyte proliferation and matrix remodeling are prerequisites for tumor progression, these findings support the role of Wnt regulation in stromal fibroblasts as crucial mechanism in cSCC progression.

## 6.2 Vemurafenib and epidermal Ras-Raf-MEK-ERK signaling in cSCC progression

Raf-MEK-ERK pathway deregulation is found in approximately one-third of human cancers (Dhillon et al., 2007), but especially melanoma heavily relies on its constant activity. This discovery led to the development of specific B-Raf inhibitors including Vemurafenib (Bollag et al., 2010) and Dabrafenib (Hauschild et al., 2012). However, while both inhibitors abrogated MEK-ERK signaling and prevented further growth of melanoma strains harboring mutated B-Raf$^{V600E/K}$, they paradoxically hyper-activated signaling via MEK-ERK in B-Raf$^{wild\text{-}type}$ melanoma cells. As result, a persistent MEK-ERK activation in B-Raf$^{wild\text{-}type}$ melanoma cells was shown to induce expression changes in a wide range of genes including IL8, increase proliferation of N-Ras$^{Q61L}$ mutant primary melanoma cells, reduce cell adhesion and enhance migration in advanced lesions (Halaban et al., 2010). Furthermore, frequently adverse effects on epidermal cells during B-Raf inhibitor therapy like hyperkeratosis and KAs/ cSCCs were also hypothesized to be the caused by MEK-ERK hyper-activation (Hatzivassiliou et al., 2010; Heidorn et al., 2010; Poulikakos et al., 2010).

### 6.2.1 MEK-ERK hyper-activation in cutaneous cells

In agreement with the literature, I observed that Vemurafenib (1 $\mu M$) blocked MEK-ERK signaling in B-Raf$^{V600E}$ A375 melanoma cells, while NHEK, HaCaT, HaCaT-RAS A-5 or HaCaT-RAS II-4

cells revealed a hyper-activation of MEK-ERK signaling. Other pathways including p38 MAPK or Akt signaling were not reproducibly altered. In general, Ras-Raf-MEK-ERK signaling was found to be normally regulated and activated by EGFR stimulation in HaCaT and HaCaT-RAS II-4 cells. By a PCR-based mutation array, the B-Raf$^{wild\text{-}type}$ status concerning common mutations was confirmed in all analyzed keratinocytes. Besides wild-type B-Raf, both currently hypothesized hyper-activation models proposed the requirement of Ras activity resulting from either a mutation or activation of upstream pathway components (Hatzivassiliou et al., 2010). In the analyzed set of cells, the somatic mutation array confirmed the known H-Ras mutations p.G12V or p.G12L in HaCaT-RAS II-4 or SCC-12 cells, respectively, while both, HaCaT-RAS A-5 and HaCaT-RAS II-4 cells were shown to have stably integrated the HRAS oncogene (Boukamp et al., 1990; Fusenig and Boukamp, 1998; Mueller and Fusenig, 1999; Rheinwald and Beckett, 1981). A so-far not described H-Ras mutation p.G12D was detected in SCC-13 cells. NHEK and HaCaT cells did not show common RAS-mutations, but Vemurafenib induced ERK phosphorylation was detected even in serum-starved HaCaT cells. However, EGFR co-stimulation increased MEK-ERK-activation, confirming upstream activity as MEK-ERK hyper-activation-promoting stimulus also in keratinocytes.

Moreover, the mechanism proposed by Poulikakos *et al.* suggested a low local concentration of a specific B-Raf inhibitor as third requirement for ERK hyper-activation. As consequence, the inhibitor stochastically binds and blocks only one Raf protein of a C-Raf/C-Raf homodimer or C-Raf/B-Raf heterodimer leading to a conformational change that trans-activates the other one causing pronounced downstream signaling (Poulikakos et al., 2010). In agreement, a high B-Raf inhibitor concentration above 10 $\mu M$ prevented a solid MEK-ERK hyper-activation also in HaCaT cells likely due to a simultaneous block of both Raf subunits. However, throughout our performed experiments, Vemurafenib related toxicity was detected at neither 1 $\mu M$ short-term and long-term nor 50 $\mu M$ short-term cultivation. Vemurafenib also led to MEK-ERK hyper-activation as well as to some p38 MAPK-activity in NHDF of two individual donors. Thus, all analyzed cutaneous cells showed MEK-ERK hyper-activation through Vemurafenib treatment with potential downstream effects.

### 6.2.2 Vemurafenib induced differentiation and invasion in OTCs and cSCCs

Melanoma patients receiving Vemurafenib develop KAs and cSCCs within a median time of 8 weeks. However, the development new KAs/ cSCCs were still observed after 52 weeks of treatment. Besides that, treatment led to the development of verrucous keratosis and hyperkeratosis (Anforth et al., 2013; Anforth et al., 2015). In order to characterize the involvement of Vemurafenib in cSCC tumorigenesis, I stimulated monolayer cultured keratinocytes representing different stages in skin carcinogenesis as well as 3D OTCs with Vemurafenib. Holderfield and co-workers showed that Vemurafenib treatment of wild-type mice led to MAPK pathway activation and enhanced epidermal proliferation, but was not sufficient for tumorigenesis (Holderfield et al., 2014). In NHEK, Vemurafenib indeed stimulated MEK-ERK hyper-activation, however, this led to neither increased proliferation nor tumorigenesis in monolayer cultures or OTCs. Besides NHEK, MEK-ERK hyper-activation was found in all analyzed keratinocyte cell lines including HaCaT, HaCaT-RAS A-5 and HaCaT-RAS II-4 cells. Although MEK-ERK signaling is historically linked to proliferation (Dhillon et al., 2007), different Vemurafenib concentrations did not stimulate proliferation of HaCaT or HaCaT-RAS A-5 cells in short-term, long-term monolayer culture or fdmOTCs.

Continuous Vemurafenib stimulation of HaCaT monolayer cultures for 5-9 weeks caused a cell cycle shift from G2 or S phase to G1/G0 phase that went along with increased differentiation. Moreover, in NHEK the differentiation-associated genes IVL and FLG were upregulated already 24 h after stimulation, supporting an early and direct differentiation induction by Vemurafenib. Importantly, KRT10 and FLG were upregulated in HaCaT cells after 8 weeks of continuous Vemurafenib stimulation showing a delayed induction of differentiation. This phenotype was also confirmed in OTCs. Accordingly, accelerated differentiation was confirmed in Vemurafenib treated HaCaT scaOTCs as well as in NHEK, HaCaT and HaCaT-RAS A-5 fdmOTCs by histology, FLG mRNA as well as by Keratin-10 and Filaggrin protein expression. Compared to NHEK cultures, induction of differentiation was delayed in HaCaT and HaCaT-RAS A-5 cells. A dose-dependent effect of Vemurafenib on differentiation was not consistent among the different keratinocytes and OTC experiments. In HaCaT-RAS A-5 fdmOTCs, Vemurafenib even led to the generation of Filaggrin-positive horn pearls. Intriguingly, the *in vitro*-observed accelerated differentiation resembled development of hyperkeratosis and well-differentiated cSCCs in Vemurafenib receiving malignant melanoma patients (Anforth et al., 2013).

To model the effects of the Vemurafenib related B-Raf$^{V600E}$ inhibitor PLX4720 in cSCCs, Su and co-workers used the two-stage skin carcinogenesis mouse model. It relies on the induction of H-Ras$^{Q61L}$ mutations in mouse keratinocytes by topical application of the carcinogen 7,12-dimethylbenz-(a) anthracene (DMBA) and subsequent long-term application of the tumor promoter 12-O-tetradecanoyl-phorbol-13-acetate (TPA) (Quintanilla et al., 1986). In this model, PLX4720 administration reduced tumor latency, but did not change tumor number. (Su et al., 2012), suggesting an accelerated progression of preexisting lesions. In the scaOTC model with a Fibrin matrix, 7 weeks of Vemurafenib treatment caused a potential early invasive phenotype by the non-tumorigenic HaCaT cells. However, when stimulating fdmOTCs, providing a more stable matrix that is not prone to self-degradation, invasion was not observed for NHEK or HaCaT cells. However, this treatment regime led to invasive growth of H-Ras$^{G12V}$ expressing benign-tumorigenic HaCaT-RAS A-5 cells, thus, confirming an accelerated progression of pre-existing lesions rather than a *de novo* development of cSCC. While low Vemurafenib concentrations in the plasma of Vemurafenib patients were associated with tumor progression, no significant correlation between elevated plasma levels and adverse effects was detected *in vivo* (Funck-Brentano et al., 2015). Similarly, a dose-dependent effect by Vemurafenib on HaCaT-RAS A-5 invasion was also not consistent among the different OTC experiments. At present, there are no studies showing B-Raf inhibitor-induced cSCC metastasis. Whether this accounts to either the close dermatological surveillance and early removal of these lesions (Anforth et al., 2013; Anforth et al., 2015) or a low tumorigenic potential of these lesions *in vivo* remains elusive.

### 6.2.3 Genetic selection by Vemurafenib and the role of Ras mutations

Vemurafenib induced invasive growth in fdmOTCs was only observed for H-Ras$^{G12V}$ transfected HaCaT-RAS A-5 cells. Besides the potential requirement of an upstream activity for a lasting MEK-ERK hyper-activation by specific B-Raf inhibitors (Hatzivassiliou et al., 2010), a predominant role of H-Ras and K-Ras in the pathology of KAs/ cSCCs was suggested (Frouin et al., 2014). In line with this, recent studies analyzed either 10 or 35 Vemurafenib induced KAs/ cSCCs and determined a high RAS mutation frequency of 30-60% in these lesions. The majority of mutations were H-Ras$^{Q61L}$

and K-Ras$^{G12D}$ (Oberholzer et al., 2012; Su et al., 2012). Moreover, South *et al.* identified the tumor suppressor NOTCH1 as a highly mutated gene in Vemurafenib induced lesions, being important for H-Ras driven skin carcinogenesis (South et al., 2014). These results were unexpected, since RAS was only mutated in 12% of KAs/ cSCCs induced by the broad-spectrum kinase inhibitor Sorafenib (Arnault et al., 2012). Furthermore, the fact that RAS mutations were only detected in 5-15% in spontaneously occurring cSCCs of elderly (Boukamp, 2005) argued that Vemurafenib triggers a clonal expansion of RAS-mutant keratinocyte populations within a lesion that subsequently progress to a full-blown cSCCs.

In order to assay, whether continuous Vemurafenib stimulation promotes growth of certain clones, a M-FISH analysis of HaCaT cells was performed. After 5 weeks, Vemurafenib indeed caused a genetic selection of a specific HaCaT subpopulation characterized by gain of i(1q), loss of i(17q) and gain of MYC. However, none of these altered chromosomes carries the genes HRAS, KRAS, NRAS, NOTCH1 or NOTCH2, suggesting that the expression of other genes was altered by Vemurafenib mediated genetic selection in HaCaT cells. Since accelerated differentiation was observed already shortly after onset of Vemurafenib stimulation in NHEK or HaCaT cells, which do not carry RAS or NOTCH mutations, this phenotype was independent of such a mutation. Furthermore, this implied that a RAS mutation may not be the only reason for the observed Vemurafenib induced invasive growth of HaCaT-RAS A-5 cells. In line with this, Yaktapour and co-workers observed as adverse effect in a Vemurafenib treated stage IV melanoma patient the development of chronic lymphocytic leukemia (CLL), which lacked any RAS mutation (Yaktapour et al., 2014). Thus, RAS independent pro-tumorigenic mechanisms account for the adverse effect by Vemurafenib also in lymphocytes.

### 6.2.4 Viruses and off-target effects

Whether viruses play a role for secondary tumor development in B-Raf inhibitor-treated patients is also controversially discussed. Falchook *et al.* reported the presence of Merkel cell polyomavirus (MCPyV) and the beta-human papillomavirus subtype 17 (HPV-17) in cSCCs of a patient receiving the specific B-Raf inhibitor Dabrafenib (Falchook et al., 2013). By analysis of 69 Vemurafenib/ Dabrafenib-induced cSCCs (29 patients), Cohen and co-workers detected no oncogenic alpha-HPV genotypes, but frequent beta-HPV infections. MCPyV was also detected in some lesions mostly as co-infection with beta-HPV (Cohen et al., 2015). In a further study of 62 Vemurafenib related tumors (44 patients), HPV DNA was detected in 13%, while a co-occurrence with mutated H-Ras could only be detected in one tumor. In contrast, Dika *et al.* could not observe HPV signatures in 7 Vemurafenib-induced human cutaneous SCCs (Dika et al., 2015) and Ganzenmueller and co-workers did not detect any human virus by next generation sequencing in 5 benign skin tumors (Ganzenmueller et al., 2013). A third study analyzing 27 skin lesions of 12 Vemurafenib patients proposed that neither HPV nor human polyomavirus (HPyV) are involved in Vemurafenib induced adverse effects such as verrucous keratosis, KAs and SCCs (Frouin et al., 2014). Since we excluded the presence of HPV in the spontaneously-transformed HaCaT cells, the observed Vemurafenib induced effects on MEK-ERK signaling and differentiation of all analyzed keratinocytes as well as on HaCaT-RAS A-5 invasion were independent of a viral infection.

Off-target effects of B-Raf inhibitors affecting signaling pathways or cellular structures besides Ras-Raf-MEK-ERK MAPK signaling could also be an explanation for the occurrence of cSCCs. However,

the fact that only 6-7% of patients treated with the broad-spectrum kinase inhibitor Sorafenib developed cSCCs after at least 3 months (Anforth et al., 2013; Arnault et al., 2009; Dubauskas et al., 2009; Robert et al., 2011) showed that these tumors are more frequent and arise earlier during treatment with more specific BRAF inhibitors. Treatment with the broad-spectrum kinase inhibitor Sunitinib, inhibiting all Sorafenib targets but Raf kinases, did not result in the development of any KAs or SCCs (Grimaldi et al., 2007; Robert et al., 2011). Thus, cutaneous adverse events that develop during treatment with specific B-Raf inhibitors depend on the Ras-Raf-MEK-ERK pathway, arguing against off-target effects.

### 6.2.5 Gene regulation by Vemurafenib stimulation of cutaneous cells

Intensive tumor-stroma cross-talks via direct contacts or soluble factors are well-known events driving tumor progression (Mueller and Fusenig, 2004). In melanoma, B-Raf$^{V600E}$ mutant cells activated stromal fibroblasts to express CXCL-12 and its receptor CXCR-4 (Whipple and Brinckerhoff, 2014), a factor known to increase malignancy of many cancer types (Mishra et al., 2011). Similar to Wnt/Beta-catenin stimulation (Sobel, Tham et al., 2015), the hyper-activation of NHDF suggested that Vemurafenib stimulation of NHDF could also promote the observed effects in OTCs and *in vivo*. As accelerated differentiation and genetic selection were observed in monolayer stimulation experiments, these phenotypes were mediated by direct stimulation of keratinocytes. Whether NHDF secreted factors play a role in the invasive behavior of Vemurafenib stimulated HaCaT-RAS A-5 cells can only be analyzed in a tissue setting, which involves the interaction of tumor and stromal cells. Gene expression analysis of known NHDF-derived paracrine factors including cytokines, growth factors, matrix remodeling factors and others did not show major regulation by Vemurafenib in NHDF. Certainly, we cannot exclude additional NHDF or keratinocyte-derived factors initiating a cross-talk. However, the gene expression data pointed towards a direct effect of Vemurafenib on keratinocytes, which subsequently led to increased differentiation, genetic selection as well as invasive growth also in co-culture.

To identify oncogenic factors in Vemurafenib hyper-activated epithelial cells, gene regulation of cytokines, growth factors, matrix remodeling factors and others was analyzed. After 24 h, Vemurafenib slightly upregulated IL1A and IL1B in NHEK, HaCaT and HaCaT-RAS A-5 cells. IL-1 is a well-described secretory factor of keratinocytes that enhances expression of growth factors in stromal cells (Maas-Szabowski et al., 2003). TGFA and IL8 were slightly upregulated in HaCaT-RAS A-5 cell, representing potential factors that activate NHDF, as well. Thus, Vemurafenib may well induce a paracrine cross-talk with NHDF that requires further investigations. Similarly, B-Raf$^{V600E}$ mutant melanoma cells with constitutive active MEK-ERK signaling were shown to express higher levels the cytokines IL1B, IL6 and IL8 than B-Raf$^{wild\text{-}type}$ counterparts (Whipple and Brinckerhoff, 2014), suggesting that the observed gene expression indeed depended on Ras-Raf-MEK-ERK activity. However, the contribution of these factors on the invasive phenotype remained elusive. Intriguingly, Vemurafenib induced high MMP1 and MMP3 expression in a dose-dependent manner in all analyzed keratinocytes. MMP9 was upregulated in HaCaT-RAS A-5 cells, as well. HaCaT cells that were constantly stimulated with Vemurafenib still demonstrated increased MMP1 and MMP3 expression after 4 and 8 weeks, revealing a stable induction by Vemurafenib. Furthermore, the fact that MMP9 was upregulated in HaCaT-RAS A-5 cells already after 24 h, while been expressed by continuously treated HaCaT cells after 4 weeks implied a delayed MMP9 response to Vemurafenib in HaCaT cells.

MMP1 is normally induced in wound-edge basal keratinocytes by contact of Integrin alpha-1 beta-2 and dermal Collagen type I leading to p38 MAPK and ERK signaling (Rohani et al., 2014). In fibroblasts, Westermarck *et al.* detected that activation of stress-activated c-Jun N-terminal kinase and p38 pathways did not enhance MMP1 promoter activity (Westermarck et al., 2001), while other studies showed either a p38-dependent MMP1 and MMP3 mRNA stabilization (Reunanen et al., 2002) or increased MMP1 transcription in fibroblasts (Brauchle et al., 2000). Furthermore, ERK was also described to be the major inducer of MMP1 expression in fibroblasts (Brauchle et al., 2000; Reunanen et al., 2002; Westermarck et al., 2001). Despite having detected MEK-ERK hyper-activation as well as some p38-activity, I could not confirm an upregulation of MMP1 in NHDF cultured in 2D and 3D. In invasive melanoma cell lines, MMP-1 is also constitutively expressed in a MEK-ERK dependent manner, arguing that constitutive activation of this pathway allows melanoma cells to acquire an invasive phenotype (Huntington et al., 2004). In cutaneous SCCs, Van Haren *et al.* identified MMP-1 upregulation across multiple microarray studies (Van Haren et al., 2009). A recent transcriptome analysis of 10 AKs and 30 cSCCs demonstrated upregulation of MMP-1, MMP-10, migratory and focal adhesion genes by MAPK-activity as key event in the transition from AKs to cSCCs (Lambert et al., 2014). Moreover, we add MMP1 and MMP3 as universal target genes of Vemurafenib induced MEK-ERK-activity in keratinocytes representing different skin carcinogenesis stages, which correlated with invasion of benign-tumorigenic keratinocytes.

### 6.2.6 Ras-Raf-MEK-ERK dependence of cSCC progression

To answer whether the observed phenotypes in keratinocytes are due to a MEK-ERK induction or other Vemurafenib related effects, the MEK inhibitor Cobimetinib was used to block Vemurafenib effects that depend on ERK-activity. MEK inhibitors were developed to prevent resistance development, the major problem of melanoma treatment with specific B-Raf inhibitors in patients. In particular, the primary resistance pathway appears to be the reactivation of the parallel MAP kinases ERK, JNK and p38 by additional mutations, amplifications or alternative splicing. Further mechanisms of acquired resistance involve activation of PI3K–PTEN–Akt signaling and others. Interestingly, multiple mechanisms were detected within the same tumor biopsy implying a crucial contribution of tumor heterogeneity in resistance development (Lidsky et al., 2014; Shi et al., 2014; Sun et al., 2014). The combination of B-Raf and MEK inhibitors increased apoptosis and delayed onset of resistance in melanoma monolayer cultures and spheroids (Paraiso et al., 2010). Co-administration of Dabrafenib and Trametinib also enhanced the inhibition of human tumor xenograft growth in mouse models (King et al., 2013). This led to the investigation of a combination therapy for treatment of malignant melanoma also in clinics. As result, combined B-Raf and MEK inhibition improved response rates, PFS and OS compared to mono-therapy with each inhibitor (Larkin et al., 2014a; Long et al., 2014; Robert et al., 2015).

Of importance, cutaneous adverse events were also decreased by combination treatment. In a Phase III clinical trial, 495 patients with previously untreated unresectable locally advanced or metastatic B-Raf$^{V600}$ mutation positive melanoma received Vemurafenib plus Cobimetinib combination therapy or Vemurafenib plus placebo. Combination therapy correlated with a decrease in new skin cancers and other hyper-proliferative skin lesions. In particular, reduction rates for KAs/ SCCs from 19% to 8% and hyperkeratosis from 29% to 10% were achieved (Larkin et al., 2014a). In a second Phase III trial comparing, Dabrafenib plus Trametinib combination therapy vs. the B-Raf inhibitor Dabrafenib alone,

a comparable reduction in cutaneous side effects was monitored (Long et al., 2014). Noteworthy monotherapy with the MEK-inhibitor Trametinib caused adverse events except for SCCs (Jang and Atkins, 2013). These observations are consistent with the suggested pathogenesis of these lesions i.e. MEK-ERK hyper-activation by specific B-Raf inhibitors that is abrogated at the level of MEK through the additional MEK inhibitor (Hatzivassiliou et al., 2010; Heidorn et al., 2010; Poulikakos et al., 2010). Here, 0.1 $\mu M$ Cobimetinib was sufficient to prevent ERK hyper-activation by 1-5 $\mu M$ Vemurafenib in monolayer cultures as well as in HaCaT and HaCaT-RAS A-5 fdmOTCs. Cobimetinib caused some toxicity at a concentration of 0.1 $\mu M$, led to major atrophy of the epithelium at 1 $\mu M$, but did not affect NHDF. Of interest is that HaCaT cells were more sensitive to Cobimetinib than HaCaT-RAS A-5 cells, which was likely due to an elevated basal ERK activity through H-Ras$^{G12V}$ of the latter.

When co-administered, Cobimetinib prevented the Vemurafenib induced accelerated differentiation, which was determined by histology and Filaggrin staining, thus, confirming that this phenotype was indeed dependent on increased ERK signaling. Furthermore, Cobimetinib co-treatment prevented invasive growth of HaCaT-RAS A-5 cells in our fdmOTC model. Invasion and metastasis to different body sites is observed during progression of many human tumors. Several classes of proteins involved in tethering cells to each other or to ECM structures are altered in invasive cells (Hanahan and Weinberg, 2000). To further unravel the invasion mechanism of HaCaT-RAS A-5 cells, I investigated changes in gene regulation upon Vemurafenib and Vemurafenib plus Cobimetinib co-treatment. As result, upregulation of Vemurafenib induced genes in HaCaT-RAS A-5 cells such as TGFA, IL1A, IL1B, IL8, MMP1 MMP3 and MMP9 was abolished with additional Cobimetinib treatment, thus, confirming that these genes and in particular MMP1, MMP3 and MMP9 were upregulated through ERK-activity. Interestingly, MMP14 expression was not affected by any inhibitor, suggesting an alternative regulation. Despite direct MEK-ERK regulation, only pro MMP-1 secretion was upregulated by Vemurafenib in HaCaT fdmOTCs. Since Cobimetinib combination treatment restored control levels, this demonstrated also for HaCaT cells an ERK-dependent gene regulation of MMP-1. In HaCaT-RAS A-5 cells both, MMP-1 and MMP-3 were significantly upregulated by Vemurafenib, although basal pro MMP-1 levels were already a 3-fold higher compared to HaCaT cells. MMP-9 secretion was downregulated by Vemurafenib in HaCaT and HaCaT-RAS A-5 fdmOTCs and therefore, unlikely played a role in the invasive phenotype. Moreover, we generally observed a lower basal level of MMP-3 compared to pro MMP-1 in HaCaT and HaCaT-RAS A-5 fdmOTCs as described previously (Berning et al., 2015). By Cobimetinib co-treatment, MMP-1 and MMP-3 secretion were significantly downregulated in HaCaT-RAS A-5 fdmOTCs, confirming the ERK-dependent expression of both MMPs. From these findings it is tempting to speculate that the higher MMP-1 levels and the additional induction of MMP-3 in HaCaT-RAS A-5 vs. HaCaT fdmOTCs may be triggered by an increased ERK-activity through H-Ras$^{G12V}$ in HaCaT-RAS A-5 cells. Thus, the expressed set of MMPs appeared to be dependent on the stage in carcinogenesis and/or the presence of an additional RAS mutation. This may well explain the difference in invasive behavior between Vemurafenib stimulated HaCaT and HaCaT-RAS A-5 cells.

Besides MMP expression in 2D + 3D, gelatinolytic activity was also increased in HaCaT-RAS A-5 fdmOTCs by Vemurafenib. As Gelatin degradation was strongly reduced by Cobimetinib co-treatment, we concluded that MMP secretion and activation depended on ERK-activation. Furthermore, as we observed increased MMP-activity and the BM components Collagen IV and Collagen VII are known substrates of either MMP-3+MMP-9 or MMP-1+MMP-3 (Visse and Nagase, 2003), the distribution of

both Collagens was determined in fdmOTCs. While Vemurafenib did not reproducibly alter both BM proteins in HaCaT cells, Collagen IV as well as Collagen VII appeared to be reduced by Vemurafenib induced ERK-activation in HaCaT-RAS A-5 fdmOTCs. This suggested that Vemurafenib induced ERK-activation directly induced MMP-1 and MMP-3 expression, which subsequently remodeled or degraded BM components like Collagen IV and VII. These observations could explain the mechanism of invasion by HaCaT-RAS A-5 cells in fdmOTCs.

In a recent study, Vemurafenib treatment in a K5-SOS-F mouse model led to growth of preexisting tumors, epidermal thickening of tail, eyelids, and ears after 5-7 days. These effects were reduced by additional MEK inhibition using Trametinib and led the authors to conclude that Vemurafenib induced proliferation and de-differentiation (Doma et al., 2013). Moreover, Roh and co-workers found that stimulation of HaCaT cells with 2 $\mu M$ Vemurafenib causes MEK-ERK phosphorylation, increased proliferation and invasiveness in a matrigel assay after 24 h (Roh et al., 2015). In contrast, we did not observe de-differentiation as the EMT marker SNAI2 was not upregulated in keratinocytes, but rather demonstrated highly increased differentiation by Vemurafenib treatment in all analyzed keratinocytes. Second, although employing Vemurafenib concentrations ranging from 1-5 $\mu M$ Vemurafenib and having observed MEK-ERK hyper-activation, we did not detect significantly increased proliferation in NHEK, HaCaT or HaCaT-RAS A-5 cells in monolayer cultures or OTCs. This Vemurafenib concentration even prevented growth of NHEK. In agreement with both publications, we describe growth of preexisting keratinocyte lesions characterized by MMP expression, activation and BM degradation that promoted invasive growth of benign-tumorigenic human keratinocytes. Invasive growth of HaCaT cells already after 24 h in Matrigel as shown by Roh *et al.* (Roh et al., 2015) probably accounted to the presence of multiple growth factors and an ECM lacking complexity (Hughes et al., 2010; Vukicevic et al., 1992). We could also demonstrate early invasive steps in HaCaT scaOTCs after 7 weeks of Vemurafenib stimulation, which was prevented in the fdmOTCs model due to the more stringent conditions. Similar to our results, Roh and co workers also identified increased MMP expression and activation by Vemurafenib particularly of MMP-2 and MMP-9 as possible mediators for tumor progression and invasion (Roh et al., 2015). We did not investigate MMP-2 levels as this MMP was recently described to be highly expressed in unstimulated HaCaT fdmOTCs, while being downregulated in cultures with SCC cell lines (Berning, 2015), thus questioning its contribution to tumorigenesis in the fdmOTC model. Furthermore, MMP-9 was also upregulated by Vemurafenib in monolayer cultured HaCaT-RAS A-5 cells after 8-24 h and in HaCaT cells after 4-8 weeks, but we could not determine a Vemurafenib induced secretion in fdmOTCs. Different from Roh *et al.*, we found MMP-1 and MMP-3 to be upregulated by ERK activation in both HaCaT-RAS A-5 monolayer cultures and fdmOTCs in combination with an increased MMP-activity in 3D, thus being most likely responsible for the invasive growth.

Taken together, this study revealed that Vemurafenib mediated MEK-ERK hyper-activation in dermal fibroblasts and keratinocytes induced differentiation as well as MMP1 and MMP3 gene expression in keratinocytes. High pro MMP-1 and MMP-3 secretion especially in Vemurafenib activated benign-tumorigenic HaCaT-RAS A-5 fdmOTCs correlated with Collagen remodeling or degradation, allowing invasive growth into the dermal equivalent. These effects were directly dependent on ERK-activation as they were prevented by co-treatment with the MEK inhibitor Cobimetinib. The invasive behavior of HaCaT-RAS A-5 cells was even higher in Vemurafenib compared to Wnt-3a stimulated fdmOTCs. Vemurafenib also mediated genetic selection pressure on HaCaT cells. A cross-talk between NHDF and

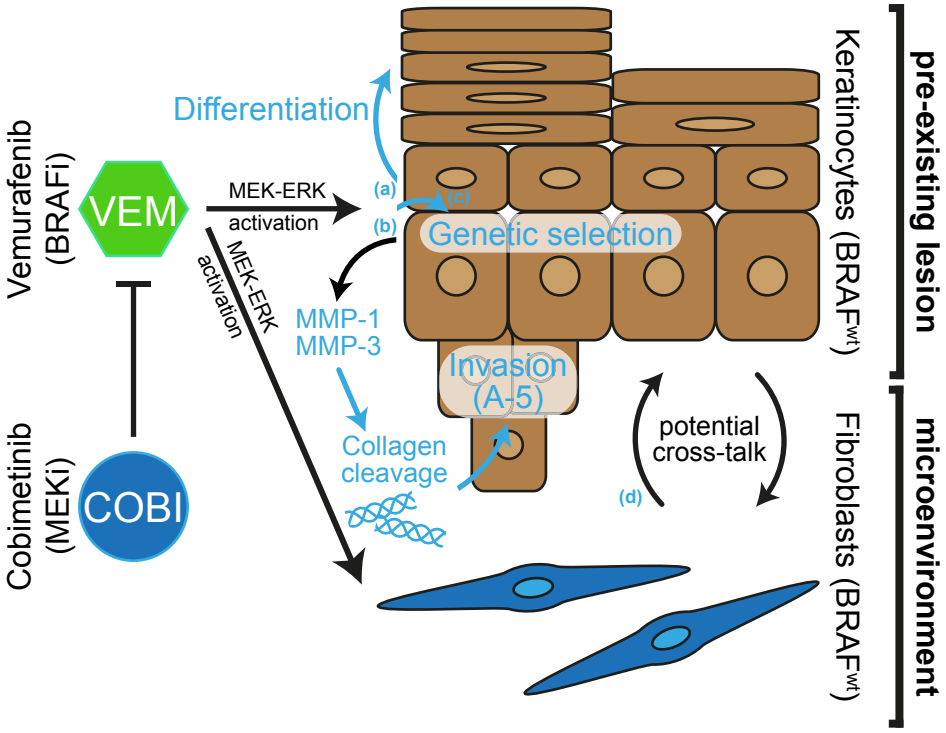


Figure 53 | **Vemurafenib and Ras-Raf-MEK-ERK MAPK signaling in skin carcinogenesis.**
Vemurafenib mediated MEK-ERK hyper-activation in dermal fibroblasts and keratinocytes directly induces differentiation (**a**) as well as MMP1 and MMP3 gene expression in keratinocytes. High pro MMP-1 and MMP-3 secretion especially by Vemurafenib-activated benign-tumorigenic HaCaT-RAS A-5 cells correlates with Collagen remodeling/ degradation and subsequent invasive growth in fdmOTCs (**b**). These effects are directly dependent on ERK-activation as both are prevented by co-treatment with the MEK inhibitor Cobimetinib. Vemurafenib also mediates genetic selection of HaCaT cells (**c**). A cross-talk between NHDF and keratinocytes that further increases differentiation or invasion was not detected, but cannot be fully excluded (**d**).

keratinocytes that further increased differentiation or invasion was not detected, however, cannot be fully excluded as Vemurafenib induced MEK-ERK hyper-activation also in these cells (Fig. 53).

## 6.3 Conclusion and future perspective

In this thesis, the impact of stromal Wnt/Beta-catenin as well as of Ras-Raf-MEK-ERK signaling on human cSCC development and progression was investigated. The performed experiments allowed obtaining a more detailed understanding of the oncogenic events leading to spontaneously occurring cSCCs. Together with aberrant Wnt signaling in tumor cells, a novel Wnt-dependent cross-talk between human skin carcinoma cells and their stromal fibroblasts was identified. Upon Wnt/Beta-catenin activation NHDF secrete proliferation and invasion inducing factors that further promote carcinogenesis. While this Wnt-regulatory mechanism represents a locally confined tumor-stroma cross-talk indirectly acting on keratinocytes, Vemurafenib-induced MEK-ERK hyper-activation was of direct consequence for the keratinocytes. ERK-activity subsequently triggered keratinocyte differentiation and invasive growth only of benign-tumorigenic keratinocytes, showing that a tumor-permissive genetic make-up is required for Vemurafenib-driven invasion. Interestingly, the invasion of HaCaT-RAS A-5 cells was even advanced in Vemurafenib compared to Wnt-3a-treated OTCs, demonstrating the power of Vemurafenib to cause cSCC formation within a very short time. Moreover, Vemurafenib directly caused a genetic

selection of keratinocytes. Thus, both, canonical Wnt and ERK-activity promoted tumor progression. A cross-talk between canonical Wnt signaling and EGFR induced Ras-Raf-MEK-ERK signaling in development and cancer is largely unknown. However, both pathways can transactivate one another. In particular, Wnt ligands can activate EGFR signaling through Frizzled, while EGFR activates Beta-catenin via RTK-Akt pathway. EGFR was also shown to form a complex with Beta-catenin, which increased invasion and metastasis of cancer cells (Hu and Li, 2010). Although cross-activation was not discovered in this study, both investigated mechanism could cooperate *in vivo* to promote cSCC development or progression.

While monoculture experiments and organotypic cultures allow unravelling mechanisms leading to cSCC, it was necessary to validate the obtained results in also primary human cSCCs. Wnt-2 and Wnt-3 ligands, Wnt pathway activation as well as IL-8, CCL-2, MMP-1 expression and collagen cleavage by MMPs were validated in cSCCs. Similar to our *in vitro* results, highly-differentiated human cSCCs emerged during B-Raf inhibitor therapy *in vivo*. Hence, these cSCCs should also be analyzed for ERK hyper-activation, keratinocyte differentiation, MMP expression and invasive growth on a molecular level in future. The role of the immune system could also not be addressed in the models used in this study. As it is well appreciated that precancerous lesions are under tight control of the immune system (Boukamp, 2005) and B-Raf signaling is central for lymphocyte regulation (Comin-Anduix et al., 2010), MEK-ERK hyper-activation could also render immune cells as additional players in cSCC tumorigenesis. A detailed understanding of the involved mechanisms would allow designing improved drugs with increased specificity and reduced adverse events assigned for melanoma therapy.

# 7. References

Airola, K., and Fusenig, N.E. (2001). Differential stromal regulation of MMP-1 expression in benign and malignant keratinocytes. The Journal of investigative dermatology *116*, 85-92.

Anforth, R., Carlos, G., Clements, A., Kefford, R., and Fernandez-Peñas, P. (2015). Cutaneous Adverse Events in Patients Treated with BRAF Inhibitor Based Therapies for Metastatic Melanoma for Longer than 52 Weeks. The British journal of dermatology *172*, 239-243.

Anforth, R., Fernandez-Penas, P., and Long, G.V. (2013). Cutaneous toxicities of RAF inhibitors. The lancet oncology *14*, e11-18.

Arnault, J.-P., Mateus, C., Escudier, B., Tomasic, G., Wechsler, J., Hollville, E., Soria, J.-C., Malka, D., Sarasin, A., Larcher, M.*, et al.* (2012). Skin tumors induced by sorafenib; paradoxic RAS-RAF pathway activation and oncogenic mutations of HRAS, TP53, and TGFBR1. Clinical cancer research : an official journal of the American Association for Cancer Research *18*, 263-272.

Arnault, J.-P., Wechsler, J., Escudier, B., Spatz, A., Tomasic, G., Sibaud, V., Aractingi, S., Grange, J.-D., Poirier-Colame, V., Malka, D.*, et al.* (2009). Keratoacanthomas and squamous cell carcinomas in patients receiving sorafenib. Journal of clinical oncology : official journal of the American Society of Clinical Oncology *27*, e59-61.

Ashton, K.J., Weinstein, S.R., Maguire, D.J., and Griffiths, L.R. (2003). Chromosomal aberrations in squamous cell carcinoma and solar keratoses revealed by comparative genomic hybridization. Archives of dermatology *139*, 876-882.

Aumailley, M., and Timpl, R. (1986). Attachment of cells to basement membrane collagen type IV. The Journal of cell biology *103*, 1569-1575.

Barbacid, M. (1987). ras genes. Annual review of biochemistry *56*, 779-827.

Bello, D.M., Ariyan, C.E., and Carvajal, R.D. (2013). Melanoma mutagenesis and aberrant cell signaling. Cancer control : journal of the Moffitt Cancer Center *20*, 261-281.

Bergers, G., and Benjamin, L.E. (2003). Tumorigenesis and the angiogenic switch. Nature reviews Cancer *3*, 401-410.

Bergers, G., Brekken, R., McMahon, G., Vu, T.H., Itoh, T., Tamaki, K., Tanzawa, K., Thorpe, P., Itohara, S., Werb, Z.*, et al.* (2000). Matrix metalloproteinase-9 triggers the angiogenic switch during carcinogenesis. Nature cell biology *2*, 737-744.

Berning, M. (2015). Three-dimensional in vitro skin and skin cancer models based on fibroblast-derived matrix.

Berning, M., Prätzel-Wunder, S., Bickenbach, J.R., and Boukamp, P. (2015). Three-Dimensional In Vitro Skin and Skin Cancer Models Based on Human Fibroblast-Derived Matrix. Tissue engineering Part C, Methods, 150507120623001.

Bhatia, N., and Spiegelman, V.S. (2005). Activation of Wnt/beta-catenin/Tcf signaling in mouse skin carcinogenesis. Molecular carcinogenesis *42*, 213-221.

Bollag, G., Hirth, P., Tsai, J., Zhang, J., Ibrahim, P.N., Cho, H., Spevak, W., Zhang, C., Zhang, Y., Habets, G.*, et al.* (2010). Clinical efficacy of a RAF inhibitor needs broad target blockade in BRAF-mutant melanoma. Nature *467*, 596-599.

Boukamp, P. (2005). UV-induced skin cancer: similarities--variations. *3*, 493-503.

Boukamp, P., Peter, W., Pascheberg, U., Altmeier, S., Fasching, C., Stanbridge, E.J., and Fusenig, N.E. (1995). Step-wise progression in human skin carcinogenesis in vitro involves mutational inactivation of p53, rasH oncogene activation and additional chromosome loss. Oncogene *11*, 961-969.

Boukamp, P., Petrussevska, R.T., Breitkreutz, D., Hornung, J., Markham, A., and Fusenig, N.E. (1988). Normal keratinization in a spontaneously immortalized aneuploid human keratinocyte cell line. The Journal of cell biology *106*, 761-771.

Boukamp, P., Popp, S., Altmeyer, S., Hülsen, A., Fasching, C., Cremer, T., and Fusenig, N.E. (1997). Sustained nontumorigenic phenotype correlates with a largely stable chromosome content during long-term culture of the human keratinocyte line HaCaT. Genes, chromosomes & cancer *19*, 201-214.

Boukamp, P., Stanbridge, E.J., Foo, D.Y., Cerutti, P.A., and Fusenig, N.E. (1990). c-Ha-ras oncogene expression in immortalized human keratinocytes (HaCaT) alters growth potential in vivo but lacks correlation with malignancy. Cancer research *50*, 2840-2847.

Boukamp, P., Tilgen, W., Dzarlieva, R.T., Breitkreutz, D., Haag, D., Riehl, R.K., Bohnert, A., and Fusenig, N.E. (1982). Phenotypic and genotypic characteristics of a cell line from a squamous cell carcinoma of human skin. Journal of the National Cancer Institute *68*, 415-427.

Brabletz, T., Jung, A., Dag, S., Hlubek, F., and Kirchner, T. (1999). beta-catenin regulates the expression of the matrix metalloproteinase-7 in human colorectal cancer. The American journal of pathology *155*, 1033-1038.

Brabletz, T., Jung, A., Hermann, K., Günther, K., Hohenberger, W., and Kirchner, T. (1998). Nuclear overexpression of the oncoprotein beta-catenin in colorectal cancer is localized predominantly at the invasion front. Pathology, research and practice *194*, 701-704.

Brasanac, D., Boricic, I., Todorovic, V., Tomanovic, N., and Radojevic, S. (2005). Cyclin A and beta-catenin expression in actinic keratosis, Bowen's disease and invasive squamous cell carcinoma of the skin. The British journal of dermatology *153*, 1166-1175.

Brash, D.E. (2006). Roles of the transcription factor p53 in keratinocyte carcinomas. The British journal of dermatology *154 Suppl 1*, 8-10.

Brash, D.E., Ziegler, A., Jonason, A.S., Simon, J.A., Kunala, S., and Leffell, D.J. (1996). Sunlight and sunburn in human skin cancer: p53, apoptosis, and tumor promotion. The journal of investigative dermatology Symposium proceedings / the Society for Investigative Dermatology, Inc [and] European Society for Dermatological Research *1*, 136-142.

Brauchle, M., Glück, D., Di Padova, F., Han, J., and Gram, H. (2000). Independent role of p38 and ERK1/2 mitogen-activated kinases in the upregulation of matrix metalloproteinase-1. Experimental cell research *258*, 135-144.

Brooks, P.C., Strömblad, S., Sanders, L.C., von Schalscha, T.L., Aimes, R.T., Stetler-Stevenson, W.G., Quigley, J.P., and Cheresh, D.A. (1996). Localization of matrix metalloproteinase MMP-2 to the surface of invasive cells by interaction with integrin alpha v beta 3. Cell *85*, 683-693.

Burnworth, B., Arendt, S., Muffler, S., Steinkraus, V., Bröcker, E.B., Birek, C., Hartschuh, W., Jauch, A., and Boukamp, P. (2007). The multi-step process of human skin carcinogenesis: a role for p53, cyclin D1, hTERT, p16, and TSP-1. European journal of cell biology *86*, 763-780.

Burnworth, B., Popp, S., Stark, H.-J., Steinkraus, V., Bröcker, E.B., Hartschuh, W., Birek, C., and Boukamp, P. (2006). Gain of 11q/cyclin D1 overexpression is an essential early step in skin cancer development and causes abnormal tissue organization and differentiation. Oncogene *25*, 4399-4412.

Cadet, J., Sage, E., and Douki, T. (2005). Ultraviolet radiation-mediated damage to cellular DNA. Mutation research *571*, 3-17.

Callahan, M.K., Rampal, R., Harding, J.J., Klimek, V.M., Chung, Y.R., Merghoub, T., Wolchok, J.D., Solit, D.B., Rosen, N., Abdel-Wahab, O.*, et al.* (2012). Progression of RAS-Mutant Leukemia during RAF Inhibitor Treatment. The New England journal of medicine *367*, 2316-2321.

Castro, F., Dirks, W.G., Fähnrich, S., Hotz-Wagenblatt, A., Pawlita, M., and Schmitt, M. (2013). High-throughput SNP-based authentication of human cell lines. International journal of cancer Journal international du cancer *132*, 308-314.

Chang, F., Steelman, L.S., Lee, J.T., Shelton, J.G., Navolanic, P.M., Blalock, W.L., Franklin, R.A., and McCubrey, J.A. (2003). Signal transduction mediated by the Ras/Raf/MEK/ERK pathway from cytokine receptors to transcription factors: potential targeting for therapeutic intervention. Leukemia : official journal of the Leukemia Society of America, Leukemia Research Fund, UK *17*, 1263-1293.

Chua, A.W.C., Ma, D., Gan, S.U., Fu, Z., Han, H.C., Song, C., Sabapathy, K., and Phan, T.T. (2011). The role of R-spondin2 in keratinocyte proliferation and epidermal thickening in keloid scarring. The Journal of investigative dermatology *131*, 644-654.

Clark, I.M., Swingler, T.E., Sampieri, C.L., and Edwards, D.R. (2008). The regulation of matrix metalloproteinases and their inhibitors. The international journal of biochemistry & cell biology *40*, 1362-1378.

Clevers, H. (2006). Wnt/beta-catenin signaling in development and disease. Cell *127*, 469-480.

Cohen, D.N., Lawson, S.K., Shaver, A.C., Du, L., Nguyen, H.P., He, Q., Johnson, D.B., Lumbang, W.A., Moody, B.R., Prescott, J.L.*, et al.* (2015). Contribution of Beta-HPV Infection and UV-Damage to Rapid-onset Cutaneous Squamous Cell Carcinoma during BRAF-inhibition Therapy. Clinical cancer research : an official journal of the American Association for Cancer Research *21*, 2624-2634.

Comin-Anduix, B., Chodon, T., Sazegar, H., Matsunaga, D., Mock, S., Jalil, J., Escuin-Ordinas, H., Chmielowski, B., Koya, R.C., and Ribas, A. (2010). The oncogenic BRAF kinase inhibitor PLX4032/RG7204 does not affect the viability or function of human lymphocytes across a wide range of concentrations. Clinical cancer research : an official journal of the American Association for Cancer Research *16*, 6040-6048.

Condeelis, J., and Pollard, J.W. (2006). Macrophages: obligate partners for tumor cell migration, invasion, and metastasis. Cell *124*, 263-266.

Conti, I., and Rollins, B.J. (2004). CCL2 (monocyte chemoattractant protein-1) and cancer. Seminars in cancer biology *14*, 149-154.

Coussens, L.M., and Werb, Z. (2002). Inflammation and cancer. Nature *420*, 860-867.

Crawford, H.C., Fingleton, B.M., Rudolph-Owen, L.A., Goss, K.J., Rubinfeld, B., Polakis, P., and Matrisian, L.M. (1999). The metalloproteinase matrilysin is a target of beta-catenin transactivation in intestinal tumors. Oncogene *18*, 2883-2891.

Davies, H., Bignell, G.R., Cox, C., Stephens, P., Edkins, S., Clegg, S., Teague, J., Woffendin, H., Garnett, M.J., Bottomley, W.*, et al.* (2002). Mutations of the BRAF gene in human cancer. Nature *417*, 949-954.

de Gruijl, F.R. (1999). Skin cancer and solar UV radiation. European journal of cancer (Oxford, England : 1990) *35*, 2003-2009.

Deshmane, S.L., Kremlev, S., Amini, S., and Sawaya, B.E. (2009). Monocyte chemoattractant protein-1 (MCP-1): an overview. *29*, 313-326.

Dhillon, A.S., Hagan, S., Rath, O., and Kolch, W. (2007). MAP kinase signalling pathways in cancer. Oncogene *26*, 3279-3290.

Dika, E., Patrizi, A., Venturoli, S., Fanti, P.A., Barbieri, D., Strammiello, R., Melotti, B., and La Placa, M. (2015). Human papillomavirus evaluation of vemurafenib induced skin epithelial tumors: a case series. The British journal of dermatology *172*, 540-542.

Doglioni, C., Piccinin, S., Demontis, S., Cangi, M.G., Pecciarini, L., Chiarelli, C., Armellin, M., Vukosavljevic, T., Boiocchi, M., and Maestro, R. (2003). Alterations of beta-catenin pathway in non-melanoma skin tumors: loss of alpha-ABC nuclear reactivity correlates with the presence of beta-catenin gene mutation. The American journal of pathology *163*, 2277-2287.

Doma, E., Rupp, C., Varga, A., Kern, F., Riegler, B., and Baccarini, M. (2013). Skin tumorigenesis stimulated by Raf inhibitors relies upon Raf functions that are dependent and independent of ERK. Cancer research *73*, 6926-6937.

Dong, J., Phelps, R.G., Qiao, R., Yao, S., Benard, O., Ronai, Z., and Aaronson, S.A. (2003). BRAF oncogenic mutations correlate with progression rather than initiation of human melanoma. Cancer research *63*, 3883-3885.

Dubauskas, Z., Kunishige, J., Prieto, V.G., Jonasch, E., Hwu, P., and Tannir, N.M. (2009). Cutaneous squamous cell carcinoma and inflammation of actinic keratoses associated with sorafenib. Clinical genitourinary cancer *7*, 20-23.

Durinck, S., Ho, C., Wang, N.J., Liao, W., Jakkula, L.R., Collisson, E.A., Pons, J., Chan, S.-W., Lam, E.T., Chu, C.*, et al.* (2011). Temporal dissection of tumorigenesis in primary cancers. Cancer discovery *1*, 137-143.

Egeblad, M., and Werb, Z. (2002). New functions for the matrix metalloproteinases in cancer progression. Nature reviews Cancer *2*, 161-174.

Elias, P.M. (2005). Stratum corneum defensive functions: an integrated view. The Journal of investigative dermatology *125*, 183-200.

Euvrard, S., Kanitakis, J., and Claudy, A. (2003). Skin cancers after organ transplantation. The New England journal of medicine *348*, 1681-1691.

Falchook, G.S., Rady, P., Hymes, S., Nguyen, H.P., Tyring, S.K., Prieto, V.G., Hong, D.S., and Kurzrock, R. (2013). Merkel cell polyomavirus and HPV-17 associated with cutaneous squamous cell carcinoma arising in a patient with melanoma treated with the BRAF inhibitor dabrafenib. JAMA dermatology *149*, 322-326.

Fathke, C., Wilson, L., Shah, K., Kim, B., Hocking, A., Moon, R., and Isik, F. (2006). Wnt signaling induces epithelial differentiation during cutaneous wound healing. BMC cell biology *7*, 4.

Flaherty, K.T., Infante, J.R., Daud, A., Gonzalez, R., Kefford, R.F., Sosman, J., Hamid, O., Schuchter, L., Cebon, J., Ibrahim, N.*, et al.* (2012). Combined BRAF and MEK inhibition in melanoma with BRAF V600 mutations. The New England journal of medicine *367*, 1694-1703.

Flaherty, K.T., Puzanov, I., Kim, K.B., Ribas, A., McArthur, G.A., Sosman, J.A., O'Dwyer, P.J., Lee, R.J., Grippo, J.F., Nolop, K.*, et al.* (2010). Inhibition of mutated, activated BRAF in metastatic melanoma. The New England journal of medicine *363*, 809-819.

Frouin, E., Guillot, B., Larrieux, M., Tempier, A., Boulle, N., Foulongne, V., Girard, C., Costes, V., and Solassol, J. (2014). Cutaneous epithelial tumors induced by vemurafenib involve the MAPK and Pi3KCA pathways but not HPV nor HPyV viral infection. PloS one *9*, e110478.

Fuchs, E. (1990). Epidermal differentiation: the bare essentials. The Journal of cell biology *111*, 2807-2814.

Fuchs, E. (1993). Epidermal differentiation and keratin gene expression. Journal of cell science Supplement *17*, 197-208.

Fuchs, E. (2007). Scratching the surface of skin development. Nature *445*, 834-842.

Fuchs, E., and Raghavan, S. (2002). Getting under the skin of epidermal morphogenesis. Nature reviews Genetics *3*, 199-209.

Funck-Brentano, E., Alvarez, J.C., Longvert, C., Abe, E., Beauchet, A., Funck-Brentano, C., and Saiag, P. (2015). Plasma vemurafenib concentrations in advanced BRAFV600mut melanoma patients: impact on tumour response and tolerance. Annals of Oncology, mdv189.

Fusenig, N.E., and Boukamp, P. (1998). Multiple stages and genetic alterations in immortalization, malignant transformation, and tumor progression of human skin keratinocytes. Molecular carcinogenesis *23*, 144-158.

Ganzenmueller, T., Hage, E., Yakushko, Y., Kluba, J., Woltemate, S., Schacht, V., Schulz, T.F., and Gutzmer, R. (2013). No human virus sequences detected by next-generation sequencing in benign verrucous skin tumors occurring in BRAF-inhibitor-treated patients. Experimental dermatology *22*, 725-729.

Gat, U., DasGupta, R., Degenstein, L., and Fuchs, E. (1998). De Novo hair follicle morphogenesis and hair tumors in mice expressing a truncated beta-catenin in skin. Cell *95*, 605-614.

Geigl, J.B., Uhrig, S., and Speicher, M.R. (2006). Multiplex-fluorescence in situ hybridization for chromosome karyotyping. Nature protocols *1*, 1172-1184.

Giannelli, G., Falk-Marzillier, J., Schiraldi, O., Stetler-Stevenson, W.G., and Quaranta, V. (1997). Induction of cell migration by matrix metalloprotease-2 cleavage of laminin-5. Science (New York, NY) *277*, 225-228.

Gillitzer, R., and Goebeler, M. (2001). Chemokines in cutaneous wound healing. Journal of leukocyte biology *69*, 513-521.

Gray, S.T., Wilkins, R.J., and Yun, K. (1992). Interstitial collagenase gene expression in oral squamous cell carcinoma. The American journal of pathology *141*, 301-306.

Green, H. (1977). Terminal differentiation of cultured human epidermal cells. Cell *11*, 405-416.

Grey, A., Cooper, A., McNeil, C., O'Toole, S., Thompson, J., and Grimison, P. (2014). Progression of KRAS mutant pancreatic adenocarcinoma during vemurafenib treatment in a patient with metastatic melanoma. Internal medicine journal *44*, 597-600.

Grimaldi, A.M., Guida, T., D'Attino, R., Perrotta, E., Otero, M., Masala, A., and Cartenì, G. (2007). Sunitinib: bridging present and future cancer treatment. Annals of oncology : official journal of the European Society for Medical Oncology / ESMO *18 Suppl 6*, vi31-34.

Haake, A., GA, S., Holbrook, K., Freinkel, R., and Woodley, D. (2001). Structure and function of the skin: Overview of the epidermis and dermis.

Haider, A.S., Peters, S.B., Kaporis, H., Cardinale, I., Fei, J., Ott, J., Blumenberg, M., Bowcock, A.M., Krueger, J.G., and Carucci, J.A. (2006). Genomic analysis defines a cancer-specific gene expression signature for human squamous cell carcinoma and distinguishes malignant hyperproliferation from benign hyperplasia. The Journal of investigative dermatology *126*, 869-881.

Halaban, R., Zhang, W., Bacchiocchi, A., Cheng, E., Parisi, F., Ariyan, S., Krauthammer, M., McCusker, J.P., Kluger, Y., and Sznol, M. (2010). PLX4032, a selective BRAF(V600E) kinase inhibitor, activates the ERK pathway and enhances cell migration and proliferation of BRAF melanoma cells. Pigment cell & melanoma research *23*, 190-200.

Hanahan, D., and Weinberg, R.A. (2000). The hallmarks of cancer. Cell *100*, 57-70.

Hanahan, D., and Weinberg, R.A. (2011). Hallmarks of cancer: the next generation. Cell *144*, 646-674.

Hatzivassiliou, G., Song, K., Yen, I., Brandhuber, B.J., Anderson, D.J., Alvarado, R., Ludlam, M.J.C., Stokoe, D., Gloor, S.L., Vigers, G.*, et al.* (2010). RAF inhibitors prime wild-type RAF to activate the MAPK pathway and enhance growth. Nature *464*, 431-435.

Hauschild, A., Grob, J.J., Demidov, L.V., Jouary, T., Gutzmer, R., Millward, M., Rutkowski, P., Blank, C.U., Miller, W.H., Kaempgen, E.*, et al.* (2012). Dabrafenib in BRAF-mutated metastatic melanoma: a multicentre, open-label, phase 3 randomised controlled trial. Lancet *380*, 358-365.

Heidorn, S.J., Milagre, C., Whittaker, S., Nourry, A., Niculescu-Duvas, I., Dhomen, N., Hussain, J., Reis-Filho, J.S., Springer, C.J., Pritchard, C.*, et al.* (2010). Kinase-dead BRAF and oncogenic RAS cooperate to drive tumor progression through CRAF. Cell *140*, 209-221.

Hembruff, S.L., Jokar, I., Yang, L., and Cheng, N. (2010). Loss of transforming growth factor-beta signaling in mammary fibroblasts enhances CCL2 secretion to promote mammary tumor progression through macrophage-dependent and -independent mechanisms. Neoplasia (New York, NY) *12*, 425-433.

Holderfield, M., Lorenzana, E., Weisburd, B., Lomovasky, L., Boussemart, L., Lacroix, L., Tomasic, G., Favre, M., Vagner, S., Robert, C.*, et al.* (2014). Vemurafenib cooperates with HPV to promote initiation of cutaneous tumors. Cancer research *74*, 2238-2245.

Hu, T., and Li, C. (2010). Convergence between Wnt-β-catenin and EGFR signaling in cancer. Molecular cancer *9*, 236.

Hughes, C.S., Postovit, L.M., and Lajoie, G.A. (2010). Matrigel: a complex protein mixture required for optimal growth of cell culture. Proteomics *10*, 1886-1890.

Huntington, J.T., Shields, J.M., Der, C.J., Wyatt, C.A., Benbow, U., Slingluff, C.L., and Brinckerhoff, C.E. (2004). Overexpression of collagenase 1 (MMP-1) is mediated by the ERK pathway in invasive melanoma cells: role of BRAF mutation and fibroblast growth factor signaling. The Journal of biological chemistry *279*, 33168-33176.

Jang, S., and Atkins, M.B. (2013). Which drug, and when, for patients with BRAF-mutant melanoma? The lancet oncology *14*, e60-69.

Jones, J.C., and Green, K.J. (1991). Intermediate filament-plasma membrane interactions. Current opinion in cell biology *3*, 127-132.

Kaler, P., Augenlicht, L., and Klampfer, L. (2009). Macrophage-derived IL-1beta stimulates Wnt signaling and growth of colon cancer cells: a crosstalk interrupted by vitamin D3. Oncogene *28*, 3892-3902.

Kalluri, R. (2003). Basement membranes: structure, assembly and role in tumour angiogenesis. Nature reviews Cancer *3*, 422-433.

Kalluri, R., and Zeisberg, M. (2006). Fibroblasts in cancer. Nature reviews Cancer *6*, 392-401.

King, A.J., Arnone, M.R., Bleam, M.R., Moss, K.G., Yang, J., Fedorowicz, K.E., Smitheman, K.N., Erhardt, J.A., Hughes-Earle, A., Kane-Carson, L.S.*, et al.* (2013). Dabrafenib; preclinical characterization, increased efficacy when combined with trametinib, while BRAF/MEK tool combination reduced skin lesions. PloS one *8*, e67583.

Klaus, A., and Birchmeier, W. (2008). Wnt signalling and its impact on development and cancer. Nature reviews Cancer *8*, 387-398.

Lambert, S.R., Mladkova, N., Gulati, A., Hamoudi, R., Purdie, K., Cerio, R., Leigh, I., Proby, C., and Harwood, C.A. (2014). Key differences identified between actinic keratosis and cutaneous squamous cell carcinoma by transcriptome profiling. British journal of cancer *110*, 520-529.

Larkin, J., Ascierto, P.A., Dréno, B., Atkinson, V., Liszkay, G., Maio, M., Mandalà, M., Demidov, L., Stroyakovskiy, D., Thomas, L.*, et al.* (2014a). Combined Vemurafenib and Cobimetinib in BRAF-Mutated Melanoma. The New England journal of medicine *371*, 1867-1876.

Larkin, J., Del Vecchio, M., Ascierto, P.A., Krajsova, I., Schachter, J., Neyns, B., Espinosa, E., Garbe, C., Sileni, V.C., Gogas, H.*, et al.* (2014b). Vemurafenib in patients with BRAF(V600) mutated metastatic melanoma: an open-label, multicentre, safety study. The lancet oncology *15*, 436-444.

Lederle, W., Depner, S., Schnur, S., Obermueller, E., Catone, N., Just, A., Fusenig, N.E., and Mueller, M.M. (2011). IL-6 promotes malignant growth of skin SCCs by regulating a network of autocrine and paracrine cytokines. International journal of cancer Journal international du cancer *128*, 2803-2814.

Lehman, T.A., Modali, R., Boukamp, P., Stanek, J., Bennett, W.P., Welsh, J.A., Metcalf, R.A., Stampfer, M.R., Fusenig, N., and Rogan, E.M. (1993). p53 mutations in human immortalized epithelial cell lines. *14*, 833-839.

Lewis, C.E., and Pollard, J.W. (2006). Distinct role of macrophages in different tumor microenvironments. Cancer research *66*, 605-612.

Li, A., Varney, M.L., Valasek, J., Godfrey, M., Dave, B.J., and Singh, R.K. (2005). Autocrine role of interleukin-8 in induction of endothelial cell proliferation, survival, migration and MMP-2 production and angiogenesis. Angiogenesis *8*, 63-71.

Libra, M., Malaponte, G., Navolanic, P.M., Gangemi, P., Bevelacqua, V., Proietti, L., Bruni, B., Stivala, F., Mazzarino, M.C., Travali, S.*, et al.* (2005). Analysis of BRAF mutation in primary and metastatic melanoma. Cell cycle (Georgetown, Tex) *4*, 1382-1384.

Lidsky, M., Antoun, G., Speicher, P., Adams, B., Turley, R., Augustine, C., Tyler, D., and Ali-Osman, F. (2014). MAP kinase hyper-activation and enhanced NRAS expression drive acquired vemurafenib resistance in V600E BRAF melanoma cells. The Journal of biological chemistry *289*, 27714-27726.

Liu, Z.-L., Li, Y., Kong, Q.-Y., Zhan, C., Wang, Q., Chen, X.-Y., Sun, Y., Wen, S., Tu, C.-X., Liu, J.*, et al.* (2008). Immunohistochemical profiling of Wnt, NF-kappaB, Stat3 and Notch signaling in human epidermal tumors. Journal of dermatological science *52*, 133-136.

Logan, C.Y., and Nusse, R. (2004). The Wnt signaling pathway in development and disease. Annual review of cell and developmental biology *20*, 781-810.

Long, G.V., Stroyakovskiy, D., Gogas, H., Levchenko, E., de Braud, F., Larkin, J., Garbe, C., Jouary, T., Hauschild, A., Grob, J.J.*, et al.* (2014). Combined BRAF and MEK inhibition versus BRAF inhibition alone in melanoma. The New England journal of medicine *371*, 1877-1888.

Lowy, A.M., Clements, W.M., Bishop, J., Kong, L., Bonney, T., Sisco, K., Aronow, B., Fenoglio-Preiser, C., and Groden, J. (2006). beta-Catenin/Wnt signaling regulates expression of the membrane type 3 matrix metalloproteinase in gastric cancer. Cancer research *66*, 4734-4741.

Luger, T.A., and Schwarz, T. (1990). Evidence for an epidermal cytokine network. The Journal of investigative dermatology *95*, 100S-104S.

Lyakhovitsky, A., Barzilai, A., Fogel, M., Trau, H., and Huszar, M. (2004). Expression of e-cadherin and beta-catenin in cutaneous squamous cell carcinoma and its precursors. The American Journal of dermatopathology *26*, 372-378.

Lynch, C.C., and Matrisian, L.M. (2002). Matrix metalloproteinases in tumor-host cell communication. Differentiation; research in biological diversity *70*, 561-573.

Maas-Szabowski, N., Stärker, A., and Fusenig, N.E. (2003). Epidermal tissue regeneration and stromal interaction in HaCaT cells is initiated by TGF-alpha. Journal of cell science *116*, 2937-2948.

Malanchi, I., Peinado, H., Kassen, D., Hussenet, T., Metzger, D., Chambon, P., Huber, M., Hohl, D., Cano, A., Birchmeier, W.*, et al.* (2008). Cutaneous cancer stem cell maintenance is dependent on beta-catenin signalling. Nature *452*, 650-653.

Manola, J., Atkins, M., Ibrahim, J., and Kirkwood, J. (2000). Prognostic factors in metastatic melanoma: a pooled analysis of Eastern Cooperative Oncology Group trials. Journal of clinical oncology : official journal of the American Society of Clinical Oncology *18*, 3782-3793.

Marshall, C.J. (1995). Specificity of receptor tyrosine kinase signaling: transient versus sustained extracellular signal-regulated kinase activation. Cell *80*, 179-185.

McArthur, G.A., Chapman, P.B., Robert, C., Larkin, J., Haanen, J.B., Dummer, R., Ribas, A., Hogg, D., Hamid, O., Ascierto, P.A.*, et al.* (2014). Safety and efficacy of vemurafenib in BRAF(V600E) and BRAF(V600K) mutation-positive melanoma (BRIM-3): extended follow-up of a phase 3, randomised, open-label study. The lancet oncology *15*, 323-332.

Mebratu, Y., and Tesfaigzi, Y. (2009). How ERK1/2 activation controls cell proliferation and cell death: Is subcellular localization the answer? Cell cycle (Georgetown, Tex) *8*, 1168-1175.

Menzies, A.M., Long, G.V., and Murali, R. (2012). Dabrafenib and its potential for the treatment of metastatic melanoma. Drug design, development and therapy *6*, 391-405.

Michel, G., Kemény, L., Peter, R.U., Beetz, A., Ried, C., Arenberger, P., and Ruzicka, T. (1992). Interleukin-8 receptor-mediated chemotaxis of normal human epidermal cells. FEBS letters *305*, 241-243.

Mishra, P., Banerjee, D., and Ben-Baruch, A. (2011). Chemokines at the crossroads of tumor-fibroblast interactions that promote malignancy. Journal of leukocyte biology *89*, 31-39.

Molho-Pessach, V., and Lotem, M. (2007). Ultraviolet radiation and cutaneous carcinogenesis. Current problems in dermatology *35*, 14-27.

Molina-Arcas, M., and Downward, J. (2012). How to fool a wonder drug: truncate and dimerize. Cancer cell *21*, 7-9.

Mueller, M.M., and Fusenig, N.E. (1999). Constitutive expression of G-CSF and GM-CSF in human skin carcinoma cells with functional consequence for tumor progression. International journal of cancer Journal international du cancer *83*, 780-789.

Mueller, M.M., and Fusenig, N.E. (2002). Tumor-stroma interactions directing phenotype and progression of epithelial skin tumor cells. Differentiation; research in biological diversity *70*, 486-497.

Mueller, M.M., and Fusenig, N.E. (2004). Friends or foes - bipolar effects of the tumour stroma in cancer. Nature reviews Cancer *4*, 839-849.

Negus, R.P., Stamp, G.W., Hadley, J., and Balkwill, F.R. (1997). Quantitative assessment of the leukocyte infiltrate in ovarian cancer and its relationship to the expression of C-C chemokines. The American journal of pathology *150*, 1723-1734.

Nemes, Z., and Steinert, P.M. (1999). Bricks and mortar of the epidermal barrier. Experimental and Molecular Medicine, 5.

O-Charoenrat, P., Rhys-Evans, P.H., and Eccles, S.A. (2001). Expression of matrix metalloproteinases and their inhibitors correlates with invasion and metastasis in squamous cell carcinoma of the head and neck. Archives of otolaryngology--head & neck surgery *127*, 813-820.

Oberholzer, P.A., Kee, D., Dziunycz, P., Sucker, A., Kamsukom, N., Jones, R., Roden, C., Chalk, C.J., Ardlie, K., Palescandolo, E.*, et al.* (2012). RAS Mutations Are Associated With the Development of Cutaneous Squamous Cell Tumors in Patients Treated With RAF Inhibitors. Journal of clinical oncology : official journal of the American Society of Clinical Oncology *30*, 316-321.

Ohta, M., Kitadai, Y., Tanaka, S., Yoshihara, M., Yasui, W., Mukaida, N., Haruma, K., and Chayama, K. (2002). Monocyte chemoattractant protein-1 expression correlates with macrophage infiltration and tumor vascularity in human esophageal squamous cell carcinomas. International journal of cancer Journal international du cancer *102*, 220-224.

Ohta, M., Kitadai, Y., Tanaka, S., Yoshihara, M., Yasui, W., Mukaida, N., Haruma, K., and Chayama, K. (2003). Monocyte chemoattractant protein-1 expression correlates with macrophage infiltration and tumor vascularity in human gastric carcinomas. International journal of oncology *22*, 773-778.

Okada, Y., Meguro, M., Ohyama, H., Yoshizawa, S., Takeuchi-Hatanaka, K., Kato, N., Matsushita, S., Takashiba, S., and Nishimura, F. (2009). Human leukocyte histocompatibility antigen class II-induced cytokines from human gingival fibroblasts promote proliferation of human umbilical vein endothelial cells: potential association with enhanced angiogenesis in chronic periodontal inflammation. Journal of periodontal research *44*, 103-109.

Orimo, A., Tomioka, Y., Shimizu, Y., Sato, M., Oigawa, S., Kamata, K., Nogi, Y., Inoue, S., Takahashi, M., Hata, T.*, et al.* (2001). Cancer-associated myofibroblasts possess various factors to promote endometrial tumor progression. Clinical cancer research : an official journal of the American Association for Cancer Research *7*, 3097-3105.

Papadavid, E., Pignatelli, M., Zakynthinos, S., Krausz, T., and Chu, A.C. (2001). The potential role of abnormal E-cadherin and alpha-, beta- and gamma-catenin immunoreactivity in the determination of the biological behaviour of keratoacanthoma. The British journal of dermatology *145*, 582-589.

Papadavid, E., Pignatelli, M., Zakynthinos, S., Krausz, T., and Chu, A.C. (2002). Abnormal immunoreactivity of the E-cadherin/catenin (alpha-, beta-, and gamma-) complex in premalignant and malignant non-melanocytic skin tumours. The Journal of pathology *196*, 154-162.

Paraiso, K.H.T., Fedorenko, I.V., Cantini, L.P., Munko, A.C., Hall, M., Sondak, V.K., Messina, J.L., Flaherty, K.T., and Smalley, K.S.M. (2010). Recovery of phospho-ERK activity allows melanoma cells to escape from BRAF inhibitor therapy. British journal of cancer *102*, 1724-1730.

Paulsson, M. (1992). Basement membrane proteins: structure, assembly, and cellular interactions. Critical reviews in biochemistry and molecular biology *27*, 93-127.

Peifer, M., McCrea, P.D., Green, K.J., Wieschaus, E., and Gumbiner, B.M. (1992). The vertebrate adhesive junction proteins beta-catenin and plakoglobin and the Drosophila segment polarity gene armadillo form a multigene family with similar properties. The Journal of cell biology *118*, 681-691.

Peters, S., Michielin, O., and Zimmermann, S. (2013). Dramatic response induced by vemurafenib in a BRAF V600E-mutated lung adenocarcinoma. Journal of clinical oncology : official journal of the American Society of Clinical Oncology *31*, e341-344.

Pfaffl, M.W. (2001). A new mathematical model for relative quantification in real-time RT-PCR. Nucleic acids research *29*, e45.

Popp, S., Waltering, S., Herbst, C., Moll, I., and Boukamp, P. (2002). UV-B-type mutations and chromosomal imbalances indicate common pathways for the development of Merkel and skin squamous cell carcinomas. International journal of cancer Journal international du cancer *99*, 352-360.

Popp, S., Waltering, S., Holtgreve-Grez, H., Jauch, A., Proby, C., Leigh, I.M., and Boukamp, P. (2000). Genetic characterization of a human skin carcinoma progression model: from primary tumor to metastasis. The Journal of investigative dermatology *115*, 1095-1103.

Poulikakos, P.I., Zhang, C., Bollag, G., Shokat, K.M., and Rosen, N. (2010). RAF inhibitors transactivate RAF dimers and ERK signalling in cells with wild-type BRAF. Nature *464*, 427-430.

Proby, C.M., Purdie, K.J., Sexton, C.J., Purkis, P., Navsaria, H.A., Stables, J.N., and Leigh, I.M. (2000). Spontaneous keratinocyte cell lines representing early and advanced stages of malignant transformation of the epidermis. Experimental dermatology *9*, 104-117.

Queirolo, P., Picasso, V., and Spagnolo, F. (2015). Combined BRAF and MEK inhibition for the treatment of BRAF-mutated metastatic melanoma. Cancer Treatment Reviews *41*, 519-526.

Quintanilla, M., Brown, K., Ramsden, M., and Balmain, A. (1986). Carcinogen-specific mutation and amplification of Ha-ras during mouse skin carcinogenesis. Nature *322*, 78-80.

Reunanen, N., Li, S.-P., Ahonen, M., Foschi, M., Han, J., and Kähäri, V.-M. (2002). Activation of p38 alpha MAPK enhances collagenase-1 (matrix metalloproteinase (MMP)-1) and stromelysin-1 (MMP-3) expression by mRNA stabilization. The Journal of biological chemistry *277*, 32360-32368.

Reya, T., and Clevers, H. (2005). Wnt signalling in stem cells and cancer. Nature *434*, 843-850.

Rheinwald, J.G., and Beckett, M.A. (1981). Tumorigenic keratinocyte lines requiring anchorage and fibroblast support cultures from human squamous cell carcinomas. Cancer research *41*, 1657-1663.

Robert, C., Arnault, J.-P., and Mateus, C. (2011). RAF inhibition and induction of cutaneous squamous cell carcinoma. Current opinion in oncology *23*, 177-182.

Robert, C., Karaszewska, B., Schachter, J., Rutkowski, P., Mackiewicz, A., Stroiakovski, D., Lichinitser, M., Dummer, R., Grange, F., Mortier, L.*, et al.* (2015). Improved overall survival in melanoma with combined dabrafenib and trametinib. The New England journal of medicine *372*, 30-39.

Roh, M.R., Kim, J.M., Lee, S.H., Jang, H.S., Park, K.H., Chung, K.Y., and Rha, S.Y. (2015). Low-concentration vemurafenib induces the proliferation and invasion of human HaCaT keratinocytes through mitogen-activated protein kinase pathway activation. The Journal of dermatology.

Rohani, M.G., Pilcher, B.K., Chen, P., and Parks, W.C. (2014). Cdc42 inhibits ERK-mediated collagenase-1 (MMP-1) expression in collagen-activated human keratinocytes. The Journal of investigative dermatology *134*, 1230-1237.

Rollins, B.J. (1997). Chemokines. Blood *90*, 909-928.

Rush, S., Foreman, N., and Liu, A. (2013). Brainstem Ganglioglioma Successfully Treated With Vemurafenib. Journal of clinical oncology : official journal of the American Society of Clinical Oncology *31*, e159-e160.

Ryle, C.M., Breitkreutz, D., Stark, H.-J., Leigh, I.M., Steinert, P.M., Roop, D., and Fusenig, N.E. (1989). Density-dependent modulation of synthesis of keratins 1 and 10 in the human keratinocyte line HACAT and in ras-transfected tumorigenic clones. Differentiation; research in biological diversity *40*, 42-54.

Samuel, M.S., Lopez, J.I., McGhee, E.J., Croft, D.R., Strachan, D., Timpson, P., Munro, J., Schröder, E., Zhou, J., Brunton, V.G.*, et al.* (2011). Actomyosin-Mediated Cellular Tension Drives Increased Tissue Stiffness and β-Catenin Activation to Induce Epidermal Hyperplasia and Tumor Growth. Cancer cell *19*, 776-791.

Sano, M., Driscoll, D.R., De Jesus-Monge, W.E., Klimstra, D.S., and Lewis, B.C. (2014). Activated wnt signaling in stroma contributes to development of pancreatic mucinous cystic neoplasms. Gastroenterology *146*, 257-267.

Schmitt, M., and Pawlita, M. (2009). High-throughput detection and multiplex identification of cell contaminations. Nucleic acids research *37*, e119-e119.

Schoop, V.M., Mirancea, N., and Fusenig, N.E. (1999). Epidermal organization and differentiation of HaCaT keratinocytes in organotypic coculture with human dermal fibroblasts. The Journal of investigative dermatology *112*, 343-353.

Shi, H., Hugo, W., Kong, X., Hong, A., Koya, R.C., Moriceau, G., Chodon, T., Guo, R., Johnson, D.B., Dahlman, K.B.*, et al.* (2014). Acquired resistance and clonal evolution in melanoma during BRAF inhibitor therapy. Cancer discovery *4*, 80-93.

Sobel, K., Tham, M., Stark, H.-J., Stammer, H., Prätzel-Wunder, S., Bickenbach, J.R., and Boukamp, P. (2015). Wnt-3a-activated human fibroblasts promote human keratinocyte proliferation and matrix destruction. International journal of cancer Journal international du cancer *136*, 2786-2798.

Søndergaard, J.N., Nazarian, R., Wang, Q., Guo, D., Hsueh, T., Mok, S., Sazegar, H., MacConaill, L.E., Barretina, J.G., Kehoe, S.M.*, et al.* (2010). Differential sensitivity of melanoma cell lines with BRAFV600E mutation to the specific Raf inhibitor PLX4032. Journal of translational medicine *8*, 39.

South, A.P., Purdie, K.J., Watt, S.A., Haldenby, S., den Breems, N.Y., Dimon, M., Arron, S.T., Kluk, M.J., Aster, J.C., McHugh, A.*, et al.* (2014). NOTCH1 Mutations Occur Early during Cutaneous Squamous Cell Carcinogenesis. The Journal of investigative dermatology *134*, 2630-2638.

Steude, J., Kulke, R., and Christophers, E. (2002). Interleukin-1-stimulated secretion of interleukin-8 and growth-related oncogene-alpha demonstrates greatly enhanced keratinocyte growth in human raft cultured epidermis. The Journal of investigative dermatology *119*, 1254-1260.

Su, F., Viros, A., Milagre, C., Trunzer, K., Bollag, G., Spleiss, O., Reis-Filho, J.S., Kong, X., Koya, R.C., Flaherty, K.T.*, et al.* (2012). RAS mutations in cutaneous squamous-cell carcinomas in patients treated with BRAF inhibitors. The New England journal of medicine *366*, 207-215.

Sun, C., Wang, L., Huang, S., Heynen, G.J.J.E., Prahallad, A., Robert, C., Haanen, J., Blank, C., Wesseling, J., Willems, S.M.*, et al.* (2014). Reversible and adaptive resistance to BRAF(V600E) inhibition in melanoma. Nature *508*, 118-122.

Takahashi, M., Tsunoda, T., Seiki, M., Nakamura, Y., and Furukawa, Y. (2002). Identification of membrane-type matrix metalloproteinase-1 as a target of the beta-catenin/Tcf4 complex in human colorectal cancers. Oncogene *21*, 5861-5867.

Tap, W.D., Gong, K.-W., Dering, J., Tseng, Y., Ginther, C., Pauletti, G., Glaspy, J.A., Essner, R., Bollag, G., Hirth, P.*, et al.* (2010). Pharmacodynamic characterization of the efficacy signals due to selective BRAF inhibition with PLX4032 in malignant melanoma. Neoplasia (New York, NY) *12*, 637-649.

Tilgen, W., Boukamp, P., Breitkreutz, D., Dzarlieva, R.T., Engstner, M., Haag, D., and Fusenig, N.E. (1983). Preservation of morphological, functional, and karyotypic traits during long-term culture and in vivo passage of two human skin squamous cell carcinomas. Cancer research *43*, 5995-6011.

Tuschil, A., Lam, C., Haslberger, A., and Lindley, I. (1992). Interleukin-8 stimulates calcium transients and promotes epidermal cell proliferation. The Journal of investigative dermatology *99*, 294-298.

Utikal, J., Udart, M., Leiter, U., Kaskel, P., Peter, R.U., and Krähn, G. (2005). Numerical abnormalities of the Cyclin D1 gene locus on chromosome 11q13 in non-melanoma skin cancer. Cancer letters *219*, 197-204.

Van Haren, R., Feldman, D., and Sinha, A.A. (2009). Systematic comparison of nonmelanoma skin cancer microarray datasets reveals lack of consensus genes. The British journal of dermatology *161*, 1278-1287.

Vermeulen, L., De Sousa E Melo, F., van der Heijden, M., Cameron, K., de Jong, J.H., Borovski, T., Tuynman, J.B., Todaro, M., Merz, C., Rodermond, H.*, et al.* (2010). Wnt activity defines colon cancer stem cells and is regulated by the microenvironment. Nature cell biology *12*, 468-476.

Vigarios, E., Lamant, L., Delord, J.P., Fricain, J.C., Chevreau, C., Barrés, B., Gomez-Roca, C., Boulanger, M., and Sibaud, V. (2015). Oral squamous cell carcinoma and hyperkeratotic lesions with BRAF inhibitors. The British journal of dermatology *172*, 1680-1682.

Visse, R., and Nagase, H. (2003). Matrix metalloproteinases and tissue inhibitors of metalloproteinases: structure, function, and biochemistry. Circulation research *92*, 827-839.

Vukicevic, S., Kleinman, H.K., Luyten, F.P., Roberts, A.B., Roche, N.S., and Reddi, A.H. (1992). Identification of multiple active growth factors in basement membrane Matrigel suggests caution in interpretation of cellular activity related to extracellular matrix components. Experimental cell research *202*, 1-8.

Vultur, A., Villanueva, J., and Herlyn, M. (2010). BRAF inhibitor unveils its potential against advanced melanoma. Cancer cell *18*, 301-302.

Vultur, A., Villanueva, J., and Herlyn, M. (2011). Targeting BRAF in advanced melanoma: a first step toward manageable disease. Clinical cancer research : an official journal of the American Association for Cancer Research *17*, 1658-1663.

Wang, N.J., Sanborn, Z., Arnett, K.L., Bayston, L.J., Liao, W., Proby, C.M., Leigh, I.M., Collisson, E.A., Gordon, P.B., Jakkula, L.*, et al.* (2011). Loss-of-function mutations in Notch receptors in cutaneous and lung squamous cell carcinoma. Proceedings of the National Academy of Sciences of the United States of America *108*, 17761-17766.

Watt, F.M. (1989). Terminal differentiation of epidermal keratinocytes. Current opinion in cell biology *1*, 1107-1115.

Watt, F.M., and Collins, C.A. (2008). Role of beta-catenin in epidermal stem cell expansion, lineage selection, and cancer. Cold Spring Harbor symposia on quantitative biology *73*, 503-512.

Watt, F.M., and Hogan, B.L. (2000). Out of Eden: stem cells and their niches. Science (New York, NY) *287*, 1427-1430.

Watt, F.M., Lo Celso, C., and Silva-Vargas, V. (2006). Epidermal stem cells: an update. Current opinion in genetics & development *16*, 518-524.

Waugh, D.J.J., and Wilson, C. (2008). The interleukin-8 pathway in cancer. Clinical cancer research : an official journal of the American Association for Cancer Research *14*, 6735-6741.

Westermarck, J., Li, S.P., Kallunki, T., Han, J., and Kahari, V.M. (2001). p38 mitogen-activated protein kinase-dependent activation of protein phosphatases 1 and 2A inhibits MEK1 and MEK2 activity and collagenase 1 (MMP-1) gene expression. Molecular and Cellular Biology *21*, 2373-2383.

Whipple, C.A., and Brinckerhoff, C.E. (2014). BRAF(V600E) melanoma cells secrete factors that activate stromal fibroblasts and enhance tumourigenicity. British journal of cancer *111*, 1625-1633.

Wischermann, K. (2009). UV-induced Skin Carcinogenesis: The Role of a Deregulated Wnt Signaling Pathway. Dissertation

Yaktapour, N., Meiss, F., Mastroianni, J., Zenz, T., Andrlova, H., Mathew, N.R., Claus, R., Hutter, B., Fröhling, S., Brors, B.*, et al.* (2014). BRAF inhibitor-associated ERK activation drives development of chronic lymphocytic leukemia. The Journal of clinical investigation *124*, 5074-5084.

Yoshimura, T., Robinson, E.A., Tanaka, S., Appella, E., and Leonard, E.J. (1989). Purification and amino acid analysis of two human monocyte chemoattractants produced by phytohemagglutinin-stimulated human blood mononuclear leukocytes. Journal of immunology (Baltimore, Md : 1950) *142*, 1956-1962.

Yu, L., Favoino, E., Wang, Y., Ma, Y., Deng, X., and Wang, X. (2011). The CSPG4-specific monoclonal antibody enhances and prolongs the effects of the BRAF inhibitor in melanoma cells. Immunologic research *50*, 294-302.

Zaravinos, A., Kanellou, P., Baritaki, S., Bonavida, B., and Spandidos, D.A. (2009). BRAF and RKIP are significantly decreased in cutaneous squamous cell carcinoma. Cell cycle (Georgetown, Tex) *8*, 1402-1408.

Zhou, L.-L., Lin, Z.-X., Fung, K.-P., Cheng, C.H., Che, C.-T., Zhao, M., Wu, S.-H., and Zuo, Z. (2011). Celastrol-induced apoptosis in human HaCaT keratinocytes involves the inhibition of NF-κB activity. European Journal of Pharmacology *670*, 399-408.

Zimmer, L., Hillen, U., Livingstone, E., Lacouture, M.E., Busam, K., Carvajal, R.D., Egberts, F., Hauschild, A., Kashani-Sabet, M., Goldinger, S.M.*, et al.* (2012). Atypical melanocytic proliferations and new primary melanomas in patients with advanced melanoma undergoing selective BRAF inhibition. Journal of clinical oncology : official journal of the American Society of Clinical Oncology *30*, 2375-2383.

# 8. Appendix

## 8.1 Author's Publications

### 8.1.1 Original Articles

Sobel, K.*, Tham, M.*, Stark, H.-J., Stammer, H., Prätzel-Wunder, S., Bickenbach, J.R., and Boukamp, P. (2015). Wnt-3a-activated human fibroblasts promote human keratinocyte proliferation and matrix destruction. Int J Cancer 136, 2786–2798. (* Authors contributed equally to this work)

### 8.1.2 Oral Presentations

Tham, M., Berning, M., Jauch, A., and Boukamp, P. (09/ 2015). Vemurafenib induces proliferation, differentiation, invasion and stromal activation in a 3D human skin carcinoma model. 15th World Congress on Cancers of the Skin, Edinburgh, United Kingdom

### 8.1.3 Poster Presentations

Tham, M., Berning, M., and Boukamp, P. (02/ 2014). Vemurafenib induces differentiation, invasion and stromal activation in a 3D human skin carcinoma model. AACR Special Conference: Cellular Heterogeneity in the Tumor Microenvironment, San Diego/ CA, USA

Tham, M., Sobel, K., Schardt, L., Stammer, H., and Boukamp, P. (07/ 2013). Wnt/Beta-catenin-activated stromal fibroblasts: A decisive role for tumor-stroma cross-talk in human skin carcinogenesis. 8th World Congress of Melanoma, Hamburg, Germany

Tham, M., Sobel, K., Stammer, H., and Boukamp, P. (06/ 2013). Wnt/Beta-catenin-activated stromal fibroblasts: A decisive role for tumor-stroma cross-talk in human skin carcinogenesis. 7th International PhD Student Cancer Conference, London, United Kingdom

Tham, M., Sobel, K., Stammer, H., and Boukamp, P. (03/ 2013). Wnt/Beta-catenin-activated stromal fibroblasts: A decisive role for tumor-stroma cross-talk in human skin carcinogenesis. 17th International AEK Cancer Congress, Heidelberg, Germany

Tham, M., Sobel, K., Stammer, H., and Boukamp, P. (11/ 2012). Wnt/b-catenin-activated fibroblasts: A decisive role for tumor-stroma cross-talk in skin carcinogenesis. Helmholtz International Graduate School for Cancer Research PhD Poster Presentation 2012, Heidelberg, Germany

Tham, M., Sobel, K., Stammer, H., and Boukamp, P. (10/ 2012). Wnt/Beta-catenin-activated stromal fibroblasts: A decisive role for tumor-stroma cross-talk in human skin carcinogenesis. 7th Heinrich F. C. Behr Symposium on Stem Cells and Cancer, Heidelberg, Germany

Tham, M., Wischermann, K., Stammer, H., Stark, H.-J., and Boukamp, P. (06/ 2012). Wnt/b-catenin activated fibroblasts induce tumor-stroma cross-talk in skin carcinogenesis. Helmholtz International Graduate School for Cancer Research PhD Retreat 2012, Weil der Stadt, Germany

Tham, M., Wischermann, K., Stammer, H., Stark, H.-J., and Boukamp, P. (02/ 2012). Wnt/β-catenin-activated stromal fibroblasts: A decisive role for tumor-stroma cross-talk in human skin carcinogenesis. 2nd Heidelberg Forum for Young Life Scientists, Heidelberg, Germany

## 8.2 Eidesstattliche Erklärung

Ich erkläre hiermit, dass ich die vorgelegte Dissertation selbst verfasst und mich dabei keiner anderen als der von mir ausdrücklich bezeichneten Quellen und Hilfen bedient habe. Diese Dissertation wurde in dieser oder anderer Form weder bereits als Prüfungsarbeit verwendet, noch einer anderen Fakultät als Dissertation vorgelegt. An keiner anderen Stelle ist ein Prüfungsverfahren beantragt.

Heidelberg, 08. Juli 2015

_____

(Marius Tham)